Title

Design, Synthesis, and Characterization of Bioinspired Functional Coatings and Adhesives

Author

Delparastan, Amir Peyman

Publication Date

2021

Peer reviewed|Thesis/dissertation

Design, Synthesis, and Characterization of Bioinspired Functional Coatings and Adhesives

by

Amir Peyman Delparastan

A dissertation submitted in partial satisfaction of the

requirements for the degree of

Doctor of Philosophy

in

Engineering - Materials Science and Engineering

in the

Graduate Division

of the

University of California, Berkeley

Committee in charge:

Professor Phillip B. Messersmith, Chair
Professor Niren Murthy
Professor Ting Xu

Spring 2021

Design, Synthesis, and Characterization of Bioinspired Functional Coatings and Adhesives

Abstract

Design, Synthesis, and Characterization of Bioinspired Functional Coatings and Adhesives

by

Amir Peyman Delparastan

Doctor of Philosophy in Engineering - Materials Science and Engineering

University of California, Berkeley

Professor Phillip B. Messersmith, Chair

Catechol-based molecules have been identified as one of the key elements responsible for many important functions in natural systems owing to their intrinsic physicochemical properties. Capitalizing on these universal design principles found in nature, catecholic molecules have been increasingly considered in the field of materials science as possible bioinspired structural motif candidates to synthesize and fabricate advanced engineering materials. This thesis begins with a short introduction to the structural diversity of the most important families of catecholic molecules found in biological systems, with an emphasis on elucidating the structure-property relationships arising from the chemical functionalities present in their molecular structures. In chapter 1 the fundamental physicochemical interactions undertaken by catecholic molecules at interfaces, both in nature and in bioinspired materials, and common strategies for productive manipulation of these interactions are further described. Chapter 2 aims to provide a more complete picture of marine mussel adhesion, particularly at the molecular level, and facilitate developing a solid framework for the rational design of mussel-inspired wet adhesives. In this chapter the interplay between chemical sequence and topological structure in the mussel adhesive proteins is illustrated by highlighting the results of our molecular level study on the interfacial adhesion of a library of mussel-inspired peptides to organic and inorganic substrates. In chapters 3-6 a summary of the research on design, synthesis, and characterization of catechol-based bioinspired functional materials for implementation in diverse applications ranging from hybrid materials and coatings to high-performance dry/wet adhesives is provided. In chapter 3, bioinspired catechol-based material polydopamine (pDA), one of the most widely employed surface modification methods due to its versatility and simplicity, is introduced and the results of the research undertaken to elucidate the formation mechanism, structure, and molecular mechanics of this fascinating material is discussed. In chapter 4 some of the main shortcomings of these coatings including their poor mechanical performance are described followed by reporting a simple post-treatment approach via thermal annealing at a moderate temperature as a facile route to enhance mechanical robustness of pDA coatings without compromising their inherent

functionality. A suite of characterization techniques are employed and analysis of the results shows fundamental changes in the molecular and bulk mechanical behavior of pDA after thermal annealing, leading to considerable improvements in the ability of the coatings to resist mechanical deformations. Chapters 5 and 6 describe developing catechol-based pressure-sensitive adhesives (PSAs) by exploiting the mussel adhesion principles. In chapter 5 a combination of microscopic and macroscopic adhesion assays are used to study the effect of catechol on dry and wet adhesion performance of the catechol-containing PSAs. Chapter 6 describes developing a new generation of synthetic amino-catechol adhesives inspired by the adhesive synergy between flanking amine and catechol residues in the mussel adhesive proteins. Comprehensive multi-scale adhesion characterization is used to probe performance at the molecular, microscopic, and macroscopic levels, showing that coupling of catechols and amines together within the same hybrid monomer architecture produced optimal cooperative effects in improving macroscopic adhesion performance.

To my wonderful mother

For her support and constant love that have sustained me throughout my life. I am forever indebted to you mom.

Contents

List of Figures

List of Tables

List of Schemes

Preface

Catechol-based molecules have been identified as one of the key elements responsible for many important functions in natural systems owing to their intrinsic physicochemical properties. Capitalizing on these universal design principles found in nature, catecholic molecules have been increasingly considered in the field of materials science as possible bioinspired structural motif candidates to synthesize and fabricate advanced materials. Chapter 1 of this thesis begins with a consideration of the building block diversity in nature, introducing important families of catechols, catecholamines, and plant-based polyphenols found in biological systems, with an emphasis on elucidating the structure-property relationships arising from the chemical functionalities present in their molecular structures. Next, I review the fundamental physicochemical interactions undertaken by catechols, which dictate the behavior of catechols at interfaces, in solution and in condensed phases, both in nature and in bioinspired materials. Recognizing that assembling or fabricating functional materials from catechols is often complicated by their unique reactive nature, I later discuss strategies for productive manipulation of catechol building blocks during synthesis and fabrication of materials. In the next chapters of this thesis I provide an overview of my doctorate research on design, synthesis, and characterization of catechol-based bioinspired functional materials for implementation in diverse applications ranging from hybrid materials and coatings to high-performance dry/wet adhesives.

Binding in the presence of water, salts, and surface contaminants remains one of the greatest challenges faced by man-made adhesives. The remarkable wet adhesion of marine mussels has long been a source of inspiration for the adhesion community. However, despite significant progress in the past few years, the true potential of mussel inspiration may not be fully harnessed until a deeper understanding of the effects of chemical composition and topological structure of the mussel adhesive proteins on adhesion strength is achieved. Interestingly, the adhesive synergy between flanking lysine (Lys, K) and 3,4-Dihydroxyphenylalanine (DOPA, Y) residues in the mussel foot proteins have recently attracted notable attention. However, unfortunately the complex topological relationship of DOPA and Lys as well as the interfacial adhesive roles of other amino acids in mussel foot proteins have been understudied. In chapter 2, I present the results of our research that was originally appeared as a peer-reviewed article co-first-authored by me in Nature Communications journal. In this work, we reported on a study into the adhesion of a library of DOPA-lysine peptides to

organic and inorganic surfaces and demonstrated the effects of chemical composition and topological structural on wet adhesion and energy dissipation. Specifically, the results indicated that increasing binding site density by simply adding more adhesive units to the sequence contribute little to enhancing the overall interaction strength. This may explain why natural proteins never have more than ∼25% of the adhesive amino acid DOPA. We also demonstrated that incorporating non-adhesive motifs as spacer in between the adhesive sites can mimic function of the 'hidden length' in mussel proteins and lead to dissipating more energy during the detachment process, ultimately resulting in enhanced wet adhesion performance. Finally, the results revealed that although Phenylalanine (Phe) can perform as well as DOPA on hydrophobic surfaces that can accommodate π-π or cation-π interactions, DOPA is a more versatile adhesive motif and has clear advantages for improving interfacial adhesion on a broader range of substrates. The research presented in this chapter enabled us to reveal previously unknown molecular features of mussel adhesion, which will inform the future rational design of biomimetic wet adhesives.

In Chapter 3, which is adapted from the work originally appeared as a peer-reviewed article co-first-authored by me in Angewandte Chemie journal, I describe the research focused on understanding the structure and molecular mechanics of bioinspired coatings. Inspired by mussel adhesive proteins, polydopamine (pDA) is one of the simplest and most versatile surface coatings that has been widely adopted for various areas ranging from energy harvest and storage, as consumer coatings, and in therapeutic and diagnostic health care applications. However, pDA remains a poorly understood material, with the dominant view in the literature being that pDA is a noncovalent supramolecular aggregate of small molecules. Our research challenged this view by directly showing with single molecule force spectroscopy (SMFS) that pDA is a high molecular weight polymer. The novel approach employed in this work enabled us to, for the first time, perform molecular mechanics measurements of pDA on the single molecule level and reveal important insights into pDA structure. The key findings in this work provided a new perspective to the field and established a rational basis for future design of advanced pDA materials with tailorable properties. The article has collected more than 62 citations at the time of writing this thesis and has been selected as the top 0.1% articles in the field based on Essential Science Indicators (ESI) database.

Chapter 4 describes an approach to improve the mechanical properties of the mussel inspired nanocoating material pDA. In chapter 1, I introduce mussel inspired coatings and provide background information about their chemistry and physicochemical properties. In chapter 3, I discuss the findings of the research that shed light on the molecular structure and mechanics of the coatings and briefly conclude with the outstanding challenges and opportunities in the field. pDA offers a simple and versatile approach to surface modification and has been widely adopted for use in various areas. However, despite its widespread use, pDA coatings are not mechanically robust and exhibit poor resistance to delamination and abrasion. In Chapter 4, I present an approach that involves a facile thermal treatment at modest temperatures to enhance the mechanical robustness of pDA coatings. I describe results of

chemical spectroscopic, x-ray scattering analyses, and molecular mechanical characterization which indicated that the thermal treatment induced fundamental chemical and structural changes in the pDA nanocoating. Importantly, scratch resistance measurements showed that the residual scratch depth of thermally annealed pDA was 4 times lower compared to the pristine pDA coatings. This unique thermal post-processing approach offers a facile route to improving mechanical properties of pDA, and may lead to more effective utilization of pDA nanocoatings.

Chapter 5 is adapted based on the research originally appeared as a peer-reviewed article co-authored by me published in ACS Applied Materials & Interfaces in 2019. Inspired by the adhesive proteins of marine mussels, catechol-containing synthetic polymers have been extensively explored for wet adhesion. However, practical potential of incorporation of catechols into pressure sensitive adhesives (PSAs) remains to be unrealized. In this work we reported synthesis of mussel-inspired PSAs by copolymerization of dopamine methacrylamide (DMA) with common PSA monomers. A combination of microscopic and macroscopic adhesion assays were used to study the effect of catechol on adhesion performance of acrylic PSAs. We observed that incorporating only 3 mol% of catechols can lead to stark increases in shear and peel adhesion for the adhesives over PSAs with noncatecholic motifs. The enhanced wet shear holding power of the catecholic PSA was illustrated by preparing a prototype sticky note and assessing its underwater performance as compared to Post-it Extreme note, a product marketed as water-resistant and engineered for tough conditions.

As mentioned before and described in detail in chapter 2, the presence of the catehcolic amino acid DOPA in the adhesive proteins of marine mussels has long inspired researchers to develop catechol-containing synthetic polymers. Recent findings have suggested that close association of DOPA with cationic amino acids such as lysine can lead to significant improvements in adhesion through synergistic effects between catechols and amines. In chapter 6, I report our research on design and synthesis of a new generation of amino-catechol PSAs by copolymerization of traditional PSA monomers with lysine- and aromatic-rich monomers. This work reports the most advanced catecholamine monomer design to date, in which the amine and catechol functional groups optimally arranged so as to enhance force transmission from the substrate to the adhesive. The polymers were subjected to the most comprehensive dry/wet adhesion characterization to date, including AFM-assisted molecular and microscopic force spectroscopy as well as standard macroscopic static shear and peel adhesion tests. The molecular and microscopic force experiments confirmed the synergistic effects between catechols and amines. Macroscopic adhesion results further showed that incorporating lysine-catechol pairs into PSAs can lead to optimization of overall performance of the catechol-amine adhesives. The results also demonstrated the key role of cation-aromatic pairs as compelling molecular modules in enabling robust cohesion of mussel-inspired adhesives and developing PSAs with remarkable resistance to flow under shear. The logical approach to polymer design combined with multi-scale adhesion characterizations allowed us to decouple the interfacial adhesive and intermolecular cohesive contributions and inves-

tigate the effects of molecular architecture and aromatic structure on the overall performance.

Finally, I conclude the dissertation by highlighting some of the acknowledged limitations and challenges associated with the translation of catechol-based molecules into functional materials and provide possible directions and future trends for further exploitation of these diverse family of molecules as building blocks for advanced materials.

Acknowledgments

I would not have been able to complete my graduate studies and write this dissertation if it was not for the support and help of so many people. First and foremost, I have to wholeheartedly thank my family for their love and support throughout my life and especially during the last six years of my graduate studies that we had to endure an unavoidable separation. Thank you mom for giving me strength throughout all these years and for your countless sacrifices to help me reach for my dreams and achieve my goals.

I would like to offer my sincere gratitude and appreciation to my advisor, Prof. Phillip B. Messersmith, for his continuous guidance and support throughout my PhD program. In the very last year of my undergraduate program when I was contemplating pursuing an advanced degree, you believed in my capabilities and encouraged me to join his research lab at UC Berkeley. Coming to Berkeley and completing my PhD under your supervision has been a honor and an absolutely rewarding experience for me. I am grateful for your confidence in me from the early days till now. I would also like to express my heartfelt thankfulness for your exquisite attention to detail and for your demand for excellence that has challenged me to do the best work that I could do. Thank you many times! I would also like to thank Prof. Ting Xu of the Materials Science & Engineering Department and Prof. Niren Murthy of the Bioengineering Department for serving as members on my thesis committee. I am also most grateful to Prof. Andrew Minor and Prof. Gerbrand Ceder of the Materials Science & Engineering Department as well as Prof. Niren Murthy and Prof. Seung-Wuk Lee of the Bioengineering Department for serving in my PhD qualifying exam committee and for sharing their valuable insights and expertise regarding my PhD projects. A special thanks to all the collaborators outside our group for all your help and support. In particular I would like to offer my gratitude to Prof. Haeshin Lee from Korea Advanced Institute of Science and Technology (KAIST) and Prof. Yi Cao from Nanjing University for their insights and continuous guidance that led me to develop a better understanding of some of the more subtle challenges in our collaborative projects. I would also like to thank Joshua Speros and Matthias Gerst for providing me with a unique research experience in California Research Alliance (CARA). Thank you for all your technical help and support throughout the last few years—I have learned so much from you.

During the past few years I have met many wonderful people that without their help completion of this work would have not been possible. A very special thanks to Katerina, my colleague and dearest friend who was always there for me when I needed her the most. Thank you for your practical help, kindness, and emotional support. You have been a source of encouragement and inspiration for my personal and professional development in the past years. Your brilliant mind, persistent help, and enthusiasm did make our works together a truly fulfilling experience. My PhD journey would have not been the same without you. Thank you, Kat, now and always. I also wish to express my sincere appreciation and thanks to all the current and former colleagues and friends in Messersmith lab. I have been fortunate

to work alongside so many talented people and learn from the best during my PhD—thank you all so much! I want to thank our postdocs and visiting scholars for their invaluable assistance and guidance that helped me construct my own scientific thoughts, research design and methodology. Dr. Brylee Tiu, Dr. Yiran Li, Dr. Jing Cheng, Dr. Kyueui Lee, Prof. Helen Zha, Dr. Diederik Balkenende, Dr. Cody Higginson, Dr. Severin Sigg, Dr. Caroline Sugnaux, Dr. Patrick Burch, Dr. Patrick Rühs, Dr. Rafael Libanori, Dr. Farid Behboodi Sadabad, Prof. Suhair Sunoqrot, Dr. Iho Kamimura, Dr. Joakim Engstrom, Dr. Jisoo Shin, Livius Muff, Benzi Estipona, Chao Liang, and Miriam Zintl—thank you for all your technical help, support and friendship! I would like to specifically thank Brylee who played an essential role along the journey as we collaborated closely together during the last few years of my PhD. Thank you for the project feedbacks, for your immeasurable help, and for your technical and professional guidance. This thesis would have not been completed without you, thank you! I am also grateful to my other postdoc project collaborators Yiran, Jing, and Severin for their continuous help and technical guidance. I also offer my sincere appreciation to Cody and Dirk for their excellent suggestions and myriad of ways in which they supported me along the way. And last but not least, my heartfelt thanks to all the graduate and undergraduate students in our lab who were always there for me when I needed experimental guidance or someone to talk. Many thanks to Dr. Devang Amin, Dr. Sally Winkler, Angie Korpusik, Kelsey DeFrates, Arianna Avellan, Max Ney, Haoqi Wang, Rachel Huang, Caroline Sobek, Aimee Nguyen, and Luis Caldera for your friendship, technical help and contributions, and providing encouragement at the many challenging times in my journey. You made my PhD a wonderful experience and you are always on my mind.

Peyman Delparastan
May 2021

Chapter 1

Catechol-based Functional Materials

Abstract

Catechol-based molecules have been identified as one of the key elements responsible for many important functions in natural systems owing to their intrinsic physicochemical properties. Capitalizing on these universal design principles found in nature, catecholic molecules have been increasingly considered in the field of materials science as possible bioinspired structural motif candidates to synthesize and fabricate advanced engineering materials. This chapter provides a short introduction to the biological background and structural diversity of catecholic molecules found in nature, with an emphasis on elucidating the structure-property relationships arising from the chemical functionalities present in their molecular structures. Here, I review the fundamental interfacial and non-interfacial interactions undertaken by catechols and discuss important strategies for productive manipulation of catechol building blocks during synthesis and fabrication of functional bioinspired materials.

1.1 Introduction

Modern technological breakthroughs have generated a high demand for the design of novel functional materials. In this regard, nature and the evolution of functional building blocks by living organisms, can serve as a unique and vast reservoir of inspiration.[1, 2] Harnessing nature's wisdom and utilizing its design principles can be a viable approach to addressing emerging challenges in engineering materials.[3] Enhanced functionalities of many natural systems are attributed to their molecular features and assembly mechanisms from small-molecule building blocks. For instance, protein-based mussel adhesion serves as one of many model systems utilizing catecholic building blocks for attachment to wet surfaces. These proteins are rich in 3,4-dihydroxyphenyl-L-alanine (DOPA), a catecholic amino acid residue formed by the post translational modification of protein-bound tyrosine.[4, 5] Dopa is also found in other marine organisms such as the cement of sandcastle worms and tunicates.[6] This peculiar but abundant catecholic moiety found in mussel adhesive proteins is a key

amino acid in the context of the diverse adhesive and cohesive interactions of these proteins. Mussels' adhesive prowess, which relies on both the regulation and processing of catechol chemistry, has inspired the design and development of numerous high performance synthetic adhesives and primers.[7–9] Beyond mussels, many organisms including a wide variety of bacteria, fungi and mammals produce melanin pigments that are composed of polymerized catecholamine and/or indolic compounds. Melanin building blocks have been associated with diverse functions ranging from UV protection of skin,[10] camouflage in response to danger,[11] energy transduction in cellular integrity,[12] and immune response and melanization at the injury sites in insects.[13] Melanin, due to its diverse physicochemical properties have been extensively exploited in the recent years to develop new materials for energy, medical and environmental applications.[14] In the plant kingdom, polyphenols are widely distributed secondary metabolites with a high concentration of catecholic and phenolic hydroxyls in their molecular structures. In addition to their role as secondary metabolites, polyphenols are linked to important biological functions such as chemical and radiation defense, pigmentation, and structural support.[15–17] The ability of polyphenolic molecules to transform into complex oligo-assemblies provides them with a remarkably diverse range of physicochemical properties, making them intriguing natural products that are increasingly appreciated as building blocks in the context of designing novel materials for various applications ranging from biomaterials to hybrids and photonics.[18–20]

The progress towards capitalizing on the unique properties and rich chemistry of natural catecholic building blocks has been rapid, leading to many breakthroughs in novel materials.[18, 21–23] Here, I aim to further discuss the current demands and the existing challenges regarding the expanding field of bioinspired functional materials. Fig. 1 summarizes some of the emerging roles of these catecholic and polyphenolic building blocks as natural and functional materials.

1.2 Structural Diversity in Catecholic Building Blocks

Although several thousand catecholic building blocks in nature have been identified and categorized up to now,[24, 25] the list of molecules that have been practically explored for developing integrated functional materials has been somewhat limited. Most of the representatives that have been adopted in this context are catecholamines such as dopamine,[26–28] L-DOPA, norepinephrine, as well as a few gallol-based derivatives such as pyrogallol and tannic acid.[21, 23, 29–32] As the physicochemical properties for each of these catecholic building blocks vary, developing a set of design principles for utilizing this bioinspired toolbox would be advantageous for fabricating functional materials. Towards this end, I will be focusing the discussion on the three main classes of catechol-based building blocks as depicted in Fig. 2, namely catechol- and gallol-based molecules as well as selected members of the catecholamine family. In this section, these main structural categories will be introduced, with an emphasis on discussing the underlying differences between them in terms of structure-property relationships.

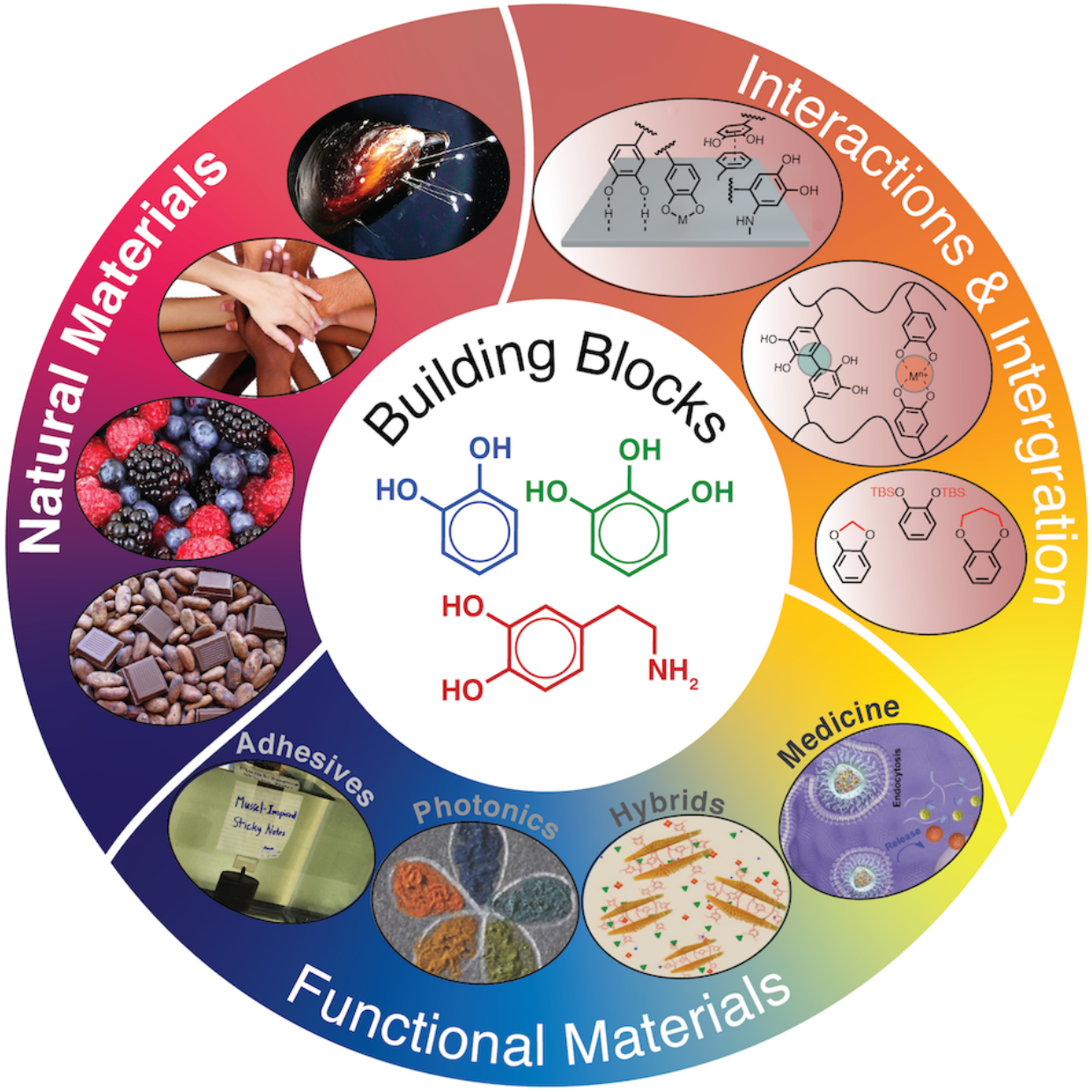

Figure 1.1: Translation of bioinspired building blocks into emerging functional materials. Pyrocatechol, pyrogallol and catecholamine moieties found in mussel, melanin pigment, berries, cacao beans serve as main inspiration for the design of complex functional materials applied in applications such as energy, photonics, adhesives, hybrids and medicine.

Catechol-based Molecules

A closer look at the structures shown in Fig. 2 indicates the pivotal role of ortho-dihydroxy (catechol) as the shared functional group. Many fungi, plants and animals[18, 21, 33] employ catechol-based molecules including pyrocatechols[19, 33] and pyrogallols[16] as essential molecules in biochemical reactions and as building blocks of tissues. A notable example is the holdfast or byssus of marine mussels, whose threads contain specialized proteins with high contents of the post-translationally modified amino-acid 3,4-dihydroxyphenyl-L-alanine (DOPA).[4] The catechol side chain in DOPA has been identified as a key motif enabling strong adhesion of mussel threads to a variety of substrates in both dry and wet conditions.[9, 34] Among the many proteins present in the byssus, mussel foot proteins Mfp-1, Mfp-3 and Mfp-5 have been shown to have the highest concentrations of DOPA. Mfp-1, abundant in the cuticle of the thread and the plaque, acts mainly as a protective varnish layer for the soft collagenous interior matrix. Mfp-3 and Mfp-5 are predominantly found at the plaque-substrate interface and play an essential role in interfacial interactions contributing to strong wet adhesion.[5] Besides fulfilling the role of interfacial binding, presence of catechol in the threads is also speculated to be critical for solidification of the byssus. The participation of catechols in a myriad of non-covalent and covalent chemical interactions is best manifested makes it essential to the exceptional mechanical performance of mussel byssus.[33]

Catechin, usually found in high concentrations in tea leaves, is another example of the catechol-based molecules in nature and has been recognized as an emerging building block for developing bioinspired functional coatings.[25, 35, 36] The thin coatings formed on the inner walls of tea cups represents the most common and everyday-life case of catechin oligomerization.[37, 38] In general, catechol-based building blocks undergo oligomerization via two distinct pathways: 1) salt-mediated non-covalent assembly and 2) enzyme-catalyzed or UV-induced oxidative coupling. The first mechanism is usually favored in slightly basic condition and is facilitated in the presence of high concentrations of salts which leads to strengthening of the cation-π interactions.[36] Presence of enzymes or UV-irradiation, on the other hand, can result in generation of free radicals which can further trigger oligomerization and cross-linking of the catechol-based molecules.[39–41] Although both of these pathways result in formation of aggregated structures from small-molecule building blocks, salt-mediated mechanism leads only to physical stacking of the monomers rather than formation of covalently cross-linked species. This further highlights that oxidative cross-linking of unsubstituted catechols is hindered in the slightly basic conditions due to the relatively high pK_a values of hydroxyl groups ($\sim$9.5-11.5),[42] which suppresses deprotonation of catechols and formation of *o*-quinones.[43] Nevertheless, catechol-based molecules have been successfully used to form conformal coatings on a variety of target substrates in solutions with high concentration of salts. However, as these coatings are mostly assembled only through relatively weak non-covalent interactions, they generally do not exhibit remarkable stabilities. Unfortunately, not many fundamental studies have focused on investigating physical and mechanical integrity of this family of coatings.[44–46] Nonetheless, unlike the salt-mediated assembly method, UV-irradiation can trigger the polymerization of catecholic monomers through aryl-aryl coupling

induced by free-radicals. Levkin and colleagues have investigated UV-polymerization of a range of catechol-based plant-derived polyphenols in detail and have successfully demonstrated viability of this approach to control the deposition and photo-patterning of these compounds on different substrates.[39, 47] Oxidase enzymes such as laccase can also enable assembly of catecholic building blocks through oxidative coupling and formation of hetero-oligomers.[41]

Urushiol Molecules and Lacquer Chemistry

Urushiol and its analogs (Fig. 2) are catecholic compounds that exist in lacquer tree, mostly distributed in South and Southeast Asia.[48] In addition to their unique glossy appearance when hardened, they possess high shear strength, chemical and heat resistance, as well as strong insulation and waterproofing properties, explaining their historical use as protective coating layers during the past thousands of years.[49, 50] Due to its amphiphilic structure composed of a relatively hydrophilic head (catechol) and an aliphatic hydrophobic tail, urushiol is usually prepared as concentrated water-in-oil emulsion which can be used for painting protective coatings.[51, 52] The urushiol in the paint can be further polymerized in air due to the presence of trace amount of the enzyme laccase in the extraction mixture of lacquer tree which can facilitate the oxidative process of *o*-quinone formation.[53] In order to circumvent the need for long curing times, synthetic mimics of urushiol have been synthesized and cured with metal ions followed by high temperature treatment to promote the cross-linking reactions.[54] UV-induced photocuring has also been investigated as another alternative method to stimulate the oxidative cross-liking of urushiol.[55]

Gallol-based Molecules

Gallol-based molecules have been widely explored as potential building blocks for developing multifunctional engineering materials.[21, 23] A number of most commonly investigated molecules are listed in Fig. 2. Rather than discuss all known gallol-based molecules, instead I focus on only the main molecules such as pyrogallol, gallate derivatives, and tannic acid that have been more frequently employed in the context of building blocks for functional materials. One prominent example of gallol-based functional materials in nature is melanin that is being incorporated by plants to strengthen their cell walls (Fig. 3). In contrast to melanin found in animal pigments, plant melanin is lacking amine-derived moieties and the main precursors include catecholic units such as caffeic acid and gallic acid.[56] During an injury, polyphenol oxidases are released from the vesicles and catalyze the oxidation of tannins to produce quinone species in the presence of oxygen.[57] These highly reactive quinone species can crosslink through reaction with nucleophilic groups such as amines and thiols generating a melano-protein which leads to the sclerotization and browning of the injury site. Similar to oxidative oligomerization of catechols, assembly of gallol-based molecules starts with the formation of *o*-quinone species.[16] However, unlike catechols, the additional hydroxyl group in gallol-based molecules enhances the intermolecular interactions through formation

of auxiliary hydrogen and ionic bonds as well as adducts from the nucleophilic reactions of the extra hydroxyl moiety with the quinone species (Fig. 3). The magnified intermolecular interactions of tannic acid and gallol-based molecules can promote the formation of relatively stable coatings as compared to those fabricated from catechol-based building blocks.[36] For instance, kinetics of the oligomerization for the pyrocatechol and pyrogallol at the air/water interface have been studied and it was demonstrated that interfacial films can be formed about an order of magnitude faster for the case of pyrogallol compared to pyrocatechol.[16] Another striking feature of these coatings is their colorless nature; although many alternative building blocks such as catecholamines have been investigated for fabrication of thin-films, gallol-based molecules present the unique opportunity to develop colorless coatings.[25] In the case of catecholamines, cyclization and intermolecular cross-linking reactions owing to the presence of amine groups can result in formation of extended conjugated structures that interact strongly with the light in the visible spectrum.[58] Since coloration can limit implementation of the coatings in many aesthetic applications, gallol-based building blocks can be potential candidates for developing colorless multifunctional materials.

Catecholamine-based Molecules

Even though hundreds of catechol-based molecules have been investigated as building block candidates, catecholamines have attracted the most interest and been widely adopted to develop synthetic functional materials. Polydopamine (pDA),[29, 59] poly-norepinephrine,[31] and melanin-mimic poly-DOPA[60] are just a few examples of the most well-established members of this family that have been extensively studied for more than a decade.[32, 61] Presence of a nucleophilic amine group in the these molecules play an essential role in accelerating the oligomerization of building blocks through formation of a number of important intermediates including dihydroxyindole (DHI) or its analogs. As shown in Fig. 3 and discussed in detail in many outstanding reviews before,[29, 33, 62, 63] these intermediates can strongly contribute to the formation of hierarchical structures such as those identified in eumelanin[30, 58] and pDA.[64–66] In addition, catecholamines and DHI intermediates have been shown to play essential roles in the stiffening and hardening of insect exoskeletons during cuticle formation or sclerotization.[67] The process is initiated by the action of phenoloxidase enzyme on catecholamine sclerotizing precursors, such as N-acetyldopamine and N-b-alanydopamine, to generate quinones which in turn form adducts with the side chain hydroxyl groups of chitin protein, a major structural component of the cuticle.[57, 68] It has been demonstrated that substituting dopamine for amine-protected derivatives such as N-acetyldopamine and N-β-alanyldopamine could result in improving the mechanical integrity of the cuticle, further highlighting the important role of catecholamines in the reaction mechanism.[68]

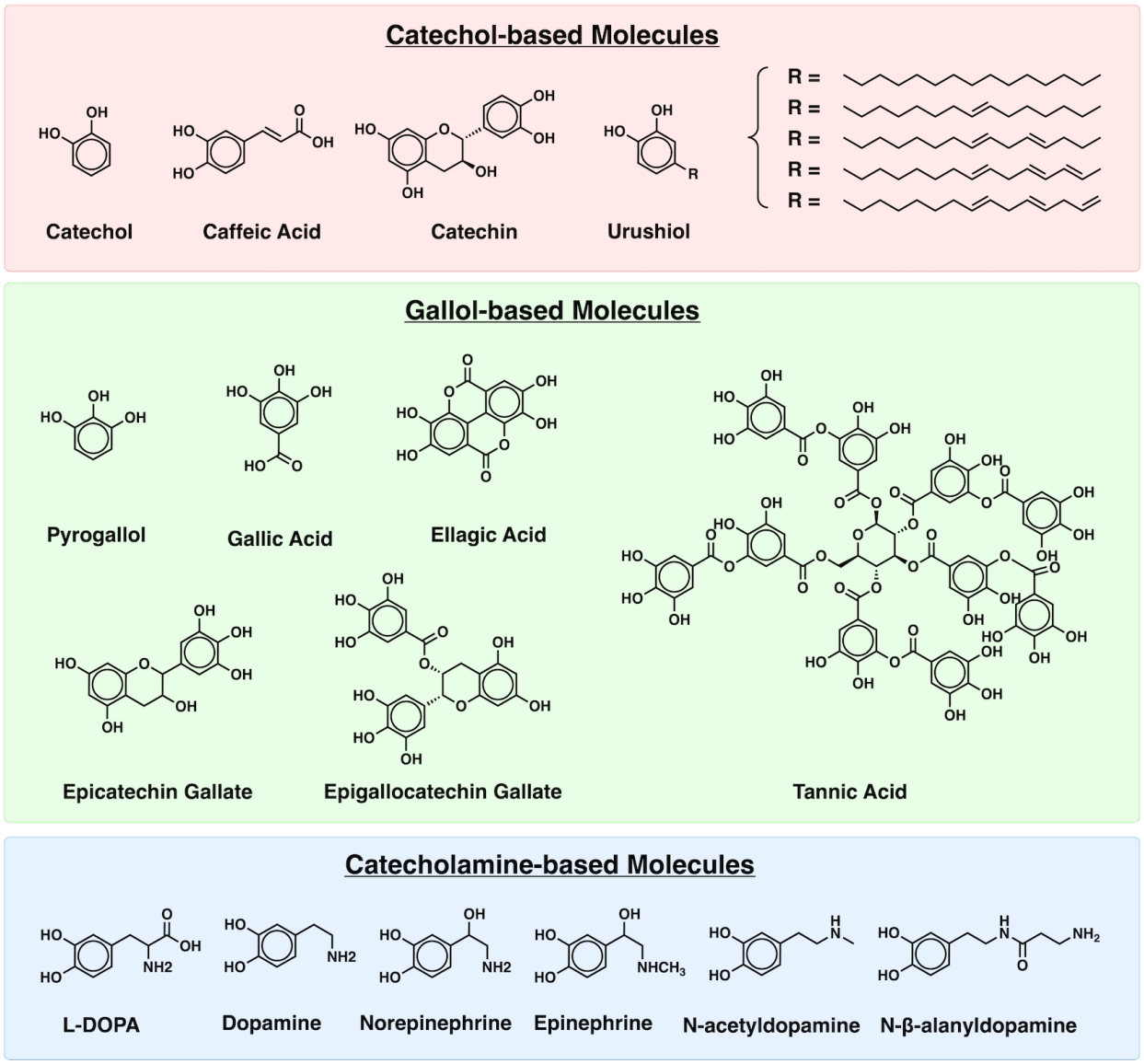

Figure 1.2: Families of catechol-based molecules. Chemical structures of most commonly used catechol-, gallol-, and catecholamine-based molecules as building blocks for functional materials.

L-DOPA: A Basic Building Block for Eumelanin Formation

Melanin is a ubiquitous biological pigment found in organisms throughout nature. Eumelanin is the black-brown subgroup of melanin pigments and is present in the skin, hair, and feathers of animal species.[57] Formation of eumelanin initially involves the enzymatic oxidation of L-DOPA into dopaquinone by tyrosinase. Dopaquinone itself can undergo subsequent cycliza-

tion and rearrangements with or without decarboxylation leading to 5,6-dihydroxyindole-2-carboxylic acid (DHICA) or 5,6-dihydroxyindole (DHI) monomer precursors, respectively, which are then further oxidized and polymerized to produce the black insoluble eumelanin pigment.[69–71] At the molecular level, crosslinking of eumelanin building blocks can occur at several reactive sites, conferring on eumelanin with a degree of chemical disorder in addition to its aggregation-dependent functional properties.[57] Nevertheless, despite the disorder observed at the primary levels, Watt et al., Clancy et al., and others have reported compelling evidence demonstrating that melanin, both in natural and synthetic forms, can assemble into stacked structures defined by heteroatomic non-covalent interactions with a characteristic inter-plane spacing of ∼3.7Å.[72–74] The extent of macroscopic stacking of layers and aggregation of protomolecules in eumelanin highly depends on its formation pathway and relative proportion of DHI- and DHICA-derived units.[30, 60, 75, 76] Eumelanin is a remarkable example of a hierarchical material formed through aggregation and assembly of small molecules and is responsible for many different functions ranging from photoprotection and camouflage to metal ion chelation and free radical sequestration in natural materials.[77, 78] Endowed with diverse physicochemical properties, eumelanin and melanin-inspired materials have attracted significant scientific attention and have become a real possibility for many cutting-edge applications in electronics, optics, and sensors.[71, 79]

Dopamine: A Mussel-inspired Building Block for Multifunctional Materials

Although the multiple and important roles of DOPA residues in mussel byssus have been studied for decades, the distinct advantages of utilizing small-molecule catecholamines as alternative models for mussel adhesive proteins has become apparent only in the last decade.[29, 61, 80] Inspired by the co-presence and high concentration of catechol- and amine-containing residues in the mussel adhesive proteins, dopamine, generally known as a neurotransmitter, was conceived as a small molecule alternative to the adhesive proteins since it is uniquely equipped with both catechol and amine moieties in its molecular structure.[61] pDA, derived from auto-oxidation and polymerization of dopamine monomers has become the most widely utilized multifunctional poly(catecholamine) material since it was first introduced in 2007.[61] Following a similar mechanism to that of the eumelanin formation, the initial stages in oligomerization of dopamine into pDA involve auto-oxidation of catechol groups giving rise to *o*-quinones, which can further undergo intramolecular cyclization reactions to yield DHI (Fig. 3c). For the next stages of the pDA assembly two main pathways have been proposed: 1) formation of supramolecular aggregates of monomeric and/or oligomeric species held together via relatively weak intermolecular interactions such as hydrogen bonding, π–π stacking, and cation-π, or 2) alternatively formation of linear polymer chains due to covalent coupling of the oxidized and cyclized dopamine monomers via aryl–aryl linkages.[45, 58] Polymerization of dopamine into pDA by a simple and low-cost dip-coating procedure results in deposition of conformal coatings on a variety of substrates as well as formation of particles as suspension, both of which have been extensively investigated as versatile platforms to develop complex functional materials for various applications.[29, 59, 78, 81] In

addition, reactivity of the chemical residues in its structure towards nucleophilic amines and thiols endows pDA with superior capacity to immobilize and conjugate variety of molecules through Michael addition or Schiff base formation.

Norepinephrine and Epinephrine: Neurotransmitters as Functional Building Blocks

Norepinephrine (NE, also known as noradrenaline, NA) and epinephrine (EPI, also known as adrenaline) are neurotransmitters derived from dopamine. Although these molecules can follow a similar aggregation pathway to those of the eumelanin and pDA formation, presence of an extra hydroxyl group on their aliphatic chain can lead to the formation of additional intermediates. For instance, a 3,4-dihydroxybenzaldehyde (DHBA) intermediate can be formed during oxidation of NE, which can further react with the amine group in norepinephrine to form DHBA-NE adducts. It has been suggested that these intermediates and adducts can contribute to the reduced roughness of the pNE coatings compared to pDA.[31, 32] Unlike dopamine and NE, EPI lacks the primary amine group in its structure which can presumably adversely affect its assembly due to diminished intermolecular interactions. Nevertheless, it has been reported that self-oligomerization of EPI can result in more homogenous and uniform coatings on TiO_2 substrates as compared to pDA coatings.[82] Unfortunately, the potential of using EPI as building block for functional materials has not been investigated in detail and its assembly mechanism still remains unclear.

1.3 Molecular Mechanics of Catecholic Building Blocks

Incorporating polyphenolic and catecholic building blocks into materials can imbue the structures with a wide range of functional properties.[21] However, to adhere onto templates and form different architectures, these molecules should possess two fundamental characteristics: first, the interfacial adhesion should be strong enough for the molecules to effectively adsorb onto the substrates or templates, and second, the intermolecular interactions between the subunits should be sufficiently large to hold them firmly together. In addition, the molecules should be able to undergo further reactions with secondary components in order to generate hybrid assemblies with integrated functional properties. The essential utility of the catechol as a building block for developing functional materials is rooted in its versatility in forming a broad range of both non-covalent and covalent interactions.[33, 83] This section aims to provide a brief summary of the most important interfacial and non-interfacial interaction mechanisms for catechol-based molecules.

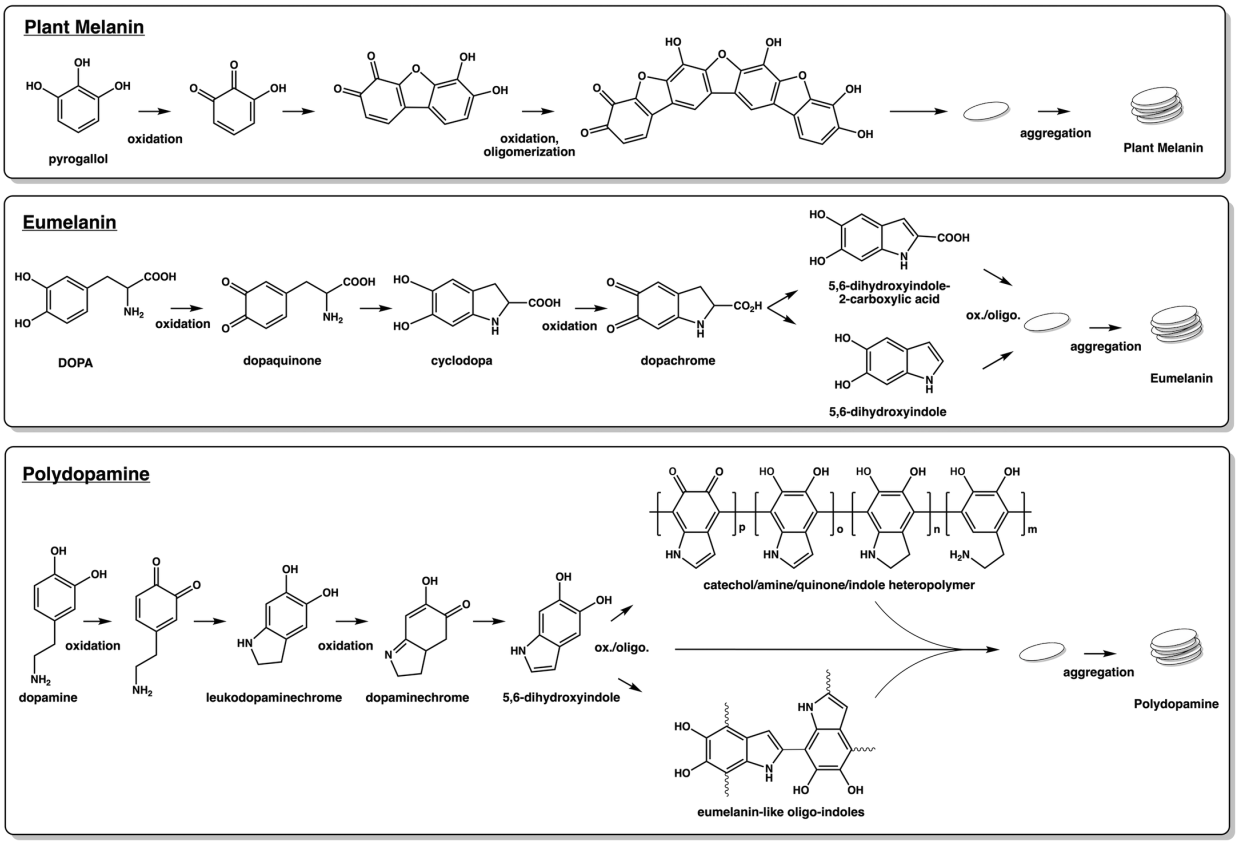

Figure 1.3: Formation pathways for gallol-based melanin, eumelanin, and pDA. Oxidation of catechol results in formation of *o*-quinone species which can further trigger aryl-aryl coupling and nucleophilic addition reactions to yield oligomers and protomolecules. Aggregation of these building blocks lead to formation of stacked structures. Unlike pyrogallol-derived plant-melanin, presence of primary amine group in the DOPA molecule results in intermolecular cyclization reactions to form DHI and DHICA intermediates, which can further oligomerize and assemble into eumelanin. Besides the eumelanin-like pathway, and additional formation mechanism has been proposed for pDA based on the formation of linear heteropolymer chains of catechol- and indole-based monomers.

Interfacial Adhesive Interactions

The interfacial adhesion of polyphenolic and catechol-based molecules and building blocks is attributed to the broad range of mechanisms that catechol moiety employs to interact with different inorganic or organic surfaces. These mechanisms have been thoroughly investigated before and reported in many great reviews.[5, 33, 34, 62, 63, 84, 85] Here I briefly describe some of the main adhesive and cohesive interactions of catechol as depicted in Fig. 4. For instance, catechol groups can bind to a variety of substrates, inorganic metal oxides and

organic materials with polar groups, via hydrogen bonding. On hydrophobic surfaces weak van der Waals forces play an important role in the adsorption process.[62] If the surface contains aromatic groups (e.g. polystyrene, graphene, carbon nanotubes), the π-π stacking interactions between the phenyl ring of catechols and aromatic-rich surfaces are proposed to prevail over other weak non-covalent interactions.[62, 86] For the case of metal oxide and metallic substrates, the main adhesion mechanism of catechols is through coordination bonding and complexation.[86, 87] Catechol group can also bind to organic substrates that contain nucleophilic groups through covalent attachments via Michael addition or Schiff base formation.[33] This outstanding reactivity of catechols towards nucleophiles such as amine or thiol has been extensively utilized to conjugate a variety of biomolecules onto the catechol-containing materials.[33, 88] For the case of catecholamines, the presence of primary amine group has been proved to be an important contributor to the adsorption process. For instance, it has been demonstrated that adhesive strength of polycatecholamine coatings is almost 30 times higher than that of polycatechol coatings, possibly due to the surface salt displacement by the primary amine and improved cation-π interactions.[89] In addition, for organic surfaces bearing primary amino groups, the aromatic ring of catechol can further establish cation-π interactions with protonated amines and facilitate the adsorption and assembly process.[90]

Non-interfacial Cohesive Interactions

Besides enjoying a myriad of adhesive mechanisms for the attachment to different substrates and templates, catechol-based molecules should also be able to interact strongly with one another in order to form a stable assembled structure. Owing to the versatile chemistry of catechol, both non-covalent and covalent interactions can contribute to the structural integrity and provide the bulk material with cohesive strength.[33] For example, catechols and catecholamines are known to be prone to electron oxidation resulting in formation of *o*-quinone species (Fig. 4).[33] These species play a key role in cross-linking and formation of covalent interactions between the subunits through arylaryl coupling reactions. Quinone-mediated coupling reaction can be facilitated in the presence of enzymes or redox-active metal ions such as Fe^{3+} or Cu^{2+} and has been recognized as a major contributor to solidification of the catechol-containing proteins in the mussel threads.[33, 91–94] The *o*-quinones formed during catechol oxidation can also contribute to intra- and/or inter-molecular interactions through reaction with a variety of nucleophiles including amines or thiols via Michael addition or Schiff base formation pathways as shown in examples in Fig. 4.[33] For instance, primary amines can react with quinone species to form cyclic DHI products. As a result, compared to the amine-free catecholic molecules, catecholamines can benefit from supplementary mechanisms to enhance their intermolecular interactions and produce more robust structures. In addition to the covalent interactions, catecholic building blocks can also use a variety of non-covalent strategies including hydrophobic interactions, cation-π, hydrogen bonding, and coordination complexation with metal ions (e.g. Fe^{3+}, Cu^{2+}, Ca^{2+}) to form stable assembled structures. Although non-covalent in nature, the metal-catechol coordination bonds

offer stiffness and strength approaching those of a covalent bond, which strongly depend on the coordination state of metal ion.[95–97] The critical role of cation-π interactions in enhancing the cohesive strength of catecholamine aggregates has also been highlighted in the recent years.[98–100] Another striking feature of catechols and catecholamine building blocks is their ability to form dynamic covalent bonds with boronic acids. The catechol-boronic acid complexes are stimuli-responsive in nature towards pH, temperature, and presence of competing species.[101, 102] These dynamic covalent interactions have been applied to develop a broad range of functional materials including therapeutics, biosensors, and self-healing hydrogels due to the fast kinetics and pH-responsiveness of the interactions in the physiological range.[102–105]

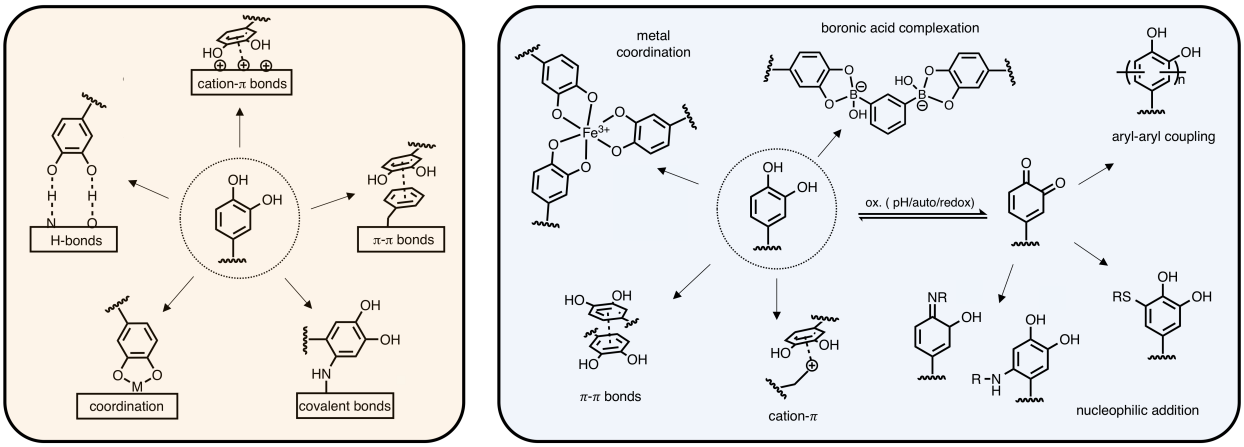

Figure 1.4: Physicochemical interactions of catecholic molecules. A brief representation of the main interfacial interactions (left) and non-interfacial molecular interactions (right) utilized by catecholic building blocks.

1.4 Manipulation Strategies for Integration of Catecholic Molecules into Functional Materials

As described earlier in detail, phenolic hydroxyl groups of catechols and polyphenols can take part in a wide range of reactions to form covalent and non-covalent interactions.[33] Although these interactions result in embedding the catechol-containing materials with many unique characteristic properties, the high reactivity of the phenolic hydroxyls towards many substrates and reagents can render developing catechol-functionalized materials a synthetically challenging task. As a result, protection of the labile hydroxyl groups is often necessary to prevent the side reactions during the synthesis of catechol-containing materials.[106, 107] Over the past decades many protection strategies have been adopted and developed to accomplish this goal and resulted in successful incorporation of catechol moiety into synthetic

schemes. For instance, despite the important distinctions between phenolic hydroxyls and alcohols in terms of their chemical reactivity, many of the protective groups developed for alcohols have also been utilized for catechol protection due to similarities that exist between these two functional groups.[106, 107] As a case in point, similar to protection of alcohols, the chemical reactivity of catechol moiety can be temporarily restricted through installation of ether or ester protective groups. Moreover, the presence of the vicinal hydroxyl groups in catecholic molecules enables additional protection strategies using bidentate groups to form cyclic derivatives such as acetals, ketals, and borate esters.[106] This section aims to provide the readers with a brief overview of the commonly used catechol protection strategies and demonstrate their utilization for developing catechol-containing materials in the recent years. For a more thorough description of the catechol protection methods, I refer the interested readers to some of the focused articles on the subject.[106, 107]

Alkyl Ether Protective Groups

Ethers along with esters and carbonates are some of the most widely used strategies to block the phenolic hydroxyl groups during synthesis of catechol-containing materials. Although similarities exist between ether and ester protection of alcohols and phenols, phenolic ethers and esters are generally more labile to cleavage and hydrolysis compared to alcohol derivatives due to the differences in the chemical reactivity and pK_a of phenolic hydroxyls.[106, 107] It should be also noted that when using these strategies to selectively protect the hydroxyl groups of catecholamine molecules, it is often necessary to first mask the amino group in order to avoid alkylation or acylation on the nitrogen.[108] A few distinct synthetic pathways are generally employed to alkylate phenolic hydroxyls. Simple alkyl ethers can be formed through nucleophilic substitution reaction on an alkyl halide (e.g. MeI) or sulphate (e.g. Me_2SO_4) with the phenol or phenolate anion in the presence of a base (e.g. K_2CO_3 or NaOH).[106, 107, 109, 110] A similar approach can be used to form phenolic ethers from benzyl halides. Alternatively, other methods have been developed for alkylation via a relatively fast, room temperature reaction between the free phenol with a diazoalkane such as CH_2N_2 or CH_3CHN_2 in an inert solvent.[106, 107] Depending on the stability of the alkoxy or aryloxy leaving groups, the deprotection can be carried out using strong Bronsted acids such as TFA, H_2SO_4, HBr or HCl in appropriate reaction conditions.[107] For instance, while the t-butyl protecting group can be removed by treatment with TFA at room temperature, removal of the methyl ether group requires harsh reaction conditions and is usually performed in the presence of concentrated hydrogen halides with reflux at high temperatures.[106] Cleavage of the ether bonds can alternatively be realized in the presence of strong Lewis acids such as $AlCl_3$ or BBr_3 in inert solvents such as CH_2Cl_2 at moderate temperatures.[106, 107] Ether protection strategy has been shown to be effective in masking hydroxyl groups during the synthesis of catechol-containing functional materials. For instance, Yoshie and colleagues employed this protection/deprotection route to incorporate catechol and gallol functional motifs into polymers for developing tunicate-inspired underwater adhesives.[111] Very recently, Fischer et al. studied the effects of catechol-amine spacing and positioning on the adhesion of

peptides by employing a similar approach for protection of catechols during the synthesis their systems.[112] However, despite many successful examples alkyl ether strategy used to protect catechols, the efficacy of the installation methods are typically highly influenced by the nucleophilicity and steric hindrance of the reagents.[106, 110, 113] More importantly, removal of the ether protecting groups often requires harsh reaction conditions that might adversely affect other functional groups present in the molecule. As a result, efforts have been made to develop ether protection strategies that offer more flexibility in the installation and cleavage reaction conditions.[110, 113] A prominent example in this area is silyl ether strategy that has been extensively used in the recent years for catechol protection.[114]

Silyl Ether Protective Groups

Over the recent years silyl protecting groups have gained prominence as a viable strategy for the protection of catechols mainly owing to the relative simplicity of their installation and removal.[114] Silyl protection of catechols can be readily accomplished using reactive common silylating reagents such as trimethylsilyl (TMS), tert-butyldimethylsilyl (TBS), or tert-butyldiphenylsilyl (TBDPS) in the presence of a base such as 1,8-diazabicyclo[5.4.0]undec-7-ene (DBU).[115, 116] Removal of the silyl ether groups is typically achieved by acid-catalyzed hydrolysis or alternatively via nucleophilic fluoride reagents such as tetrabutylammonium fluoride (TBAF).[116, 117] Reactivity and stability of the silyl ethers is highly dependent on the steric volume and electronic properties of the Si substituents.[106] For instance, while TBS is a widely used silyl protective group owing to its relative good stability to acid and base, TMS ethers are often used as a transient protection strategy in synthetic schemes as they are easily hydrolyzed even in the presence of weak acids.[114] Due to this wide range of reactivity, new silylating agents and methods are constantly being developed to enable a more precise manipulation of the functional groups during complex chemical schemes.[114] The silyl ether protection strategy has been successfully employed to incorporate catechol groups into functional materials. For instance, Hawker, Waite and colleagues demonstrated a simple synthetic strategy using silyl protection for introducing catecholic moieties into polysiloxane derivatives for fabrication into 3D microstructures as well as 2D patterned surfaces.[118] Bioinspired high performance structural and pressure-sensitive adhesives, as well as toughened elastomers have also been recently synthesized utilizing silyl ether protecting groups as strategy for masking catechols during synthesis and preparation.[119, 120]

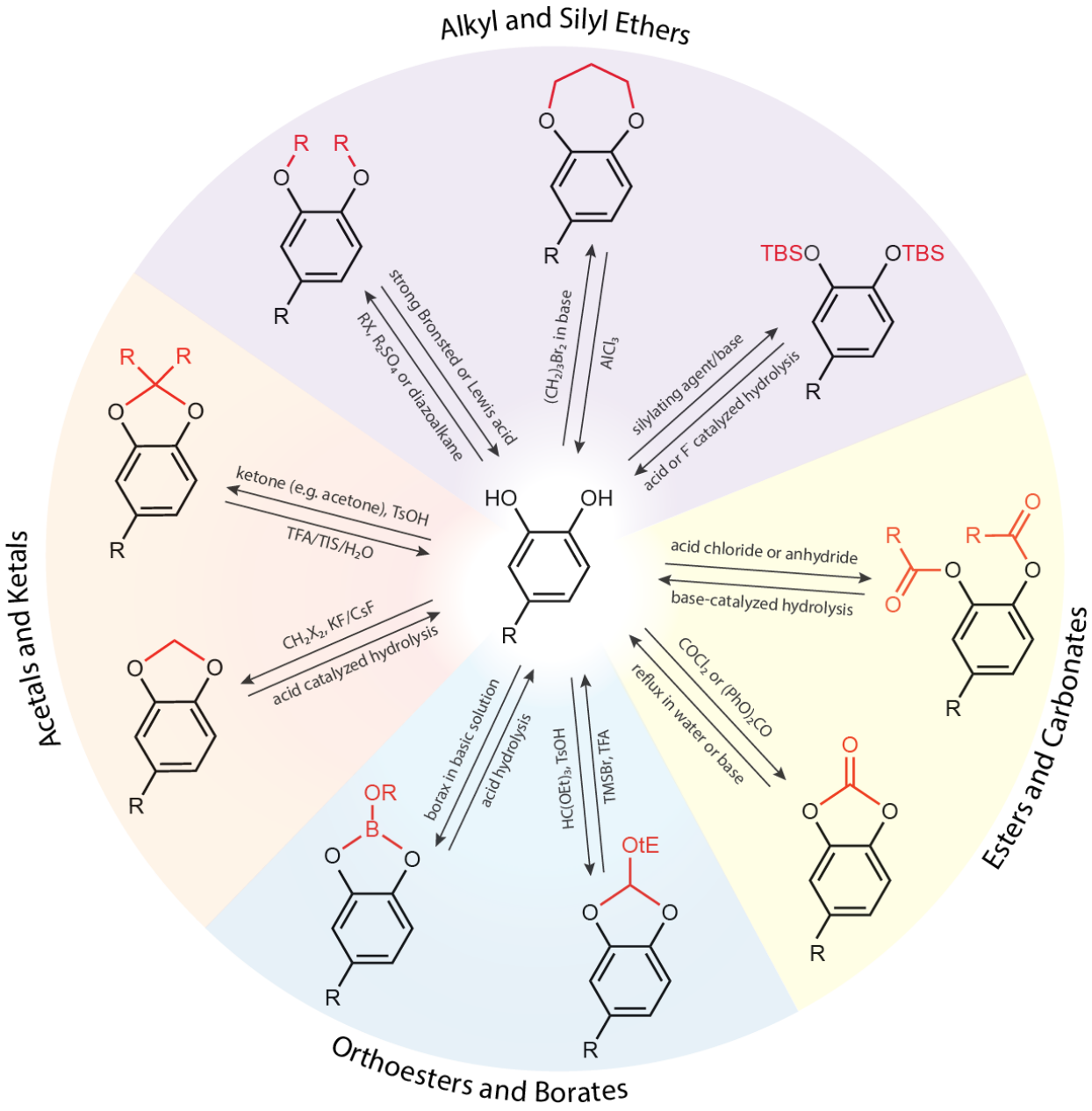

Figure 1.5: Overall view of the main protection strategies for catechols and polyphenols.

Ester and Carbonate Protective Groups

In addition to what was discussed above on the use of alkyl and silyl ether blocking groups for phenolic hydroxyls, polyphenols and catecholic molecules can alternatively be protected

through formation of aryl esters or carbonates.[107] Acylated polyphenols and catechols can be prepared from the reaction of the phenolic hydroxyls with an acid chloride or anhydride in the presence of a base.[106, 107] For instance, aryl acetates can be prepared through reaction of phenols and acetic anhydride in isopropyl alcohol (IPA) at slightly basic conditions.[106] Aryl esters are generally less stable compared to esters of alcohols and can be readily cleaved through room temperature saponification in the presence of even mild bases such as sodium bicarbonate in methanol.[107, 121] As a result, the ester blocking strategy method is often used for protection of catecholic derivatives with functional groups that are sensitive to strong acids or reducing agents.[107] Moreover, although the lability towards based catalyzed cleavage can limit the range of subsequent reaction conditions, this method provides with the opportunity to selectively remove phenolic esters while preserving the other ester linkages in the molecule. Polyphenols and catechol derivatives may also be blocked using cyclic carbonate ester protective groups.[106] Although a few derivatives have shown to be effective in blocking the catecholic hydroxyls, carbonate esters have not been frequently used protecting group strategy, most likely due to their relative inaccessibility and lability.[106]

Borate and Ortho Ester Protective Groups

Boric acid derivatives can be used to protect catechol group in basic environment through formation of a cyclic borate ester.[122–125] The protection is usually performed in the presence of borax buffer at slightly basic pH to form a borate ester or with addition of phenylboronic acid to form a cyclic phenylboronate ester.[122] The borate protection group can be readily removed via hydrolysis by dilute acid (typically HCl at pH of 1-2) since the equilibrium is highly influenced by the pH.[122, 123, 126] At any given pH, stability of the borate-catechol esters is highly dependent on the pK_a of both boric acid derivative and the catecholic molecules.[127] As a result, the formation of borate-catechol complexes is usually facilitated in a typical pH range of 8 to 10, though chemical modifications of boric acid or catecholic molecules (e.g. presence of electron withdrawing groups such as NO_2) is shown to decrease the pK_a and therefore drive the formation of esters at lower pH values.[127–129] The unique pH sensitivity of the catechol protection through boronate ester formation has been successfully utilized to control the adhesive properties of catechol-containing smart adhesives.[130] In addition to borates, ortho esters have also been used as protecting groups for catechols and catechol-derived molecules.[131] Ortho esters are generally stable in neutral or basic conditions but are labile to acid hydrolysis. As a result, ortho esters have found applications for masking catecholic hydroxyls in peptide synthesis due to their compatibility with a variety of base-labile protective groups.[131, 132] For instance, methyl chloroformate and cyclic ethyl orthoformate (Ceof) have been successfully used in the past for protection of catecholic hydroxyl groups and been applied in the solid-phase peptide synthesis of mussel-mimetic DOPA-containing peptides.[132]

Acetal and Ketal Protective Groups

Both hydroxyl groups of catechols can be protected simultaneously through reaction with aldehydes or ketones to form cyclic diethers known as acetals or ketals.[116, 133, 134] This strategy can be especially useful for selectively protecting the vicinal hydroxyl groups in the presence of isolated phenol groups. Moreover, acetals and ketals are generally stable in basic conditions, providing some degree of freedom in performing chemical reactions at other functional sites of catechol-containing molecules without interfering with the catechol protecting groups.[106] However, these groups can be removed through acid catalyzed hydrolysis in a similar fashion to what described previously for the ether protection strategy. The deprotection typically involves protonation of the phenolic oxygen and breakage of the dioxole ring.[106] Consequently, substituents on the C-O ether bonds can significantly affect the stability of the intermediates and eventually rate of the hydrolysis reaction. For instance, methylene acetals can be used for masking catechols and are commonly formed through high temperature condensation reaction of catechols with CH_2X_2 (X=Cl, Br, or I) in the presence of KF/CsF in DMF.[106] Due to the unique chemical structure and minimum steric hindrance on the ring, methylene acetals demonstrate ultra-high stability towards many deprotection reagents and requires harsh acidic conditions such as 4M HCl/AcOH at $\sim$130°C for removal.[135] By substituting hydrogen atoms for alkyl chains or aryl groups, the stability of the intermediate decreases, and as a result, the acetal or ketal protecting groups can be removed at more moderate reaction conditions. For example, acetonide is one of the most commonly used methods for masking of catechols due to its ease of installation and removal.[106, 116] The acetonide groups can be installed on catecholic molecules through reaction with 2,2-dimethoxypropane (DMP) and toluenesulfonic acid (TsOH) in DMF or benzene, or alternatively via reaction of catechol with Acetone and TsOH in IPA.[133, 134, 136] However, to prevent side reactions, amine group of catecholamine molecules should be first protected as phthalimide, trifluoroacetamide, or Fmoc derivative.[132] The acetonide group can be removed using a mixture of TFA/H_2O/TIS or TFA/TIS/H_2O/DMSO.[134, 136–138] This strategy has been used frequently to block the reactivity of catecholic hydroxyls during synthesis of functional materials. For example, very recently acetonide protective groups were used in the synthesis of a hybrid monomer architecture with catechol and amine moieties coexisting adjacent to each other that were subsequently copolymerized to develop high performance pressure-sensitive adhesives.[139] Acetonide protection has also been elegantly used by Dichtel and colleagues to develop covalent organic frameworks (COFs) through formation of crystalline boronate ester-linked COFs via reaction between protected polyfunctional catechols and arylboronic acids.[140]

References

[1] U. G. Wegst et al. "Bioinspired structural materials". In: *Nat Mater* 14.1 (2015), pp. 23–36. ISSN: 1476-1122 (Print) 1476-1122 (Linking) (cit. on p. 1).

[2] G. M. Whitesides. "Bioinspiration: something for everyone". In: *Interface Focus* 5.4 (2015). ISSN: 2042-8898 (cit. on p. 1).

[3] R. R. Naik and S. Singamaneni. "Introduction: Bioinspired and Biomimetic Materials". In: *Chemical Reviews* 117.20 (2017), pp. 12581–12583. ISSN: 0009-2665 (cit. on p. 1).

[4] J. H. Waite and M. L. Tanzer. "Polyphenolic Substance of Mytilus-Edulis - Novel Adhesive Containing L-Dopa and Hydroxyproline". In: *Science* 212.4498 (1981), pp. 1038–1040. ISSN: 0036-8075 (cit. on pp. 1, 4).

[5] B. P. Lee et al. "Mussel-Inspired Adhesives and Coatings". In: *Annual Review of Materials Research, Vol 41* 41 (2011), pp. 99–132. ISSN: 1531-7331 (cit. on pp. 1, 4, 10).

[6] D. W. R. Balkenende, S. M. Winkler, and P. B. Messersmith. "Marine-inspired polymers in medical adhesion". In: *European Polymer Journal* 116 (2019), pp. 134–143. ISSN: 0014-3057 (cit. on p. 1).

[7] Q. Guo et al. "Recent progress in synthesis and application of mussel-inspired adhesives". In: *Nanoscale* 12.3 (2020), pp. 1307–1324. ISSN: 2040-3364 (cit. on p. 2).

[8] B. K. Ahn. "Perspectives on Mussel-Inspired Wet Adhesion". In: *Journal of the American Chemical Society* 139.30 (2017), pp. 10166–10171. ISSN: 0002-7863 (cit. on p. 2).

[9] J. H. Waite. "Mussel adhesion - essential footwork". In: *J Exp Biol* 220.Pt 4 (2017), pp. 517–530. ISSN: 1477-9145 (Electronic) 0022-0949 (Linking) (cit. on pp. 2, 4).

[10] Helene Z Hill. "Melanins in the photobiology of skin cancer and the radiobiology of melanomas". In: *Cancer biology and biosynthesis. Telford Press, Caldwell, NJ* (1991), pp. 31–53 (cit. on p. 2).

[11] Gabriella Fiore et al. "Dopamine in the ink defence system of Sepia officinalis: biosynthesis, vesicular compartmentation in mature ink gland cells, nitric oxide (NO)/cGMP-induced depletion and fate in secreted ink". In: *Biochemical Journal* 378.3 (2004), pp. 785–791. ISSN: 0264-6021 (cit. on p. 2).

[12] Joshua D Nosanchuk and Arturo Casadevall. "The contribution of melanin to microbial pathogenesis". In: *Cellular microbiology* 5.4 (2003), pp. 203–223. ISSN: 1462-5814 (cit. on p. 2).

[13] AJ Nappi and BM Christensen. "Melanogenesis and associated cytotoxic reactions: applications to insect innate immunity". In: *Insect biochemistry and molecular biology* 35.5 (2005), pp. 443–459. ISSN: 0965-1748 (cit. on p. 2).

[14] Marco d'Ischia et al. "Melanin biopolymers: Tailoring chemical complexity for materials design". In: *Angewandte Chemie International Edition* 59.28 (2020), pp. 11196–11205. ISSN: 1433-7851 (cit. on p. 2).

[15] Edwin Haslam. *Practical polyphenolics : from structure to molecular recognition and physiological action*. Cambridge, UK ; New York, NY, USA: Cambridge University Press, 1998, xv, 422 p. ISBN: 0521465133 (hb) (cit. on p. 2).

[16] S. Quideau et al. "Plant Polyphenols: Chemical Properties, Biological Activities, and Synthesis". In: *Angewandte Chemie-International Edition* 50.3 (2011), pp. 586–621. ISSN: 1433-7851 (cit. on pp. 2, 4–6).

[17] T. M. Robson et al. "A perspective on ecologically relevant plant-UV research and its practical application". In: *Photochem Photobiol Sci* 18.5 (2019), pp. 970–988. ISSN: 1474-9092 (Electronic) 1474-905X (Linking) (cit. on p. 2).

[18] J. Sedo et al. "Catechol-Based Biomimetic Functional Materials". In: *Advanced Materials* 25.5 (2013), pp. 653–701. ISSN: 0935-9648 (cit. on pp. 2, 4).

[19] Q. Ye, F. Zhou, and W. M. Liu. "Bioinspired catecholic chemistry for surface modification". In: *Chemical Society Reviews* 40.7 (2011), pp. 4244–4258. ISSN: 0306-0012 (cit. on pp. 2, 4).

[20] M. d'Ischia. "Melanin-Based Functional Materials". In: *International Journal of Molecular Sciences* 19.1 (2018). ISSN: 1422-0067 (cit. on p. 2).

[21] M. A. Rahim et al. "Phenolic Building Blocks for the Assembly of Functional Materials". In: *Angewandte Chemie-International Edition* 58.7 (2019), pp. 1904–1927. ISSN: 1433-7851 (cit. on pp. 2, 4, 5, 9).

[22] R. Pinnaratip et al. "Multifunctional Biomedical Adhesives". In: *Adv Healthc Mater* 8.11 (2019), e1801568. ISSN: 2192-2659 (Electronic) 2192-2640 (Linking) (cit. on p. 2).

[23] Mikyung Shin, Eunsook Park, and Haeshin Lee. "Plant-Inspired Pyrogallol-Containing Functional Materials". In: *Advanced Functional Materials* 78 (2019), pp. 1903022–26 (cit. on pp. 2, 5).

[24] Jr. Erdman John W. et al. "Flavonoids and heart health: Proceedings of the ILSI North America Flavonoids Workshop, May 31-June 1, 2005, Washington, DC". In: *Journal of Nutrition* 137.3 (2007), 718S–737S (cit. on p. 2).

[25] T. S. Sileika et al. "Colorless Multifunctional Coatings Inspired by Polyphenols Found in Tea, Chocolate, and Wine". In: *Angewandte Chemie-International Edition* 52.41 (2013), pp. 10766–10770. ISSN: 1433-7851 (cit. on pp. 2, 4, 6).

[26] Vincent Ball. "Polydopamine Nanomaterials: Recent Advances in Synthesis Methods and Applications". In: *Frontiers in Bioengineering and Biotechnology* 6 (2018), pp. 17–12 (cit. on p. 2).

[27] Ik Soo Kwon and Christopher J. Bettinger. "Polydopamine nanostructures as biomaterials for medical applications". In: *Journal of Materials Chemistry B* 6.43 (2018), pp. 6895–6903 (cit. on p. 2).

[28] Rahila Batul et al. "Recent progress in the biomedical applications of polydopamine nanostructures". In: *Biomaterials Science* 5.7 (2017), pp. 1204–1229 (cit. on p. 2).

[29] J. H. Ryu, P. B. Messersmith, and H. Lee. "Polydopamine Surface Chemistry: A Decade of Discovery". In: *Acs Applied Materials Interfaces* 10.9 (2018), pp. 7523–7540. ISSN: 1944-8244 (cit. on pp. 2, 6, 8).

[30] M. d'Ischia et al. "Polydopamine and Eumelanin: From Structure-Property Relationships to a Unified Tailoring Strategy". In: *Accounts of Chemical Research* 47.12 (2014), pp. 3541–3550. ISSN: 0001-4842 (cit. on pp. 2, 6, 8).

[31] S. Hong et al. "Poly(norepinephrine): Ultrasmooth Material-Independent Surface Chemistry and Nanodepot for Nitric Oxide". In: *Angewandte Chemie-International Edition* 52.35 (2013), pp. 9187–9191. ISSN: 1433-7851 (cit. on pp. 2, 6, 9).

[32] S. M. Kang et al. "Norepinephrine: Material-Independent, Multifunctional Surface Modification Reagent". In: *Journal of the American Chemical Society* 131.37 (2009), pp. 13224–13225. ISSN: 0002-7863 (cit. on pp. 2, 6, 9).

[33] J. Yang, M. A. C. Stuart, and M. Kamperman. "Jack of all trades: versatile catechol crosslinking mechanisms". In: *Chemical Society Reviews* 43.24 (2014), pp. 8271–8298. ISSN: 0306-0012 (cit. on pp. 4, 6, 9–12).

[34] E. Carrington et al. "Mussels as a Model System for Integrative Ecomechanics". In: *Annual Review of Marine Science, Vol 7* 7 (2015), pp. 443–469. ISSN: 1941-1405 (cit. on pp. 4, 10).

[35] Devin G. Barrett, Tadas S. Sileika, and Phillip B. Messersmith. "Molecular diversity in phenolic and polyphenolic precursors of tannin-inspired nanocoatings". In: *Chemical Communications* 50.55 (2014), pp. 7265–7268. ISSN: 1359-7345;1364-548X (cit. on p. 4).

[36] J. S. Lee et al. "Plant Flavonoid-Mediated Multifunctional Surface Modification Chemistry: Catechin Coating for Enhanced Osteogenesis of Human Stem Cells". In: *Chemistry of Materials* 29.10 (2017), pp. 4375–4384. ISSN: 0897-4756 (cit. on pp. 4, 6).

[37] K. Yamada, T. Abe, and Y. Tanizawa. "Black tea stain formed on the surface of teacups and pots. Part 2 - Study of the structure change caused by aging and calcium addition". In: *Food Chemistry* 103.1 (2007), pp. 8–14. ISSN: 0308-8146 (cit. on p. 4).

[38] Y. Tanizawa, T. Abe, and K. Yamada. "Black tea stain formed on the surface of teacups and pots. Part 1 - Study on the chemical composition and structure". In: *Food Chemistry* 103.1 (2007), pp. 1–7. ISSN: 0308-8146 (cit. on p. 4).

[39] F. Behboodi-Sadabad et al. "Bioinspired Strategy for Controlled Polymerization and Photopatterning of Plant Polyphenols". In: *Chemistry of Materials* 30.6 (2018), pp. 1937–1946. ISSN: 0897-4756 (cit. on pp. 4, 5).

[40] Hui-Ling Ma et al. "Laccase-catalyzed oxidation of phenolic compounds in organic media". In: *Journal of Molecular Catalysis B-Enzymatic* 57.1-4 (2009), pp. 89–95 (cit. on p. 4).

[41] Jong-Rok Jeon, Jae-Hwan Kim, and Yoon-Seok Chang. "Enzymatic polymerization of plant-derived phenols for material-independent and multifunctional coating". In: *Journal of Materials Chemistry B* 1.47 (2013), pp. 6501–6509 (cit. on pp. 4, 5).

[42] José M. Herrero-Martínez et al. "Determination of dissociation constants of flavonoids by capillary electrophoresis". In: *Electrophoresis* 26.10 (2005), pp. 1886–1895 (cit. on p. 4).

[43] Greg P. Maier, Christopher M. Bernt, and Alison Butler. "Catechol oxidation: considerations in the design of wet adhesive materials". In: *Biomaterials Science* 6.2 (2018), pp. 332–339 (cit. on p. 4).

[44] K. G. Malollari et al. "Mechanical Enhancement of Bioinspired Polydopamine Nanocoatings". In: *Acs Applied Materials Interfaces* 11.46 (2019), pp. 43599–43607. ISSN: 1944-8244 (cit. on p. 4).

[45] P. Delparastan et al. "Direct Evidence for the Polymeric Nature of Polydopamine". In: *Angewandte Chemie-International Edition* 58.4 (2019), pp. 1077–1082. ISSN: 1433-7851 (cit. on pp. 4, 8).

[46] K. Lee et al. "Laser-induced graphitization of polydopamine leads to enhanced mechanical performance while preserving multifunctionality". In: *Nature Communications* 11.1 (2020). ISSN: 2041-1723 (cit. on p. 4).

[47] F. Behboodi-Sadabad et al. "UV-Triggered Polymerization, Deposition, and Patterning of Plant Phenolic Compounds". In: *Advanced Functional Materials* 27.22 (2017). ISSN: 1616-301x (cit. on p. 5).

[48] Noriyasu Niimura and Tetsuo Miyakoshi. "Characterization of Natural Resin Films and Identification of Ancient Coating". In: *Journal of the Mass Spectrometry Society of Japan* 51.4 (2003), pp. 439–457 (cit. on p. 5).

[49] Rong Lu, Takashi Yoshida, and Tetsuo Miyakoshi. "Oriental Lacquer: A Natural Polymer". In: *Polymer Reviews* 53.2 (2013), pp. 153–191. ISSN: 1558-3724 (cit. on p. 5).

[50] M. Wu et al. "Natural lacquer was used as a coating and an adhesive 8000 years ago, by early humans at Kuahuqiao, determined by ELISA". In: *Journal of Archaeological Science* 100 (2018), pp. 80–87. ISSN: 0305-4403 (cit. on p. 5).

[51] Jan Bartus et al. "Oriental Lacquer III. Composition of the Urushiol Fraction of the Sap of Rhus verniciflua". In: *Polymer Journal* 26.1 (1994), pp. 67–78 (cit. on p. 5).

[52] J. Kumanotani. "Urushi (oriental lacquer) - A natural aesthetic durable and future-promising coating". In: *Progress in Organic Coatings* 26.2-4 (1995), pp. 163–195 (cit. on p. 5).

[53] Rong Lu et al. "Development of a fast drying hybrid lacquer in a low-relative-humidity environment based onkurome lacquer sap". In: *Journal of Applied Polymer Science* 98.3 (2005), pp. 1055–1061 (cit. on p. 5).

[54] Hirohmi Watanabe, Aya Fujimoto, and Atsushi Takahara. "Characterization of catechol-containing natural thermosetting polymer "urushiol" thin film". In: *Journal of Polymer Science Part A: Polymer Chemistry* 51.17 (2013), pp. 3688–3692 (cit. on p. 5).

[55] Jianrong Xia et al. "On the UV-Induced Polymeric Behavior of Chinese Lacquer". In: *ACS Applied Materials Interfaces* 3.2 (2011), pp. 482–489. ISSN: 1944-8244 (cit. on p. 5).

[56] D. H. Scharf, T. Heinekamp, and A. A. Brakhage. "Human and Plant Fungal Pathogens: The Role of Secondary Metabolites". In: *Plos Pathogens* 10.1 (2014). ISSN: 1553-7374 (cit. on p. 5).

[57] M. d'Ischia et al. "Melanins and melanogenesis: from pigment cells to human health and technological applications". In: *Pigment Cell Melanoma Research* 28.5 (2015), pp. 520–544. ISSN: 1755-1471 (cit. on pp. 5–8).

[58] Jürgen Liebscher. "Chemistry of Polydopamine – Scope, Variation, and Limitation". In: *European Journal of Organic Chemistry* 2019.31-32 (2019), pp. 4976–4994. ISSN: 1434-193X (cit. on pp. 6, 8).

[59] Y. L. Liu, K. L. Ai, and L. H. Lu. "Polydopamine and Its Derivative Materials: Synthesis and Promising Applications in Energy, Environmental, and Biomedical Fields". In: *Chemical Reviews* 114.9 (2014), pp. 5057–5115. ISSN: 0009-2665 (cit. on pp. 6, 8).

[60] Andrzej Slominski et al. "Melanin Pigmentation in Mammalian Skin and Its Hormonal Regulation". In: *Physiological Reviews* 84.4 (2004), pp. 1155–1228 (cit. on pp. 6, 8).

[61] H. Lee et al. "Mussel-inspired surface chemistry for multifunctional coatings". In: *Science* 318.5849 (2007), pp. 426–430. ISSN: 0036-8075 (cit. on pp. 6, 8).

[62] J. Saiz-Poseu et al. "The Chemistry behind Catechol-Based Adhesion". In: *Angewandte Chemie-International Edition* 58.3 (2019), pp. 696–714. ISSN: 1433-7851 (cit. on pp. 6, 10, 11).

[63] Q. H. Lyu, N. Hsueh, and C. L. L. Chai. "The Chemistry of Bioinspired Catechol(amine)-Based Coatings". In: *Acs Biomaterials Science Engineering* 5.6 (2019), pp. 2708–2724. ISSN: 2373-9878 (cit. on pp. 6, 10).

[64] Radosław Mrówczyński, Roksana Markiewicz, and Jürgen Liebscher. "Chemistry of polydopamine analogues". In: *Polymer International* 65.11 (2016), pp. 1288–1299 (cit. on p. 6).

[65] Qinghua Lyu, Nathanael Hsueh, and Christina L. L. Chai. "The Chemistry of Bioinspired Catechol(amine)-Based Coatings". In: *ACS Biomaterials Science Engineering* 5.6 (2019), pp. 2708–2724 (cit. on p. 6).

[66] Marco d'Ischia et al. "Polydopamine and Eumelanin: From Structure–Property Relationships to a Unified Tailoring Strategy". In: *Accounts of Chemical Research* 47.12 (2014), pp. 3541–3550 (cit. on p. 6).

[67] S. O. Andersen. "Insect cuticular sclerotization: A review". In: *Insect Biochemistry and Molecular Biology* 40.3 (2010), pp. 166–178. ISSN: 0965-1748 (cit. on p. 6).

[68] K. Lee et al. "Role of Dopamine Chemistry in the Formation of Mechanically Strong Mandibles of Grasshoppers". In: *Chemistry of Materials* 27.19 (2015), pp. 6478–6481. ISSN: 0897-4756 (cit. on p. 6).

[69] M. Arzillo et al. "Eumelanin buildup on the nanoscale: aggregate growth/assembly and visible absorption development in biomimetic 5,6-dihydroxyindole polymerization". In: *Biomacromolecules* 13.8 (2012), pp. 2379–90. ISSN: 1526-4602 (Electronic) 1525-7797 (Linking) (cit. on p. 8).

[70] M. d'Ischia, A. Napolitano, and A. Pezzella. "5,6-Dihydroxyindole Chemistry: Unexplored Opportunities Beyond Eumelanin". In: *European Journal of Organic Chemistry* 2011.28 (2011), pp. 5501–5516. ISSN: 1434-193x (cit. on p. 8).

[71] M. d'Ischia et al. "Chemical and Structural Diversity in Eumelanins: Unexplored Bio-Optoelectronic Materials". In: *Angewandte Chemie-International Edition* 48.22 (2009), pp. 3914–3921. ISSN: 1433-7851 (cit. on p. 8).

[72] S. Meng and E. Kaxiras. "Theoretical models of eumelanin protomolecules and their optical properties". In: *Biophys J* 94.6 (2008), pp. 2095–105. ISSN: 1542-0086 (Electronic) 0006-3495 (Linking) (cit. on p. 8).

[73] C. M. R. Clancy and J. D. Simon. "Ultrastructural organization of eumelanin from Sepia officinalis measured by atomic force microscopy". In: *Biochemistry* 40.44 (2001), pp. 13353–13360. ISSN: 0006-2960 (cit. on p. 8).

[74] A. A. R. Watt, J. P. Bothma, and P. Meredith. "The supramolecular structure of melanin". In: *Soft Matter* 5.19 (2009), pp. 3754–3760. ISSN: 1744-683x (cit. on p. 8).

[75] N. F. Della Vecchia et al. "Building-Block Diversity in Polydopamine Underpins a Multifunctional Eumelanin-Type Platform Tunable Through a Quinone Control Point". In: *Advanced Functional Materials* 23.10 (2013), pp. 1331–1340. ISSN: 1616-301x (cit. on p. 8).

[76] A. Bungeler, B. Hamisch, and O. I. Strube. "The Supramolecular Buildup of Eumelanin: Structures, Mechanisms, Controllability". In: *Int J Mol Sci* 18.9 (2017). ISSN: 1422-0067 (Electronic) 1422-0067 (Linking) (cit. on p. 8).

[77] Y. Liu and J. D. Simon. "Metal-ion interactions and the structural organization of Sepia eumelanin". In: *Pigment Cell Res* 18.1 (2005), pp. 42–8. ISSN: 0893-5785 (Print) 0893-5785 (Linking) (cit. on p. 8).

[78] T. G. Barclay et al. "Versatile Surface Modification Using Polydopamine and Related Polycatecholamines: Chemistry, Structure, and Applications". In: *Advanced Materials Interfaces* 4.19 (2017). ISSN: 2196-7350 (cit. on p. 8).

[79] A. Corani et al. "Superior Photoprotective Motifs and Mechanisms in Eumelanins Uncovered". In: *Journal of the American Chemical Society* 136.33 (2014), pp. 11626–11635. ISSN: 0002-7863 (cit. on p. 8).

[80] J. H. Waite. "Surface chemistry - Mussel power". In: *Nature Materials* 7.1 (2008), pp. 8–9. ISSN: 1476-1122 (cit. on p. 8).

[81] W. Cheng et al. "Versatile Polydopamine Platforms: Synthesis and Promising Applications for Surface Modification and Advanced Nanomedicine". In: *ACS Nano* 13.8 (2019), pp. 8537–8565. ISSN: 1936-086X (Electronic) 1936-0851 (Linking) (cit. on p. 8).

[82] H. M. Ma et al. "Formation of Homogeneous Epinephrine-Melanin Solutions to Fabricate Electrodes for Enhanced Photoelectrochemical Biosensing". In: *Langmuir* 34.26 (2018), pp. 7744–7750. ISSN: 0743-7463 (cit. on p. 9).

[83] Seonki Hong et al. "Non-Covalent Self-Assembly and Covalent Polymerization Co-Contribute to Polydopamine Formation". In: *Advanced Functional Materials* 22.22 (2012), pp. 4711–4717 (cit. on p. 9).

[84] P. K. Forooshani and B. P. Lee. "Recent approaches in designing bioadhesive materials inspired by mussel adhesive protein". In: *Journal of Polymer Science Part a-Polymer Chemistry* 55.1 (2017), pp. 9–33. ISSN: 0887-624x (cit. on p. 10).

[85] E. Faure et al. "Catechols as versatile platforms in polymer chemistry". In: *Progress in Polymer Science* 38.1 (2013), pp. 236–270. ISSN: 0079-6700 (cit. on p. 10).

[86] Y. R. Li et al. "Molecular design principles of Lysine-DOPA wet adhesion". In: *Nature Communications* 11.1 (2020). ISSN: 2041-1723 (cit. on p. 11).

[87] H. Lee, N. F. Scherer, and P. B. Messersmith. "Single-molecule mechanics of mussel adhesion". In: *Proceedings of the National Academy of Sciences of the United States of America* 103.35 (2006), pp. 12999–13003. ISSN: 0027-8424 (cit. on p. 11).

[88] H. Lee, J. Rho, and P. B. Messersmith. "Facile Conjugation of Biomolecules onto Surfaces via Mussel Adhesive Protein Inspired Coatings". In: *Advanced Materials* 21.4 (2009), pp. 431–+. ISSN: 0935-9648 (cit. on p. 11).

[89] C. Lim et al. "Nanomechanics of Poly(catecholamine) Coatings in Aqueous Solutions". In: *Angewandte Chemie-International Edition* 55.10 (2016), pp. 3342–3346. ISSN: 1433-7851 (cit. on p. 11).

[90] G. P. Maier et al. "Adaptive synergy between catechol and lysine promotes wet adhesion by surface salt displacement". In: *Science* 349.6248 (2015), pp. 628–632. ISSN: 0036-8075 (cit. on p. 11).

[91] L. A. Burzio and J. H. Waite. "Cross-linking in adhesive quinoproteins: Studies with model decapeptides". In: *Biochemistry* 39.36 (2000), pp. 11147–11153. ISSN: 0006-2960 (cit. on p. 11).

[92] J. H. Waite. "The Phylogeny and Chemical Diversity of Quinone-Tanned Glues and Varnishes". In: *Comparative Biochemistry and Physiology B-Biochemistry Molecular Biology* 97.1 (1990), pp. 19–29. ISSN: 0305-0491 (cit. on p. 11).

[93] A. Andersen, Y. Q. Chen, and H. Birkedal. "Bioinspired Metal-Polyphenol Materials: Self-Healing and Beyond". In: *Biomimetics* 4.2 (2019). ISSN: 2313-7673 (cit. on p. 11).

[94] D. E. Fullenkamp et al. "pH-dependent cross-linking of catechols through oxidation via Fe3+ and potential implications for mussel adhesion". In: *Rsc Advances* 4.48 (2014), pp. 25127–25134. ISSN: 2046-2069 (cit. on p. 11).

[95] Z. P. Xu. "Mechanics of metal-catecholate complexes: The roles of coordination state and metal types". In: *Scientific Reports* 3 (2013). ISSN: 2045-2322 (cit. on p. 12).

[96] C. N. Z. Schmitt et al. "Mechanical homeostasis of a DOPA-enriched biological coating from mussels in response to metal variation". In: *Journal of the Royal Society Interface* 12.110 (2015). ISSN: 1742-5689 (cit. on p. 12).

[97] E. Khare, N. Holten-Andersen, and M. J. Buehler. "Transition-metal coordinate bonds for bioinspired macromolecules with tunable mechanical properties". In: *Nature Reviews Materials* (2021). ISSN: 2058-8437 (cit. on p. 12).

[98] S. Hong et al. "Progressive fuzzy cation-pi assembly of biological catecholamines". In: *Sci Adv* 4.9 (2018), eaat7457. ISSN: 2375-2548 (Electronic) 2375-2548 (Linking) (cit. on p. 12).

[99] M. A. Gebbie et al. "Tuning underwater adhesion with cation-pi interactions". In: *Nat Chem* 9.5 (2017), pp. 473–479. ISSN: 1755-4349 (Electronic) 1755-4330 (Linking) (cit. on p. 12).

[100] M. V. Rapp et al. "Defining the Catechol-Cation Synergy for Enhanced Wet Adhesion to Mineral Surfaces". In: *Journal of the American Chemical Society* 138.29 (2016), pp. 9013–9016. ISSN: 0002-7863 (cit. on p. 12).

[101] W. L. A. Brooks, C. C. Deng, and B. S. Sumerlin. "Structure-Reactivity Relationships in Boronic Acid-Diol Complexation". In: *Acs Omega* 3.12 (2018), pp. 17863–17870. ISSN: 2470-1343 (cit. on p. 12).

[102] B. Marco-Dufort and M. W. Tibbitt. "Design of moldable hydrogels for biomedical applications using dynamic covalent boronic esters". In: *Materials Today Chemistry* 12 (2019), pp. 16–33. ISSN: 2468-5194 (cit. on p. 12).

[103] Jennifer N. Cambre and Brent S. Sumerlin. "Biomedical applications of boronic acid polymers". In: *Polymer* 52.21 (2011), pp. 4631–4643 (cit. on p. 12).

[104] Ying Guan and Yongjun Zhang. "Boronic acid-containing hydrogels: synthesis and their applications". In: *Chemical Society Reviews* 42.20 (2013), pp. 8106–8121 (cit. on p. 12).

[105] G. Lang et al. "Mechanical Testing of Engineered Spider Silk Filaments Provides Insights into Molecular Features on a Mesoscale". In: *Acs Applied Materials Interfaces* 9.1 (2017), pp. 892–900. ISSN: 1944-8244 (cit. on p. 12).

[106] Peter G. M. Wuts and Theodora W. Greene. *Greene's protective groups in organic synthesis*. 5th. Hoboken, New Jersey: John Wiley Sons, 2014. ISBN: 9781118905128 (cit. on pp. 12–14, 16, 17).

[107] E. Haslam. "Protection of Phenols and Catechols". In: *Protective Groups in Organic Chemistry*. Ed. by J. F. W. McOmie. Boston, MA: Springer US, 1973, pp. 145–182. ISBN: 978-1-4684-7218-9 (cit. on pp. 12, 13, 16).

[108] A. Ishida et al. "Synthesis of 3,4-Dihydroisoquinolines and 1,2,3,4-Tetrahydroisoquinolines". In: *Chemical Pharmaceutical Bulletin* 34.5 (1986), pp. 1994–2006. ISSN: 0009-2363 (cit. on p. 13).

[109] H. Yamamoto and T. Hayakawa. "Synthesis and Conformational Studies of Polymers and Copolymers of O,O'-Dimethyl-L-Beta-3,4-Dihydroxyphenyl-Alpha-Alanine with Gamma-Benzyl-L-Glutamate". In: *Polymer* 19.8 (1978), pp. 963–968. ISSN: 0032-3861 (cit. on p. 13).

[110] D. Y. Sang et al. "Cleavage of Catechol Monoalkyl Ethers by Aluminum Triiodide-Dimethyl Sulfoxide". In: *Synthesis-Stuttgart* 51.3 (2019), pp. 704–712. ISSN: 0039-7881 (cit. on pp. 13, 14).

[111] K. Zhan et al. "Tunicate-Inspired Gallol Polymers for Underwater Adhesive: A Comparative Study of Catechol and Gallol". In: *Biomacromolecules* 18.9 (2017), pp. 2959–2966. ISSN: 1525-7797 (cit. on p. 13).

[112] L. Fischer et al. "Sequence-defined positioning of amine and amide residues to control catechol driven wet adhesion". In: *Chemical Science* 11.36 (2020), pp. 9919–9924. ISSN: 2041-6520 (cit. on p. 14).

[113] W. B. Huang et al. "An Efficient Strategy for Protecting Dihydroxyl Groups of Catechols". In: *Synlett* 24.6 (2013), pp. 741–746. ISSN: 0936-5214 (cit. on p. 14).

[114] R. D. Crouch. "Recent Advances in Silyl Protection of Alcohols". In: *Synthetic Communications* 43.17 (2013), pp. 2265–2279. ISSN: 0039-7911 (cit. on p. 14).

[115] B. P. Lee et al. "Synthesis of 3,4-dihydroxyphenylalanine (DOPA) containing monomers and their co-polymerization with PEG-diacrylate to form hydrogels". In: *Journal of Biomaterials Science-Polymer Edition* 15.4 (2004), pp. 449–464. ISSN: 0920-5063 (cit. on p. 14).

[116] M. J. Sever and J. J. Wilker. "Synthesis of peptides containing DOPA (3,4-dihydroxyphenylalanine)" In: *Tetrahedron* 57.29 (2001), pp. 6139–6146. ISSN: 0040-4020 (cit. on pp. 14, 17).

[117] J. L. Dalsin et al. "Protein resistance of titanium oxide surfaces modified by biologically inspired mPEG-DOPA". In: *Langmuir* 21.2 (2005), pp. 640–646. ISSN: 0743-7463 (cit. on p. 14).

[118] J. Heo et al. "Improved Performance of Protected Catecholic Polysiloxanes for Bioinspired Wet Adhesion to Surface Oxides". In: *Journal of the American Chemical Society* 134.49 (2012), pp. 20139–20145. ISSN: 0002-7863 (cit. on p. 14).

[119] E. Filippidi et al. "Toughening elastomers using mussel-inspired iron-catechol complexes". In: *Science* 358.6362 (2017), pp. 502–505. ISSN: 0036-8075 (cit. on p. 14).

[120] C. J. Higginson et al. "Bioinspired Design Provides High-Strength Benzoxazine Structural Adhesives". In: *Angewandte Chemie-International Edition* 58.35 (2019), pp. 12271–12279. ISSN: 1433-7851 (cit. on p. 14).

[121] G. Buchi and S. M. Weinreb. "Total Syntheses of Aflatoxins-M1 and G1 and an Improved Synthesis of Aflatoxin-B1". In: *Journal of the American Chemical Society* 93.3 (1971), 746–. ISSN: 0002-7863 (cit. on p. 16).

[122] K. Yoshino et al. "B-11-Nmr Study of the Complex-Formation of Borate with Catechol and L-Dopa". In: *Bulletin of the Chemical Society of Japan* 52.10 (1979), pp. 3005–3009. ISSN: 0009-2673 (cit. on p. 16).

[123] Christopher C. Deng et al. "Boronic acid-based hydrogels undergo self-healing at neutral and acidic pH". In: *ACS Macro Letters* 4.2 (2015), pp. 220–224 (cit. on p. 16).

[124] Santiago Lascano et al. "The third orthogonal dynamic covalent bond". In: *Chemical Science* 7.7 (2016), pp. 4720–4724 (cit. on p. 16).

[125] R. R. Scheline. "A Rapid Synthesis of 3-O-Methylgallic Acid". In: *Acta Chemica Scandinavica* 20.4 (1966), 1182–. ISSN: 0904-213x (cit. on p. 16).

[126] Stuart J. Rowan et al. "Dynamic covalent chemistry". In: *Angewandte Chemie International Edition* 41.6 (2002), pp. 898–952 (cit. on p. 16).

[127] Jun Yan et al. "The relationship among pKa, pH, and binding constants in the interactions between boronic acids and diols—it is not as simple as it appears". In: *Tetrahedron* 60.49 (2004), pp. 11205–11209. ISSN: 0040-4020 (cit. on p. 16).

[128] Louis P. Hammett. "The effect of structure upon the reactions of organic compounds. Benzene derivatives". In: *Journal of the American Chemical Society* 59.1 (1937), pp. 96–103 (cit. on p. 16).

[129] J. W. Tomsho et al. "Ring Structure and Aromatic Substituent Effects on the pK a of the Benzoxaborole Pharmacophore". In: *ACS Med Chem Lett* 3.1 (2012), pp. 48–52. ISSN: 1948-5875 (Linking) (cit. on p. 16).

[130] A. R. Narkar et al. "pH Responsive and Oxidation Resistant Wet Adhesive based on Reversible Catechol-Boronate Complexation". In: *Chemistry of Materials* 28.15 (2016), pp. 5432–5439. ISSN: 0897-4756 (cit. on p. 16).

[131] F. Vellaccio et al. "Catechol and Substituted Catechol-Derived Ortho Esters, Models for Protected Active Esters in Peptide-Synthesis". In: *Journal of Organic Chemistry* 46.15 (1981), pp. 3087–3091. ISSN: 0022-3263 (cit. on p. 16).

[132] B. H. Hu and P. B. Messersmith. "Protection of 3,4-dihydroxyphenylalanine (DOPA) for Fmoc solid-phase peptide synthesis". In: *Tetrahedron Letters* 41.31 (2000), pp. 5795–5798. ISSN: 0040-4039 (cit. on pp. 16, 17).

[133] Z. Q. Liu, B. H. Hu, and P. B. Messersmith. "Convenient synthesis of acetonide-protected 3,4-dihydroxyphenylalanine (DOPA) for Fmoc solid-phase peptide synthesis". In: *Tetrahedron Letters* 49.38 (2008), pp. 5519–5521. ISSN: 0040-4039 (cit. on p. 17).

[134] V. A. Soloshonok and H. Ueki. "Efficient and practical protection of the catechol residue of 3,4-dihydroxyphenylalanine (DOPA) derivative as acetonide". In: *Synthesis-Stuttgart* 5 (2008), pp. 693–695. ISSN: 0039-7881 (cit. on p. 17).

[135] F. Y. Chen and B. J. Uang. "Enantioselective synthesis of (R)-3-(3,4-dihydroxyphenyl)alanine from tert-butyl glycinate". In: *Journal of Organic Chemistry* 66.10 (2001), pp. 3650–3652. ISSN: 0022-3263 (cit. on p. 17).

[136] K. Fujiwara et al. "Total Synthesis of Thelephantin O, Vialinin A/Terrestrin A, and Terrestrins B-D". In: *Journal of Organic Chemistry* 77.11 (2012), pp. 5161–5166. ISSN: 0022-3263 (cit. on p. 17).

[137] Z. Q. Liu, B. H. Hu, and P. B. Messersmith. "Acetonide protection of dopamine for the synthesis of highly pure N-docosahexaenoyldopamine". In: *Tetrahedron Letters* 51.18 (2010), pp. 2403–2405. ISSN: 0040-4039 (cit. on p. 17).

[138] A. R. Statz et al. "New peptidomimetic polymers for antifouling surfaces". In: *Journal of the American Chemical Society* 127.22 (2005), pp. 7972–7973. ISSN: 0002-7863 (cit. on p. 17).

[139] B. D. B. Tiu et al. "Cooperativity of Catechols and Amines in High-Performance Dry/Wet Adhesives". In: *Angewandte Chemie-International Edition* 59.38 (2020), pp. 16616–16624. ISSN: 1433-7851 (cit. on p. 17).

[140] E. L. Spitler and W. R. Dichtel. "Lewis acid-catalysed formation of two-dimensional phthalocyanine covalent organic frameworks". In: *Nature Chemistry* 2.8 (2010), pp. 672–677. ISSN: 1755-4330 (cit. on p. 17).

Chapter 2

Molecular Design Principles of Mussel Adhesion

* This chapter is adapted based on the research originally appeared as a peer-reviewed article co-first-authored by me published in Nature Communications.
Y. Li†, J. Cheng†, P. Delparastan†, H.Wang†, S. J. Sigg, K. G. DeFrates, Y. Cao, P. B. Messersmith, Molecular design principles of Lysine-DOPA wet adhesion. Nature Communications 11, 3895 (2020)

Abstract

The byssus of marine mussels has been a major source of inspiration for the adhesion community over the last few decades. DOPA (DOPA, Y), via its catechol side chain, has long been considered to be a key adhesive moiety in the byssal interfacial proteins. Recently, adhesive synergy between flanking lysine (Lys, K) and DOPA residues in the mussel adhesive proteins has been highlighted, inspiring a new generation of synthetic amino-catechol adhesives. However, the complex topological relationship of DOPA and Lys as well as the interfacial adhesive roles of other amino acids in mussel adhesive proteins have been understudied. The incomplete picture of mussel adhesion, particularly at the molecular level, hampers efforts to develop mussel-inspired adhesives. Herein, we synthesized a library of Lys and DOPA-containing peptides and studied their adhesion to organic and inorganic substrates using single-molecule force spectroscopy (SMFS) technique. We observed that a modest increase in peptide length, from KY to $(KY)_3$, increased adhesion strength to TiO_2. Surprisingly, further increase in peptide length to $(KY)_{10}$ offered no additional adhesive benefit, with unbinding force of both $(KY)_3$ and $(KY)_{10}$ being similar to that of a 17-mer peptide from mussel foot protein-5 (Mfp-5). Additionally and in contrast to recent reports, comparison of adhesion strength of dipeptides containing Lys and either DOPA (KY) or phenylalanine (KF) showed that DOPA is a stronger and more versatile adhesive moiety than Phe. We

furthermore demonstrated that incorporating a nonadhesive molecular spacer between (K$\underline{\text{Y}}$) repeats can mimic the 'hidden length' in the Mfp sequence and act as an effective strategy to dissipate energy during the detachment process. Our results shed light on the interplay between chemical sequence and topological structure in the mussel adhesive proteins and provide a solid framework for rational design of bioinspired wet adhesives.

2.1 Introduction

One of the great challenges faced by man-made adhesives is binding in the presence of water, salts, and surface contaminants.[1] Marine mussels, on the other hand, have perfected the art of adhering tenaciously to a variety of surfaces in wet conditions.[2] The strong attachment of mussels is mediated by the byssus, a proteinaceous holdfast that is formed by secretion and solidification of specialized adhesive proteins.[3–6] A unique feature of these interfacial proteins is the presence of large amounts of post-translationally modified amino acid 3,4-dihydroxyphenylalanine (DOPA), a catechol-containing residue that is believed to be a major contributor to wet adhesion.[7–11] Bioinspired design principles based on mimicking these interfacial proteins have been employed extensively and resulted in a variety of catechol functionalized polymers for bio-compatible adhesives, self-healing hydrogels, and surgical wound closure materials.[12–22]

Nevertheless, the true potential of mussel-inspiration may not be fully realized until the hidden complexities in the structure and biofabrication of these adhesive proteins is revealed. For instance, a large number of positively charged Lys or arginine (Arg) residues are found in proximity to DOPA along the protein backbone.[23] Recently, Maier et al. and others utilized surface forces apparatus (SFA) to study the adaptive synergy between amine and catechol in binding to wet mica, using small molecule cyclic analogs of Lys or Arg were present adjacent to catechol or phenyl groups.[1, 24, 25] Their results showed that adhesion energy is remarkably higher when both catechol and amine are present, suggesting a synergistic effect between these functional motifs. SMFS studies further revealed that the average detaching force for DOPA and Lys dipeptide is ∼300 pN on mica surface, which was observably higher than that of a dipeptide in which the Lys side chain was protected (∼90 pN).[9, 26] Although these studies indicated an amino-catechol synergy, the influence of other amino acids, peptide length and topology on adhesion and cohesion still remains unclear.

Interestingly, in recent studies a DOPA-deficient foot protein from green mussels was shown to possess strong wet adhesion capabilities.[27] Results of SFA measurements on Phe and Lys model peptides by Gebbie et al. indicated that adhesion of these peptides to mica exceeded even that of DOPA-containing analogs.[5] The surprisingly strong adhesion of these peptides was attributed to the interaction of Lys with mica surface as well as intermolecular cation-π cohesion between Lys and Phe residues. These provocative results challenged the notion that catechols are required for wet adhesion and sparked the design of Phe-based synthetic adhesives.[5, 28, 29]

Although SFA measurements elegantly revealed the important roles of DOPA, Lys and Phe in wet adhesion and cohesion, the ensemble nature of SFA experiments precludes accurate determination of the molecular mechanism and provide indirect evidence for the adhesive functions of Lys and Phe. Since incorporation of DOPA into polymers and peptides has proven to be more synthetically demanding than Phe, the enticing possibility of employing Phe instead of DOPA in bioinspired molecular designs motivates further studies of the interfacial adhesion properties of Phe, alone or in combination with Lys. Furthermore, in Mfp-5, Lys and DOPA often appear in Lys-DOPA-Lys symmetric structure with several additional amino acids located between these sites instead of the adhesive DOPA (Fig. 1a). However, the effect of binding site density and topological structure on adhesion of Mfps and synergistic effects between DOPA and Lys residues is yet to be fully understood. Addressing these questions is critical to further understanding the underlying mechanisms of mussel adhesion and guiding rational design of bioinspired adhesives.

Here, we probed the single molecule adhesive behavior of Mfp-5 analog peptides of various length and composition on organic and inorganic substrates (Fig. 1b and Fig. 2). The AFM-based SMFS approach has been widely used to measure adhesion of biomolecules and polymers and to analyze elastic protein topological structure, ligand recognition and polymer mechanics.[30–35] We first measured the detaching force of DOPA-Lys peptides of various lengths (K$\underline{\text{Y}}$), (K$\underline{\text{Y}}$)$_3$, and (K$\underline{\text{Y}}$)$_{10}$ with TiO_2. Next, we used SMFS to quantitively compare the strength of interaction of the (KF)- and (K$\underline{\text{Y}}$)-containing peptides with different surfaces and evaluated importance of cation-π mediated binding in (KF). We then synthesized an analog peptide of Mfp-5 and studied its adhesion strength by SMFS. Furthermore, by inserting short polyethylene glycol oligomers (P8) between K$\underline{\text{Y}}$ repeat units, we mimicked the hidden length in Mfps and revealed the important function of this hidden length in wet adhesion.

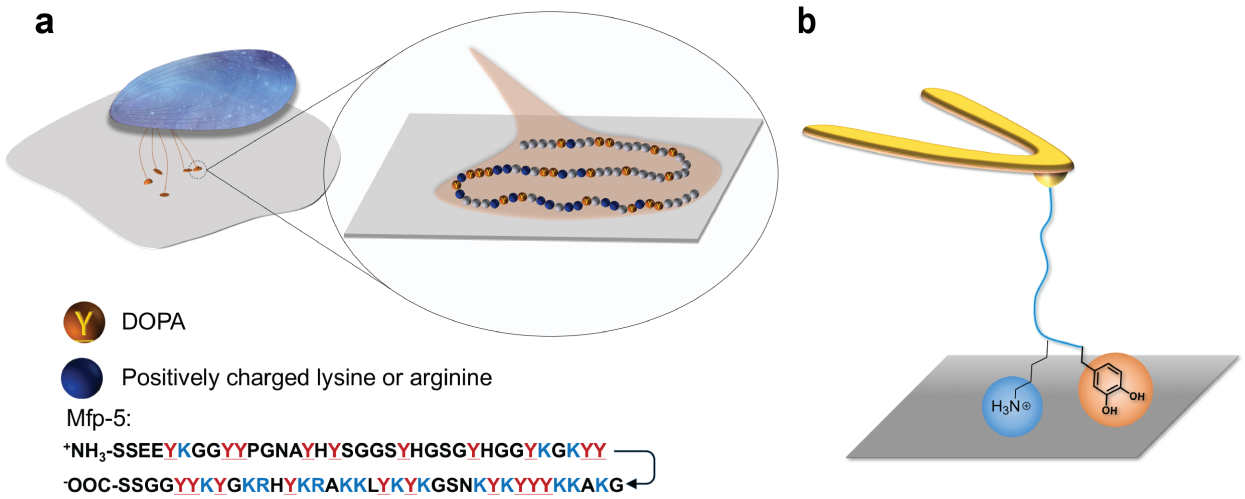

Figure 2.1: Mussel byssus adhesion. (a) Schematic of the mussel thread attachment to the surface with zoom-in showing the Mfp-5 sequence and (b) schematic of the SMFS experiments to measure the strength of interaction of the peptides with the organic and inorganic substrates.

2.2 Methods

Materials Peptide Synthesis

A detailed description of materials used and steps undertaken to synthesize monomers and polymers is provided in the published article in Nature Communications journal.

Cantilever Modification

MLCT Silicon nitride cantilever (Bruker Nano Inc.) were first treated with piranha solution (H_2SO_4:H_2O_2=1:5 (v:v), Piranha is a very aggressive solution and should be used with caution) for 30 minutes. After rinsing with excessive DI water and gently drying under a stream of nitrogen, the cantilevers were transferred into 0.5% (v/v) MPTMS/toluene solution for 2 hours for thiol functionalization. The cantilevers were then rinsed with excess toluene to remove the unreacted MPTMS and placed in oven at 120°C for 15 minutes to cure the alkoxysilane layer. Next the cantilevers were immersed in a 1:10 mixture of maleimide-PEG-NHS (5000 Da) and maleimide-PEG-methoxy (2000 Da), at a total concentration of 1 mg/ml, in DMSO for 3 hours. This ratio was used to control the binding density of bifunctional PEG and to reduce nonspecific interactions in the force spectroscopy measurements. The cantilevers were then rinsed with DMSO and incubated in a 0.5 mg/ml solution of DBCO-amine in DMSO with 0.2% (v/v) trimethylamine for 2 hours. The cantilevers were washed

with DMSO to remove unreacted reagent and were incubated in PBS (10 mM phosphate, 137 mM NaCl, pH 9) for 4 hours to hydrolyze maleimide-thiol bond to a stable ring-opened form. Finally, the cantilevers were immersed into 1 mg/ml solution of peptides in DMSO for 1 hour. The modified cantilevers were then washed with DMSO and ethanol then dried under a stream of nitrogen.

Substrate Preparation

TiO_2 substrates were treated with Piranha solution for 30 minutes to remove organic residues from the surface. The substrates were then rinsed extensively with water and dried with nitrogen. Polystyrene substrates were cleaned by sonication in ethanol for 1 hour and then rinsed with excessive water and dried with nitrogen.

AFM-based Force Spectroscopy Experiments

AFM force spectroscopy measurements were carried out using a JPK ForceRobot 300 AFM (JPK Instruments AG, Germany). The experiments were performed in 10 mM PBS buffer (containing 137 mM NaCl) which was previously bubbled with nitrogen to degas dissolved oxygen to minimize catechol oxidation during the course of measurements. Soft silicon nitride MLCT cantilevers of typical spring constant of 50-60 pN/nm were used for all experiments and calibrated using the thermal tune method after allowing the cantilever to equilibrate in solution for at least 30 minutes.[36] In a typical force measurement, the cantilever was approached to substrate at a constant speed of 1000 nm/s and held at the surface for 2 seconds to allow for the interaction between peptides and substrates. The cantilever was then retracted at the same speed. The force-extension curves were recorded using JPK data processing software and were further analyzed by a custom-written procedure in Igor Pro 6.12 (Wavemetric, Inc).

2.3 Results & Discussion

All peptides were synthesized via Fmoc-strategy on solid phase with an azide-$(PEG)_6$-COOH linker conjugated to the C-terminus and then covalently attached to 5 kDa PEG-modified AFM cantilevers via Cu-free click chemistry (Supplementary Schemes S1-2 and Fig. 2). In a typical force spectroscopy experiment, the cantilevers were approached to the substrate at a constant speed of 1000 nm/s, held on the surface with a constant force of 0.3-0.5 nN for 2 seconds, and then retracted at the same speed. In about 2-5% of total force-extension (F-X) curves, single rupture force events were observed at ∼20-60 nm, indicating the peptide surface detachment (Supplementary Fig. S2). Each individual peak was fitted with the worm-like chain (WLC) model (red line), using a persistence length range of 0.36-0.40 nm, consistent with the PEG linker and suggesting the rupture of single-peptide detachment.

Rupture events with persistence lengths either larger than 0.40 nm or smaller than 0.32 nm were discarded in the data analysis (Supplementary Fig. S3).

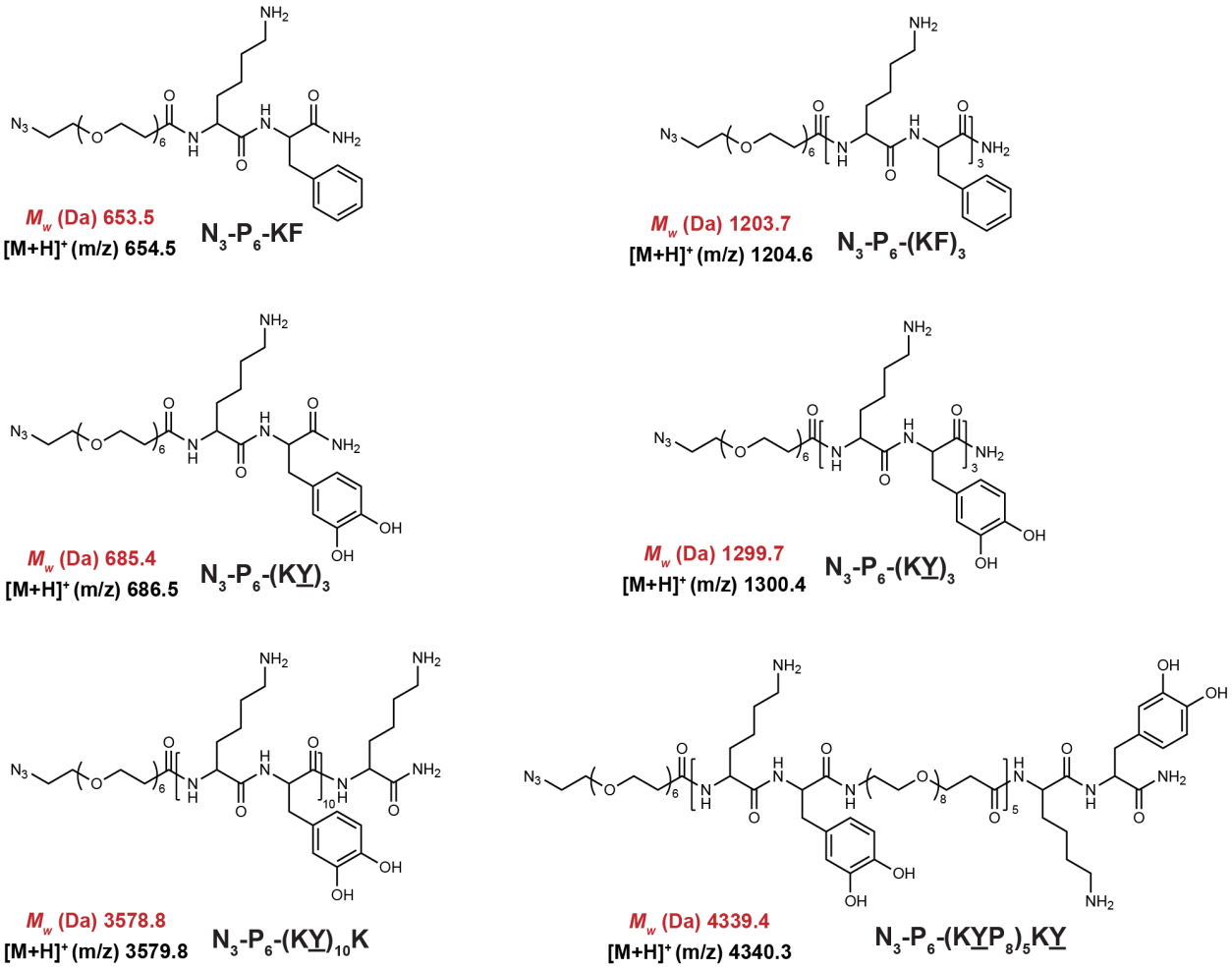

Figure 2.2: Chemical structure of the synthesized peptides. Calculated exact mass and measured mass (obtained from MALDI) are shown in red and black, respectively.

We first studied effects of number of the KY repeating units on the adhesion of mussel-inspired peptides. For this purpose, we synthesized peptides (KY), $(KY)_3$, and $(KY)_{10}$ and measured their adhesion against TiO_2. Representative F-X curves and histograms of rupture force distribution for the interaction between the peptides and the surface are shown in Fig. 2. For the (KY) peptide, the adhesion force distribution showed a narrow dominant peak located at ∼120 pN and a less probable wide distribution from 200 to 900 pN (Fig. 2a). The dominant peak located at lower force matches previously reported values and could mainly result from the rupture of individual DOPA-surface interactions.[9, 37, 38] The second broad peak may be attributed to the synergistic binding of (KY) to the TiO_2. Due

to the surface roughness, pulling direction and molecular dynamics, this synergistic effect cannot be successfully established in every pulling cycle to the same extent, leading to a broad distribution in the rupture force values.[26, 39–41] For the longer peptide $(K\underline{Y})_3$, the rupture force distribution showed only a major peak at ∼300 pN. Compared to the (K$\underline{Y}$) peptide, the $(K\underline{Y})_3$ sequence has more positively charged Lys residues which increases the strength of the coulombic charge interactions with the negatively-charged TiO_2 surface. The increased positive charges can also result in a more effective removal of the hydration layer on the surface and facilitate the binding of DOPA to the substrate.[1] Moreover, in $(K\underline{Y})_3$, the repetitive sequence allows the formation of a symmetric K$\underline{Y}$K structure, which could further promote the synergistic binding and make it more adaptable and versatile. As a consequence, the adhesion strength is enhanced and the detaching force increased to ∼300 pN (Fig. 2b). Although most of the F-X curves only exhibited one rupture peak, in some rare cases (less than 5%) we were able to observe two or three distinct rupture peaks in one F-X curve which might result from sequential detachment of individual (K$\underline{Y}$) units from the surface (Supplementary Fig. S4). The contour length increment of these peaks is ∼1 nm, consistent with the distance between repeat units in the peptide. The low observation rate of multiple detachments is likely a result of approaching the AFM detection limit, and more importantly conformational limitations that prevent all the adhesive moieties from binding effectively to the surface.

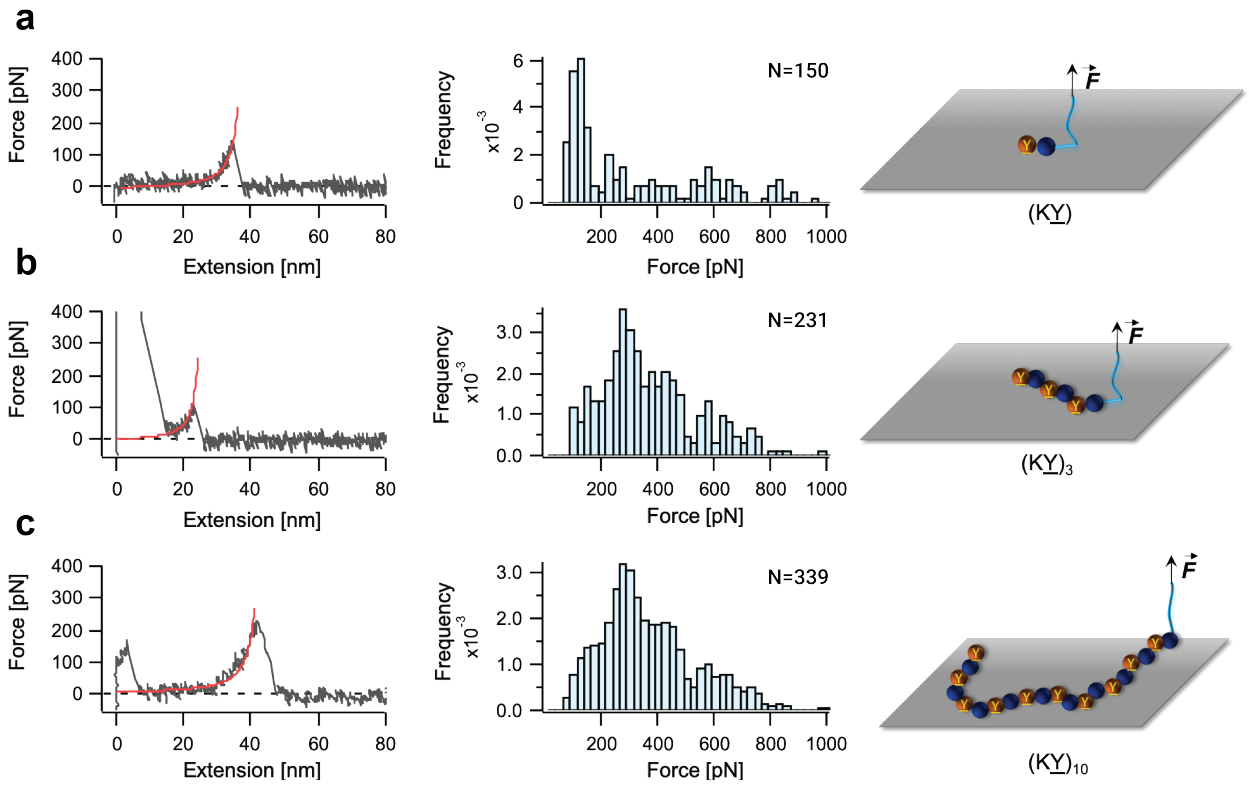

Figure 2.3: SMFS results for the interaction of (K$\underline{Y}$), (K$\underline{Y}$)$_3$, and (K$\underline{Y}$)$_{10}$ peptides with TiO_2. Representative F-X curves (left column) and rupture force distribution (middle column) are shown for (a) (K$\underline{Y}$), (b) (K$\underline{Y}$)$_3$, and (c) (K$\underline{Y}$)$_{10}$. N values represent the total number of rupture events used to plot the histograms. The red lines on the F-X curves correspond to WLC fitting. Right column shows schematic illustration of the peptides interacting with the substrate.

To study the cooperative binding of K$\underline{Y}$ units in greater depth we synthesized (K$\underline{Y}$)$_{10}$ peptides for SMFS measurements. Although it is generally expected that more adhesive units located along the peptide chain should lead to higher adhesion strength, to our surprise, simply incorporating more adhesive motifs into the structure did not enhance adhesion performance remarkably. Interestingly, the majority of the F-X curves only contained one or two rupture peaks with an average detaching rupture force of ~250 pN (Fig. 2c and Supplementary Fig. S5) similar to that of the (K$\underline{Y}$)$_3$ peptide. For the case of (K$\underline{Y}$)$_{10}$ peptide, backbone rigidity, peptide conformation, as well as surface roughness and hydration might possibly make it highly unlikely for all the (K$\underline{Y}$) units to simultaneously interact with the substrate effectively.

To investigate whether Phe residues could have the same effect on wet adhesion as DOPA, we designed peptides with (K$\underline{Y}$) or (KF) sequences and compared the binding strength of

their interactions with polystyrene (PS) and TiO_2. The representative F-X curves and the corresponding detaching force distributions are shown in Fig. 3. The rupture force distribution showed an average detachment force of ∼90 pN for the interaction of (KF) dipeptide and PS surface, while no detectable rupture force was observed for the interaction with TiO_2 surface. Previous studies have showed that DOPA can utilize hydrophobic or π-π stacking interactions with aromatic rings on the surface to bind to PS substrate.[9, 10] The (KF) peptide could also bind to PS surface in a similar way through interaction of phenyl groups. Besides, Lys residues can participate in cation-π interactions with the PS surface.[9, 10] As a consequence, an observable detaching force was measured for the interaction with PS. However, unlike DOPA that uses its catechol to form bidentate coordination bonds with TiO_2 surface,[9, 10, 37] Phe cannot form such stable interactions with TiO_2, and the charge interaction between Lys and TiO_2 surface is not strong enough to be detected by this technique. Consequently, we failed to observe detectable rupture events for the interaction of (KF) and TiO_2 surface. The (K<u>Y</u>) peptide, on the other hand, displayed detectable interactions with both PS and TiO_2 surfaces. We observed a dominant rupture force peak located at ∼100 pN for both surfaces, as well as an additional broad rupture force distribution from 200 to 900 pN for TiO_2. The results suggest that (K<u>Y</u>) is a more versatile and stronger adhesive moiety compared to (KF), possibly owing to the broader range of interfacial adhesive mechanisms of catechols. It is important to note that we sought to isolate the adhesive interactions of single molecules with substrates, and that the vanishingly low concentration of peptide on the cantilever tip precludes the formation of intramolecular peptide aggregates.[42–44] However, at relatively higher concentrations the (KF) incorporated peptides might form stable secondary nano-assemblies which can drastically increase the intermolecular interactions and cohesion strength, leading to larger separation forces detected in the previous SFA measurements.[45, 46] We further investigated the effect of incorporating more adhesive units in the peptide backbone by synthesizing $(KF)_3$ and $(K\underline{Y})_3$ sequences and measuring their interaction with TiO_2 and PS substrates using the same methodology. The representative F-X curves and rupture force distributions are shown in Supplementary Fig. S6. The average detaching force for $(KF)_3$ against PS surface was ∼90 pN, almost the same as that of the K<u>Y</u> peptide measured before. However, since multiple Lys residues increased the positive charges on the peptide, the binding strength with negatively charged TiO_2 surface was enhanced compared to before and a detaching force of ∼100 pN was observed. For the case of $(K\underline{Y})_3$ sequence, the average detaching force on PS surface was similar to that observed for (K<u>Y</u>) peptide. Overall, the results indicated that although Phe can perform similar to DOPA on hydrophobic surfaces that can accommodate π-π or cation-π interactions, DOPA is a more versatile adhesive motif and has clear advantages for improving interfacial adhesion on a broader range of substrates.

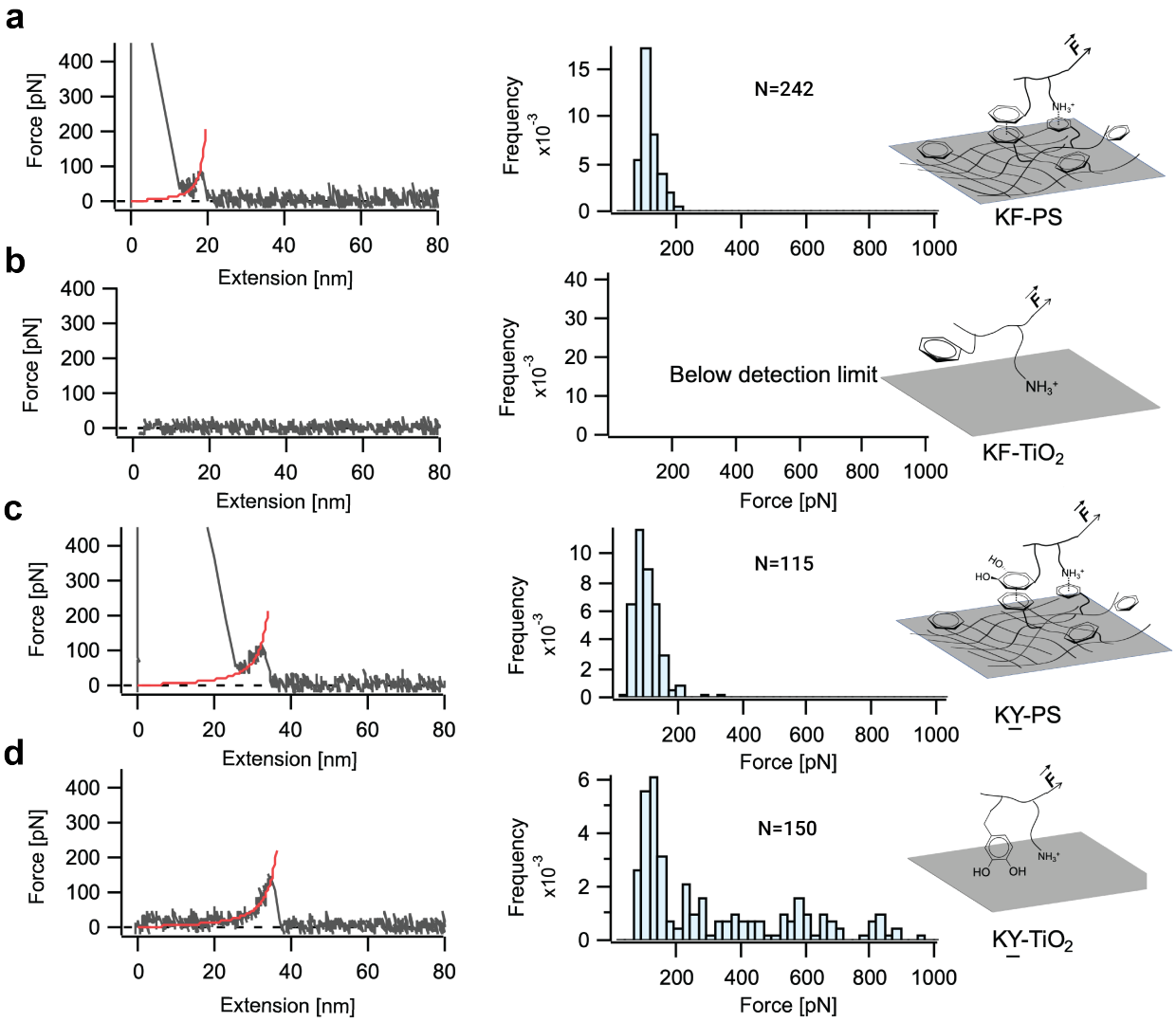

Figure 2.4: SMFS results for the interaction of (KF) and (KY) dipeptides with PS and TiO_2. Representative F-X curves (left) and rupture force distribution (right) are shown for interaction of (KF) in (a-b) and for interaction of (KY) in (c-d). N values represent the total number of rupture events used to plot the histograms. The red lines in the F-X curves correspond to the WLC fitting. Schematic illustrations for the peptide-surface interactions are shown on the right. For comparison purposes, panel (d) is reproduced here from the same dataset as shown in Fig. 2a.

Next, we studied the adhesion performance of a Lys and DOPA rich Mfp-5 segment. Mfp-5 family are interfacial proteins in the plaque and have the highest DOPA content (up to 30 mol%) among of the byssal thread proteins.[47] Although the adhesive properties of Mfp-5

and its analogs have been intensively studied by SFA measurements,[47] the molecular detachment mechanism of individual Mfp-5 proteins is still unclear. The native protein has over 74 amino acids which makes it difficult to synthesize the entire Mfp-5 chain using solid phase peptide synthesis method. Therefore, we selected a part of Mfp-5 protein with 17 amino acids and incorporated an azide functional terminus (Azide-YKGKYYGKAKKYYYKYK, and is termed as Mfp-5 analog hereafter) for coupling to the cantilever. We note that the selected segment has a higher DOPA content compared to the native Mfp-5. We then connected this Mfp-5 analog to the AFM cantilever and performed SMFS experiments as previously described for (KY) peptides. Most of the F-X curves showed a single rupture peak at ∼20 nm (Fig. 4a). However, in about 20% of F-X curves, we observed a sawtooth-like pattern indicating detachment of multiple DOPA-surface interactions. The measured rupture force showed a wide distribution with a peak located at ∼280 pN (Fig. 4b) similar to that of the $(KY)_3$ sequence. The SMFS results indicated that the $(KY)_3$ sequence has similar adhesive performance as Mfp-5, and simply adding more adhesive units contribute little to enhancing the overall interaction strength.

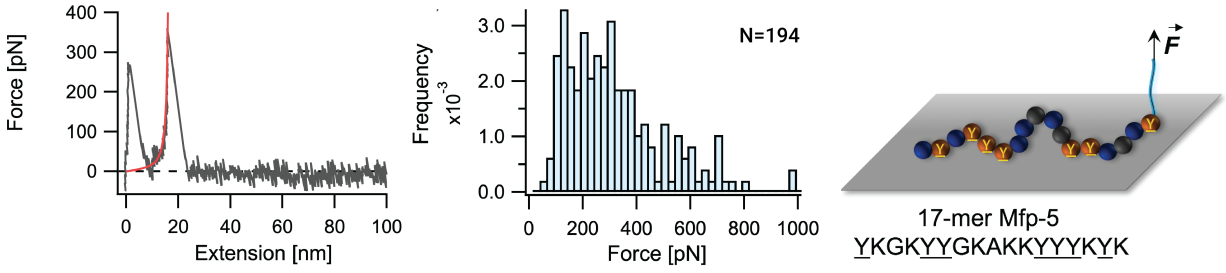

Figure 2.5: SMFS results for interaction of 17-mer Mfp-5 peptide with the TiO_2. Representative F-X curve, rupture force distribution, and schematic of the peptide interacting with the substrate are shown from left to right, respectively. N value represents the total number of rupture events used to plot the histogram.

Finally, a closer look at the Mfp-5 sequence reveals that several other amino acids are present and may have the effect of acting as spacers between (KY) repeat units.[47] Inspired by this design principle and considering the probability of observing multiple rupture peaks in the F-X curves for the Mfp-5 analog was much higher than those of $(KY)_3$ and $(KY)_{10}$ sequences, we were intrigued to synthesize and test adhesion of model peptides with similar binding-site density as Mfp-5. We used monodisperse PEG oligomers (P8) to mimic the 'spacer' residues in native Mfp-5 and synthesized peptides with multiple (KY-P8) repeat units (Fig. 5a). Same cantilever modification method and experimental conditions as before were used to measure the interaction of the peptide with the TiO_2. Most of the F-X curves displayed 3-4 distinct rupture peaks with contour length increment of ∼5 nm that is commensurate with the (KY-P8) length. The detaching force for the peptide showed a broad

distribution with a peak located at ∼200 pN (Fig. 5b and c). Compared to the peptide with 3 adjacent (KY) units, a flexible PEG linker reduces the peptide rigidity, allowing for each (KY) unit to interact with the surface effectively. Although this peptide did not show an increase in the adhesion strength as measured by SMFS, the PEG spacer can act as hidden length and lead to dissipating more energy during the detachment process.[48, 49] Unlike constructs of KY repeats with no spacing where the adhesive sites are detached almost simultaneously upon application of force, in the P8 incorporated peptide the adhesive motifs are detached sequentially followed by release of the hidden length. The energy dissipated in this process can further confer toughness and superior performance to the adhesive.[48, 49]

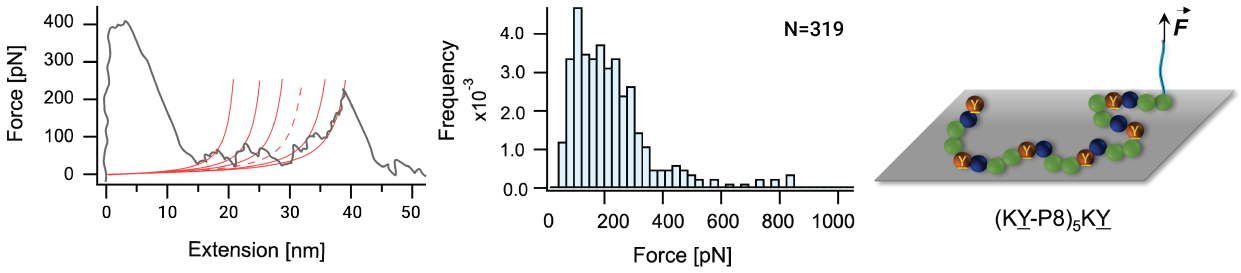

Figure 2.6: SMFS results of (KY-P8)$_5$KY peptide interacting with TiO$_2$. (a) Representative F-X curve and (b) rupture force distribution for the interaction of the peptide with the surface are shown. The retraction trace is smoothed using a 10-period moving-average filter to reduce the thermal noise. N value represents the total number of rupture events used to plot the histogram. The red lines in (a) show WLC fittings, where dashed line corresponds to the missing rupture peak. Right column shows schematic illustration of the peptides interacting with the substrate where green spheres represent the PEG spacer between the KY units.

2.4 Conclusions

We used AFM-based SMFS technique to study the influence of length, composition and topological structure on the adhesion strength of mussel-inspired peptides. We synthesized a library of peptides with different number of Lys-DOPA repeat units as well as a 17-mer peptide from Mfp-5 and demonstrated that a modest increase in the length of the peptide can lead to noticeable increase in the adhesion strength while further increasing the peptide length without incorporating nonadhesive spacer between Lys-DOPA units resulted in little benefits on the adhesion strength. Moreover, we substituted Phe for DOPA in the peptide sequences and showed that while Lys-Phe and Lys-DOPA containing peptides could interact with organic substrates similarly, no strong interfacial adhesion could be detected for the interaction of Lys-Phe sequences against inorganic substrates, further highlighting the versatility of DOPA in establishing strong interfacial adhesion to a broader range of substrates.

And finally, we designed a peptide with nonadhesive molecular spacer incorporated between Lys-DOPA repeats and showed that this 'hidden length' can enhance the overall adhesive performance by allowing for higher energy dissipation before ultimate rupture. The findings in this work can provide a solid foundation to tailor properties and further guide the deliberate design and synthesis of bioinspired wet adhesives.

2.5 Supplementary Figures

AFM Cantilever Modification

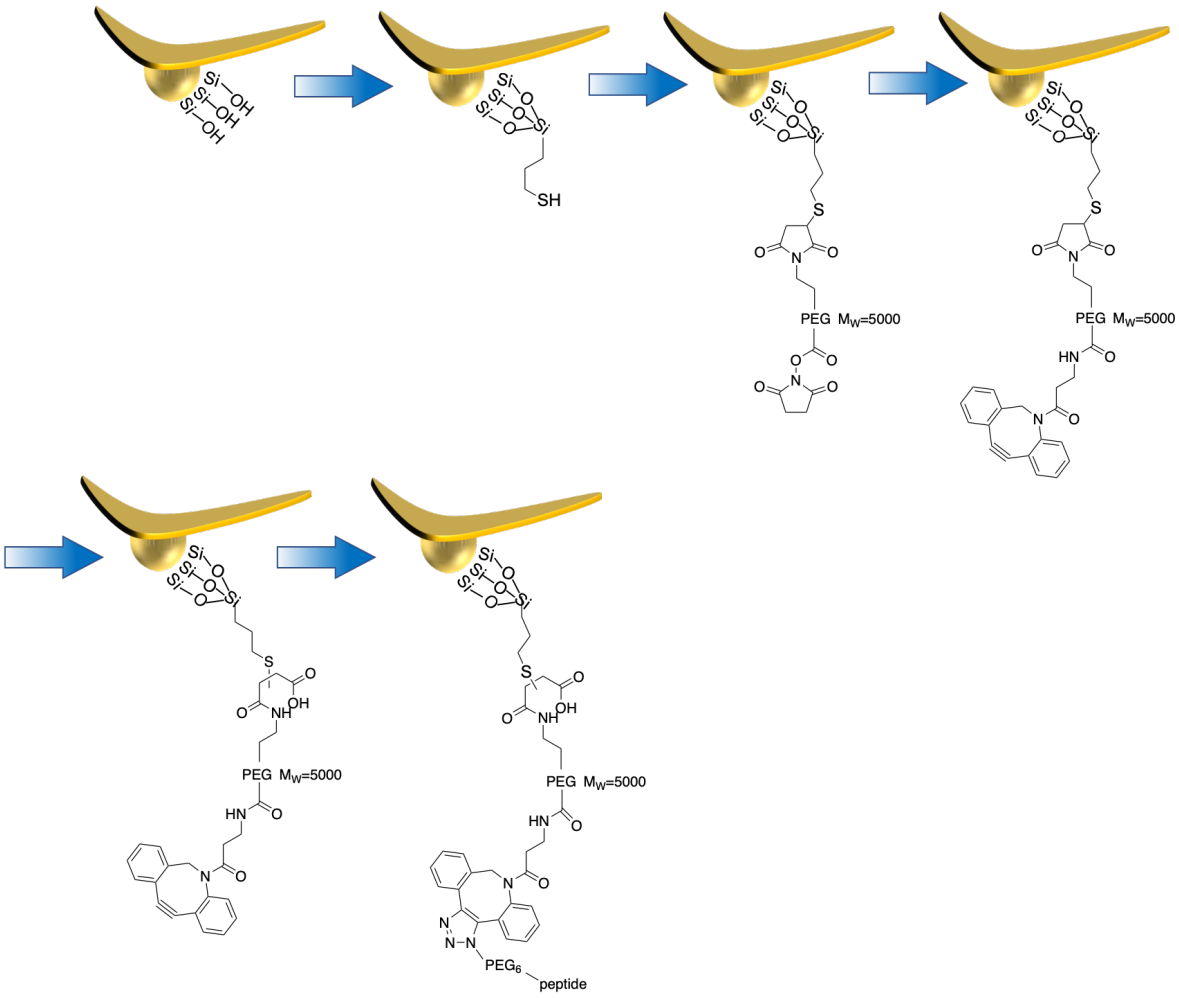

Scheme S2.1: Schematic of AFM cantilever modification steps (monofunctional methoxy-PEG is not shown).

Solid-Phase Peptide Synthesis

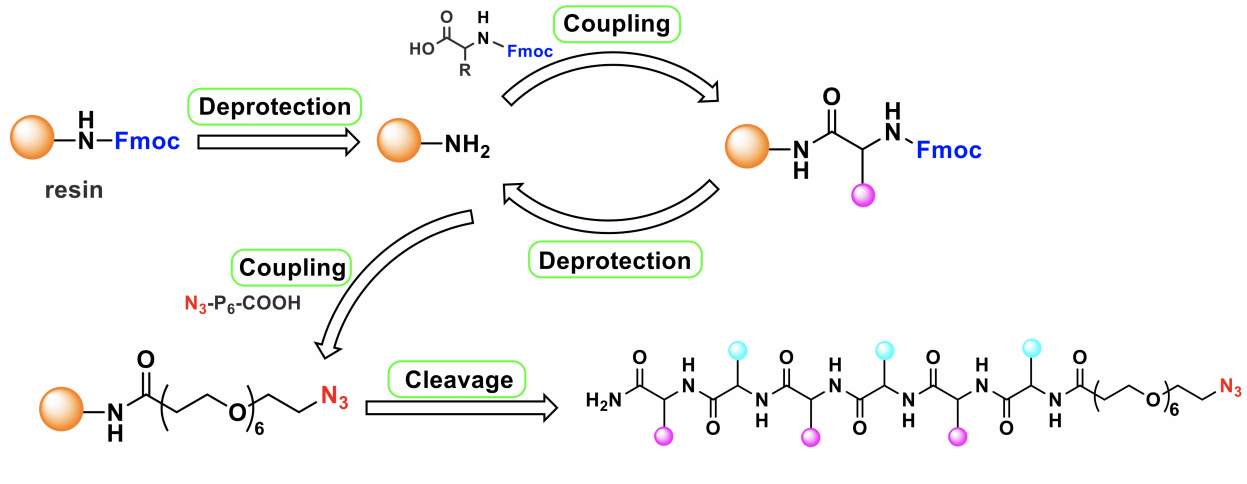

Scheme S2.2: Schematic of solid-phase peptide synthesis.

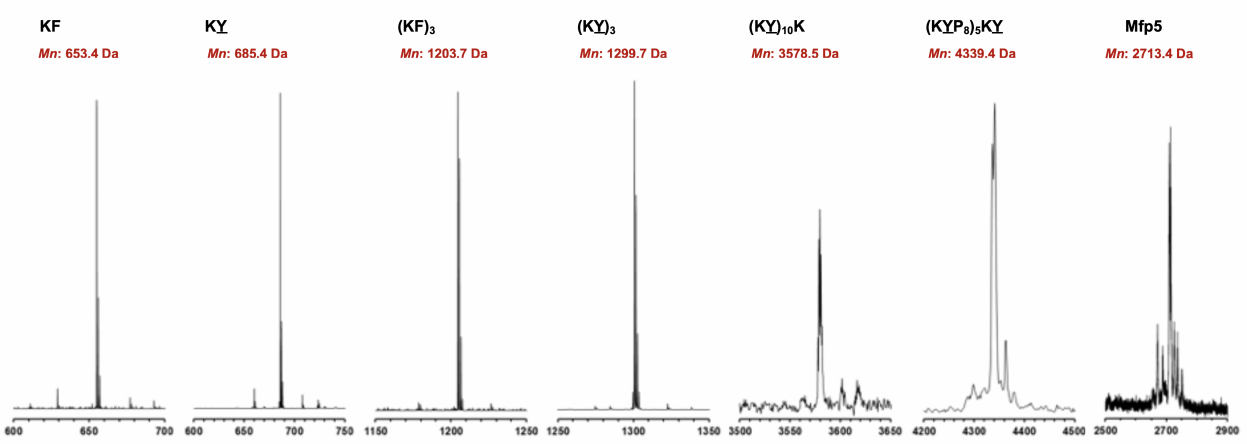

Figure S2.1: MALDI spectra of the synthesized peptides. Measured mass is shown in red.

SMFS Measurements

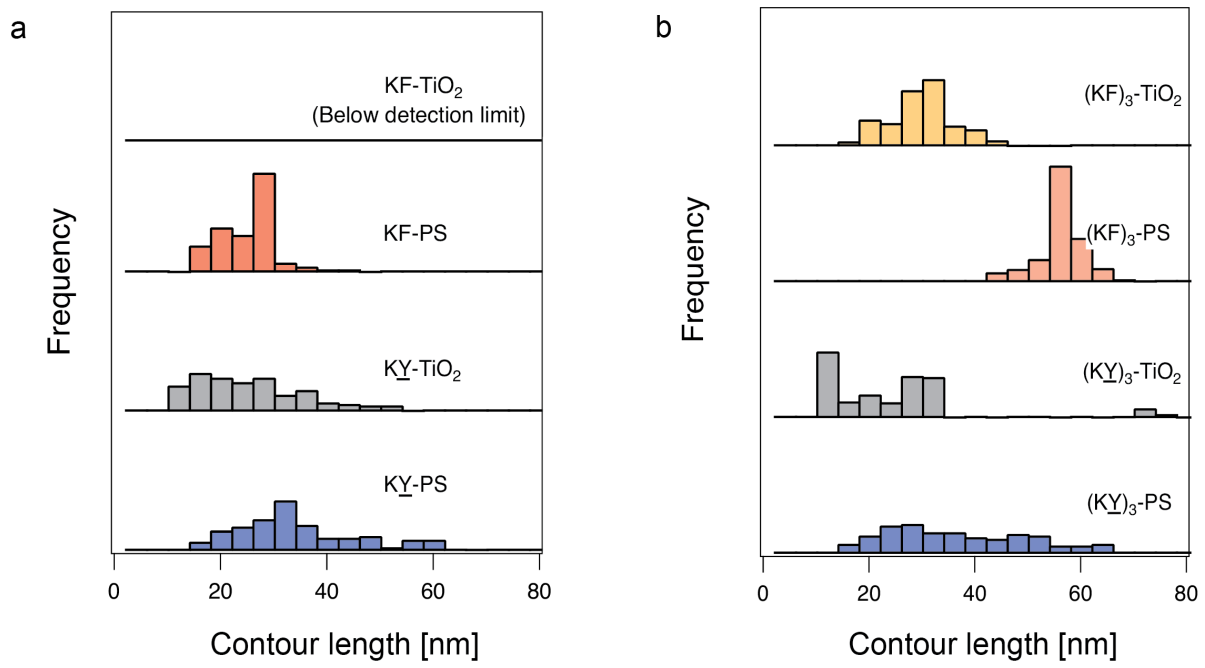

Figure S2.2: Contour length distribution for rupture events; (a) for interaction of (K$\underline{\text{Y}}$) or (KF) and (b) for interaction of (K$\underline{\text{Y}}$)$_3$ or (KF)$_3$ with different surfaces. The distribution of contour lengths is attributed to the polydispersity of the PEG linker as well as randomness in the conjugation site on the cantilever tip.

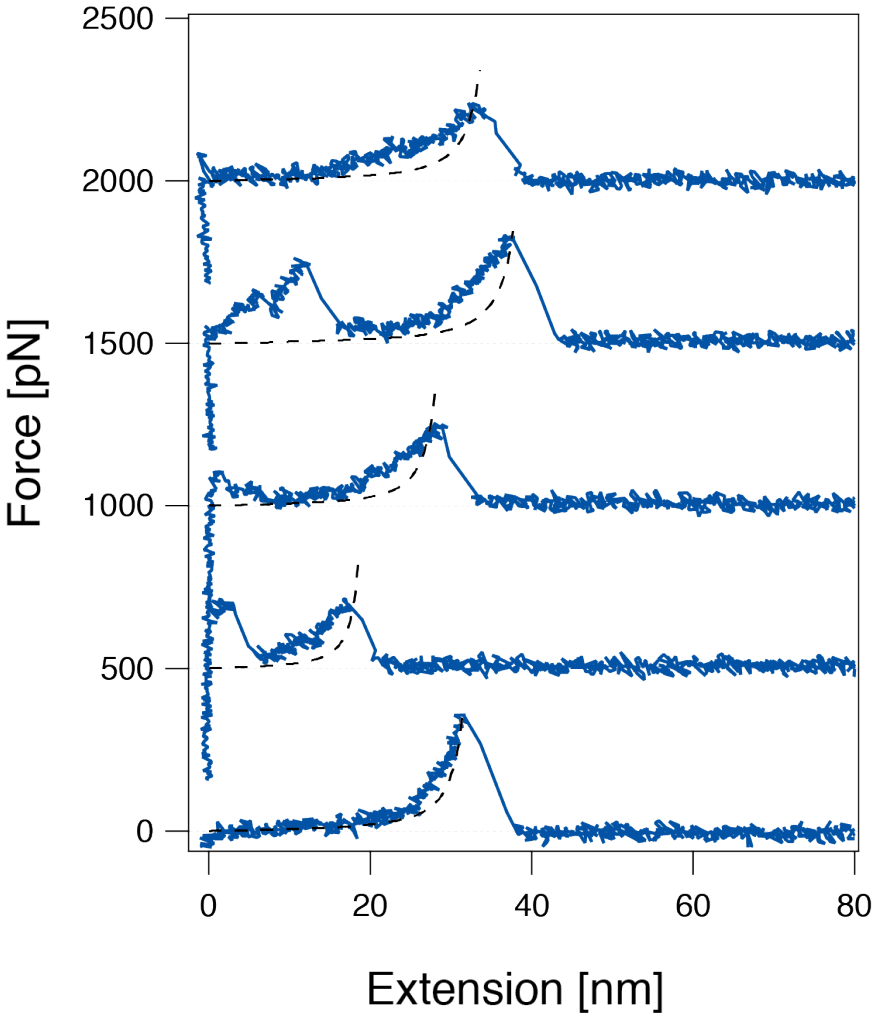

Figure S2.3: Representative discarded F-X curves for the interaction of (KY) peptide with the TiO_2 surface. The black dashed lines correspond to the worm-like chain model fitting with persistence length of 0.36 nm. The force-extension curves whose fitted persistence length are larger than 0.4 nm or smaller than 0.32 nm were discarded and not included in the data analysis for calculating rupture force distribution.

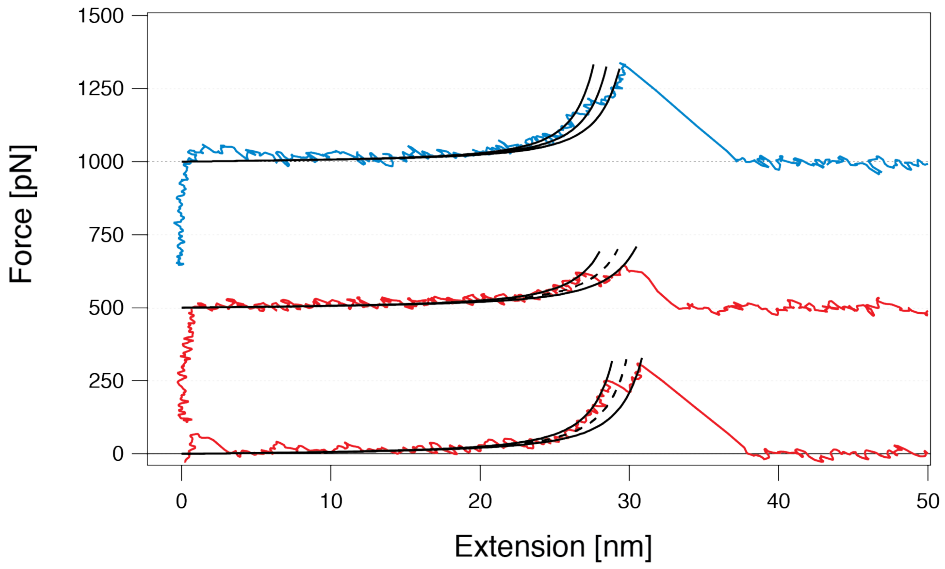

Figure S2.4: Representative F-X curves for interaction of $(K\underline{Y})_3$ peptide with TiO_2 surface. The black lines correspond to worm-like chain fitting with persistence length of 0.36 nm and the contour length increment of 1 nm. The blue curve shows three detachment events of $(K\underline{Y})_3$ peptide from the surface. The dashed lines in the red F-X curves show a possible missing rupture event. As 1 nm contour length increment reaches the AFM detection limits, distinguishing three individual rupture peaks becomes difficult.

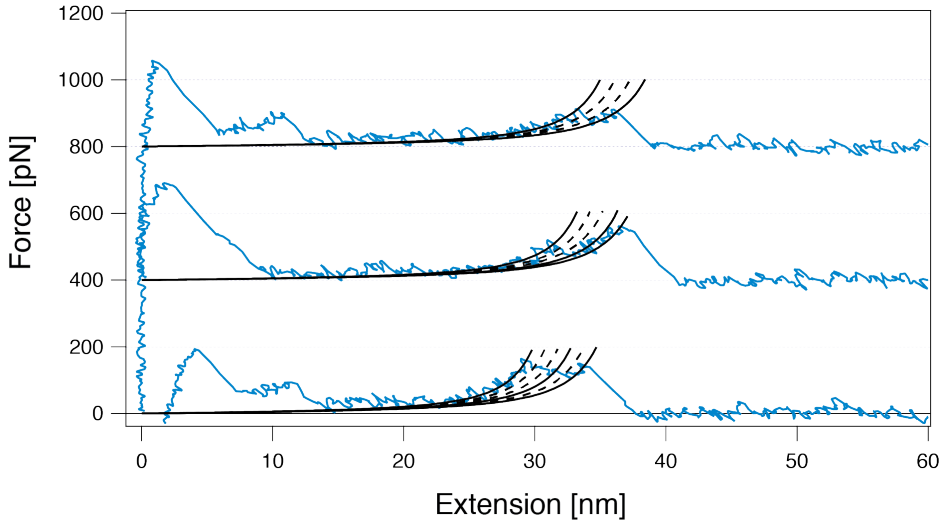

Figure S2.5: Representative F-X curves for the $(K\underline{Y})_{10}$ peptide interacting with TiO_2 substrate. Black lines correspond to the worm-like chain fitting. Dashed lines represent the expected unbinding events based on the distance between adhesive moieties. Data indicates that that not all the adhesive sites were able to successfully attach to the surface.

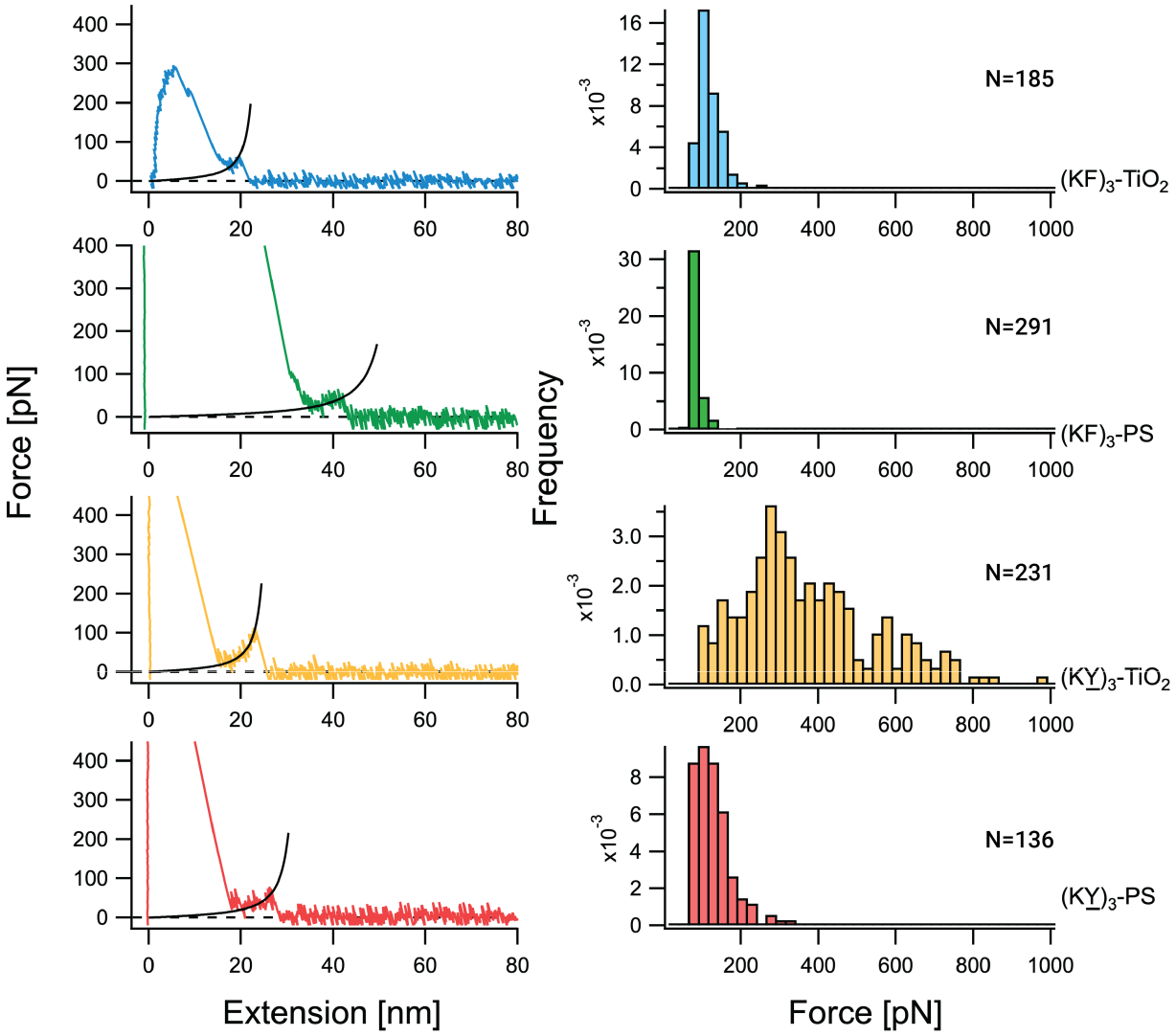

Figure S2.6: Representative F-X curves (left) and rupture force distribution (right) for the interaction $(KF)_3$ and $(K\underline{Y})_3$ peptides with PS and TiO_2 substrates. N values represent the total number of rupture events used to plot the histograms. The black lines in the F-X curves correspond to the worm-like chain fitting.

References

[1] G. P. Maier et al. "Adaptive synergy between catechol and lysine promotes wet adhesion by surface salt displacement". In: *Science* 349.6248 (2015), pp. 628–632 (cit. on pp. 30, 35).

[2] J. H. Waite. "Surface chemistry - Mussel power". In: *Nature Materials* 7.1 (2008), pp. 8–9 (cit. on p. 30).

[3] B. K. Ahn. "Perspectives on Mussel-Inspired Wet Adhesion". In: *J Am Chem Soc* 139.30 (2017), pp. 10166–10171 (cit. on p. 30).

[4] B. P. Lee et al. "Mussel-Inspired Adhesives and Coatings". In: *Annu Rev Mater Res* 41 (2011), pp. 99–132 (cit. on p. 30).

[5] M. A. Gebbie et al. "Tuning underwater adhesion with cation-pi interactions". In: *Nat Chem* 9.5 (2017), pp. 473–479 (cit. on p. 30).

[6] R. Y. Floriolli, J. von Langen, and J. H. Waite. "Marine Surfaces and the Expression of Specific Byssal Adhesive Protein Variants in Mytilus". In: *Mar Biotechnol (NY)* 2.4 (2000), pp. 352–363 (cit. on p. 30).

[7] H. Lee, N. F. Scherer, and P. B. Messersmith. "Single-molecule mechanics of mussel adhesion". In: *Proc Natl Acad Sci U S A* 103.35 (2006), pp. 12999–3003 (cit. on p. 30).

[8] Q. Lin et al. "Adhesion mechanisms of the mussel foot proteins mfp-1 and mfp-3". In: *Proc Natl Acad Sci U S A* 104.10 (2007), pp. 3782–6 (cit. on p. 30).

[9] Y. Li et al. "Single molecule evidence for the adaptive binding of DOPA to different wet surfaces". In: *Langmuir* 30.15 (2014), pp. 4358–66 (cit. on pp. 30, 34, 37).

[10] Q. Lu et al. "Adhesion of mussel foot proteins to different substrate surfaces". In: *J R Soc Interface* 10.79 (2013), p. 20120759 (cit. on pp. 30, 37).

[11] J. Yu et al. "Adhesion of Mussel Foot Protein-3 to TiO2 Surfaces: the Effect of pH". In: *Biomacromolecules* 14.4 (2013), pp. 1072–1077 (cit. on p. 30).

[12] M. Shin et al. "Complete prevention of blood loss with self-sealing haemostatic needles". In: *Nat Mater* 16.1 (2017), pp. 147–152 (cit. on p. 30).

[13] Y. Wang et al. "Biologically Inspired Materials Exhibiting Repeatable Regeneration with Self-Sealing Capabilities without External Stimuli or Catalysts". In: *Adv Mater* 28.45 (2016), pp. 9961–9968 (cit. on p. 30).

[14] Ying Li et al. "Hidden complexity of synergistic roles of Dopa and lysine for strong wet adhesion". In: *Materials Chemistry Frontiers* 1.12 (2017), pp. 2664–2668 (cit. on p. 30).

[15] C. A. Monnier, D. G. DeMartini, and J. H. Waite. "Intertidal exposure favors the soft-studded armor of adaptive mussel coatings". In: *Nat Commun* 9.1 (2018), p. 3424 (cit. on p. 30).

[16] P. M. Lopez-Perez et al. "Self-healing hydrogels formed by complexation between calcium ions and bisphosphonate-functionalized star-shaped polymers". In: *Macromolecules* 50.21 (2017), pp. 8698–8706 (cit. on p. 30).

[17] James D. White and Jonathan J. Wilker. "Underwater Bonding with Charged Polymer Mimics of Marine Mussel Adhesive Proteins". In: *Macromolecules* 44.13 (2011), pp. 5085–5088 (cit. on p. 30).

[18] C. J. Kastrup et al. "Painting blood vessels and atherosclerotic plaques with an adhesive drug depot". In: *Proc Natl Acad Sci U S A* 109.52 (2012), pp. 21444–9 (cit. on p. 30).

[19] A. R. Statz et al. "New peptidomimetic polymers for antifouling surfaces". In: *J Am Chem Soc* 127.22 (2005), pp. 7972–3 (cit. on p. 30).

[20] B. K. Ahn et al. "High-performance mussel-inspired adhesives of reduced complexity". In: *Nat Commun* 6 (2015), p. 8663 (cit. on p. 30).

[21] Cody J. Higginson et al. "Bioinspired Design Provides High-Strength Benzoxazine Structural Adhesives". In: *Angewandte Chemie International Edition* 0.0 (2019) (cit. on p. 30).

[22] Brylee David B. Tiu et al. "Enhanced Adhesion and Cohesion of Bioinspired Dry/Wet Pressure-Sensitive Adhesives". In: *ACS Applied Materials Interfaces* 11.31 (2019), pp. 28296–28306 (cit. on p. 30).

[23] B. P. Lee et al. "Mussel-Inspired Adhesives and Coatings". In: *Annual Review of Materials Research, Vol 41* 41 (2011), pp. 99–132 (cit. on p. 30).

[24] M. V. Rapp et al. "Defining the Catechol-Cation Synergy for Enhanced Wet Adhesion to Mineral Surfaces". In: *J Am Chem Soc* 138.29 (2016), pp. 9013–6 (cit. on p. 30).

[25] G. D. Degen et al. "Impact of Molecular Architecture and Adsorption Density on Adhesion of Mussel-Inspired Surface Primers with Catechol-Cation Synergy". In: *Journal of the American Chemical Society* 141.47 (2019), pp. 18673–18681 (cit. on p. 30).

[26] Yiran Li et al. "Single-molecule study of the synergistic effects of positive charges and Dopa for wet adhesion". In: *Journal of Materials Chemistry B* 5.23 (2017), pp. 4416–4420 (cit. on pp. 30, 35).

[27] D. S. Hwang et al. "Adhesion mechanism in a DOPA-deficient foot protein from green mussels()". In: *Soft Matter* 8.20 (2012), pp. 5640–5648 (cit. on p. 30).

[28] W. Wei et al. "Hydrophobic enhancement of Dopa-mediated adhesion in a mussel foot protein". In: *J Am Chem Soc* 135.1 (2013), pp. 377–83 (cit. on p. 30).

[29] Wei Zhang et al. "Molecular interactions between DOPA and surfaces with different functional groups: a chemical force microscopy study". In: *RSC Advances* 7.52 (2017), pp. 32518–32527 (cit. on p. 30).

[30] Yiran Li et al. "Single-Molecule Mechanics of Catechol-Iron Coordination Bonds". In: *ACS Biomaterials Science Engineering* 3.6 (2017), pp. 979–989 (cit. on p. 31).

[31] W. Huang et al. "Maleimide-thiol adducts stabilized through stretching". In: *Nat Chem* (2019) (cit. on p. 31).

[32] J. Li and H. Li. "Mechanical Unfolding Pathway of the High-Potential Iron-Sulfur Protein Revealed by Single-Molecule Atomic Force Microscopy: Toward a General Unfolding Mechanism for Iron-sulfur Proteins". In: *J Phys Chem B* 122.40 (2018), pp. 9340–9349 (cit. on p. 31).

[33] P. Delparastan et al. "Direct Evidence for the Polymeric Nature of Polydopamine". In: *Angew Chem Int Ed Engl* 58.4 (2019), pp. 1077–1082 (cit. on p. 31).

[34] T. Verdorfer et al. "Combining in Vitro and in Silico Single-Molecule Force Spectroscopy to Characterize and Tune Cellulosomal Scaffoldin Mechanics". In: *J Am Chem Soc* 139.49 (2017), pp. 17841–17852 (cit. on p. 31).

[35] Z. J. Huang et al. "Injectable dynamic covalent hydrogels of boronic acid polymers cross-linked by bioactive plant-derived polyphenols". In: *Biomaterials Science* 6.9 (2018), pp. 2487–2495 (cit. on p. 31).

[36] Jannis Lübbe et al. "Determining cantilever stiffness from thermal noise". In: *Beilstein Journal of Nanotechnology* 4 (2013), pp. 227–233 (cit. on p. 33).

[37] Y. Li et al. "Single-Molecule Force Spectroscopy Reveals Multiple Binding Modes between DOPA and Different Rutile Surfaces". In: *Chemphyschem* 18.11 (2017), pp. 1466–1469 (cit. on pp. 34, 37).

[38] Jijun Wang et al. "Influence of Binding-Site Density in Wet Bioadhesion". In: *Advanced Materials* 20.20 (2008), pp. 3872–3876 (cit. on p. 34).

[39] C. Ke et al. "Pulling geometry-induced errors in single molecule force spectroscopy measurements". In: *Biophys J* 92.9 (2007), pp. L76–8 (cit. on p. 35).

[40] P. Zheng et al. "Single molecule force spectroscopy reveals the molecular mechanical anisotropy of the FeS4 metal center in rubredoxin". In: *J Am Chem Soc* 135.47 (2013), pp. 17783–92 (cit. on p. 35).

[41] R. B. Best et al. "Pulling direction as a reaction coordinate for the mechanical unfolding of single molecules". In: *J Phys Chem B* 112.19 (2008), pp. 5968–76 (cit. on p. 35).

[42] S. G. Zhang. "Fabrication of novel biomaterials through molecular self-assembly". In: *Nature Biotechnology* 21.10 (2003), pp. 1171–1178 (cit. on p. 37).

[43] S. G. Zhang et al. "Spontaneous Assembly of a Self-Complementary Oligopeptide to Form a Stable Macroscopic Membrane". In: *Proceedings of the National Academy of Sciences of the United States of America* 90.8 (1993), pp. 3334–3338 (cit. on p. 37).

[44] M. R. Caplan et al. "Control of self-assembling oligopeptide matrix formation through systematic variation of amino acid sequence". In: *Biomaterials* 23.1 (2002), pp. 219–227 (cit. on p. 37).

[45] P. Tamamis et al. "Self-assembly of phenylalanine oligopeptides: insights from experiments and simulations". In: *Biophys J* 96.12 (2009), pp. 5020–9 (cit. on p. 37).

[46] A. Lakshmanan et al. "Aliphatic peptides show similar self-assembly to amyloid core sequences, challenging the importance of aromatic interactions in amyloidosis". In: *Proc Natl Acad Sci U S A* 110.2 (2013), pp. 519–24 (cit. on p. 37).

[47] E. W. Danner et al. "Adhesion of mussel foot protein Mefp-5 to mica: an underwater superglue". In: *Biochemistry* 51.33 (2012), pp. 6511–8 (cit. on pp. 38, 39).

[48] G. E. Fantner et al. "Sacrificial bonds and hidden length dissipate energy as mineralized fibrils separate during bone fracture". In: *Nat Mater* 4.8 (2005), pp. 612–6 (cit. on p. 40).

[49] Bettye L. Smith et al. "Molecular mechanistic origin of the toughness of natural adhesives, fibres and composites". In: *Nature* 399 (1999), p. 761 (cit. on p. 40).

Chapter 3

Direct Evidence for the Polymeric Nature of Polydopamine

* This chapter is adapted based on the research originally appeared as a peer-reviewed article co-first-authored by me published in Angewandte Chemie.
P. Delparastan[†], K. G. Malollari[†], H. Lee, P. B. Messersmith, Angew. Chem. Int. Ed. 2019, 58, 1077.

Abstract

Inspired by the adhesive proteins of mussels, polydopamine (pDA) has emerged as one of the most widely employed methods for functionalizing material surfaces, fueled in part by the versatility, simplicity, and spontaneity of pDA film deposition on most materials upon immersion in an alkaline aqueous solution of dopamine. However, the rapid adoption of pDA for surface modification over the last decade stands in stark contrast to the slow pace in understanding the composition of pDA. Numerous attempts to elucidate the formation mechanism and structure of this fascinating material have resulted in little consensus mainly due to the insoluble nature of pDA; which renders most conventional methods of polymer molecular weight characterization ineffective.[1, 2] Here, we employed the non-traditional approach of single molecule force spectroscopy (SMFS) to characterize pDA films. Retraction of a pDA coated cantilever from an oxide surface shows the characteristic features of a polymer with contour lengths up to 200nm. pDA polymers are generally weakly bound to the surface through much of their contour length, with occasional "sticky" points. Our findings represent the first direct evidence for the polymeric nature of pDA and provide a foundation upon which to understand and tailor its physicochemical properties.

3.1 Introduction

The building blocks and processing strategies used by biological organisms for the fabrication of natural materials often serve as inspiration for the design of novel synthetic materials.[3] Mussel adhesive proteins have attracted great interest for having high contents of catechols (3,4-dihydroxyphenylalanine, Dopa) in combination with primary and secondary amines (lysine and histidine).[4] A synergy between catechol and amine moieties has been associated with enhanced biomolecular adhesion in recent model studies of mussel adhesion.[5] Meanwhile, small molecule catecholamines such as dopamine have become widely exploited for surface modification as a result of their ability to form adherent coatings on solid surfaces.[6] The coatings derived from dopamine are referred to as dopamine-melanin or more commonly as 'polydopamine' (pDA) and represent one of the most facile and versatile approaches to surface modification. In its simplest form, deposition of a pDA coating involves simple immersion of a substrate in an aqueous alkaline solution of dopamine for a period of time, usually minutes to hours, during which time conformal coatings of thickness typically 1-100 nm spontaneously form.[6] pDA coatings have been explored in a broad range of applications including energy harvest and storage, separations, environmental remediation, healthcare, and sensing.[7]

There is general agreement that the initial stages of pDA coating formation involves auto-oxidation of dopamine giving rise to dopamine-quinone, which cyclizes to form dihydroxyindole (DHI), a key precursor to pDA.[2] However, ensuing reaction pathways leading to pDA formation are complex and remain unclear, as does the ultimate chemical structure of pDA. A confounding property of pDA that has complicated attempts at structural characterization is its nearly intractable nature-pDA is largely insoluble in aqueous and organic solvents. Furthermore, deposition of pDA coatings on substrates is accompanied by formation of particles in suspension, and most attempts to determine pDA structure have been performed on pDA isolated from solution. However, recent evidence suggests that the structural characteristics and properties of pDA films are different than those of aggregates and solution species.[8]

Nevertheless, a number of important experimental studies have been performed on pDA using mostly chemical spectroscopy (NMR, UV-Vis, Raman, FT-IR) and mass spectrometry (MALDI-ToF, LDI, ESI, ToF-SIMS), leading to several hypotheses for the structure of pDA (Supplementary Fig. S1). Proposals fall into two general categories. The most common hypothesis is that pDA is a supramolecular aggregate of monomeric and/or oligomeric species, for example consisting of dopamine-quinone, dihydroxyindole (DHI), dopamine, or eumelanin-like derivatives that are held together through relatively weak interactions such as hydrogen bonding, charge transfer, π-π stacking and π-cation assembly.[1, 2, 9–11] Others have proposed that pDA is polymeric in nature, arising from covalent coupling of the oxidized and cyclized dopamine monomers via aryl-aryl linkages.[12] Due to the insoluble nature of pDA, traditional solution based methods of polymer molecular weight characterization (e.g. gel permeation chromatography) are unsuitable, and mass spectral analyses of pDA reported in the literature have revealed primarily low molecular weight ionized and fragmented pDA

species.[10, 12] We could not find a published mass spectrum of pDA in the literature that includes masses significantly above 700 Daltons.[2, 8–11] We confirmed the absence of high molecular weight species in the MALDI-MS spectrum of pDA particles isolated from solution (Supplementary Fig. S2). Thus, despite the wide use of 'polymer' ascribed to pDA, it is largely unproven experimentally.

In this report, AFM-assisted single molecule force spectroscopy (SMFS) was applied towards investigating pDA. SMFS is a force-based characterization technique that has been recognized as a powerful tool to study noncovalent and covalent interactions at a single molecule level.[13, 14] SMFS is well suited to studying intermolecular and intramolecular interactions such as weak secondary bonds, ligand-receptor interactions, protein unfolding, DNA unwinding, polymer stretching, and even the rupture of covalent bonds.[15–21] Here, we used SMFS to study the cohesive (pDA-pDA) and adhesive (pDA-surface) interactions of pDA. The ability of SMFS to detect well-known signatures of mechanical deformation of individual macromolecules allowed us to address a specific compelling question regarding pDA: is there a significant polymeric fraction present in pDA? The results obtained here are of importance not only in understanding pDA structure but also for establishing a solid framework of structure-property relationships of pDA to help guide the further study and exploitation of this fascinating material.

3.2 Methods

Materials

Dopamine hydrochloride (99%, Alfa Aesar), bicine (99%, Alfa Aesar), sodium hydroxide (NaOH, pellets, Fisher Scientific), α-Cyano-4-hydroxycinnamic acid (CHCA) (Sigma Aldrich) isopropyl alcohol (99.5%, VWR Analytical), DMSO (VWR Analytical), acetone (Macron Fine Chemicals), and Simple Green (Sunshine Makers, Inc) were used as received. Mica discs were purchased from Ted Pella, Inc (Redding, CA). 1cm×1cm 316 stainless steel (SS) samples were cut by university machine shop (Berkeley, CA), silicon wafers (SiO_2) and silicon wafers with a layer of 100 nm titanium oxide (TiO_2) were obtained from University Wafer, Inc (Boston, MA). Ultrapure (UP) water was obtained by purification of deionized water with a Barnstead Ultrapure Water Purification System (Thermo Fisher Scientific, Waltham, MA) to a resistivity of 18.2 MΩ cm.

pDA Coating

SiO_2, TiO_2, and SS substrates were first cleaned with a 3:1 mixture of water and Simple Green solution for degreasing by placing into sonication bath for 15 minutes. The substrates were then rinsed and sonicated with water followed by isopropanol and acetone, each for 15 minutes, and dried under a stream of nitrogen. Prior immersing in dopamine.HCl solution, substrates were exposed to a plasma discharge at 100 W for 5 minutes (Harrick Plasma

Cleaner, Ithaca, NY, USA). Mica substrates were prepared by physically cleaving the top layer using scotch tape. AFM cantilevers were cleaned by UV-Ozone treatment (PSD Pro Series, Novascan Technologies, USA) for 6 minutes.[22] The substrates were immersed into 2 mg/ml DA.HCl in 100 mM Bicine buffer at pH 8.5 for 16 hours with constant shaking. The substrates were taken out and rinsed intensively with Milli-Q water and dried under a stream of nitrogen.

pDA Nanoparticle Synthesis

DA.HCl (2 mg/ml) was dissolved in Milli-Q water and pH was increased to 8.5 by adding NaOH. The solution was stirred at 400 rpm for 5 hours at 70°C and subsequently left at ambient temperature for 3 hours without stirring. Finally, the mixture was filtered with PVDF membrane filters with a pore size of 0.1 μm (Durapore VVPP) followed by drying at 50°C under vacuum.

Single Molecule Force Spectroscopy (SMFS)

Measurements were carried out using a JPK ForceRobot 300 (JPK Instruments AG, Germany) with a tip velocity of 1000 nm/s over a z-piezo distance of 500 nm with a dwell time of 1 second. The experiments were performed in Milli-Q water after allowing the cantilever to equilibrate in solution for at least 30 minutes. Soft silicon nitride cantilevers (MLCT from Bruker Nano Inc.) of typical spring constant of 50-60 pN/nm were used for all experiments and calibrated using the equipartition theorem.[2] All the experiments have been repeated at least three times using different pDA-coated cantilevers and/or substrates. The force-extension traces were recorded and analyzed using data processing software from JPK and home-written procedure in IgorPro (Wavemetrics). The spikes in the force-distance curves were fitted with the Worm-like Chain (WLC) model to measure the corresponding rupture force and persistence length.

X-Ray Photoelectron Spectroscopy (XPS)

The surface chemical composition of pDA coatings on TiO_2 substrates and AFM cantilevers was measured using X-Ray photoelectron spectroscopy (XPS). XPS analyses were performed on a Perkin Elmer Phi 5600, equipped with a monochromatic Al Ka X-ray source operating at 350 W. The neutralizer was used with an emission of 1 μA to inhibit charging of the samples. All the spectra were calibrated to a C1s peak at 284.8 eV. For each sample measured, multiple survey scans were taken, on different spots, with a pass energy of 187.85 eV.

Matrix Assisted Laser Desorption/Ionization (MALDI)

MALDI spectra were recorded on an ABI Voyager DE-Pro MALDI ToF (Applied Biosystems) instrument operating in the positive reflector mode. The mass spectrometer parameters were

set as recommended by the manufacturer and adjusted for optimal acquisition performance. The mass spectra data were acquired from averaging of 300 laser shots over a m/z range of 100-20000 Da. The solution of matrix CHCA (10 mg/mL) was prepared in ethanol. Sample was prepared by dissolving solid pDA powder in DMSO. Matrix solution was dropped onto the target plate and allowed to dry. A droplet of sample was pipetted on the plate and air-dried. Before analysis, matrix solution was added to the target plate and allowed to air dry.

3.3 Results & Discussion

We performed our SMFS measurements directly on pDA films deposited on Si_3N_4 AFM cantilevers (Fig. 1b, and Supplementary Fig. S3). In a typical experiment, pDA coated AFM cantilevers were approached onto uncoated or pDA coated substrates and then retracted while measuring the deflection of the cantilever (Fig. 1a), from which the adhesive interaction between pDA and a substrate, or between pDA and pDA, could be ascertained. A characteristic feature of the force-distance (F-D) traces for the case of interaction between a pDA coated cantilever and a bare TiO_2 substrate was the presence of variable-length plateaus of constant force punctuated by stepwise reduction in interaction force during retraction, i.e. a 'step-wise plateau' pattern (Fig. 1c). Such behavior was initially surprising given that stretching of single polymer chains with an AFM probe typically produces qualitatively different F-D curves that reflect the entropic resistance to polymer chain extension.[14] In numerous studies, however, regions of constant force plateau have been observed for cases of pulling a polymer chain out of its single crystal or force-induced peeling of weakly adsorbed biomacromolecules and polyelectrolytes from substrates.[23–28] In the latter cases, force plateaus were attributed to the rupture mode in which individual bonds connecting the molecules to the surface break in quick succession.[29] In most F-D curves obtained from pDA in contact with TiO_2, we typically observed 1-3 plateaus separated by 'steps', which we interpreted as originating from bridging of one or more pDA chains between the cantilever and substrate surfaces (Fig. 1d). At short separation distances in particular, multiple chains are being peeled off the surface simultaneously as the cantilever is retracted, and thus, the force required to detach the chains is higher (2^{nd} and 3^{rd} peaks in Fig. 1e). Since the pickup-up location could be at any point along the polymer chain and if we assume a statistical distribution of polymer chain molecular weights, detachment of the multiple bridging polymer chains at the same distance is considered to be unlikely. Thus, upon retraction of the cantilever, detachment of chains bound to the surface through variable adsorption lengths will result in abrupt steps in the F-D trace, with the 'step' height between force plateaus representing the magnitude of the interaction force between the pDA chain and the surface. A histogram of rupture force representing more than a thousand unbinding events indicated a trimodal distribution as shown in Fig. 1e, consistent with the above interpretation in which multiple pDA molecules initially tethered the cantilever to the surface. Table 1 lists the average unbinding forces for the 1^{st}, 2^{nd} and 3^{rd} steps, from which a mean desorption

force (i.e. 'step' height) of 93 ± 13 pN was observed.

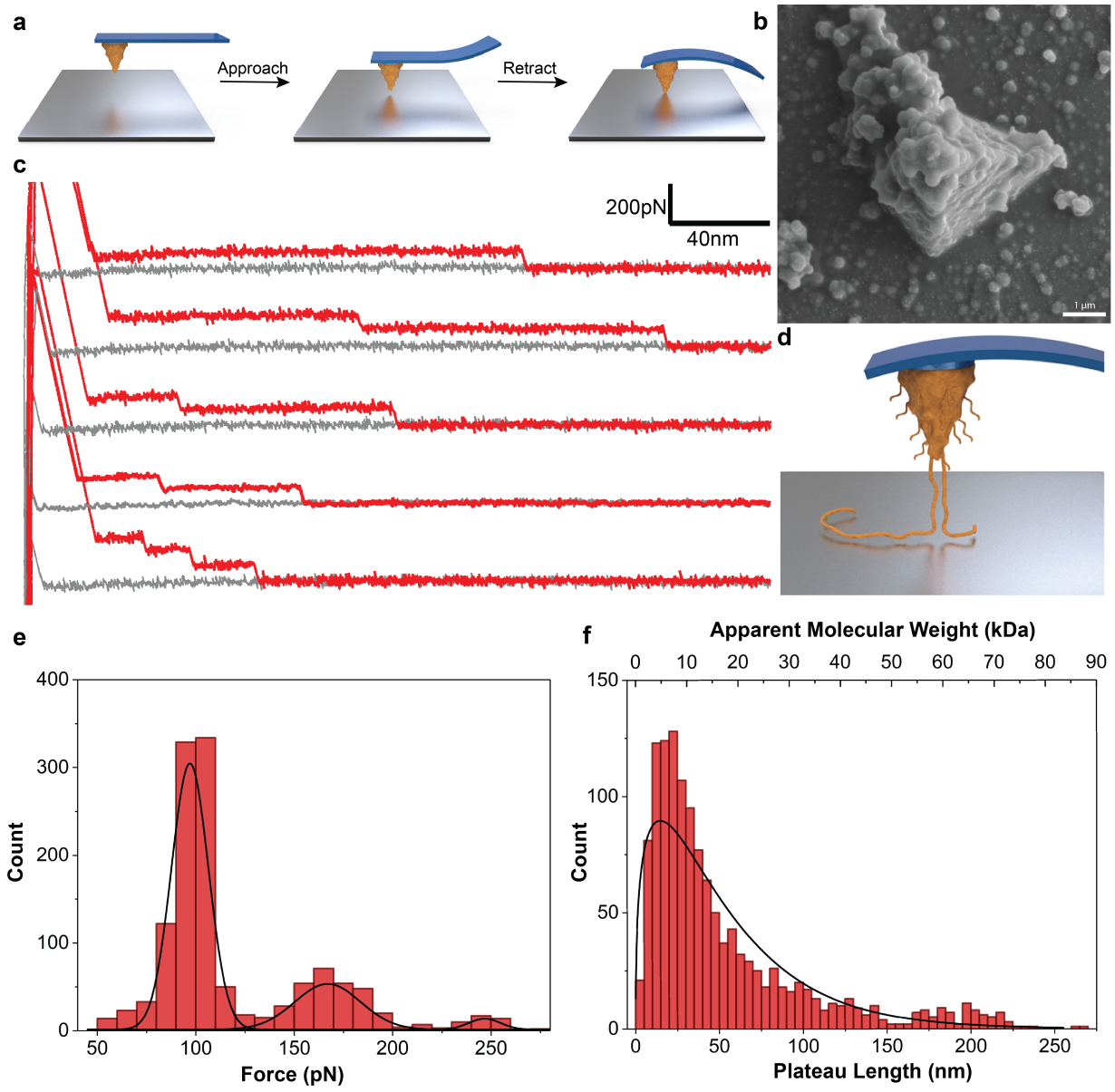

Figure 3.1: Peeling of polymer chains in SMFS. a, Schematic of the SMFS experiments showing a pDA coated cantilever approaching onto a bare substrate and deflecting when in contact with the surface. b, SEM image of a pDA coated cantilever. c, F-D traces showing plateaus of constant force. d, Schematic showing peeling off polymer chains from the surface upon retraction of the cantilever. e, Distribution of peeling force obtained by measuring the height of plateaus. f, Distribution of plateau length and the corresponding apparent molecular weight values.

Table 3.1: Statistical analysis of the step-wise plateau behavior observed in SMFS

Plateau Force (pN)			**Plateau Length (nm)**	**Molecular Weight (kDa)**
1st Peak	**2nd Peak**	**3rd Peak**	**Median**	**Median**
97 ± 12	167 ± 18	245 ± 14	34	11.2

Further analysis of the F-D curves provided important insights into the molecular weight of pDA. Previously, Gaub and coworkers have elegantly shown the capabilities of SMFS to investigate molecular weight of polymers by comparing the distribution of plateau lengths obtained from F-D traces with the distribution obtained by GPC measurements.[30, 31] Using a similar analysis, the plateau lengths from our raw data can likewise be used to characterize the contour length of individual pDA molecules, provided we assume a molecular structure for the pDA repeat unit. For example, if we assume pDA to be a linear polymer formed by aryl coupling of aromatic rings as proposed by Liebscher and coworkers[12] (Supplementary Fig. S1), we estimate 4.5 Å and 149 $g.mol^{-1}$ for the length and mass of a monomeric unit in the pDA molecule. Using this approach, the distribution of measured plateau lengths was converted to a distribution of chain lengths and molecular weights as shown in Fig. 1f, with average values listed in Table 1. The distribution resembled what is usually observed for a polydisperse polymer with an average mass of 11.2 kDa, with the notable presence of a significant fraction of pDA having masses and contour lengths well above 50 kDa and 150 nm, respectively.

In a few percent ($\sim 1\%$) of F-D curves obtained for pDA on TiO_2 we noted with great interest the presence of spikes (Langevin events) located in the midst of the constant force plateau behavior described above (Fig. 2a). The Langevin events had the appearance of classic entropic polymer chain stretching culminating in detachment and could be fitted to the worm-like chain (WLC) model of polymer chain elasticity using a persistence length of approximately 0.5 nm, confirming that they originated from a single-molecule stretching event. The forces required to rupture the interactions at the sticky points ranged from 200-800 pN, with some values as high as 1000 pN (Fig. 2b). Interestingly, these forces are similar to those measured by others using SMFS for interaction of a single DOPA amino acid or DOPA containing dipeptide with a TiO_2 surface.[32–35] However, in contrast to these previous studies where the composition of the molecular species was known, here we have performed SMFS on a heterogeneous polymer with an unknown assortment of functional groups that may include catechol, quinone, indoles and amines. It is also possible that the stronger interactions at sticky points arise from cooperative effects of neighboring repeat unit functional groups.[28, 35] Thus, without more information on the exact chemical composition of pDA we are unable to unequivocally attribute the stretching events at sticky points to any particular functional group. Nevertheless, we conclude from the F-D curves that the observed behavior represents detachment of a polymer that is bound to the surface by strong

interactions at randomly located sticky sites, but which is otherwise bound to the substrate along most of its contour length by comparatively weaker interactions.

An important implication of the observation of WLC fitting of the F-D curves and ability of pDA molecules to withstand applied forces as high as 1000 pN at the sticky points, is that these force values are well above the expected threshold for rupture of noncovalent interactions under the conditions of our experiments.[14, 36, 37] Thus, models of pDA structure that involve primarily non-covalent connectivity between subunits are inconsistent with our findings, as such interactions cannot withstand these force levels. Indeed, our data and interpretations are consistent with a covalent polymer model for pDA such as that proposed by Liebscher et al.[12] in which oxidative polymerization of dopamine culminates in the formation of a linear polymer chain containing covalently linked aromatic repeat units comprised of a mixture of catechol, quinone, indole and amine functional groups.

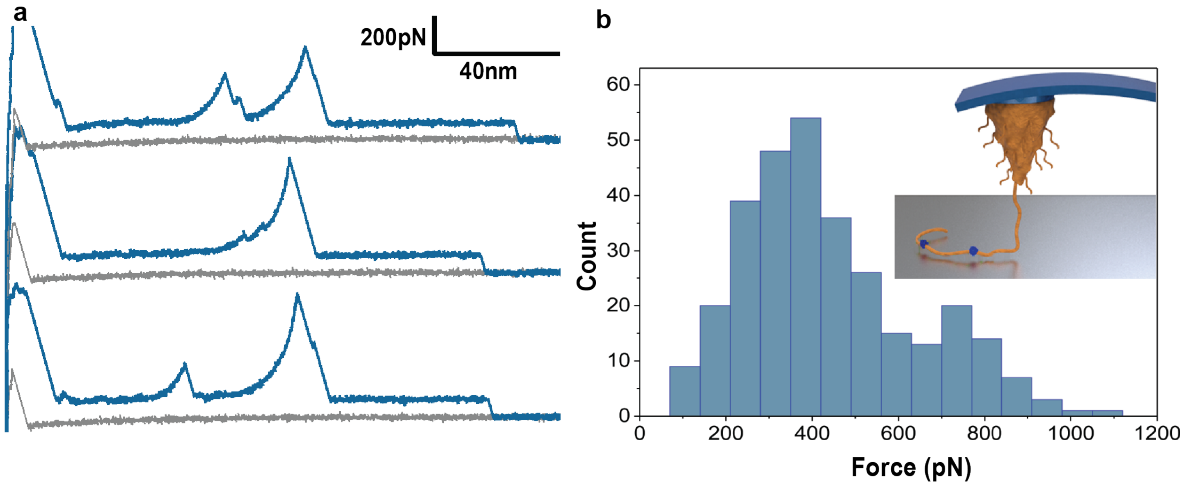

Figure 3.2: Stretching of polymer chains along sticky locations. a, Representative F-D traces showing stretching events in the middle of plateaus. b, Histogram showing the unbinding force of stretching events (N=306). Inset shows schematic visualization of a pDA polymer chain adsorbed to a surface via mostly weak interactions along its contour length with occasional strong interactions with the surface (indicated in blue). Given the heterogeneous nature of pDA, the origins of the strong interactions at sticky points are unknown, but could represent catechol, quinone or other functional groups known to be present in pDA.

To probe the intermolecular interactions between pDA molecules, we also performed experiments where a pDA coated cantilever was approached against a pDA coated substrate (Fig. 3a). Regions of constant force plateaus were observed, likely resulting from progressive rupture of intermolecular interactions between pDA molecules. Increasing the dwell time from 1 to 5 seconds led to stepwise rupture events in the F-D traces occurring at similar

separation distances during successive pulling cycles (Fig. 3b, and Supplementary Fig. 6), indicating that during mechanical relaxation the chains rapidly rebind together. Similar behavior has been observed during mechanical manipulation of amyloid fibrils and RNA molecules.[38–40] In our case, we believe that a bundle of pDA molecules dissociates from either the tip or the substrate surface and the unzipped subunits rapidly rebind to the surface prior to the subsequent mechanical cycle. Such a rapid, cooperative process can be facilitated by the high local concentration of binding sites that participate in intermolecular interaction between pDA molecules. Conceivably, similar interactions could take place during formation of pDA and be an important mechanism driving deposition of pDA coatings on solid surfaces from precursors in solution.

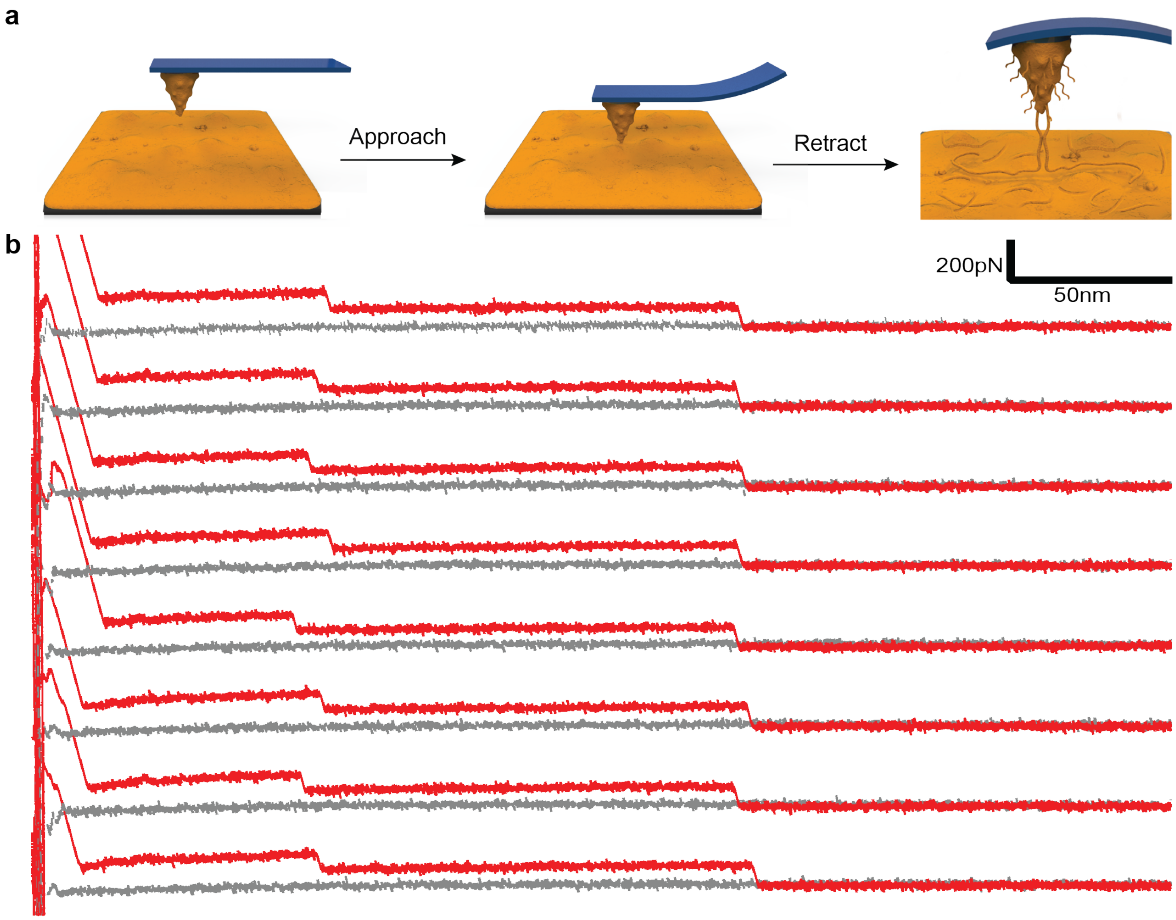

Figure 3.3: Intermolecular interactions between pDA molecules. a, Schematic of experiments showing a pDA coated cantilever approaching a pDA coated substrate. b, The F-D traces shown represent eight successive traces obtained during approach of a pDA coated cantilever onto a pDA coated substrate.

Finally, in order to demonstrate polymer growth during pDA film deposition we performed a unique in-situ time-dependent SMFS experiment in which F-D curves were collected during the early stages of pDA formation. In these experiments, the liquid cell of the AFM chamber was filled with a freshly prepared DA monomer solution and F-D curves collected continuously over a period of several hours (Fig. 4a). We detected pDA polymers on the surface soon after initiating the experiment, evident in the form of short plateaus in the F-D curves, which qualitatively increased in length with time (Fig. 4b). We attributed this behavior to the formation and peeling of short pDA chains adsorbed on the surface of the cantilever and/or substrate. As polymerization progresses, these adsorbed species can further react together through covalent interactions resulting in appearance of longer force plateaus due to chain extension. Unfortunately, this experiment was restricted to the very early stages of pDA formation, as pDA particle formation in solution ultimately interfered with laser detection as evidenced by unstable baselines in length with time (Fig. 4b). Nevertheless, the results observed are in agreement with previous studies of the early stages of pDA coating formation,[41, 42] where small molecule precursors of pDA initially adsorb on the surface followed by subsequent chain growth and supramolecular assembly at the solid-liquid interface.

3.4 Conclusions

In summary, we have been able to apply the SMFS technique towards investigation of pDA and its highly debated polymeric nature. Results showed that pDA films contain high molecular weight polymer chains with covalently connected subunits. Interactions of the pDA chains with titanium oxide is generally weak, although some subunits interact with the oxide surface through medium to high strength ($\sim$200-800 pN). The data confirm the existence of polymers in pDA, although the presence of additional small molecule and oligomer components cannot be ruled out by these experiments. Intramolecular interactions among pDA chains are weak and reversible non-covalent interactions. In addition, time dependent force spectroscopy during the early stages of pDA formation revealed that pDA chain growth occurs at the solid-liquid interface, where film formation likely starts with adsorption of small oligomeric species that undergo further polymerization and maturation to form higher molecular weight pDA chains.

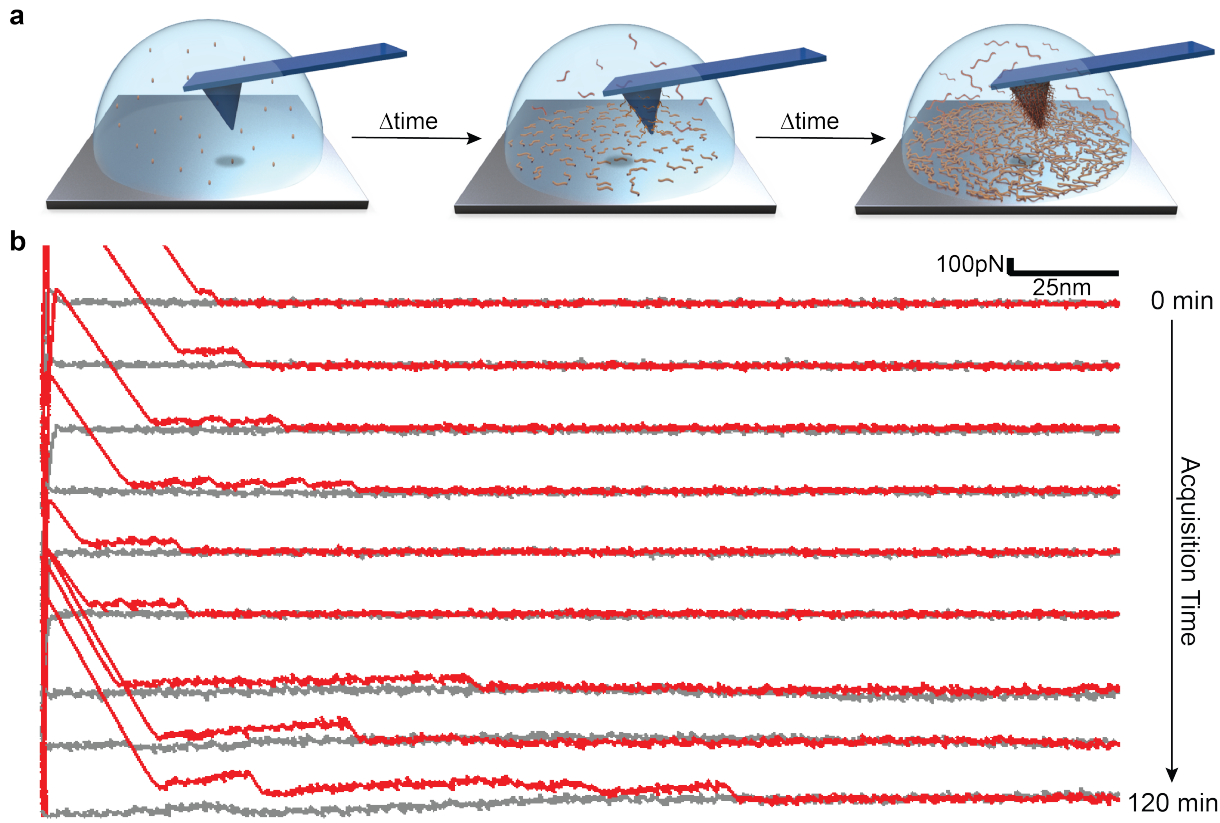

Figure 3.4: in-situ time dependent SMFS during pDA formation. a, Schematic of the in-situ experiments whereby the AFM liquid cell was filled with freshly prepared monomer solution (2 mg/ml DA.HCl in 100 mM bicine buffer at pH 8.5) and force spectroscopy was performed during the first two hours of pDA formation b, Representative F-D traces collected during in-situ polymerization of pDA; after two hours, particles formed in the solution and possibly also pDA deposition on the cantilever mirror surfaces interfered with the reflection of the laser light, making further measurements impossible.

3.5 Supplementary Figures

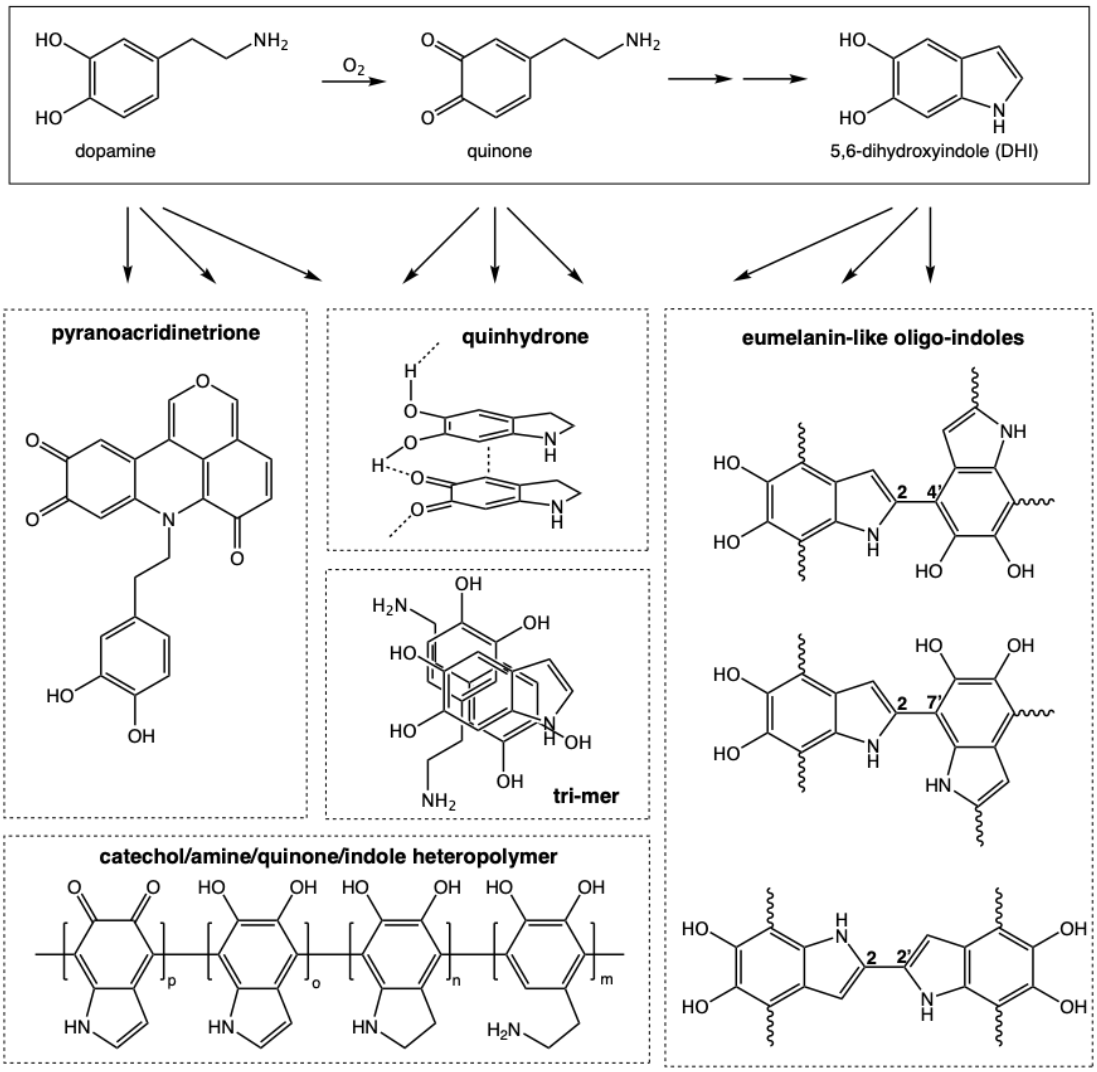

Figure S3.1: Current theories of polydopamine structure and formation. Auto-oxidation of dopamine leads to the formation of dopamine-quinone and 5,6-dihydroxyindole. Proposed mechanisms for polydopamine formation range from noncovalent self-assembly of subunits to form quinhydrone or trimer assemblies, and covalent coupling of subunits to yield a catecholamine/quinone/indole heteropolymer or eumelanin-like oligo-indoles. Adapted with permission from [43–45]. Copyright 2013 American Chemical Society, 2014 American Chemical Society, and 2012 WileyVCH.

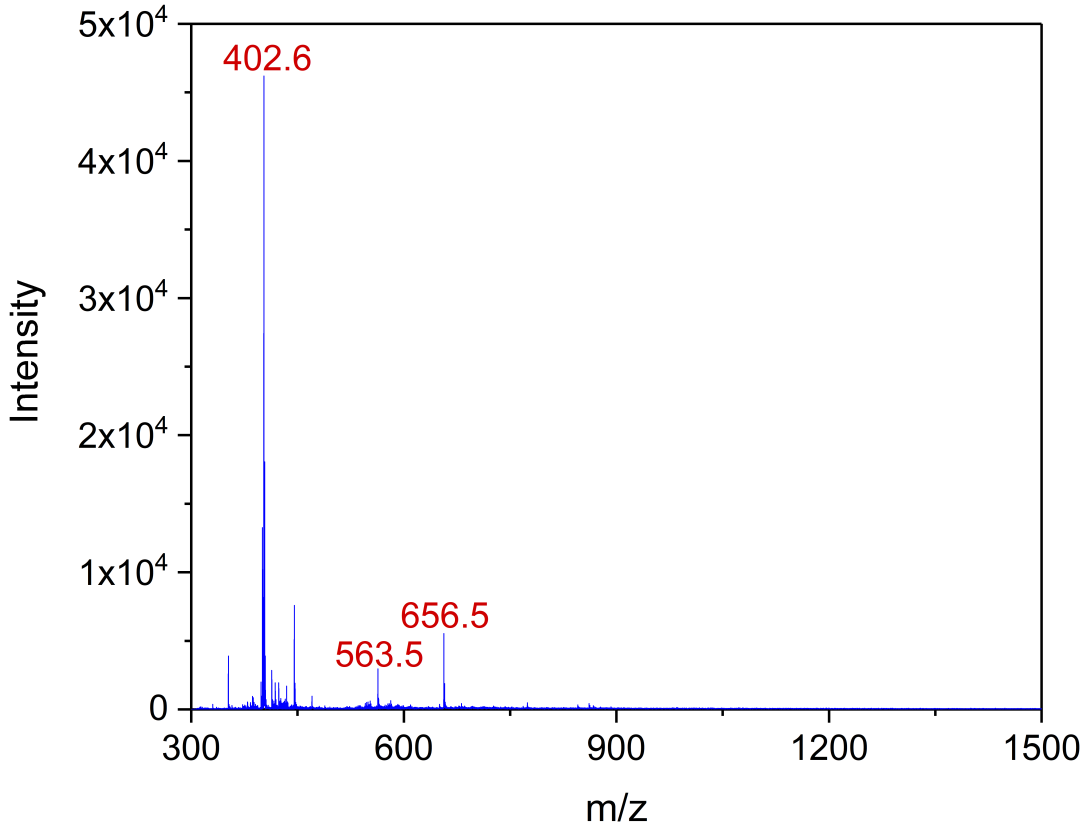

Figure S3.2: MALDI mass spectrum of pDA particles. Primary building block of pDA at m/z 402.6 was observed as previously reported in literature.[45, 46] No major fragment was collected at m/z values of 700 or above.

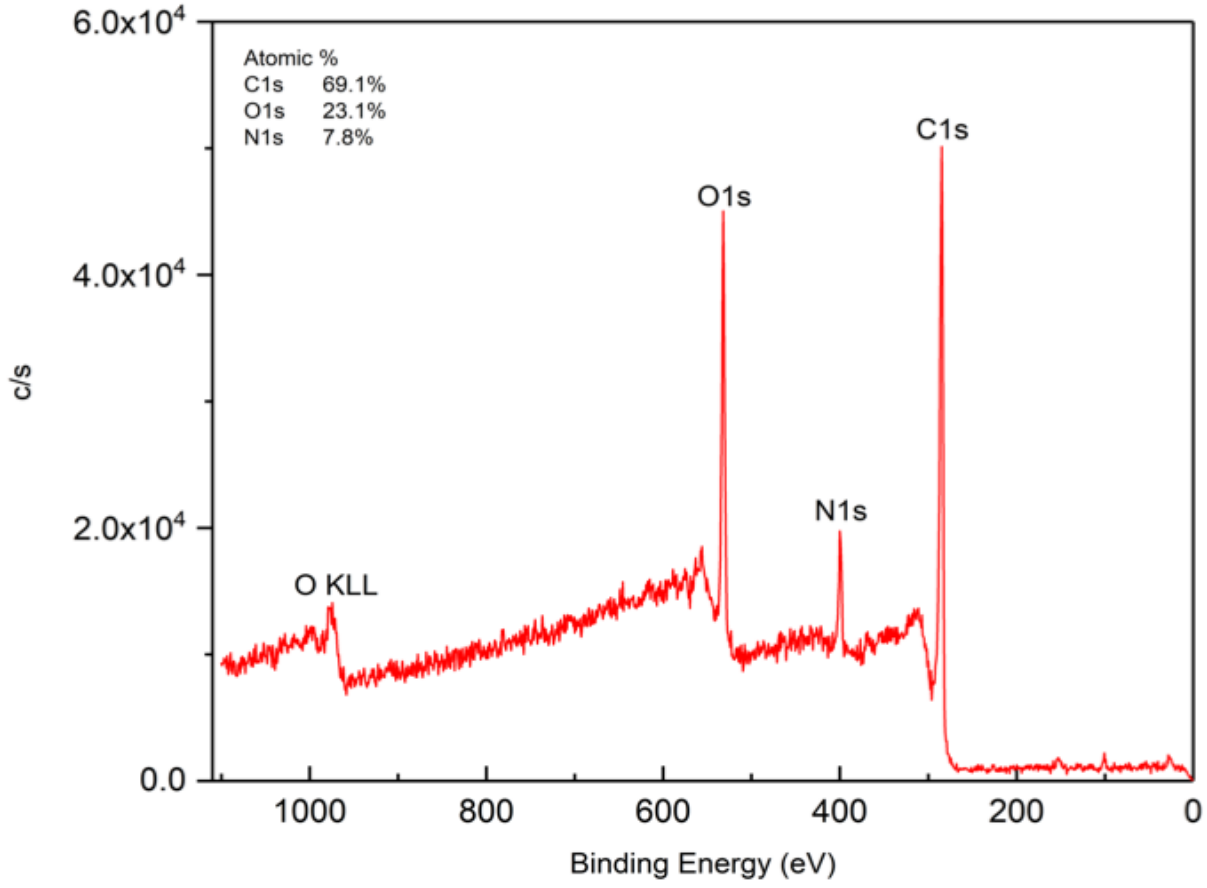

Figure S3.3: XPS spectrum of the pDA coated cantilever.

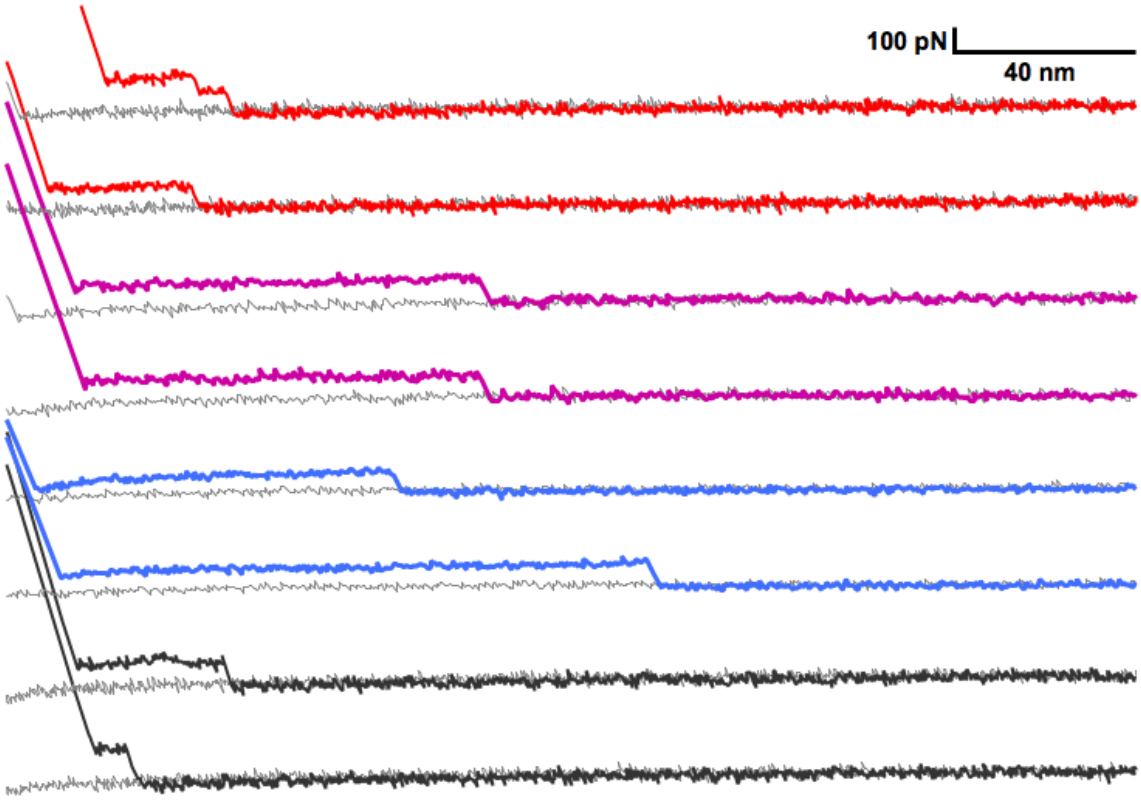

Figure S3.4: F-D traces for approach of a bare AFM cantilever onto pDA-coated substrates; mica (red), SS (purple), TiO_2 (blue), and SiO_2 (black). Force spectroscopy experiments were performed on the pDA-coated substrates to confirm that the features observed in the F-D curves are independent of the underlying substrate. In these experiments a bare AFM cantilever was approached against pDA-coated substrates and F-D traces were recorded. As shown in the figure, we observed plateaus of constant force for pDA-coated mica, SS, TiO_2, and SiO_2.

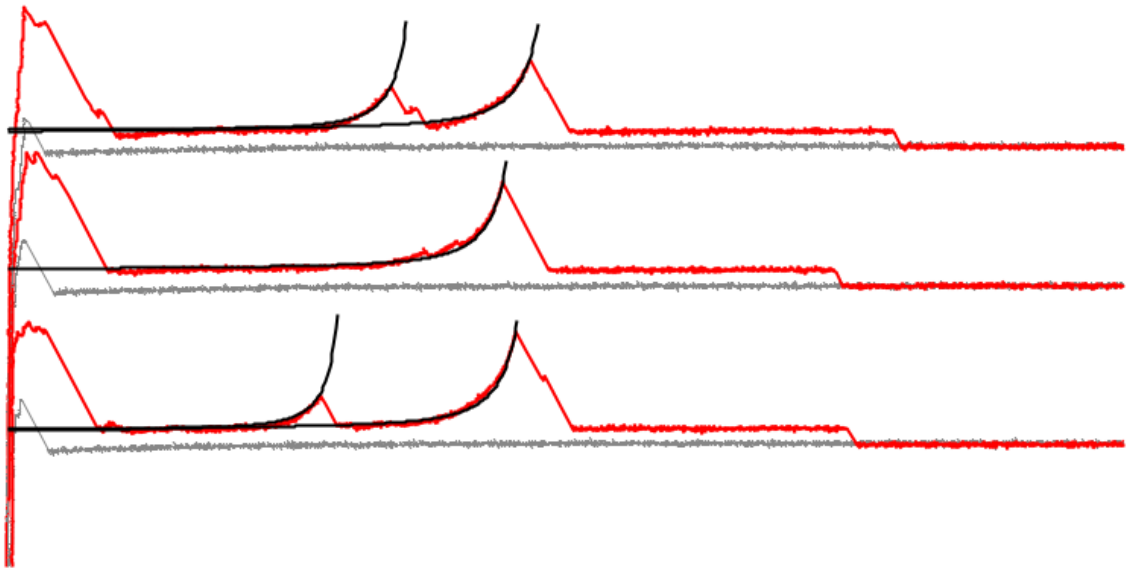

Figure S3.5: Fitting of the stretching events with polymer chain elasticity model. Stretching events have been fitted with a Worm-like Chain (WLC) model, yielding a persistence length of about 0.5 nm consistent with the values reported for stretching a single polymer molecule in water. No previous studies have been done to measure persistence length for pDA chains; however, previous reports have shown values of 0.38 nm or less for PEG,[47] 0.38 nm for amyloid fibers,[48] 0.4-0.6 for ssDNA and RNA,[49–51] 0.37 nm for PS, [52] and 0.4 for polyproteins and polypeptides.[47, 53]. The data has been fitted with WLC model according to the following equation where F is the applied force, p is the persistence length, k is the Boltzmann constant, L_c is the contour length, and T is the absolute temperature.

$$F = \frac{kT}{p} \times \left(\frac{1}{(4(1-\frac{x}{L_c})^2}\right) - \frac{1}{4} + \frac{x}{L_c}\right)$$

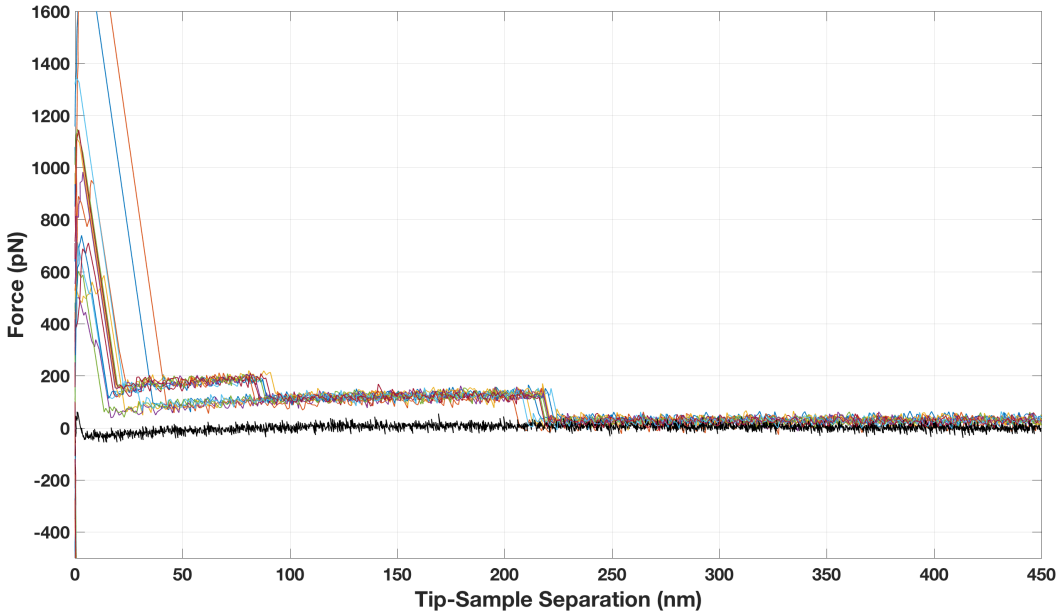

Figure S3.6: Cohesive and intermolecular interactions between the pDA molecules. The superposition of the successive F-D curves obtained upon approach of a pDA coated AFM cantilever onto a pDA coated TiO_2 substrate with a piezo speed of 100 nm/s and a dwell time of 5 seconds. The presence of superimposable features indicates that the unzipped subunits can rapidly rebind to the surface prior to the subsequent mechanical cycle once given sufficient time.

References

[1] D. R. Dreyer et al. "Elucidating the Structure of Poly(dopamine)". In: *Langmuir* 28.15 (2012), pp. 6428–6435 (cit. on pp. 53, 54).

[2] N. F. Della Vecchia et al. "Building-Block Diversity in Polydopamine Underpins a Multifunctional Eumelanin-Type Platform Tunable Through a Quinone Control Point". In: *Advanced Functional Materials* 23.10 (2013), pp. 1331–1340 (cit. on pp. 53–56).

[3] U. G. K. Wegst et al. "Bioinspired structural materials". In: *Nature Materials* 14.1 (2015), pp. 23–36 (cit. on p. 54).

[4] B. P. Lee et al. "Mussel-Inspired Adhesives and Coatings". In: *Annual Review of Materials Research, Vol 41* 41 (2011), pp. 99–132 (cit. on p. 54).

[5] G. P. Maier et al. "Adaptive synergy between catechol and lysine promotes wet adhesion by surface salt displacement". In: *Science* 349.6248 (2015), pp. 628–632 (cit. on p. 54).

[6] H. Lee et al. "Mussel-inspired surface chemistry for multifunctional coatings". In: *Science* 318.5849 (2007), pp. 426–430 (cit. on p. 54).

[7] J. H. Ryu, P. B. Messersmith, and H. Lee. "Polydopamine Surface Chemistry: A Decade of Discovery". In: *Acs Applied Materials Interfaces* 10.9 (2018), pp. 7523–7540 (cit. on p. 54).

[8] M. L. Alfieri et al. "Structural Basis of Polydopamine Film Formation: Probing 5,6-Dihydroxyindole-Based Eumelanin Type Units and the Porphyrin Issue". In: *ACS Appl Mater Interfaces* 10.9 (2018), pp. 7670–7680 (cit. on pp. 54, 55).

[9] Y. H. Ding et al. "Insights into the Aggregation/Deposition and Structure of a Polydopamine Film". In: *Langmuir* 30.41 (2014), pp. 12258–12269 (cit. on pp. 54, 55).

[10] S. Hong et al. "Non-Covalent Self-Assembly and Covalent Polymerization Co-Contribute to Polydopamine Formation". In: *Advanced Functional Materials* 22.22 (2012), pp. 4711–4717 (cit. on pp. 54, 55).

[11] Seonki Hong et al. "Progressive fuzzy cation- assembly of biological catecholamines". In: *Science Advances* 4 (2018), eaat7457 (cit. on pp. 54, 55).

[12] J. Liebscher et al. "Structure of Polydopamine: A Never-Ending Story?" In: *Langmuir* 29.33 (2013), pp. 10539–10548 (cit. on pp. 54, 55, 59, 60).

[13] Xi Zhang, Chuanjun Liu, and Zhiqiang Wang. "Force spectroscopy of polymers: Studying on intramolecular and intermolecular interactions in single molecular level". In: *Polymer* 49.16 (2008), pp. 3353–3361 (cit. on p. 55).

[14] H. Clausen-Schaumann et al. "Force spectroscopy with single bio-molecules". In: *Current Opinion in Chemical Biology* 4.5 (2000), pp. 524–530 (cit. on pp. 55, 57, 60).

[15] Yi Cao and Hongbin Li. "Polyprotein of GB1 is an ideal artificial elastomeric protein". In: *Nat Mater* 6.2 (2007), pp. 109–114 (cit. on p. 55).

[16] V. T. Moy, E. L. Florin, and H. E. Gaub. "Intermolecular Forces and Energies between Ligands and Receptors". In: *Science* 266.5183 (1994), pp. 257–259 (cit. on p. 55).

[17] M. Rief, H. Clausen-Schaumann, and H. E. Gaub. "Sequence-dependent mechanics of single DNA molecules". In: *Nat Struct Biol* 6.4 (1999), pp. 346–9 (cit. on p. 55).

[18] D. J. Muller et al. "Force probing surfaces of living cells to molecular resolution". In: *Nat Chem Biol* 5.6 (2009), pp. 383–90 (cit. on p. 55).

[19] J. S. Kim et al. "Mechanically Stretching Folded Nano-pi-stacks Reveals Pico-Newton Attractive Forces". In: *Advanced Materials* 21.7 (2009), pp. 786–789 (cit. on p. 55).

[20] L. F. Milles et al. "Molecular mechanism of extreme mechanostability in a pathogen adhesin". In: *Science* 359.6383 (2018), pp. 1527–1532 (cit. on p. 55).

[21] Z. Huang et al. "Injectable dynamic covalent hydrogels of boronic acid polymers cross-linked by bioactive plant-derived polyphenols". In: *Biomater Sci* 6.9 (2018), pp. 2487–2495 (cit. on p. 55).

[22] M. Fujihira et al. "A novel cleaning method of gold-coated atomic force microscope tips for their chemical modification". In: *Ultramicroscopy* 82.1-4 (2000), pp. 181–191 (cit. on p. 56).

[23] K. Liu et al. "Extracting a single polyethylene oxide chain from a single crystal by a combination of atomic force microscopy imaging and single-molecule force spectroscopy: toward the investigation of molecular interactions in their condensed states". In: *J Am Chem Soc* 133.10 (2011), pp. 3226–9 (cit. on p. 57).

[24] C. Friedsam et al. "Adsorption of polyacrylic acid on self-assembled monolayers investigated by single-molecule force spectroscopy". In: *New Journal of Physics* 6 (2004) (cit. on p. 57).

[25] L. Sonnenberg et al. "AFM-based single molecule force spectroscopy of end-grafted poly(acrylic acid) monolayers". In: *Macromolecules* 39.1 (2006), pp. 281–288 (cit. on p. 57).

[26] S. Manohar et al. "Peeling Single-Stranded DNA from Graphite Surface to Determine Oligonucleotide Binding Energy by Force Spectroscopy". In: *Nano Letters* 8.12 (2008), pp. 4365–4372 (cit. on p. 57).

[27] F. S. Ruggeri et al. "Identification and nanomechanical characterization of the fundamental single-strand protofilaments of amyloid alpha-synuclein fibrils". In: *Proceedings of the National Academy of Sciences of the United States of America* 115.28 (2018), pp. 7230–7235 (cit. on p. 57).

[28] J. J. Wang et al. "Influence of Binding-Site Density in Wet Bioadhesion". In: *Advanced Materials* 20.20 (2008), pp. 3872–3876 (cit. on pp. 57, 59).

[29] M. A. Nash and H. E. Gaub. "Single-Molecule Adhesion of a Stimuli-Responsive Oligo(ethylene glycol) Copolymer to Gold". In: *Acs Nano* 6.12 (2012), pp. 10735–10742 (cit. on p. 57).

[30] L. Sonnenberg et al. "Choose sides: differential polymer adhesion". In: *Langmuir* 23.12 (2007), pp. 6660–6 (cit. on p. 59).

[31] L. Sonnenberg, L. Billon, and H. E. Gaub. "Competitive adhesion reduces the effective bridging length of polymers". In: *Macromolecules* 41.10 (2008), pp. 3688–3691 (cit. on p. 59).

[32] P. Das and M. Reches. "Revealing the role of catechol moieties in the interactions between peptides and inorganic surfaces". In: *Nanoscale* 8.33 (2016), pp. 15309–15316 (cit. on p. 59).

[33] Y. R. Li et al. "Single-Molecule Force Spectroscopy Reveals Multiple Binding Modes between DOPA and Different Rutile Surfaces". In: *Chemphyschem* 18.11 (2017), pp. 1466–1469 (cit. on p. 59).

[34] H. Lee, N. F. Scherer, and P. B. Messersmith. "Single-molecule mechanics of mussel adhesion". In: *Proceedings of the National Academy of Sciences of the United States of America* 103.35 (2006), pp. 12999–13003 (cit. on p. 59).

[35] Yiran Li et al. "Single-molecule study of the synergistic effects of positive charges and Dopa for wet adhesion". In: *Journal of Materials Chemistry B* 5.23 (2017), pp. 4416–4420 (cit. on p. 59).

[36] M. Grandbois et al. "How strong is a covalent bond?" In: *Science* 283.5408 (1999), pp. 1727–1730 (cit. on p. 60).

[37] Y. Liu et al. "Host-enhanced pi-pi interaction for water-soluble supramolecular polymerization". In: *Chemistry* 17.36 (2011), pp. 9930–5 (cit. on p. 60).

[38] A. Karsai et al. "Mechanical manipulation of Alzheimer's amyloid beta 1-42 fibrils". In: *Journal of Structural Biology* 155.2 (2006), pp. 316–326 (cit. on p. 61).

[39] M. S. Z. Kellermayer et al. "Reversible mechanical unzipping of amyloid beta-fibrils". In: *Journal of Biological Chemistry* 280.9 (2005), pp. 8464–8470 (cit. on p. 61).

[40] N. N. Liu et al. "Pulling Genetic PDAA out of Tobacco Mosaic Virus Using Single-Molecule Force Spectroscopy". In: *Journal of the American Chemical Society* 132.32 (2010), pp. 11036–11038 (cit. on p. 61).

[41] F. Bernsmann et al. "Characterization of Dopamine-Melanin Growth on Silicon Oxide". In: *Journal of Physical Chemistry C* 113.19 (2009), pp. 8234–8242 (cit. on p. 62).

[42] R. A. Zangmeister, T. A. Morris, and M. J. Tarlov. "Characterization of Polydopamine Thin Films Deposited at Short Times by Autoxidation of Dopamine". In: *Langmuir* 29.27 (2013), pp. 8619–8628 (cit. on p. 62).

[43] M. d'Ischia et al. "Polydopamine and Eumelanin: From Structure-Property Relationships to a Unified Tailoring Strategy". In: *Accounts of Chemical Research* 47.12 (2014), pp. 3541–3550 (cit. on p. 64).

[44] S. Hong et al. "Non-Covalent Self-Assembly and Covalent Polymerization Co-Contribute to Polydopamine Formation". In: *Advanced Functional Materials* 22.22 (2012), pp. 4711–4717 (cit. on p. 64).

[45] M. L. Alfieri et al. "Structural Basis of Polydopamine Film Formation: Probing 5,6-Dihydroxyindole-Based Eumelanin Type Units and the Porphyrin Issue". In: *ACS Appl Mater Interfaces* 10.9 (2018), pp. 7670–7680 (cit. on pp. 64, 65).

[46] Y. H. Ding et al. "Insights into the Aggregation/Deposition and Structure of a Polydopamine Film". In: *Langmuir* 30.41 (2014), pp. 12258–12269 (cit. on p. 65).

[47] W. Ott et al. "Elastin-like Polypeptide Linkers for Single-Molecule Force Spectroscopy". In: *ACS Nano* 11.6 (2017), pp. 6346–6354 (cit. on p. 68).

[48] M. S. Z. Kellermayer et al. "Reversible mechanical unzipping of amyloid beta-fibrils". In: *Journal of Biological Chemistry* 280.9 (2005), pp. 8464–8470 (cit. on p. 68).

[49] S. B. Smith, Y. J. Cui, and C. Bustamante. "Overstretching B-DNA: The elastic response of individual double-stranded and single-stranded DNA molecules". In: *Science* 271.5250 (1996), pp. 795–799 (cit. on p. 68).

[50] M. Rief, H. Clausen-Schaumann, and H. E. Gaub. "Sequence-dependent mechanics of single DNA molecules". In: *Nat Struct Biol* 6.4 (1999), pp. 346–9 (cit. on p. 68).

[51] N. N. Liu et al. "Pulling Genetic PDASA out of Tobacco Mosaic Virus Using Single-Molecule Force Spectroscopy". In: *Journal of the American Chemical Society* 132.32 (2010), pp. 11036–11038. ISSN: 0002-7863 (cit. on p. 68).

[52] J. E. Bemis, B. B. Akhremitchev, and G. C. Walker. "Single polymer chain elongation by atomic force microscopy". In: *Langmuir* 15.8 (1999), pp. 2799–2805 (cit. on p. 68).

[53] M. Rief et al. "Single molecule force spectroscopy of spectrin repeats: Low unfolding forces in helix bundles". In: *Journal of Molecular Biology* 286.2 (1999), pp. 553–561 (cit. on p. 68).

Chapter 4

Mechanical Enhancement of Bioinspired Polydopamine Nanocoatings

* This chapter is adapted based on the research originally appeared as a peer-reviewed article co-first-authored by me published in ACS Applied Materials & Interfaces.
K. G. Malollari†, P. Delparastan†, C. Sobek, S. J. Vachhani, T. D. Fink, R. H. Zha, and P. B. Messersmith. ACS Applied Materials & Interfaces 2019, 11, 46, 43599–43607

Abstract

Inspired by the catechol and amine rich adhesive proteins of mussels, polydopamine (pDA) has become one of the most widely employed methods for functionalizing material surfaces, powered in part by the versatility and simplicity of pDA film deposition that takes place spontaneously on objects immersed in an alkaline aqueous solution of dopamine monomer. Despite the widespread adoption of pDA as a multifunctional coating for surface modification, it exhibits poor mechanical performance. Attempts to modify the physical properties of pDA by incorporation of oxidizing agents, crosslinkers or carbonization of the films at ultra-high temperatures have been reported; however, improving mechanical properties with mild post-treatments without sacrificing the functionality and versatility of pDA remains a challenge. Here, we demonstrate thermal annealing at a moderate temperature (130°C) as a facile route to enhance mechanical robustness of pDA coatings. Chemical spectroscopy, x-ray scattering, molecular force spectroscopy and bulk mechanical analyses indicate that monomeric and oligomeric species undergo further polymerization during thermal annealing, leading to fundamental changes in molecular and bulk mechanical behavior of pDA. Considerable improvements in scratch resistance were noted in terms of both penetration depth (32% decrease) and residual depth (74% decrease) for the annealed pDA coating, indicating

the enhanced ability of the annealed coating to resist mechanical deformations. Thermal annealing resulted in significant enhancement in the intermolecular and cohesive interactions between the chains in the pDA structure, attributed to cross-linking and increased entanglements, preventing desorption and detachment of the chains from the coating. Importantly, improvements in pDA mechanical performance through thermal annealing did not compromise the ability of pDA to support secondary coating reactions as evidenced by electroless deposition of a metal film adlayer on annealed pDA.

4.1 Introduction

Mussel adhesive proteins are noteworthy for containing the unusual catecholic amino acid 3,4-dihydroxyphenylalanine (DOPA),[1] which is found in close association with basic amino acid residues (lysine, histidine and arginine) in byssal proteins located near the interface. These observations have led numerous researchers to develop mussel-inspired materials that contain both catechol and amino functional groups for use as adhesives and surface modifiers.[1, 2] Most commonly these take the form of catecholamine synthetic polymers prepared by solution phase polymerization of specialty catechol and amine containing monomers,[3–5] chemical modification of amine polymers with catechols,[6, 7] or by conjugation of sequence specific DOPA-Lys peptides to a synthetic polymer.[8, 9]

The interfacial properties of dopamine, a small molecule analog of catechol and amine-rich mussel adhesive proteins, has been of high interest since it was shown to form coatings on the surfaces of solids.[10] These coatings, commonly referred to as polydopamine (pDA), are spontaneously formed by simple immersion of an organic or inorganic substrate in an aqueous alkaline solution of dopamine (DA) monomer for a period of time ranging from minutes to hours, resulting in a conformal pDA coating of thickness typically 1-100 nm.[10–12] Formation of pDA coatings is believed to involve auto-oxidation of dopamine giving rise to dopamine-quinone, which cyclizes to form dihydroxyindole (DHI), a fundamental building block of pDA.[11] Subsequent events that culminate in the formation of pDA are less well understood and remain an active area of investigation.[13] Most structural models for pDA fall into two distinct categories: the supramolecular model,[14] which describes pDA as arising from weak interactions between monomeric and/or oligomeric subunits, and the open chain model,[15] which more closely resembles a polymer resulting from covalent linking of oxidized and cyclized dopamine monomers. We recently employed the unconventional approach of single molecule force spectroscopy (SMFS) to study the molecular mechanics of pDA films, providing the first direct evidence for high molecular weight covalent polymers in pDA.[16] Considering that pDA likely also contains unpolymerized monomeric or oligomeric species,[17, 18] at this time pDA is best described as being a heterogeneous material that lacks a well-defined chemical structure, unlike most synthetic polymers.

The poorly defined and heterogeneous nature of pDA has not been a significant hindrance to development of practical applications probably due to the simplicity, scalability and versatility of pDA coatings. As a result, pDA has become arguably the most important

translational example of mussel inspired materials, achieving rapid and wide-ranging impact in the interdisciplinary fields of applied chemistry, physics, medicine and engineering.[10, 11, 19] Nevertheless, the technology does have identifiable limitations.[13] For example it is apparent to most researchers that pDA coatings are not mechanically robust and exhibit poor resistance to delamination and abrasion. Several post-processing approaches to altering pDA physical properties involving incorporation of oxidizing agents, cross-linkers or carbonization at high temperatures have been reported,[20–25] however few have focused on improving the mechanical performance of pDA.[20] For instance, annealing of pDA-coated stainless steel substrates at 150°C was shown to enhance the immobilization capacity of the coatings for albumin.[26] Qualitative inspection of heat treated coatings by SEM revealed fewer surface cracks formed upon stretching of the coated substrates, suggesting that the heat treatment might lead to improvements in the coating stability and cohesion.

Herein we investigated thermal annealing at moderate temperatures as a facile route to enhance mechanical robustness of pDA coatings. It has been asserted that as much as ∼20% of pDA is comprised of unpolymerized monomeric or oligomeric species;[17, 18] therefore we hypothesized that thermal annealing may cause reorganization and ordering in the film[27, 28] while simultaneously inducing further polymerization of the unpolymerized monomer and partially polymerized oligomers, leading to substantial enhancements in the mechanical properties of pDA coatings.[29–31] Therefore, the objective of this study was to investigate the mechanical stability of pDA coatings while examining the underlying chemical, structural and molecular changes occurring upon thermal annealing. Our results indicate that significant improvement in the mechanical performance of the coatings can be achieved after a mild post-synthesis heat treatment, further paving the way to more robust pDA coatings with tailorable properties.

4.2 Methods

Materials

Dopamine hydrochloride (99%, Alfa Aesar), sodium metaperiodate ($NaIO_4$, 98%, Alfa Aesar), bicine (99%, Alfa Aesar), sodium hydroxide (NaOH, pellets, Fisher Scientific), Silver Nitrate (99.9% Alfa Aesar), hydrogen peroxide (35 wt% H_2O_2, Acros Organics), sulfuric acid (96%, H_2SO_4, Fisher Scientific), isopropyl alcohol (99.5%, VWR Analytical), acetone (Macron Fine Chemicals), and Simple Green (Sunshine Makers, Inc) were used as received. Quartz coverslips were purchased from Ted Pella, Inc. (Redding, CA). Silicon wafers (SiO_2) with a layer of 100 nm titanium oxide (TiO_2) were obtained from University Wafer, Inc. (Boston, MA). Ultrapure (UP) water was obtained by purification of deionized water with a Barnstead Ultrapure Water Purification System (Thermo Fisher Scientific, Waltham, MA) to a resistivity of 18.2 MΩ cm.

Coating Substrates with pDA

TiO_2 substrates were first degreased with a 3:1 (v/v) mixture of water and Simple Green solution by placing into sonication bath for 15 minutes at ambient temperature (∼22°C). The substrates were then rinsed and sonicated sequentially with water, isopropanol, and acetone, each for 15 minutes, and dried under a stream of nitrogen gas. Prior to immersing in dopamine solution, substrates were exposed to a plasma discharge at 100 W for 5 minutes (Harrick Plasma Cleaner, Ithaca, NY, USA). Quartz slides were cleaned by placing into Piranha solution (H_2SO_4:H_2O_2 70:30 v/v) for 1 hour at ambient temperature and were then rinsed with UP water and dried with nitrogen. The substrates were immersed into 2 mg/ml dopamine hydrochloride in 100 mM bicine buffer at pH 8.5 for 16 hours (20 hours for quartz slides) with constant shaking. The substrates were removed and rinsed extensively with UP water and dried under a stream of nitrogen gas.

pDA-Assisted Electroless Metalization

pDA coated TiO_2 substrates were immersed into 50 mM aqueous silver nitrate solutions for 20 h at room temperature under constant stirring. Surfaces were washed extensively and dried under a stream of nitrogen gas.

pDA Nanoparticle Synthesis

TGA and TGA-MS measurements were performed on pDA particles. Dopamine hydrochloride (2 mg/ml) was dissolved in UP water and the pH was increased to 8.5 by adding 1M NaOH solution. The solution was stirred at 400 rpm for 5 hours at 70°C and subsequently left at ambient temperature for 3 hours without stirring. Finally, the mixture was filtered with PVDF membrane filters with a pore size of 0.1 μm (Durapore VVPP) followed by drying at 50°C under vacuum.

Thermal and Chemical Treatment of pDA

pDA-coated substrates and NPs were annealed for 12 hours (72 hours for quartz slides) at 130°C under vacuum. Ellipsometry, contact angle, and XPS measurements were performed on the samples after allowing them to equilibrate to room temperature. For the chemical stability test, samples were immersed for 2 hours in 1 M aqueous NaOH solution and then removed and rinsed with water and dried under nitrogen gas. For chemical stability test under sonication pristine pDA and annealed pDA coated TiO_2 were sonicated in an aqueous environment (pH∼6.9) at high power for 10 minutes.

X-Ray Photoelectron Spectroscopy (XPS)

The surface chemical composition of pristine and annealed pDA coatings on TiO_2 substrates was measured using X-ray photoelectron spectroscopy (XPS). XPS analyses were performed

on a Perkin Elmer Phi 5600, equipped with a monochromatic Al Ka X-ray source operating at 350 W. The neutralizer accessory was used with an emission of 1 μA to inhibit charging of the samples. All spectra were calibrated to a C1s peak at 284.8 eV. For each sample measured, multiple survey scans were taken at different positions, with a pass energy of 187.85 eV followed by high resolution spectra of C1s, N1s, and O1s with a pass energy of 23.50 eV. Calibrated spectra were fitted with Gaussian functions using OriginPro software. The minimum number of peaks consistent with the best fit were used, while peak position, full width at half maximum, and intensity were also considered during the peak fitting.

UV-Vis Spectroscopy

The UV–Vis absorbance spectra of the pDA-coated quartz slides were taken at a wavelength range of 200-800 nm using a UV2600 spectrophotometer (Shimadzu Scientific Instruments, Kyoto, Japan).

Thermogravimetric Analysis (TGA)/Mass Spectroscopy (TGA-MS)

Thermogravimetric analyses were conducted using a TA Instruments TGA Q5000 and decomposition trace was collected under a flow rate of 25 mL/min N_2 with a temperature ramp rate of 1.5°C/min. TGA-MS performed over a m/z range of 15 to 120 under nitrogen flow using a Perkin Elmer Pyris 1 TGA paired with a Hiden Analytical HPR20 Sampling System.

Ellipsometry

The thickness of the pristine and annealed pDA deposited on the TiO_2 substrates was measured with a spectroscopic ellipsometer (M-2000V, J.A. Woollam, USA). The spectra were fitted with multilayer slab models using CompleteEase software. The TiO_2 layer was fitted with a Cauchy model immediately prior to immersion in the dopamine solution whereas pDA deposits on the TiO_2 were fitted with a B-spline model. For the liquid cell measurements, thickness of the dry coatings in an empty, aligned 500-μL liquid cell were determined at an incidence angle of 70°. Deionized water (room temperature) was then introduced into the cell and the thickness was measured at half-hour increments for 6 hours. Best-fit for coating thicknesses and optical constants were determined from analyzing data with the CompleteEASE software.

Contact Angle

Water contact angle of the coatings on TiO_2 substrates prior and after annealing were measured using a Ramé-Hart goniometer. 6 μL of water was dropped on each sample using the automated drop volume control module and the static contact angle was measured with DropImage software.

GIWAX

GIWAXS was performed at the CMS (11-BM) of the National Synchrotron Light Source II. Silicon wafers with a 100 nm layer of TiO_2 were coated with pDA. Samples were exposed to a beam energy of 13.5 keV ($\lambda = 0.9184\mathring{A}) for 100 seconds at an incidence angle of 0.1°$. 2D scattering patterns were obtained using a square Photonic Sciences CCD detector with a size of 1042×1042 pixels with pixel dimension of 0.1017 mm×0.1017 mm. The sample-to-detector distance was 0.229 m with a detector tilt of -21° and detector orientation of 45°. Raw detector images were converted from (q_x,q_z) to (q_r,q_z) to account for Ewald sphere curvature ("missing wedge correction") using SciAnalysis, a python-based softwate developed by Brookhaven National Lab's CFN- Center for Functional Nanomaterials.[32] Additionally, raw detector images analyzed using Xi-cam software (CAMERA at Lawrence Berkeley National Laboratory) to produce 1D intensity vs. |q| plots in a line along the q_x axis.[33]

Scratch Testing

Nanoscratch tests were performed using Bruker's Hysitron TI-950 triboindenter equipped with a 2-D transducer and a 300 nm conospherical probe. The scratch load function consisted of three distinct segments: a trace segment to determine the surface profile at the site of the scratch, a 6-μm long scratch segment, and a retrace segment to determine the residual deformation after the scratch. Two scratch test load functions were used: one with a constant normal load of 50 μN applied during the scratch and the other with the normal load ramped linearly from 0 to 100 μN during the length of the scratch. Multiple tests (n=8) for each load function were performed on 3 samples of pristine and annealed pDA coatings in order to determine variation between films of the same type as well as between the two types of films tested. In addition, multiple tests (n=8) for each load function were also performed on a TiO_2 control sample. For all scratch tests, a tilt correction was performed on the scratch test data using the trace segment of the load function. Finally, using Hysitron's SPM imaging technique, the surface topography over an area of 15 μm×15 μm was mapped at each test site.

Nanoindentation

Nanoindentation tests were performed using Bruker's Hysitron TI-950 triboindenter equipped with a 2-D transducer and a 300 nm conospherical probe. The tip area function was established from an aluminum standard. All load displacement curves were analyzed using the method described by Oliver and Pharr[34] (50% of the unloading curve was used for analysis). All indentation tests were carried out in an open loop feedback mode under loading rate control. The peak load of approximately 25 μN was used and was held fixed for a period of 3 seconds and load displacement curves were acquired. The slope of the load-displacement curve, upon unloading represents the stiffness, S, evaluated at the maximum indentation

depth h_{max}. The stiffness was used to calculate reduced Young's Modulus E_r using the relationship:

$$E_r = \frac{\sqrt{\pi}}{2}\frac{S}{\sqrt{A_c}}$$

With A_c being the contact area at h_{max}. Finally, the reduced modulus can be expressed as a function of the elastic properties of the system (indenter and sample). Herein a Poisson's ratio of ν=0.35, a typical value for macromolecules, was used.

Single Molecule Force Spectroscopy (SMFS)

Measurements were carried out using a JPK ForceRobot 300 (JPK Instruments AG, Germany) with a tip velocity of 1000 nm/s over a z-piezo distance of 500 nm with a dwell time of 1 second. The experiments were performed in UP water after allowing the cantilever to equilibrate in solution for at least 30 minutes. Soft silicon nitride cantilevers (MLCT from Bruker Nano Inc.) of typical spring constant of 50-60 pN/nm were used for all experiments and calibrated using the equipartition theorem.[35] The force-extension traces were recorded and analyzed using data processing software from JPK and a home-written procedure in IgorPro (Wavemetrics).

4.3 Results & Discussion

To evaluate possible chemical transformations occurring during thermal treatment, X-ray Photoelectron Spectroscopy (XPS) measurements were performed on the pristine and annealed pDA coatings and detailed chemical composition was acquired from the deconvoluted spectra of C1s, N1s and O1s regions. Representative high-resolution spectra are shown in Fig. 1 and the percent contribution of each functional group before and after annealing are presented in Supplementary Fig. S1. The C1s spectrum was fit with four peaks corresponding to CH_x/C-NH_2 (∼284.3 eV), C-O/C-N (∼285.6 eV), C=O (287.7 eV) and π-π^* shake-up (∼291 eV) according to the literature.[36] The O1s region was deconvoluted into two components assigned to O=C (∼531.0 eV) and O-C (∼532.9 eV) species, whereas the N1s region was fit with three peaks attributed to primary (R-NH_2, ∼401.9 eV), secondary (R_2-NH, 399.9 eV) and tertiary/aromatic (=N-R,∼398.8 eV) amine functionalities.[37] After thermal annealing, a 20-25% relative increase in the carbonyl (O=C) content was observed in the C1s and O1s spectra, and a corresponding decrease in the C-O content was observed in the O1s spectrum. The observed conversion of C-O to C=O may be attributed to the oxidation of the phenolic hydroxyls and the formation of quinone species at elevated temperatures.[29, 38–40] The transformation of polar hydroxyl groups to carbonyl species was also apparent in an increase in the water contact angle of the coatings after thermal treatment (Supplementary Fig. S2). The quinone species have been extensively utilized as chemical handles for pDA surface functionalization with nucleophiles through Michael addition or

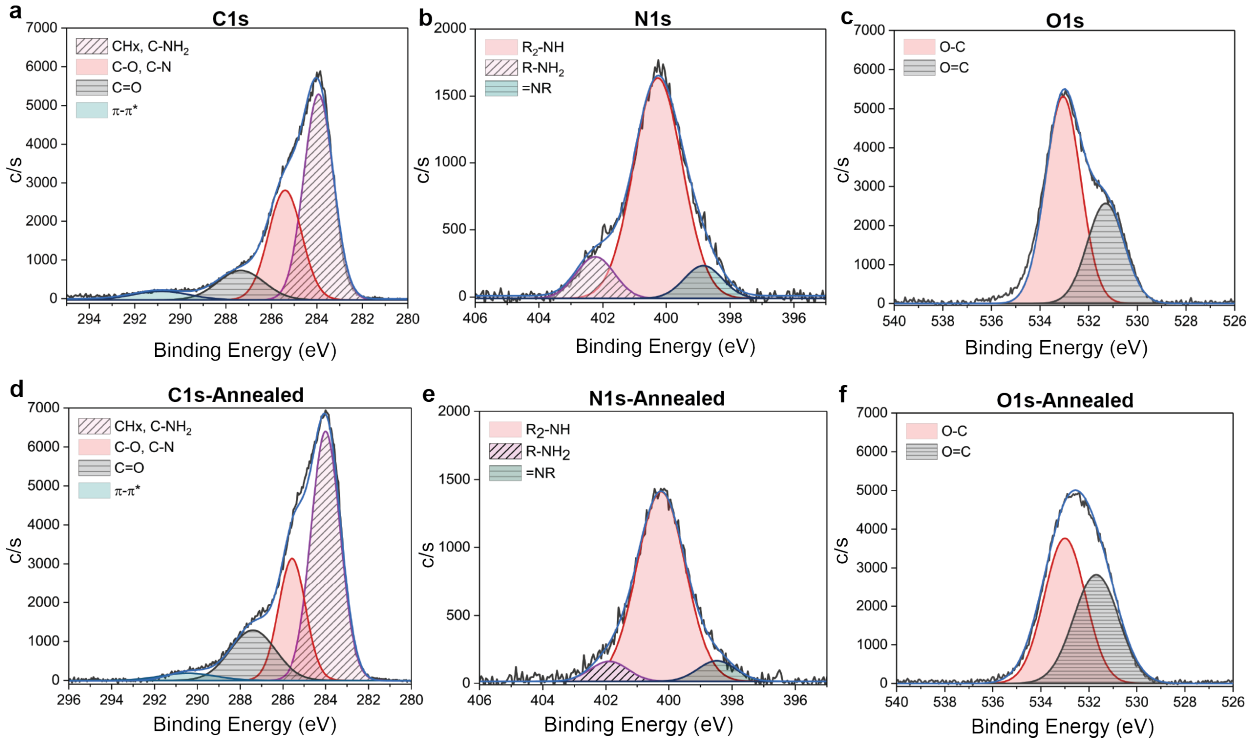

Figure 4.1: XPS elemental composition. Representative raw and deconvoluted high-resolution XPS spectra of C1s, N1s, and O1s for the pristine (a-c) and thermally annealed pDA coatings (d-f).

formation of Schiff bases.[11, 41] Thus, the increase in the carbonyl content after thermal annealing can further enhance the attachment of nucleophiles to the surface and enhance the bioconjugation capacity of the pDA coatings, as demonstrated in previous works.[38] In one example, Luo and colleagues showed that heat treatment of pDA at 150°C increases the concentration of quinone in the coatings and improves its ability to immobilize biomolecules on the surface.[38]

According to recent structural studies of pDA, the primary amine content is attributed to the presence of DA monomer and partially polymerized species (oligo-dopamine, oDA) in the structure whereas the secondary and tertiary amines are associated with the intermediate species of 5,6-dihydroxyindole (DHI) and 5,6-indolequinone (IQ) along with the cyclized amines which are products of DA polymerization.[11, 18] After thermal treatment, we observed a notable decrease (∼35%) in the primary amine content with a corresponding increase in the secondary amine species. This progressive change in the N1s spectrum can be attributed to the presence of a significant amount of uncyclized monomeric and oligomeric species which undergo further polymerization and take part in competitive inter- and intramolecular cyclization, triggering crosslinking reactions in the structure.[20, 29, 40] Indeed,

the idea of thermal treatment of pDA was previously investigated by Proks et al.[42] where they suggested that heat treatment at moderate temperatures (∼100°C) can cause reorientation within the structure due to dehydration, allowing the unreacted amines to cooperate in cyclization and cross-linking reactions resulting in stabilization of the pDA structure. However, we noted that their experiments were performed on solid pDA aggregates collected from the polymerization solution, which have been recently shown to be different from pDA films.[43] In the present study, we evaluated the effects of thermal annealing directly on the pDA films formed on substrates since the coatings have found much broader applications compared to pDA particles.

UV-Vis spectroscopy of the pDA coatings supported our hypothesis that thermal annealing triggers further polymerization of unreacted monomers and partially reacted species. It has been shown previously that absorbance of pDA films is almost a monotonic function of the wavelength, with some discontinuities in the spectrum at around 280 nm and 420 nm attributed to presence of monomeric and oligomeric species present in the pDA coating.[17, 44] Similar features have been detected and assigned to partially polymerized and low molecular weight fractions in melanin.[45] We observed a significant decrease in the intensity of these bands after thermal annealing (Supplementary Fig. S3), suggesting the conversion and further oxidation of oligomeric species present in the pDA structure.

To examine thermal stability of the pDA and to confirm that no chemical degradation occurs upon thermal annealing at 130°C, thermogravimetric analysis (TGA) was carried out within the temperature range of 25-600°C. As shown in Fig. 2a, more than 95% of the pDA mass was retained up to 130°C, with an approximate mass retention of 80% for temperatures up to 400°C. To identify the chemical species evolved upon heating we performed TGA-mass spectroscopy (TGA-MS) experiments. A notable feature of the TGA-MS data was a two-step dehydration centered at 80°C and 280°C, which we believe is related to water loss, as pDA and eumelanin are known to be hygroscopic.[46, 47] The adsorbed water exists in two forms: one in the form of weakly-bound surface water, and another that is more tightly bound.[14, 25, 42, 48, 49] Thus, our results are consistent with the literature and indicate dehydration of the structure and removal of surface and bound water at 80°C and 280°C, respectively. Moreover, a continuous evolution of CO_2 was observed upon heating, which can be attributed to the sample degassing at moderate temperatures and to the partial decomposition of pDA building blocks at elevated temperatures.[42, 50] No evolution of any other fragment in a m/z range of 15 to 120 was observed, indicating that no significant degradation is taking place at the annealing temperature used and the mass loss can be ascribed to dehydration of the pDA structure.

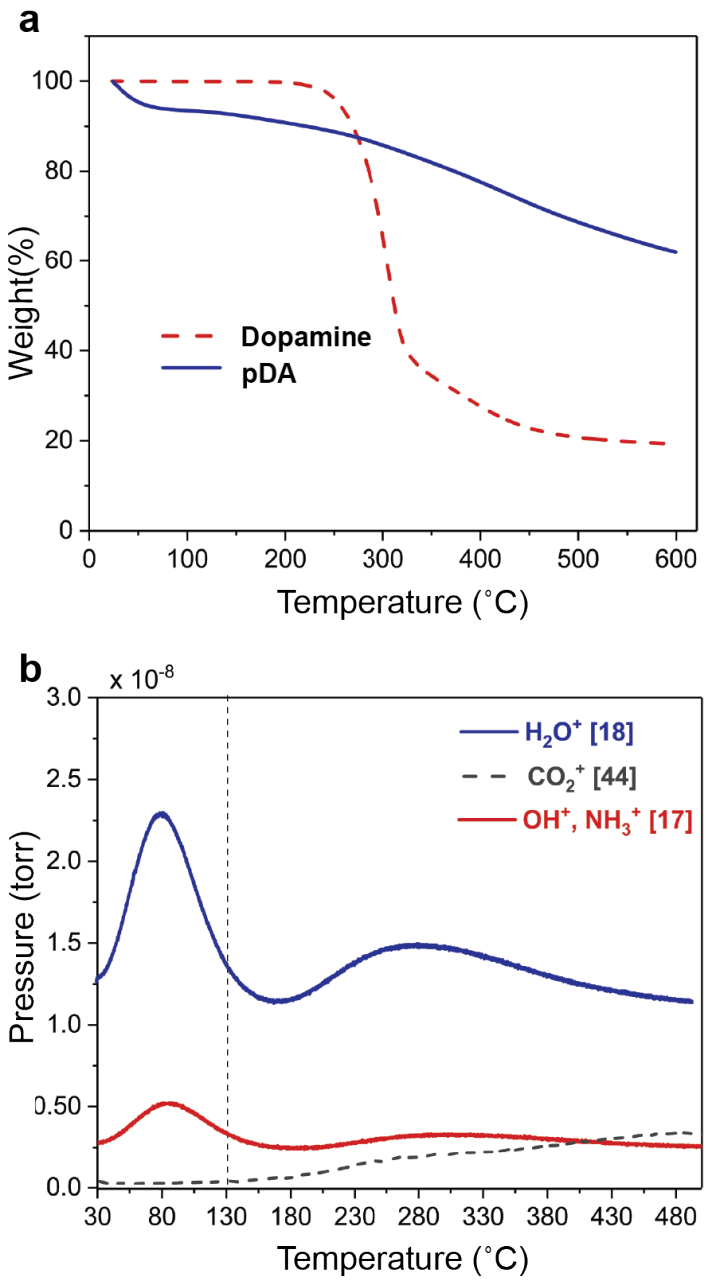

Figure 4.2: Thermal stability of pDA. TGA curve of the pDA showing more than 95% mass retention up to the annealing temperature of 130°C (a); TGA-MS spectrum of the pDA indicating that most of the mass loss at lower temperatures can be attributed to the dehydration (b).

To gauge the effect of thermal annealing on pDA physical properties, the stability of pDA coatings toward dissolution in solvent was measured using ellipsometry. In contrast to

many conventional polymers, pDA is notoriously insoluble in common organic solvents and acidic and neutral aqueous media and is only known to dissolve in strongly alkaline solutions, a characteristic that has been attributed to the deprotonation of catechols and amines in the pDA structure at basic pH causing electrostatic repulsion between subunits resulting in disruption of secondary bonding and intermolecular interactions and, consequently, detachment and/or dissolution of the coatings.[23, 44] In our experiments, the thickness of the pristine pDA coating decreased by more than 80% (from 85 nm to 16 nm) upon immersion in 1M NaOH, whereas we observed only 17% (from 89 nm to 65 nm) decrease in the thickness of the heat treated pDA films under the same conditions (Fig. 3). This sharp difference between near-quantitative removal of pristine pDA coatings and the high retention of the annealed pDA coatings can be associated with the structural changes occurring upon thermal treatment. It is generally accepted that solubility of polymer films is dependent on a number of parameters among which cross-linking density, molecular weight, and crystallinity are major contributors.[51] In this case, results suggest that further polymerization of oligomeric species during annealing leads to additional cross-linking reactions between the polymer chains. The interaction of solvent molecules and polymer chains is hindered in a strongly cross-linked polymer network, preventing the chains from being solubilized. Thus, the effect of thermal annealing was manifested in enhanced chemical stability towards alkaline conditions, a crucial consideration for pDA coatings in practical applications.

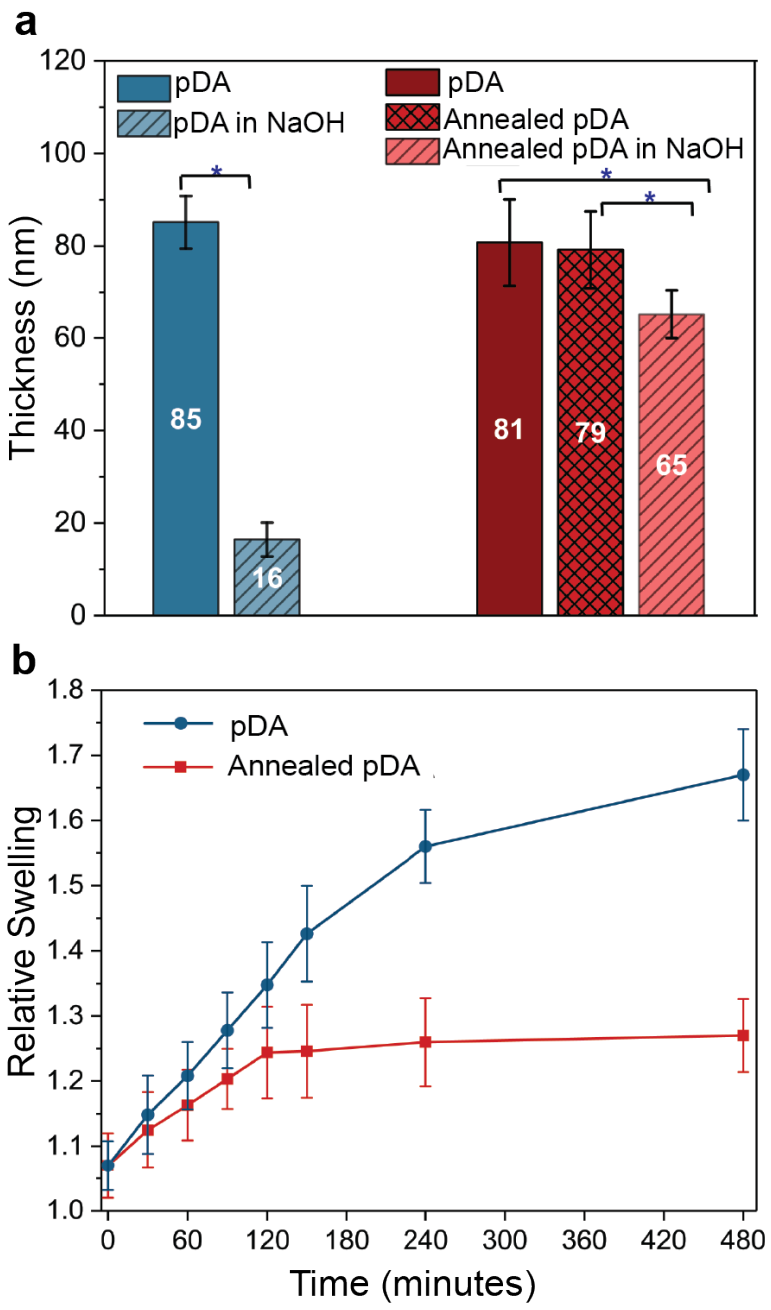

Figure 4.3: Solvent stability and aqueous swelling of pDA films. Ellipsometry measurements showing changes in thickness of the pristine and annealed pDA coatings after incubation in 1M NaOH (2 hours at room temperature) (a). Liquid cell ellipsometry results showing the relative swelling (wet thickness: dry thickness) of pristine and thermally annealed pDA coatings at room temperature in water (b).

To investigate this in more depth, we measured the aqueous swelling of pristine and annealed pDA coatings in-situ using liquid cell ellipsometry. When in contact with a penetrant solvent, the polymer usually swells as the solvent molecules diffuse into the network.[52] However, higher degree of crosslinking limits network expansion and swelling of a polymer film, as the chains are held more tightly together and the free volume is decreased.[53] Fig. 3 shows the relative thickness of the pristine and annealed pDA over time after the addition of water to the sample cell. Results showed that thermally annealed pDA coatings take up less water compared to pristine pDA coatings. Reduced film expansion after annealing may result from a combined effect of the improved structural organization within the coating due to dehydration along with the increased crosslinking which reduces the available volume for water molecules within the coating and exerts further resistance to the film expansion. However, the significant difference in functional group composition and hydrophobicity between pristine and annealed pDA may also suggest different interaction parameters with water, which could play a role in the different equilibrium swelling behavior. To investigate the possible morphological and molecular structural changes in the pDA coatings upon thermal annealing we performed grazing incidence wide angle X-ray scattering (GIWAXS) measurements on the coatings. GIWAXS has been exploited as a powerful tool for investigating the crystalline structure of macromolecules and obtaining information about the texture and phase composition of polymeric thin films.[54] GIWAXS data were collected on pristine and annealed pDA deposited onto TiO_2 substrates. A 2D detector recorded images of scattering along q_z (out-of-plane film normal direction) and q_x (in-plane-film horizontal direction) (Supplementary Fig. S5) which were converted into q_z and q_r (total in-plane momentum transfer) to account for the curvature of the Ewald sphere (Fig. 4a and b). To further unravel the structural changes of pDA coatings prior to and after annealing, 1D intensity along the radial axis were plotted from the converted GIWAXS images (Figure 4c). To the best of our knowledge, no phase transformation occurs during thermal annealing of TiO_2 at 130°C,[55] and thus, any changes observed can be attributed to the pDA structure.

The GIWAXS pattern of pristine pDA coating exhibits a broad amorphous halo at q$\simeq$1.4 $Å^{-1}$ which corresponds to a d-spacing of $\sim$4.4 Å. Upon annealing, the halo shifts to a higher q ($\sim$1.6 $Å^{-1}$), indicating a decrease in the pDA layer spacing (d=3.9 Å), which is more consistent with π-π stacked structures. The removal of adsorbed water during thermal annealing in pDA can lead to a decrease in the d-spacing of the layers. Upon dehydration, pDA chains can reorganize and come closer together leading to an increase in ordering and change in physical properties such as electrical conductivity.[56] Moreover, a broad ring observed at q$\simeq$0.84 $Å^{-1}$ corresponding to a spacing of $\sim$7.5 Å appears in the annealed sample. A similar observation has been made in annealed bulk amorphous polymers, attributed to enhanced ordering of the amorphous domains.[57] This feature can be readily identified in the 1D radial reduction (Fig. 4c) of the annealed sample as a shoulder at q$\simeq$0.84 $Å^{-1}$, which is consistent with peak changes observed during thermal annealing of eumelanin.[48, 56] Earlier studies have suggested the presence of extended layer stacking with a separation of $\sim$3.7-3.8 $Å^{-1}$ in pDA and DHI-based eumelanin, considering them as para-crystalline units with short and medium range order.[48, 49, 58, 59], Therefore, the d-spacing of 7.5 Åin annealed pDA

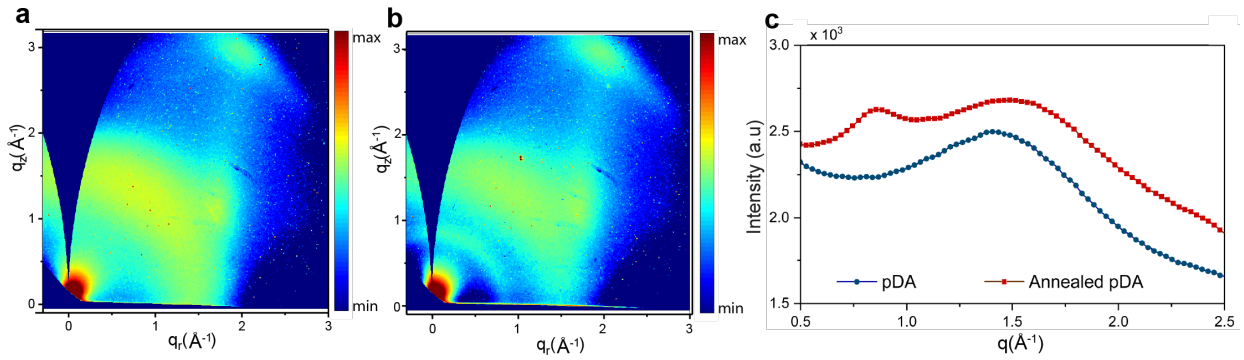

Figure 4.4: GIWAXS scattering patterns. 2D GIWAXS images of pristine pDA (a) and annealed pDA (b) coatings after conversion to q_r (in-plane) and q_z (out-of-plane) scattering vectors, which results for a "missing wedge" that accounts for curvature of the Ewald sphere. 1D radial reductions obtained from the 2D images are shown in (c).

might be ascribed to stacking of three layers of aromatic building blocks. In our case, we observed an intensification in the three-layer stacking signal, which we attributed to better ordering of pDA building block domains.[60] The results obtained indicate a clear difference in molecular structure of pristine and annealed pDA samples and are in a good agreement with previous X-ray diffraction (XRD) studies of melanin-like materials.[56]

One of the main shortcomings of pDA coatings that limits their use in some practical applications is weak mechanical properties. Thus, it was critical to assess whether thermal annealing can improve the mechanical performance of the coatings. Towards this goal, we investigated scratch resistance of pristine and thermally annealed pDA coatings. Scratch testing is one of the most widely used quality assurance techniques for evaluating shear strength and mechanical robustness of coatings and thin films.[61] A typical scratch experiment involves translation of a geometrically precise indenter across the sample surface while subjecting the indenter to a constant or progressive normal load.[62] During the scratch cycle, height profiles for the trace and retrace segments are recorded and can later be analyzed to extract penetration and residual depth values. Penetration depth corresponds to the deformation occurred during trace profile (e.g. mixture of elastic and plastic deformation) while the residual depth is calculated using the retrace profile and can be attributed to the permanent deformation of the sample after the load is removed. Scratch experiments were performed on the pristine and annealed pDA coatings to evaluate the influence of thermal annealing on the mechanical performance of the films and the results are shown in Fig. 5. The average penetration depth during the scratch was determined to be 31.4±3.0 nm and 21.4±3.2 nm for the pristine and annealed PDA films, respectively, representing a 32% decrease in the scratch depth after thermal annealing. Furthermore, the average residual scratch depth was measured to be -18.2±4 nm and -4.7±1.7 nm for the pristine and heat-treated samples, respectively, representing a significant 74% reduction in the scratch depth

after thermal treatment. Roughness, especially for thin polymeric coatings, is a significant contributor affecting deformation; however, even though pDA coatings are relatively rough, in our case, both pristine and annealed samples exhibited comparable roughness. For the bare TiO_2 substrates, the average scratch depth was negligible for the normal load values used during the measurements, and thus, the scratch depths extracted in the experiments on the coated substrates can be confidently assigned to deformation of the coating. More importantly, annealed pDA coatings displayed improved recovery capability after removal of the load as evident in the decreased residual depth. These results are in accordance with previous investigations on pristine and annealed polymer films, where enhanced scratch resistance was attributed to the higher degree of crosslinking in the molecular structure of the annealed polymeric coatings.[63] In our case a similar explanation is possible, as thermal annealing can enhance crosslinking and increase entanglements among pDA chains, resulting in mechanical interlocks that restrict segmental motion of the polymeric chains leading to an interconnected polymeric network with improved cohesive interactions, benefitting the ultimate mechanical performance of the coating.[62] Interestingly, the improvements in the mechanical performance did not come at the expense of multifunctionality and versatility of the pDA coatings. As a proof of concept, we have been able to show that transformations during thermal annealing process does not result in diminishing the ability of the pDA coatings to reduce metal ions into metallic form (Supplementary Fig. S9), as pDA-assisted electroless metallization has been widely utilized to form adherent conductive films onto a variety of substrates.[10]

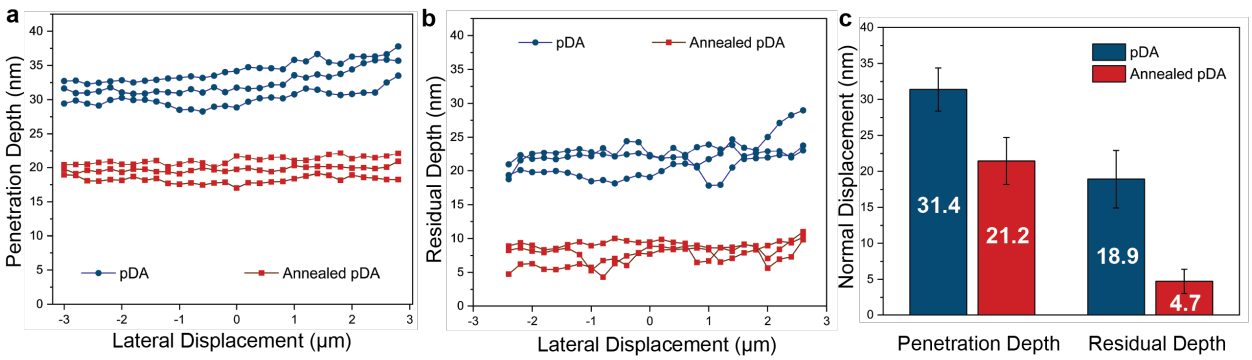

Figure 4.5: Scratch resistance measurements on pristine and annealed pDA coatings using a constant load of 50 μN. Representative penetration-lateral displacement and residual depth-lateral displacement curves are shown in (a) and (b), respectively. Improved scratch resistance of the pDA coatings after thermal annealing is shown in (c).

To complement the scratch resistance measurements and to further evaluate the effects of thermal annealing on the molecular mechanics of pDA coatings, we performed force spectroscopy experiments on annealed pDA. AFM-assisted force spectroscopy has been recog-

nized as a powerful technique enabling nano-mechanical characterization of protein and polymer coatings at a molecular level.[16, 64] The technique has been employed extensively in investigation of mechanical properties of nanoscale thin coatings including, but not limited to, evaluation of Young's modulus, adhesion to substrate, and friction coefficient.[65, 66] We recently utilized this technique to study structure and molecular mechanics of pDA coatings and to confirm its polymeric nature as revealed by the presence of step-wise plateaus of constant force in the force-displacement (F-D) curves, indicating detachment and peeling of a bundle of polymer chains from the pDA-coated cantilever due to weak, non-covalent intermolecular interactions among the chains.[16] These characteristic features of pDA F-D curves serve as a useful baseline that we can use to determine if the observed enhancements in the mechanical properties are indeed linked to changes in the molecular structure of pDA coatings.

Pristine and thermally annealed pDA coated AFM cantilevers were brought into contact with TiO_2 substrates and deflection of the cantilever was monitored during retraction (Fig. 6). In clear contrast to the step-like plateau behavior exhibited by pristine pDA,[16] the probability of observing plateaus was extremely low for the annealed samples. Among the tens of thousands of F-D curves collected on annealed pDA using different cantilevers, most were featureless- only $\sim$0.2-0.4% of F-D curves showed the characteristic step-wise plateau behavior (as compared to $\sim$5% for the pristine pDA[16]). We attribute this observation to significant enhancement in the intermolecular and cohesive interactions between the chains in the pDA structure after annealing, possibly due to cross-linking and increased entanglements, thus preventing desorption and detachment of the chains from the coating. Unexpectedly, 1-2% of F-D curves obtained from annealed pDA were characterized by a saw-tooth pattern of non-equilibrium stretching events in the form of spikes (Fig. 6). Force curves of this type can found during force-induced extension of biomacromolecules, where the sawtooth features represent rupture of non-covalent bonds or unfolding of secondary structures.[67] Whereas the plateaus can be interpreted as molecular desorption from the top layer of the pDA coating or the underlying substrate, the saw-tooth features in our F-D curves can be caused by rupture of intermolecular bonds or by release of mechanical interlocks and entanglements between the chains that are topologically trapped in the pDA network.[65, 68] These features might be interpreted as successive release of intermolecular bonds holding a cross-linked multi-chain matrix together, translating into enhanced toughness of the material.[69]

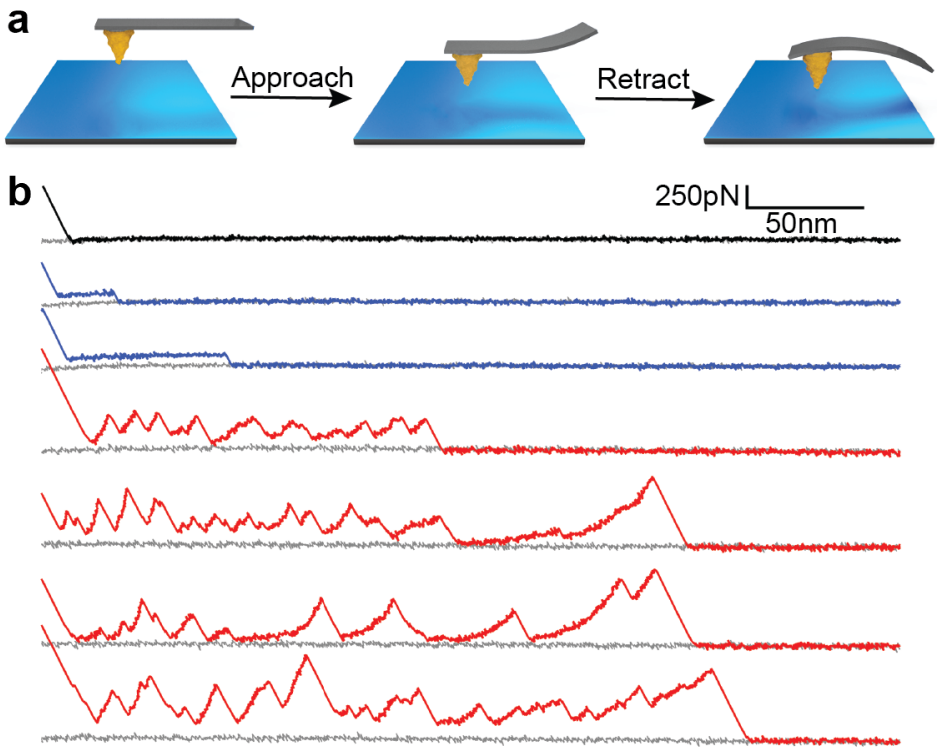

Figure 4.6: Single molecule force spectroscopy of annealed pDA. Schematic of the AFM-assisted force spectroscopy experiments is shown in (a), and representative F-D curves collected during approach of an annealed pDA-coated cantilever against TiO_2 substrate are shown in (b). Most of the F-D curves (∼98%) were featureless as shown in the top curve (black). Only 0.2-0.4% of F-D curves showed stepwise plateau behavior (blue) representative of pristine pDA and corresponding to equilibrium desorption of the polymer chains from the coating. 1-2% of F-D curves (red) showed features (spikes) corresponding to the non-equilibrium desorption of the polymer chains from the coating.

4.4 Conclusions

In summary, we demonstrated that a simple thermal post treatment process can be used to improve the mechanical performance of pDA coatings. XPS and UV-Vis results showed that thermal annealing led to observable changes in the chemical signature of pDA, consistent with a model in which thermal annealing induces chemical transformations in the structure of pDA that include further polymerization of uncyclized and partially polymerized oligo-dopamine (oDA) species. Thermal annealing also led to increased ordering as suggested by GIWAXS measurements. Thermally induced chemical transformations were accompanied by changes in physical properties such as resistance to coating dissolution under solvent

conditions that normally dissolve pDA and enhanced mechanical performance as measured by scratch resistance. Molecular mechanical analysis of thermally annealed pDA was performed by SMFS, revealing significant changes in the mechanical signature of the annealed pDA that are suggestive of enhanced intermolecular interactions and physical entanglements in the pDA structure. Altogether these results suggest that thermal annealing produces chemical and structural changes in the bulk pDA coating adhesion that likely enhance the coating mechanical performance. Importantly, these mechanical improvements were achieved with only a mild thermal treatment and preserved the ability of pDA to undergo secondary coating reactions for specific applications.

4.5 Supplementary Figures

X-ray Photoelectron Spectroscopy (XPS)

	C1s			
	CH_x, C-NH_2	C-O, C-N	C=O	π-π
pDA	48.9 ± 2.9	32.5 ± 2.0	12.1 ± 1.0	6.4 ± 1.4
pDA 130 °C	50.2 ± 1.4	28.8 ± 1.0	15.9 ± 0.9	5.2 ± 1.4

	O1s	
	O-C	O=C
pDA	64.2 ± 3.3	35.8 ± 3.2
pDA 130 °C	55.1 ± 2.4	45.1 ± 2.7

	N1s		
	R-NH_2	R_2-NH	=N-R
pDA	14.6 ± 0.8	78.8 ± 0.6	6.6 ± 0.8
pDA 130 °C	9.5 ± 0.5	84.9 ± 0.8	5.6 ± 0.7

Figure S4.1: Atomic concentration of functional groups in pDA and annealed pDA coatings obtained from the XPS measurements.

Contact Angle Measurements

The increase in the contact angle after thermal treatment may be ascribed to the disappearance and transformation of polar groups in the pDA structure. XPS spectra show transformation of phenolic hydroxyls to quinones (∼25% increase in content) as well as a significant reduction in the primary amine content. The increase in the carbonyl content after thermal treatment has been previously utilized to increase the bioconjugation capacity of the pDA coatings.[70, 71]

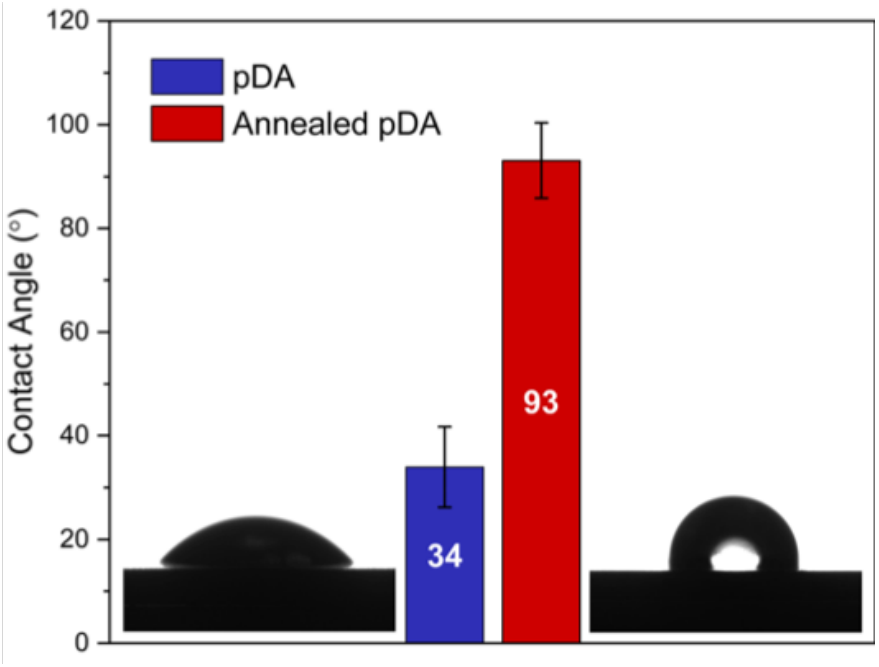

Figure S4.2: Water contact angle of the pristine pDA and annealed pDA coatings, showing a drastic increase in the surface hydrophobicity after annealing. Error bars represent standard deviation of 15 independent measurements.

UV-Vis Absorbance Spectrum

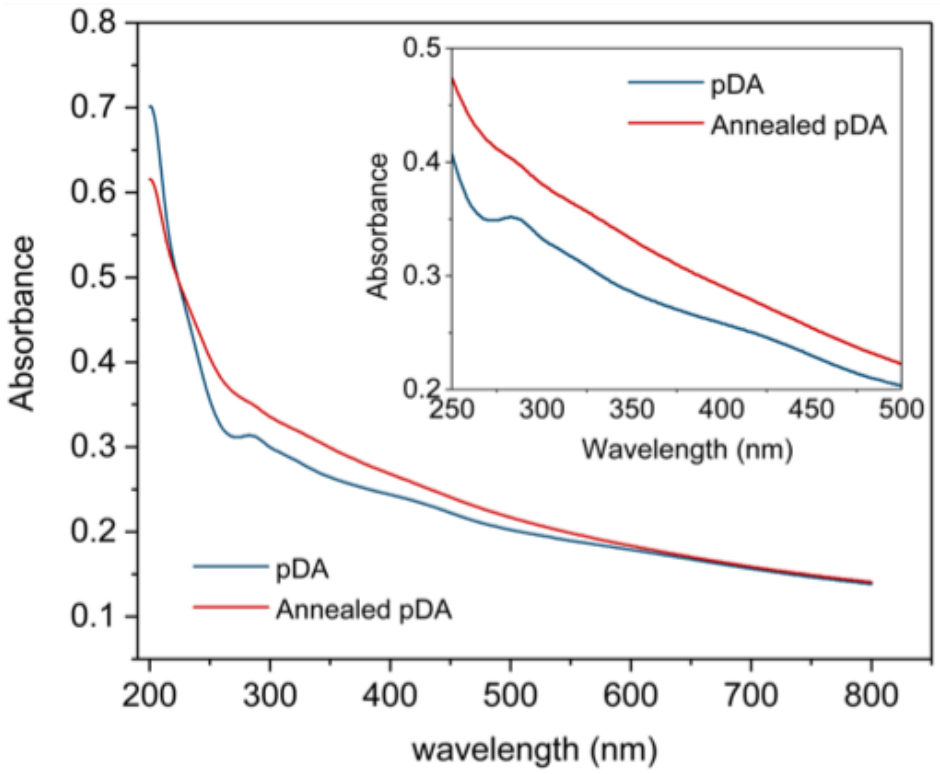

Figure S4.3: UV-Vis spectra of the pDA-coated quartz slides before and after thermal annealing at 130°C. The peak at 280 nm and the shoulder at 420 nm in the blue curve correspond to the fraction of monomeric and oligomeric species present in the pristine pDA coating. After annealing, the intensity of these features decreases significantly, indicating the conversion and further oxidation of partially polymerized species resulting in a monotonous absorption behavior. Inset shows a zoom-in of the spectrum from 250 to 500 nm.

Thickness Evaluation after Sonication

One the main drawbacks of pDA coatings is their weak stability under sonification. Pristine pDA and annealed pDA coated on TiO_2 were sonicated in an aqueous environment (pH$\sim$6.9) at high power for 10 minutes. After sonication, the thickness of pDA dropped by $\sim$35% (n=9, $p<0.05$) whereas the thickness of the annealed pDA did not show any statistically significant reduction. After thermal annealing the stability of pDA against sonication was enhanced possibly due to the enhancement in the intermolecular and cohesive interactions between pDA chains.

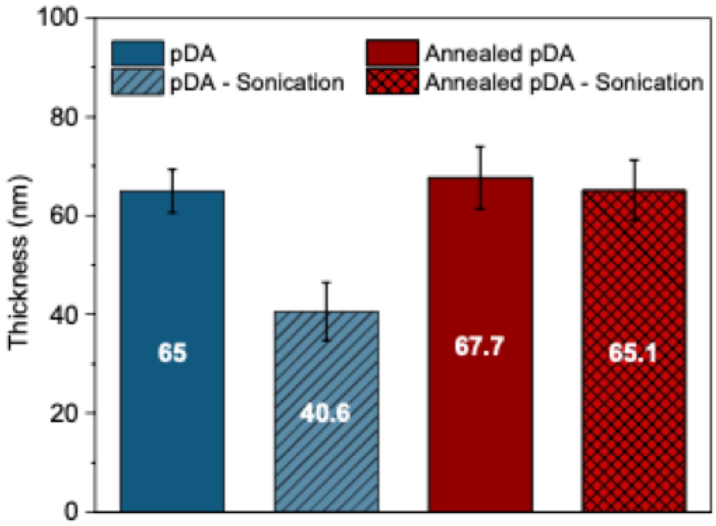

Figure S4.4: Ellipsometry measurements showing changes in thickness of the pristine and annealed pDA coatings prior to and after sonication in Milli-Q water for 10 minutes.

GIWAXS on pDA-Coated and Bare TiO_2 Substrates

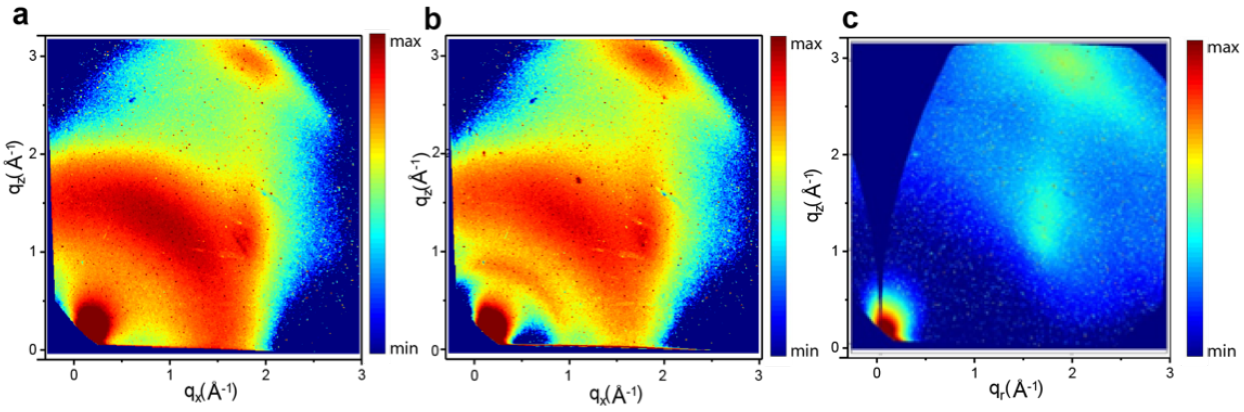

Figure S4.5: Raw 2D GIWAXS detector images of pristine pDA coatings on TiO_2 (a) and annealed pDA coatings on TiO_2 (b). 2D GIWAXS image of bare TiO_2 after missing wedge correction (c). No phase transformational changes occur during thermal annealing of TiO_2 at 130°C.[72, 73]

Scratch Resistance

Constant Load – 50 μN

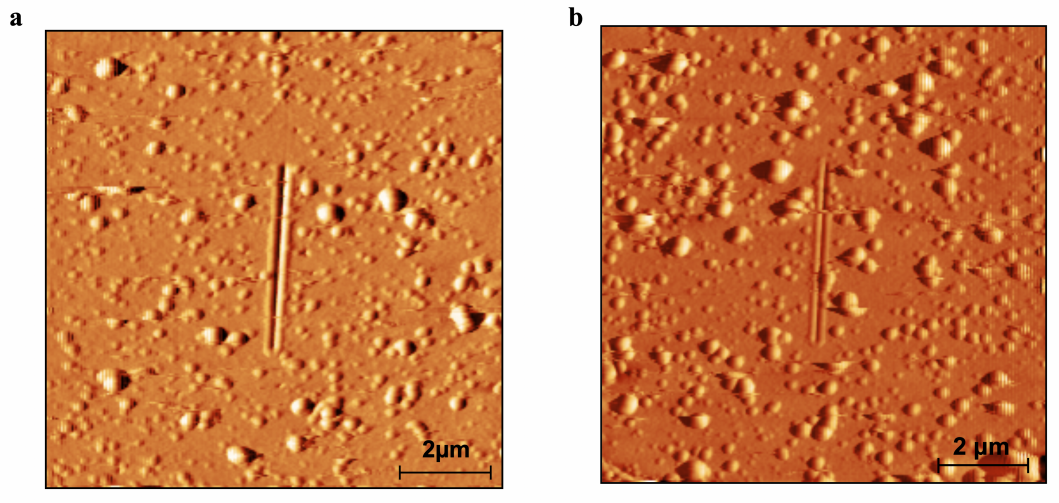

Figure S4.6: Images of scratches on the pristine pDA (a) and annealed pDA (b) using a 50 μN constant load. An improvement in the scratch resistance is noted for the annealed pDA, indicating the enhanced ability of the coating to withstand the load resulting in smaller surface deformation.

Progressive Load – 100 μN

The influence of the scratch load on the mechanical response of the pDA coatings prior to and after annealing was investigated by carrying out progressive load scratch measurements. This second set of the scratch tests, where the normal force was ramped from 0 to 100 μN during the scratch, were performed in order to induce failure of the film to compare critical loads at failure between the two sets of films. The normal displacement during the scratch segment as well as that during the retrace segments for the ramp load scratch test is shown in Supplementary Fig. S7. No evidence of cracking or delamination failure was observed in either set of films up to 100 μN normal force. However, the scratch depth was equal to or greater than the film thickness for most tests on all pristine samples tested. The penetration depth was lower while the recovery after load removal was higher for the annealed pDA coatings compared to pristine coatings evidence of the higher penetration resistance. After thermal annealing, pDA films show higher resistance to scratch as compared to pristine pDA films, consistent with the expectation that the annealing process increases the cross-linking of the polymeric chains and cohesion of pDA films, resulting in a robust coating with superior mechanical properties.

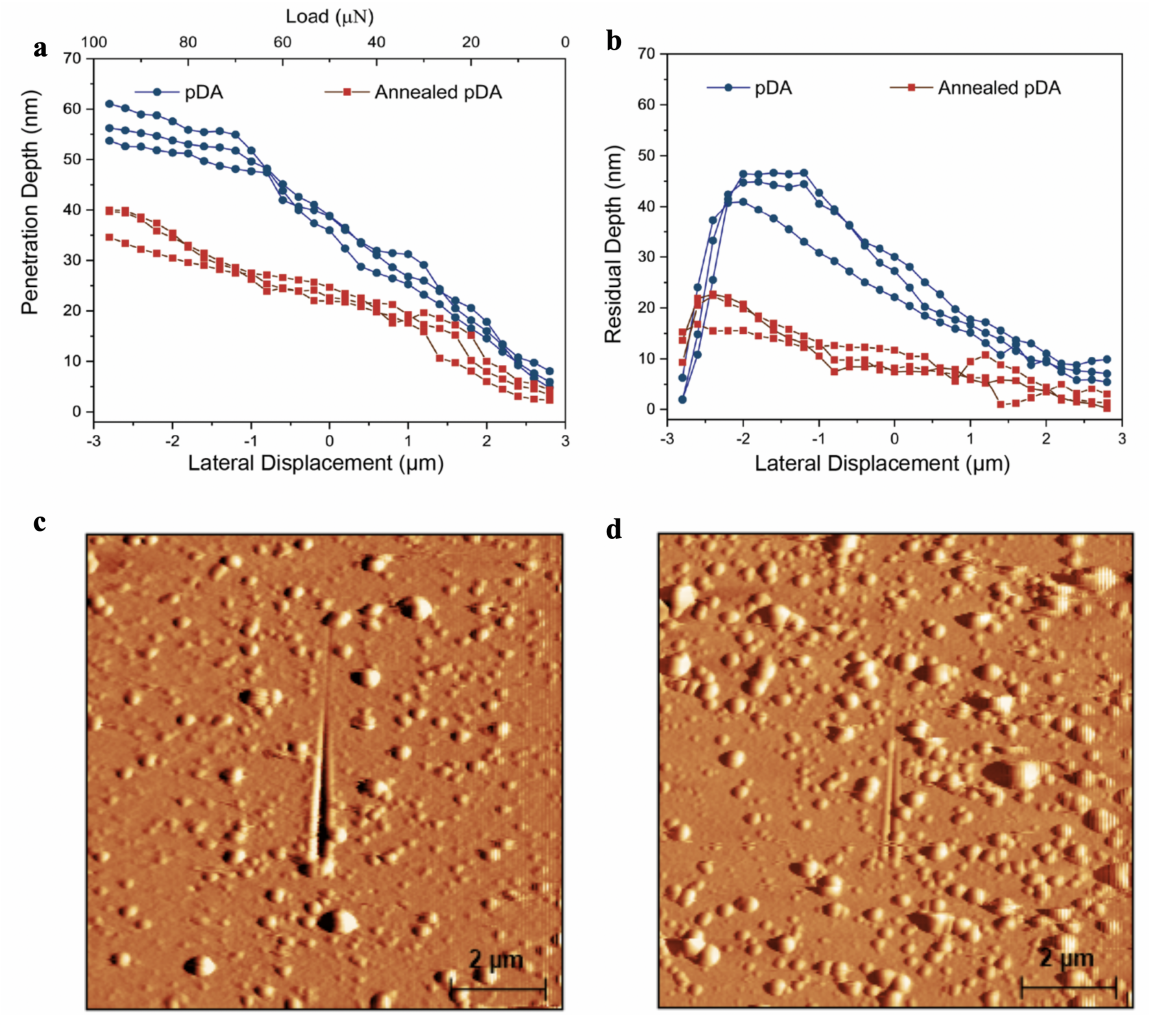

Figure S4.7: Scratch resistance measurements on the pristine and annealed pDA coatings using a progressive load up to 100 μN. Representative penetration-lateral displacement and residual depth-lateral displacement curves during scratching shown in (a) and (b), respectively. Images of the scratches on the pristine pDA (c) and annealed pDA (d) during the 100 μN progressive load.

Elastic Modulus

The elastic modulus of pristine pDA was measured ∼2.8±0.8 GPa whereas after thermal annealing the modulus increased to ∼7.4±1.2 GPa. Thermal annealing resulted in a significant increase on the elastic modulus due to the enhancement in the intermolecular and cohesive interactions between the chains which resulted in mechanical interlocks that enhanced the resistance to elastic deformation. Similar increase in the elastic modulus of pDA films has been observed before and attributed to the enhanced cross-linking. For instance, Klosterman et al. demonstrated that chemical cross-linking of the pDA films using Genipin molecules can result in almost 5 times increase in the modulus from 1.5±0.4 to 7.9±1.7 GPa.[74] More recently Li et al. showed that heat treatment of pDA films at elevated temperatures (300 to 600°C) can result in enhancing the Young's modulus of the films from 2.3±0.84 GPa to ∼7GPa after treatment at 300°C and ∼14GPa when treated at 600°C.[75]

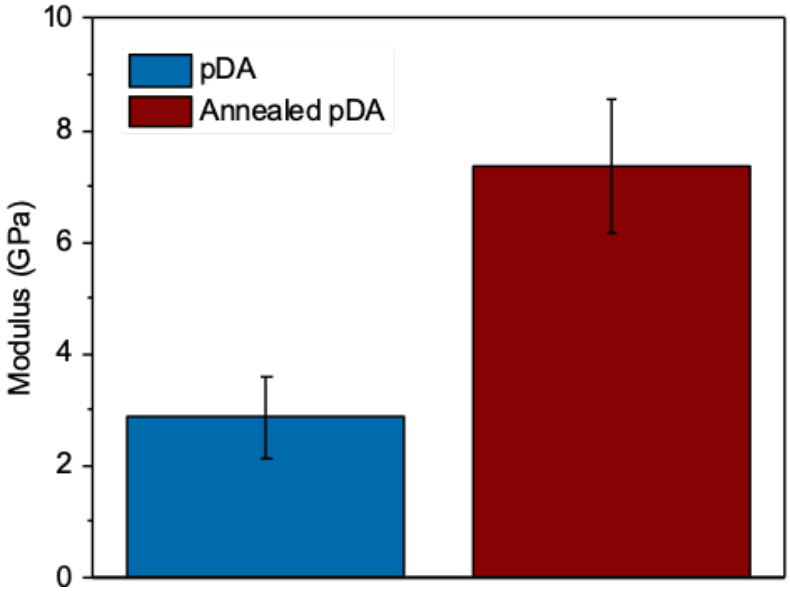

Figure S4.8: Elastic modulus determined by nanoindentation on pristine and annealed pDA.

pDA-Assisted Electroless Metallization

The metal binding ability of catechols in the pDA coating is known to assist the deposition of an adherent and uniform metal film onto substrates by electroless metallization. Here the electroless silver metal film deposition via dip coating of pDA and annealed pDA coated TiO_2 substrates into silver nitrate solution was investigated. As Supplementary Fig. S9 shows after thermal annealing the apparent reductive capacity of pDA layer was sufficient to eliminate the need for addition of a reducing agent implying the ability of the annealed pDA layer to reduce metal ions comparable to that of the pristine pDA.

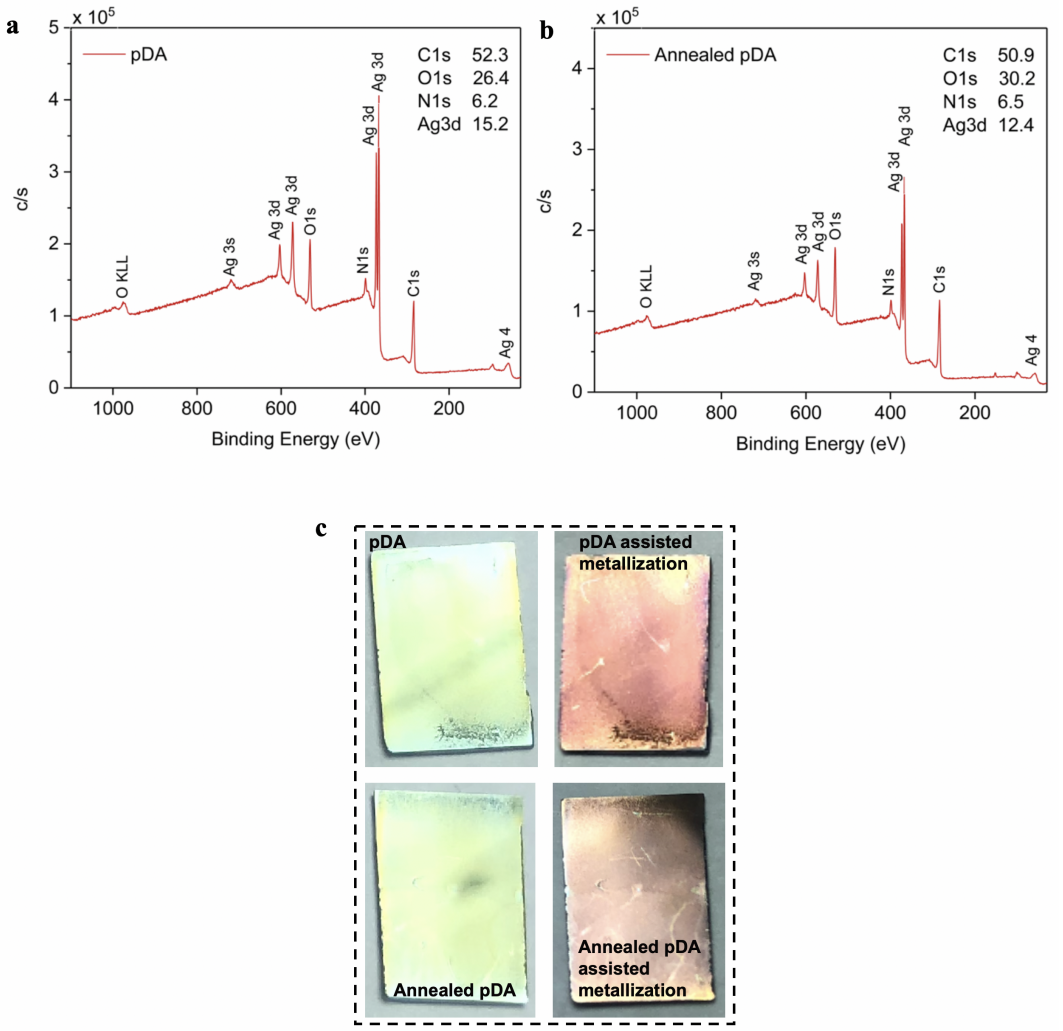

Figure S4.9: XPS spectra on (a) pDA- and (b) annealed pDA-assisted electroless metallization of pDA coated TiO_2 substrates. Representative images of pDA and annealed pDA coated TiO_2 substrates prior to (left) and after (right) the electroless metallization (c).

References

[1] B. P. Lee et al. "Mussel-Inspired Adhesives and Coatings". In: *Annual Review of Materials Research, Vol 41* 41 (2011), pp. 99–132 (cit. on p. 75).

[2] P. K. Forooshani and B. P. Lee. "Recent approaches in designing bioadhesive materials inspired by mussel adhesive protein". In: *Journal of Polymer Science Part a-Polymer Chemistry* 55.1 (2017), pp. 9–33 (cit. on p. 75).

[3] Miaoer Yu and Timothy J. Deming. "Synthetic Polypeptide Mimics of Marine Adhesives". In: *Macromolecules* 31.15 (1998), pp. 4739–4745 (cit. on p. 75).

[4] P. Podsiadlo et al. "Fusion of seashell nacre and marine bioadhesive analogs: High-strength nanocompoisite by layer-by-layer assembly of clay and L-3,4-dihydroxyphenylaianine polymer". In: *Advanced Materials* 19.7 (2007), pp. 949–+ (cit. on p. 75).

[5] J. J. Wang et al. "Influence of Binding-Site Density in Wet Bioadhesion". In: *Advanced Materials* 20.20 (2008), pp. 3872–3876 (cit. on p. 75).

[6] H. Lee et al. "Substrate-Independent Layer-by-Layer Assembly by Using Mussel-Adhesive-Inspired Polymers". In: *Adv. Mater.* 20 (2008), pp. 1916–1923 (cit. on p. 75).

[7] J. H. Ryu, S. Hong, and H. Lee. "Bio-inspired adhesive catechol-conjugated chitosan for biomedical applications: A mini review". In: *Acta Biomaterialia* 27 (2015), pp. 101–115 (cit. on p. 75).

[8] J. L. Dalsin et al. "Mussel adhesive protein mimetic polymers for the preparation of nonfouling surfaces". In: *Journal of the American Chemical Society* 125.14 (2003), pp. 4253–4258 (cit. on p. 75).

[9] A.R. Statz et al. "New peptidomimetic polymers for antifouling surfaces". In: *Journal Of the American Chemical Society* 127 (2005), pp. 7972–3 (cit. on p. 75).

[10] H. Lee et al. "Mussel-inspired surface chemistry for multifunctional coatings". In: *Science* 318.5849 (2007), pp. 426–430 (cit. on pp. 75, 76, 88).

[11] J. H. Ryu, P. B. Messersmith, and H. Lee. "Polydopamine Surface Chemistry: A Decade of Discovery". In: *Acs Applied Materials Interfaces* 10.9 (2018), pp. 7523–7540 (cit. on pp. 75, 76, 81).

[12] T. G. Barclay et al. "Versatile Surface Modification Using Polydopamine and Related Polycatecholamines: Chemistry, Structure, and Applications". In: *Advanced Materials Interfaces* 4.19 (2017) (cit. on p. 75).

[13] Jürgen Liebscher. "Chemistry of Polydopamine – Scope, Variation, and Limitation". In: *European Journal of Organic Chemistry* (), In Press. ISSN: 1434-193X (cit. on pp. 75, 76).

[14] D. R. Dreyer et al. "Elucidating the Structure of Poly(dopamine)". In: *Langmuir* 28.15 (2012), pp. 6428–6435 (cit. on pp. 75, 82).

[15] N. F. Della Vecchia et al. "Building-Block Diversity in Polydopamine Underpins a Multifunctional Eumelanin-Type Platform Tunable Through a Quinone Control Point". In: *Advanced Functional Materials* 23.10 (2013), pp. 1331–1340 (cit. on p. 75).

[16] P. Delparastan et al. "Direct Evidence for the Polymeric Nature of Polydopamine". In: *Angewandte Chemie-International Edition* 58.4 (2019), pp. 1077–1082 (cit. on pp. 75, 89).

[17] Florian Ponzio and Vincent Ball. "Persistence of dopamine and small oxidation products thereof in oxygenated dopamine solutions and in "polydopamine" films". In: *Colloids and Surfaces A: Physicochemical and Engineering Aspects* 443 (2014), pp. 540–543 (cit. on pp. 75, 76, 82).

[18] S. Hong et al. "Non-Covalent Self-Assembly and Covalent Polymerization Co-Contribute to Polydopamine Formation". In: *Advanced Functional Materials* 22.22 (2012), pp. 4711–4717 (cit. on pp. 75, 76, 81).

[19] Y. Liu, K. Ai, and L. Lu. "Polydopamine and its derivative materials: synthesis and promising applications in energy, environmental, and biomedical fields". In: *Chem Rev* 114.9 (2014), pp. 5057–115 (cit. on p. 76).

[20] L. Klosterman et al. "Synthesis and Measurement of Cohesive Mechanics in Polydopamine Nanomembranes". In: *Advanced Materials Interfaces* 4.10 (2017) (cit. on pp. 76, 81).

[21] L. Klosterman and C. J. Bettinger. "Calcium-Mediated Control of Polydopamine Film Oxidation and Iron Chelation". In: *International Journal of Molecular Sciences* 18.1 (2017) (cit. on p. 76).

[22] H. Wei et al. "Stability of polydopamine and poly(DOPA) melanin-like films on the surface of polymer membranes under strongly acidic and alkaline conditions". In: *Colloids Surf B Biointerfaces* 110 (2013), pp. 22–8 (cit. on p. 76).

[23] S. Kim, T. Gim, and S. M. Kang. "Stability-enhanced polydopamine coatings on solid substrates by iron(III) coordination". In: *Progress in Organic Coatings* 77.8 (2014), pp. 1336–1339 (cit. on pp. 76, 84).

[24] H. Q. Li et al. "Structure Evolution and Thermoelectric Properties of Carbonized Polydopamine Thin Films". In: *Acs Applied Materials Interfaces* 9.8 (2017), pp. 6655–6660 (cit. on p. 76).

[25] H. Coskun et al. "Chemical vapor deposition - based synthesis of conductive polydopamine thin-films". In: *Thin Solid Films* 645 (2018), pp. 320–325 (cit. on pp. 76, 82).

[26] H. Zhang et al. "Stability research on polydopamine and immobilized albumin on 316L stainless steel". In: *Regenerative Biomaterials* 3.5 (2016), pp. 277–284 (cit. on p. 76).

[27] P. J. Goncalves, C. A. Brunello, and C. F. O. Graeff. "Thermal annealing effects on synthetic melanin". In: *Molecular Crystals and Liquid Crystals* 374 (2002), pp. 39–44 (cit. on p. 76).

[28] G. S. Y. Yeh et al. "Annealing Effects of Polymers and Their Underlying Molecular Mechanisms". In: *Polymer* 17.4 (1976), pp. 309–318 (cit. on p. 76).

[29] P. Zhou et al. "Rapidly-Deposited Polydopamine Coating via High Temperature and Vigorous Stirring: Formation, Characterization and Biofunctional Evaluation". In: *Plos One* 9.11 (2014) (cit. on pp. 76, 80, 81).

[30] M. Lee et al. "Microwave-Accelerated Rapid, Chemical Oxidant-Free, Material-Independent Surface Chemistry of Poly(dopamine)". In: *Small* 13.4 (2017) (cit. on p. 76).

[31] J. H. Jiang et al. "Surface Characteristics of a Self-Polymerized Dopamine Coating Deposited on Hydrophobic Polymer Films". In: *Langmuir* 27.23 (2011), pp. 14180–14187 (cit. on p. 76).

[32] "GitHub SciAnalysis". In: *https://github.com/CFN-softbio/SciAnalysis* () (cit. on p. 79).

[33] R. J. Pandolfi et al. "Xi-cam: a versatile interface for data visualization and analysis". In: *Journal of Synchrotron Radiation* 25 (2018), pp. 1261–1270 (cit. on p. 79).

[34] G. M. Pharr, W. C. Oliver, and F. R. Brotzen. "On the Generality of the Relationship among Contact Stiffness, Contact Area, and Elastic-Modulus during Indentation". In: *Journal of Materials Research* 7.3 (1992), pp. 613–617 (cit. on p. 79).

[35] Jannis Lübbe et al. "Determining cantilever stiffness from thermal noise". In: *Beilstein Journal of Nanotechnology* 4 (2013), pp. 227–233 (cit. on p. 80).

[36] Y. H. Ding et al. "Insights into the Aggregation/Deposition and Structure of a Polydopamine Film". In: *Langmuir* 30.41 (2014), pp. 12258–12269 (cit. on p. 80).

[37] S. Rella et al. "Investigation of polydopamine coatings by X-ray Photoelectron Spectroscopy as an effective tool for improving biomolecule conjugation". In: *Applied Surface Science* 447 (2018), pp. 31–39 (cit. on p. 80).

[38] R. F. Luo et al. "Improved immobilization of biomolecules to quinone-rich polydopamine for efficient surface functionalization". In: *Colloids and Surfaces B-Biointerfaces* 106 (2013), pp. 66–73 (cit. on pp. 80, 81).

[39] S. Lomnicki, H. Truong, and B. Dellinger. "Mechanisms of product formation from the pyrolytic thermal degradation of catechol". In: *Chemosphere* 73.4 (2008), pp. 629–633 (cit. on p. 80).

[40] X. W. Dong et al. "Superlithiated Polydopamine Derivative for High-Capacity and High-Rate Anode for Lithium-Ion Batteries". In: *Acs Applied Materials Interfaces* 10.44 (2018), pp. 38101–38108 (cit. on pp. 80, 81).

[41] H. Lee, J. Rho, and P. B. Messersmith. "Facile Conjugation of Biomolecules onto Surfaces via Mussel Adhesive Protein Inspired Coatings". In: *Advanced Materials* 21.4 (2009), pp. 431–+ (cit. on p. 81).

[42] V. Proks et al. "Thermal-Induced Transformation of Polydopamine Structures: An Efficient Route for the Stabilization of the Polydopamine Surfaces". In: *Macromolecular Chemistry and Physics* 214.4 (2013), pp. 499–507 (cit. on p. 82).

[43] M. L. Alfieri et al. "Structural Basis of Polydopamine Film Formation: Probing 5,6-Dihydroxyindole-Based Eumelanin Type Units and the Porphyrin Issue". In: *ACS Appl Mater Interfaces* (2017) (cit. on p. 82).

[44] F. Bernsmann et al. "Characterization of Dopamine-Melanin Growth on Silicon Oxide". In: *Journal of Physical Chemistry C* 113.19 (2009), pp. 8234–8242 (cit. on pp. 82, 84).

[45] K. M. Hanson, B. L. Li, and J. D. Simon. "A spectroscopic study of the epidermal ultraviolet chromophore trans-urocanic acid". In: *Journal of the American Chemical Society* 119.11 (1997), pp. 2715–2721 (cit. on p. 82).

[46] D. Hafner et al. "Mussel-Inspired Polymer Carpets: Direct Photografting of Polymer Brushes on Polydopamine Nanosheets for Controlled Cell Adhesion". In: *Advanced Materials* 28.7 (2016), pp. 1489–1494 (cit. on p. 82).

[47] M. S. Blois, J. E. Maling, and A. B. Zahlan. "Electron Spin Resonance Studies on Melanin". In: *Biophysical Journal* 4.6 (1964), 471– (cit. on p. 82).

[48] J. Cheng et al. "X-Ray Characterization of Melanins .1." In: *Pigment Cell Research* 7.4 (1994), pp. 255–262 (cit. on pp. 82, 86).

[49] J. Cheng, S. C. Moss, and M. Eisner. "X-Ray Characterization of Melanins .2." In: *Pigment Cell Research* 7.4 (1994), pp. 263–273 (cit. on pp. 82, 86).

[50] A. Napolitano et al. "Structural analysis of synthetic melanins from 5,6-dihydroxyindole by matrix-assisted laser desorption ionization mass spectrometry". In: *Rapid Communications in Mass Spectrometry* 10.4 (1996), pp. 468–472 (cit. on p. 82).

[51] B. A. Miller-Chou and J. L. Koenig. "A review of polymer dissolution". In: *Progress in Polymer Science* 28.8 (2003), pp. 1223–1270 (cit. on p. 84).

[52] Y. Tang et al. "Swelling of zwitterionic polymer films characterized by spectroscopic ellipsometry". In: *Macromolecules* 34.25 (2001), pp. 8768–8776 (cit. on p. 86).

[53] Y. Tang et al. "Structural effects on swelling of thin phosphorylcholine polymer films". In: *Macromolecules* 35.10 (2002), pp. 3955–3964 (cit. on p. 86).

[54] Y. Kim et al. "A strong regioregularity effect in self-organizing conjugated polymer films and high-efficiency polythiophene: fullerene solar cells". In: *Nature Materials* 5.3 (2006), pp. 197–203 (cit. on p. 86).

[55] D. A. H. Hanaor and C. C. Sorrell. "Review of the anatase to rutile phase transformation". In: *Journal of Materials Science* 46.4 (2011), pp. 855–874 (cit. on p. 86).

[56] L. Migliaccio et al. "Evidence of Unprecedented High Electronic Conductivity in Mammalian Pigment Based Eumelanin Thin Films After Thermal Annealing in Vacuum". In: *Frontiers in Chemistry* 7 (2019) (cit. on pp. 86, 87).

[57] T. Xiao et al. "Molecular Packing and Electronic Processes in Amorphous-like Polymer Bulk Heterojunction Solar Cells with Fullerene Intercalation". In: *Scientific Reports* 4 (2014) (cit. on p. 86).

[58] X. Yu et al. "Characterization of carbonized polydopamine nanoparticles suggests ordered supramolecular structure of polydopamine". In: *Langmuir* 30.19 (2014), pp. 5497–505 (cit. on p. 86).

[59] C. T. Chen et al. "Self-Assembly of Tetramers of 5,6-Dihydroxyindole Explains the Primary Physical Properties of Eumelanin: Experiment, Simulation, and Design". In: *Acs Nano* 7.2 (2013), pp. 1524–1532 (cit. on p. 86).

[60] F. Panzer, H. Bassler, and A. Kohler. "Temperature Induced Order-Disorder Transition in Solutions of Conjugated Polymers Probed by Optical Spectroscopy". In: *Journal of Physical Chemistry Letters* 8.1 (2017), pp. 114–125 (cit. on p. 87).

[61] Y. L. Liang et al. "Effect of high temperature annealing on scratch behavior of acrylonitrile styrene acrylate copolymers". In: *Polymer* 53.2 (2012), pp. 604–612 (cit. on p. 87).

[62] M. Sangermano and M. Messori. "Scratch Resistance Enhancement of Polymer Coatings". In: *Macromolecular Materials and Engineering* 295.7 (2010), pp. 603–612 (cit. on pp. 87, 88).

[63] J. F. Gonzalez-Martinez et al. "The role of cross-linking in the scratch resistance of organic coatings: An investigation using Atomic Force Microscopy". In: *Wear* 418 (2019), pp. 151–159 (cit. on p. 88).

[64] R. H. Zha et al. "Universal nanothin silk coatings via controlled spidroin self-assembly". In: *Biomaterials Science* 7.2 (2019), pp. 683–695 (cit. on p. 89).

[65] B. N. Balzer et al. "Adhesion Property Profiles of Supported Thin Polymer Films". In: *Acs Applied Materials Interfaces* 5.13 (2013), pp. 6300–6306 (cit. on p. 89).

[66] M. Chyasnavichyus et al. "Probing elastic properties of soft materials with AFM: Data analysis for different tip geometries". In: *Polymer* 102 (2016), pp. 317–325 (cit. on p. 89).

[67] M. Rief et al. "Reversible unfolding of individual titin immunoglobulin domains by AFM". In: *Science* 276.5315 (1997), pp. 1109–1112 (cit. on p. 89).

[68] S. Kienle et al. "Effect of Molecular Architecture on Single Polymer Adhesion". In: *Langmuir* 30.15 (2014), pp. 4351–4357 (cit. on p. 89).

[69] B. L. Smith et al. "Molecular mechanistic origin of the toughness of natural adhesives, fibres and composites". In: *Nature* 399.6738 (1999), pp. 761–763 (cit. on p. 89).

[70] M. Martin et al. "Quinone-Rich Poly(dopamine) Magnetic Nanoparticles for Biosensor Applications". In: *Chemphyschem* 15.17 (2014), pp. 3742–3752 (cit. on p. 93).

[71] R. F. Luo et al. "Improved immobilization of biomolecules to quinone-rich polydopamine for efficient surface functionalization". In: *Colloids and Surfaces B-Biointerfaces* 106 (2013), pp. 66–73 (cit. on p. 93).

[72] J. A. Eastman. "Microstructural Development in Nanophase Tio2 during Annealing". In: *Journal of Applied Physics* 75.2 (1994), pp. 770–779 (cit. on p. 96).

[73] H. Rath et al. "Phase Transformation of TiO2 from Anatase to Rutile by Thermal Annealing and Swift Heavy Ion Irradiation". In: *Mesoscopic, Nanoscopic, and Macroscopic Materials* 1063 (2008) (cit. on p. 96).

[74] L. Klosterman et al. "Synthesis and Measurement of Cohesive Mechanics in Polydopamine Nanomembranes". In: *Advanced Materials Interfaces* 4.10 (2017) (cit. on p. 99).

[75] H. Q. Li et al. "Mechanical properties of polydopamine (PDA) thin films". In: *Mrs Advances* 4.7 (2019), pp. 405–412 (cit. on p. 99).

Chapter 5

Enhanced Adhesion and Cohesion of Bioinspired Adhesives

* This chapter is adapted based on the research originally appeared as a peer-reviewed article co-authored by me published in ACS Applied Materials & Interfaces.
B. D. B. Tiu, P. Delparastan, M. R. Ney, M. Gerst, and P. B. Messersmith, Enhanced Adhesion and Cohesion of Bioinspired Dry/Wet Pressure-Sensitive Adhesives. ACS Appl. Mater. Interfaces 2019, 11, 31, 28296–28306

Abstract

The byssus-mediated adhesion of marine mussels is a widely mimicked system for robust adhesion in both dry and wet conditions. Mussel holdfasts are fabricated from proteins that contain a significant amount of the unique catecholic amino acid dihydroxyphenylalanine (DOPA), which plays a key role in enhancing interfacial adhesion to organic and inorganic marine surfaces, and contributes to cohesive strength of the holdfast. In this work, pressure sensitive adhesives (PSAs) were synthesized by copolymerization of dopamine methacrylamide (DMA) with common PSA monomers, butyl acrylate (BA) and acrylic acid (AA), with careful attention paid to the effects of catechol on adhesive and cohesive properties. A combination of microscopic and macroscopic adhesion assays were used to study the effect of catechol on adhesion performance of acrylic PSAs. Addition of only 5% DMA to a conventional PSA copolymer containing butyl acrylate and acrylic acid resulted in a 6-fold and 2.5-fold increase in work required to separate the PSA from silica and polystyrene, respectively, and a large increase in 180° peel adhesion against stainless steel after 24 h storage in both ambient and underwater conditions. Moreover, the holding power of the catechol PSAs on both steel and high density polyethylene (HDPE) under shear load continuously increased as a function of catechol concentration, up to a maximum of 10% DMA. We also observed stark increases in shear and peel adhesion for the catecholic adhesives over PSAs

with noncatecholic aromatic motifs, further underlining the benefits of catechols in PSAs. Overall, catechol PSAs perform extremely well on polar and metallic surfaces. The advantage of incorporating catechols in PSA formulations, however, is less straightforward for peel adhesion in nonpolar, organic substrates and tackiness of the PSAs.

5.1 Introduction

PSAs are ubiquitous industrial and consumer products that are an integral part of everyday life. Common examples include adhesive tapes, sticky notes, hanging strips, and medical bandages. PSAs commonly take the form of viscoelastic polymeric adhesive thin films coated on a backing material, ideally adhering to substrates with only light pressure.[1] For temporary adhesion applications such as sticky notes, the PSA with backing should have the ability to be removed without transfer of adhesive residue to the adherend. Optimizing PSAs for specific target applications is a multifaceted problem involving balancing the adhesive and cohesive properties of the material, as improving one property often comes at the expense of the other. For example, the PSA polymer must either flow or have a sufficiently low modulus to allow for maximal contact with the substrate, but also be stiff enough to resist flow and dissipate energy when stress is applied to the system. Fine tuning of PSA properties is typically accomplished through control of molecular weight, polydispersity, branching and crosslinking of the polymer, or by introducing tackifiers, plasticizers or other additives into the PSA formulation.[2]

One general requirement of a polymer PSA is that it has a low glass transition temperature (T_g), which in the case of the (meth)acrylic polymer family of PSAs is often achieved by linear or slightly cross-linked polymers with a high content of butyl acrylate, 2-ethylhexyl acrylate, or other monomers that contribute low T_g. However, PSA composition varies widely by manufacturer and the intended application, and other monomers are often included for functionality. For example, a few percent of a hydrophilic monomer such as acrylic acid can be added to enhance adhesion of poly(butyl acrylate) PSAs onto polar substrates such as glass, steel or aluminum.[3] Common strategies to improve PSA adhesion onto low surface energy substrates like polyethylene and polypropylene include introduction of nonpolar hydrophobic monomers, and physical or chemical treatment of the surface,[4] or applying solvent-based adhesion promoters.[5] Adhesive performance of PSAs under water is generally poor compared to that in air, with the magnitude of the decrease depending on several factors including the effects of water on bulk viscoelastic properties, wettability of the contact surface, and whether water is present during contact formation.[6] Repositionable PSA sticky notes designed for use under difficult conditions (hot/cold, humid/wet), are now commercially available. Interestingly, the manufacturer's marketing guidance specifies the product to be used on (initially) dry surfaces for holding under wet conditions.[7]

A fascinating observation about mussel adhesion is that two situations historically challenging for PSAs, namely adhesion to low surface energy substrates and adhesion under water, apparently do not pose significant problems for mussels, which are known to ad-

here to a wide range of substrates including rocks, wood, animal skins, painted surfaces, fluorinated polymers and paraffin wax.[8] The byssal threads of the mussel are each terminally glued onto surfaces by specialized adhesive proteins that permanently anchor the threads onto substrates. Mussel foot proteins (Mfps) contain the catecholic amino acid 3,4-dihydroxyphenylalanine (DOPA) at concentrations ranging from 3-27%, with the highest catechol concentration found in the proteins located near the plaque-substrate interface.[9–11] Molecular adhesion studies performed on Mfps, small molecule catechols and catechol containing macromolecules have shown that catechols can enhance adhesive interactions to inorganic and organic surfaces.[12–16] Even though the DOPA content of proteins found in the interior of the byssal plaque and in the byssal cuticle is lower than at the interface, DOPA still contributes to the overall cohesive strength by participating in metal coordination and covalent protein cross-links.[10, 11]

As summarized in several excellent reviews,[10, 17, 18] incorporating catechol motifs into polymers has been shown to improve adhesive performance in dry and wet conditions. Applications proposed for catechol-polymers include structural adhesives,[19–21] biomedical adhesives for tissues,[22–25] denture adhesives,[26] self-healing materials,[27, 28] adhesives with stimuli-responsive behavior,[29] surface modification of nanomaterials,[30] antibacterial and corrosion-resistant coatings,[31, 32] and adhesion-promoting hydrogel-based electronics.[33]

Although a number of studies have reported catechol-containing (meth)acrylate polymers,[33–36] reports on the use of catechol polymers in developing PSAs have been somewhat limited. In 2003, our group first synthesized catechol-functionalized acrylic polymers via the free radical copolymerization of a monomer modified with an unprotected catechol group for bioadhesive hydrogel applications.[37] Subsequently, we used the same strategy and copolymerized dopamine methacrylamide (DMA) with methoxyethyl acrylate (MEA) to make a catechol copolymer that was adsorbed as a molecular film on a gecko-inspired structured PDMS tape, resulting in significant increases in wet adhesion.[38] Since then, several studies on bioinspired poly(dopamine methacrylamide-co-alkyl (meth)acrylate) adhesives have been reported,[34, 35] often using only one adhesion test such as lap-shear (most common)[19–21, 39] or probe-tack/indentation.[35, 40] Although these studies were successful in highlighting the potential of catechols in improving an aspect of adhesion, a more comprehensive evaluation of PSA performance should include industry-standard tests such as 180° peel adhesion, loop tack/quickstick and static shear tests. Furthermore, most catechol-based adhesives have primarily focused on adhering onto polar surfaces such as glass or steel because low surface energy adhesion is less straightforward.[35] It would be interesting to investigate whether mussel-inspired chemistry can translate into robust pressure sensitive adhesive systems for hydrophobic and polyolefin-based adherends.

In this work we report a comprehensive evaluation of the ability of DOPA-mimicking motifs to improve the adhesive and cohesive properties of PSAs as applied onto low and high surface energy surfaces in both dry and wet conditions. Interfacial adhesion was characterized at the microscale by colloidal probe spectroscopy, and at the macroscale by several industry-standard adhesion tests (static shear, 180° peel, and loop tack/quickstick). This multifaceted

approach allowed us to decouple the adhesive and cohesive contributions of catechol to PSA performance.

5.2 Methods

Synthesis & Characterization

A detailed description of materials used and steps undertaken to synthesize and characterize monomers and polymers is provided in the published article in ACS Applied Materials & Interfaces journal.

Colloidal Probe Spectroscopy

Colloidal probe spectroscopy experiments were performed using the JPK ForceRobot 300 atomic force microscope (JPK Instruments AG, Berlin, Germany). Colloidal AFM probes with nominal spring constant of 0.2 N/m and diameters of 3.5 μm (SiO_2) and 14.45 μm (Polystyrene) were obtained from sQube (Bickenbach, Germany). Polyethylene colloidal probes with nominal spring constant of 0.24 N/m and diameter of 10 μm were acquired from Novascan Technologies (Iowa, US). For the sample preparation, the polymers were dissolved at a concentration of 1 wt% in ethanol and drop casted on mica substrates (Ted Pella, Inc, Redding, CA) that were freshly cleaved using scotch tape in order to provide a pristine surface. The polymer-coated mica substrates were then directly used for AFM force spectroscopy experiments in the presence of ethanol. The sensitivity and spring constant of the cantilevers were calibrated using the equipartition theorem.[41] The cantilever was approached to the surface with a piezo speed of 1000 nm/s, hold for a dwell time (time of contact between probe and surface) of 1 s with a contact force of 25 nN and then retracted at a piezo speed of 1000 nm/s. Thousands of F-D curves were recorded on more than 5 samples in each group to achieve statistically representative results. The area under the retraction curve in F-D traces were calculated using the JPK data processing software.

Pressure Sensitive Adhesive (PSA) Testing

Fabrication of Pressure Sensitive Adhesive (PSA) Tape Samples

The synthesized PSAs were dissolved in methyl ethyl ketone (MEK) in 1:1 (wv) ratio and coated onto Hostaphan RN36 polyethylene terephthalate films (thickness = 36 μm) with a wet coating thickness of 120 μm using a wire-round K-bar hand coater (Testing Machines, Inc., New Castle, DE) to target a final coating thickness of 60 gsm (g/m^2) (Supplementary Fig. S1). The PET films coated with PSAs were heated at 100°C for 5 min to remove the solvent and stored in ambient conditions for 24 h prior to use. In order to temporarily protect the adhesive layer, the PSA-coated PET films were adhered onto silicone release

layers. Then, 1 in-wide strips of PSA-coated films were cut for PSA evaluation tests (shear, 180° peel, and loop tack).

Preparation of Test Panels

PSA performance was tested against stainless steel and high-density polyethylene (HDPE) test plates. Based on the FINAT Technical Handbook, the substrates were cleaned prior to testing by dispensing ethyl acetate onto the surface and wiping it dry with Kimwipes. The process was repeated at least three times. Acetone was used in the last rinse. The cleaned substrates were placed in a vacuum desiccator for at least an hour before testing.

Static Shear Test

The shear holding power of the PSA was measured using the Room Temperature 10 Bank Shear Tester (ChemInstruments, Fairfield, OH) according to FINAT Test Method no. 8. The silicone-release layer was removed from the prepared 1 in-wide strip, which was then adhered on a clean test plate in such a way that a 25 mm×25 mm area of the PSA-coated PET film was attached onto the substrate. Initially, contact was made using light finger pressure. To standardize the applied pressure, the standard 2 kg-hand roller was rolled twice in each direction at approximately 10 mm/sec. The other end of the tape was looped through a Shear Test Clip (part STC-100, ChemInstruments) and carefully attached back on itself. The test sample (test plate with attached PSA strip and Shear Test Clip) was mounted onto the substrate holder of the shear tester. Then, a 500 g weight was carefully inserted into the Shear Test Clip. The static shear test was performed in both dry and wet conditions, which means that the contact between the PSA and the test panel and the 'roll-down' methodology to standardize the applied pressure were done either in dry/ambient condition or while submerged under water. For the wet condition, the PSA attached to the test panel was patted dry with a Kimwipe and were placed in the Shear tester. Shear test results of 5 samples per condition were averaged and reported.

180° Peel Adhesion

The peeling resistance of the PSA samples were measured by the conventional 180° peel adhesion test as defined by FINAT Test Method no. 1. The PSA tape was cut into 25 mm×175 mm strips and, after removing the release layer, was adhered onto the test substrates using light finger pressure. To achieve similar contact between the adhesive layer and the substrate, a standard FINAT 2 kg-hand roller was rolled twice in each direction at approximately 10 mm/sec. The test samples were stored in ambient conditions for 24 h before testing. The end of the tape was pulled back at 180°, mounted in an Instron 3345 single column universal testing system, and pulled at 300 mm/min. Peel tests were repeated 5 times and the results averaged. In addition to the dry 180° peel test, the peel adhesion after immersion in deionized water for 24 h was also measured. The setup for the wet 180° peel test is similar to the dry test except that the test samples were assembled and stored under

water for 24 h before measuring the peel adhesion. First, the test substrate was submerged in water. The silicone release layer of the pressure-sensitive tape was removed and the PSA was adhered onto the test substrate while still submerged under water. Contact between the adhesive and the substrate was standardized by rolling the FINAT hand roller twice in each direction at 10 mm/sec. The test samples were then incubated in water for 24 h, dried with lint free wipe and then mounted in the Instron tensile testing system for the peel adhesion test.

Loop Tack Test (Quickstick)

Tack, or the ability of the PSA to immediately wet and adhere onto surfaces under low external pressure, was characterized using the loop tack test as explained in the FINAT test method no. 8 or PSTC-16. To perform this test, 25 mm×175 mm-sized PSA strips were folded into a loop in such a way that the adhesive layer was in the outer side. The ends of the PSA tape were then clamped onto the upper jaw of the Instron Tensile tester. The test panel (30 mm×200 mm) was then mounted onto a Loop Tack Fixture (TT-LTF-100, ChemInstruments, Fairfield, OH), which was clamped onto the lower jaw of the Instron Tensile Tester. The longer axis of the looped PSA tape should be at a right angle to the long axis of the test substrate. Then, the looped tape sample was made to approach a test substrate at 300 mm/min to form a contact area of 25 mm×30 mm. Once the contact area was fully covered by the PSA, the motion was reversed immediately also at 300 mm/min. The maximum force measured to completely remove the tape from the substrate was recorded, as specified in the test method. Five PSA strips were tested and the results averaged.

5.3 Results & Discussion

Synthesis and Characterization of Catechol-PSAs

The PSA polymer platform used for this study is based on a standard PSA composition[42–44] synthesized by copolymerization of BA (95 wt%) with AA (5 wt%). Catechol PSAs were synthesized by replacing a portion of the BA monomer with DMA (5 wt% or 10 wt%), an acrylamide monomer with a tethered catechol motif prepared via a highly scalable one-step reaction using the starting material dopamine hydrochloride. Despite the radical scavenging ability of catechols,[35] DMA was successfully copolymerized with other monomers under anhydrous conditions to make catechol-PSAs, as revealed by ^{1}H NMR analysis. For comparison purposes, we also synthesized aromatic PSAs by using phenethyl methacrylamide (PMA) in place of DMA in order to isolate the effect of phenolic hydroxyls on PSA performance. As shown in Table 1, samples are identified based on the feed wt% and type of aromatic monomer and the molecular weight of the polymer, using (L) to designate the low M_w polymers synthesized in ethanol and (H) for the higher molecular weight PSAs prepared in DMF. For instance, the copolymer synthesized using a monomer feed ratio of 90% BA,

Table 5.1: Monomer feed composition (wt%), molecular and thermal characterization of the synthesized pressure sensitive adhesives.

Polymer	Polymerization Solvent	Feed Composition (wt%)				M_n (kDa)	M_w (kDa)	Dispersity	T_g (°C)
		BA	AA	PMA	DMA				
PSA-L	Ethanol	95	5	-	-	42	164	3.9	-39
PSA-H	DMF	95	5	-	-	116	346	3.0	-41
PSA-5PMA-H	DMF	90.6	5	4.4	-	289	484	1.7	-30
PSA-10PMA-H	DMF	86.2	5.1	8.7	-	179	406	2.2	-27
PSA-5DMA-L	Ethanol	90	5	-	5	98	388	4.0	-36
PSA-5DMA-H	DMF	90	5	-	5	289	908	3.1	-31
PSA-10DMA-H	DMF	85	5	-	10	485	1018	2.1	-18

5% AA, and 5% DMA in DMF will be denoted as PSA-5DMA-H. Control polymers without DMA or PMA will simply be referred to as either PSA-L or PSA-H corresponding to copolymerization of 95% BA and 5% AA in ethanol or DMF, respectively. Finally, T_g values of the resulting PSAs ranged from -41°C to -18°C, which should be taken into consideration when interpreting the mechanical performance of the PSAs.

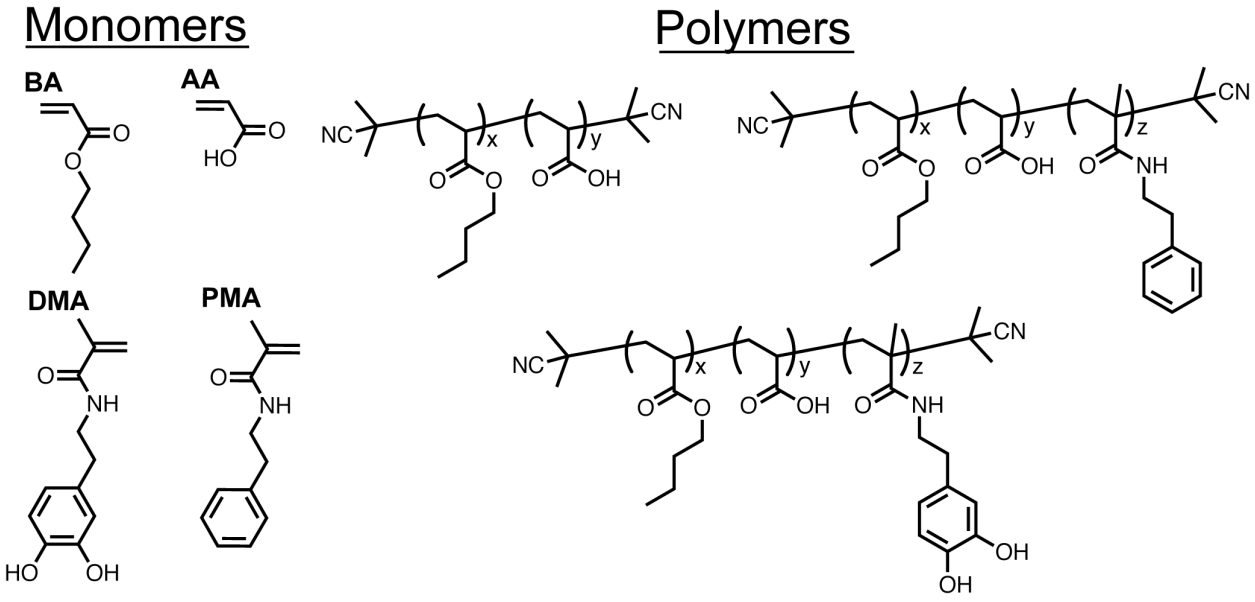

Scheme 5.1: Structure of PSA monomers and polymers. Structures of monomers and mussel-inspired pressure-sensitive adhesive polymers (with omitted end groups) synthesized via free-radical polymerization.

Colloidal Probe Spectroscopy

AFM-based force spectroscopy has become widely used in the past few years due to its high sensitivity and ability to study molecular or micro-scale interfacial phenomena on various substrates.[45] In particular, colloidal probe force spectroscopy technique is a versatile tool to measure adhesive forces acting between a colloidal particle (i.e., micrometer-sized spherical particle) and a planar substrate.[46–48] In the present work, colloidal probe force spectroscopy was used to gain a microscopic view of adhesion performance of the synthesized PSA polymers, in addition to macroscopic bulk adhesion testing. In a typical force spectroscopy experiment (Fig. 1A), an AFM cantilever with a colloidal probe tip is brought into contact with a PSA film and retracted at a specified speed while the force of interaction between the probe and the polymer film is measured. In our experiments we chose three different colloidal probes to evaluate the effect of catechols on PSA polymer adhesion to different surfaces; silica (SiO_2, diameter=3.5 μm), polystyrene (PS, diameter=14.45 μm), and polyethylene (PE, diameter=10 μm). Based on Derjaguin-Muller-Toporov (DMT) and Johnson-Kendall-Roberts (JKR) models for adhesive contact mechanics, both the contact radius and the adhesive force are dependent on the probe diameter.[45, 49, 50] Since larger probes will lead to higher values for separation work, comparisons of results obtained using probes with different diameters should be done with caution.

Shown in Fig. 1B are representative force-distance (F-D) curves for catechol-free (PSA-L) and catechol-containing (PSA-5DMA-L) PSAs using an SiO_2 probe, as examples of typical raw data obtained in our experiments. Representative F-D curves collected using PS and PE probes are included in Supplementary Fig. S2 in the Supporting Information. The appearance of multiple spikes in the retraction part of the curve was characteristic of most F-D curves and is suggestive of the presence of multiple adhesion and detachment points during the retraction of the AFM cantilever from the polymer film. Presence of these spikes can be attributed to detachment of multiple polymer chains from either the colloidal probe or the substrate upon retraction of the cantilever or alternatively to rupture of specific interactions between the individual polymer chains and the surface. Thus, the maximum detachment force value obtained from F-D curves is not a reliable measure of the overall adhesive interaction of the polymer with the probe. Moreover, extracting adhesion values based on estimating contact radius can itself introduce large errors into calculations due to the viscoelastic nature of the polymer as well as roughness and asperities on the colloidal particle. Instead, we chose to integrate the area under the F-D curve as an estimate of the magnitude of the overall adhesive strength between the polymer and the substrate in the contact area, which we refer to as "separation work" (W, in Joules) here.[51–53] This work is the product of thermodynamic work of adhesion (due to surface tension) and a function describing viscoelastic properties of the adhesive as well as an additional interfacial component reflecting factors such as probe diameter, surface roughness, and dwell time. The separation work calculated here is related to the energy that is required to detach the probe from the substrate.[47]

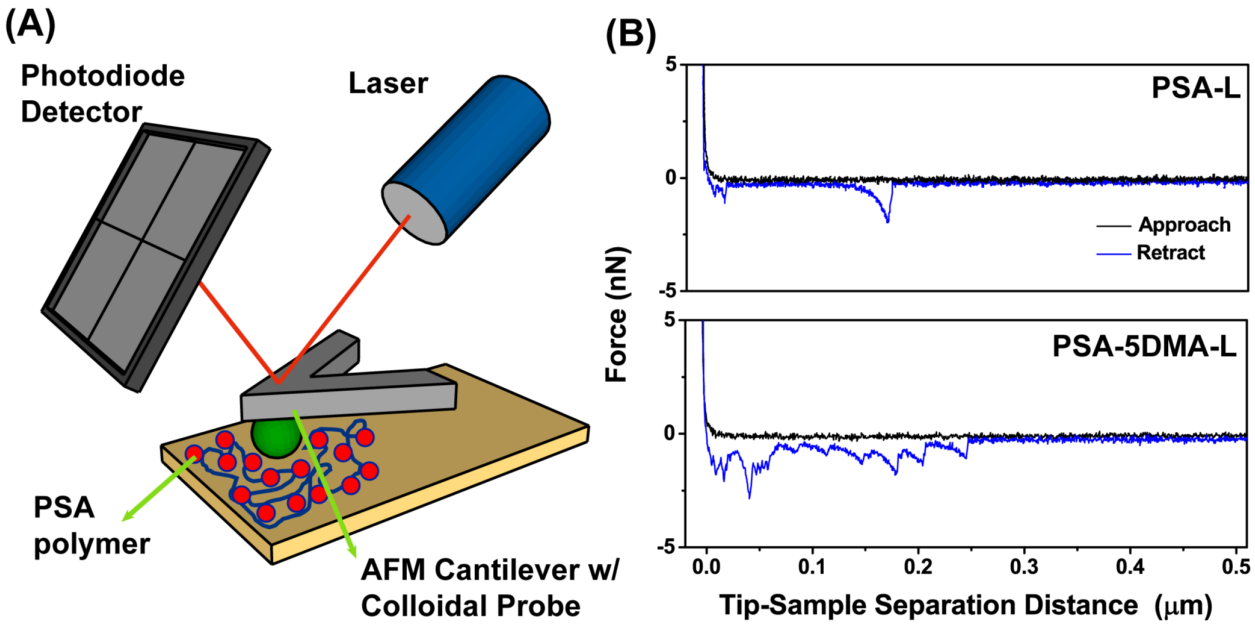

Figure 5.1: Colloidal probe spectroscopy on PSA polymers. (A) Schematic illustration of the colloidal probe spectroscopy technique. (B) Representative F-D curves for PSA-L and PSA-5DMA-L collected using an SiO_2 probe (d=3.5 μm).

Histograms and average values of W for the PSA polymers using different probes are presented in Fig. 2 and Table 2. Results show that incorporating 5 wt% of DMA into the PSA leads to a 6-fold and 2.5-fold increase in the separation work for SiO_2 and PS probes, respectively, but no significant increase in the separation work for the PE colloidal probe. The large increase in adhesion to silica upon incorporation of 5 wt% DMA may be attributed to strong binding mechanisms such as bidentate complexation as described previously.[12, 17] While we cannot invoke such mechanisms on PS, the surface of PS is nevertheless rich in phenyl rings which can accommodate π-π interactions with the catechol groups on the polymer. This can explain why we observed an increase in the separation work for catechol-containing PSAs as compared to the catechol-free PSAs when using PS probes. These observations further highlight the capability of catechols, even when incorporated at low molar ratios, to improve PSA performance on oxide and certain organic substrates via bidentate complexes, hydrogen-bonding, and π-π interactions as compared to polyolefins such as PE, which cannot accommodate such interactions.[16, 54]

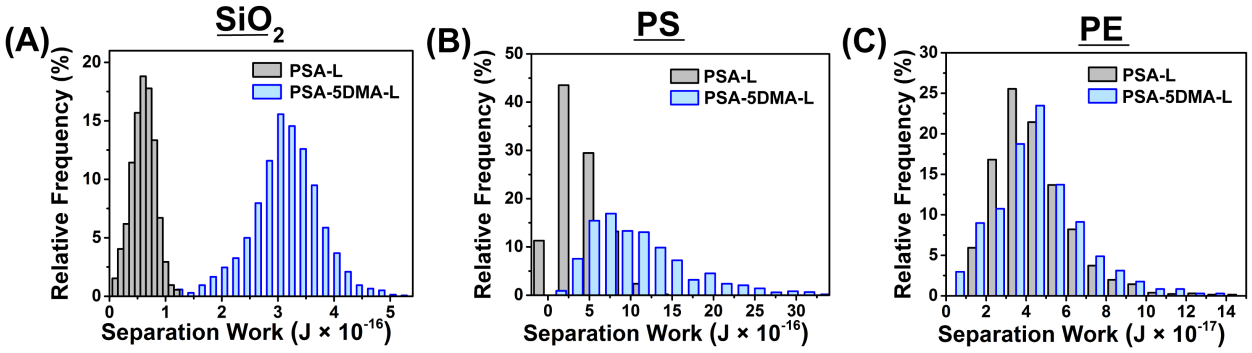

Figure 5.2: Separation work and adhesion of PSA polymers. Histograms of separation work on catechol-free and catechol-containing PSAs in contact with silica (A), polystyrene (B), and polyethylene (C) colloidal probes.

Table 5.2: Colloidal probe spectroscopy measurements for the synthesized pressure sensitive adhesives using SiO_2 (d=3.5 μm), PS (d=14.45 μm), and PE probes (D=10 μm). The number of F-D curves analyzed to calculate the average are indicated in the parentheses.

	Separation Work (J×10^{-17})		
Polymer	SiO_2	PS	PE
PSA-L	5.5±2.1 (3977)	40.3±26.8 (1266)	3.82±1.24 (1315)
PSA-5DMA-L	31.9±6.0 (1381)	105.0±59.2 (1218)	4.07±1.68 (1415)

Adhesive and Cohesive Properties of the Catechol-PSAs

Several macroscopic adhesion tests were performed on PSAs cast as thin films onto PET backing (Fig. 3A). PSA performance was measured against both stainless steel and high-density polyethylene (HDPE) test substrates. First, we evaluated PSA shear strength, which is related mostly to the cohesive strength and resistance of the adhesive to flow under shear (Fig. 3B).[55] As compared to other types of adhesives such as structural adhesives, PSAs generally experience viscous flow, resulting in very low shear strength when the evaluation is performed using conventional lap shear tests.[1] Nevertheless, in service PSAs tapes are often expected to persist for long periods of time under constant shear stress; thus the PSA industry uses static shear tests (constant load creep test) for determining the shear failure time as a measure of the cohesive strength or shear holding power of PSAs. For the low M_w polymers tested under both dry and wet conditions, the catechol-free system PSA-L failed almost immediately whereas the PSA-5DMA-L failed at approximately 12 min on average for both steel and HDPE. Statistical analysis showed that the shear test results for the low M_w polymers were not statistically significant (Supplementary Tables S1-S4).

Synthesis of PSAs in DMF resulted in higher M_w values and significantly improved shear holding power of the adhesives in ambient (dry) conditions, particularly those containing catechol motifs. For example, the high molecular weight catechol-free PSA (PSA-H) failed at an average of 9 minutes on both steel and HDPE, whereas catechol PSA with 5 wt% DMA (PSA-5DMA-H) survived for over 260 min for both substrates (Fig. 3B and 3C). Doubling the DMA feed concentration to 10 wt% extended the shear failure time to ∼380 min. This may be due at least in part to an increase in T_g (-41, -31, and -18°C for PSA-H, PSA-5DMA-H and PSA-5DMA-H, respectively) but also potentially to noncovalent intermolecular interactions among catechol motifs. In order to isolate the contributions of phenolic hydroxyls to adhesion, PSAs containing N-phenethyl methacrylamide (PMA) were also analyzed. Incorporating PMA into the copolymer increased the shear failure times compared to aromatic-free PSA-H (9, 62 and 157 min for PSA-H, PSA-5PMA-H and PSA-10PMA-H, respectively), although these values are much less than those of the catechol polymers. The increase in shear holding power of PSA-5DMA-H over PSA-5PMA-H was statistically significant ($p<0.05$) and cannot be attributed to a T_g effect. This enhancement in cohesive strength may have been a result of the non-covalent hydrogen bonding bonds between catechols in addition to the π-stacking interactions of the aromatic motifs.

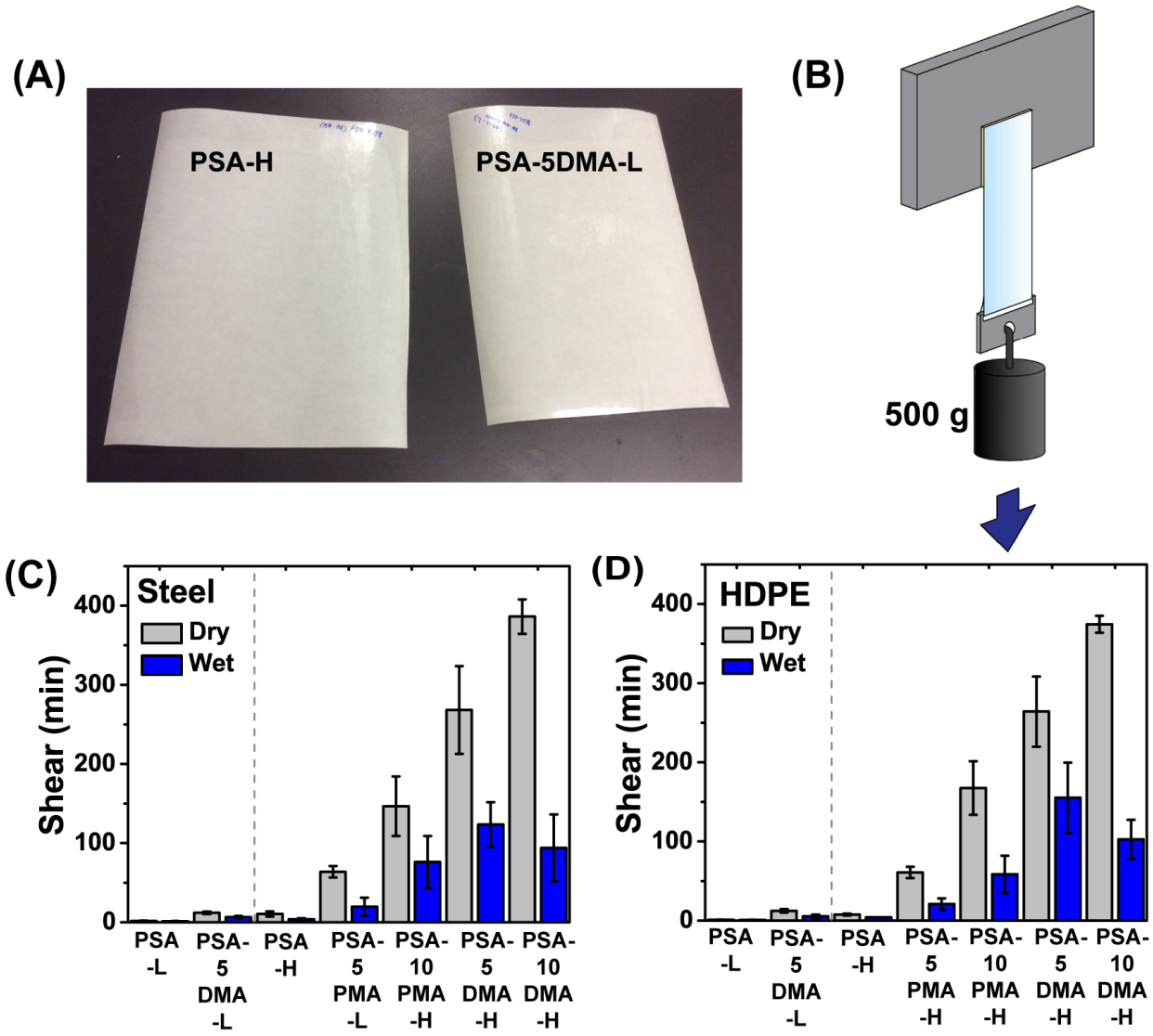

Figure 5.3: Fabrication of PSA tapes and static shear test results.(A) Photograph of the PSA tapes prepared from catechol-free (left) and catechol-containing (right) polymer. (B) Schematic of static shear test with 1 in×1 in bonded surface area and 500 g hanging weight. The experiment measures the elapsed time at which the adhesive bond fails. Shear failure times for (C) steel and (D) HDPE after 10 min conditioning in ambient and wet conditions. A vertical dashed line separates the results of the low (left) and high (right) M_w PSAs. Statistical analysis was performed using a one-way analysis of variance (ANOVA) and Tukey's multiple comparisons post-test to verify significant differences ($p<0.05$). Data are expressed as mean±standard deviation (N=5 independent test samples). A summary of statistical test results are presented in Supplementary Tables S1-S4.

In the case of PSAs brought into contact with test substrates under water, a general trend of 20-30% shorter shear failure times in wet versus dry conditions was observed for all PSAs tested (Fig. 3C-D). Notably, the catechol PSAs exhibited the longest shear failure times of all PSAs studied, with the difference between conventional PSA-H (4 min) and PSA-5DMA-H (139 min) being particularly striking. Improvement in wet shear performance can be attributed in part to enhancement of interfacial interactions by phenolic hydroxyls, although as described above an increase in T_g and intermolecular π-π stacking interactions between aromatic side chains likely contribute to strengthening the cohesive properties of the PSA. Surprisingly, further increasing the DMA content to 10% resulted in a decrease in wet shear failure time (97 min). Since we typically compensate increases in DMA concentration by decreasing the more hydrophobic BA monomer, it is possible that at 10% DMA, water had a plasticizing effect and decreased the shear strength of PSA-10DMA-H.

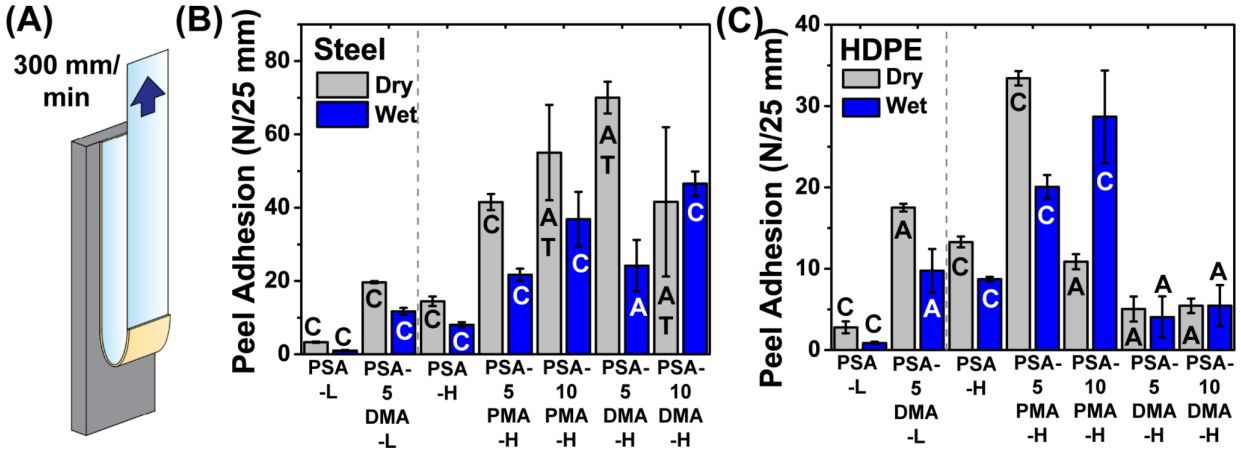

Figure 5.4: 180° peel adhesion test on PSA polymers. (A) Schematic of the 180° peel adhesion test in which 25 mm wide PSA strips are brought into contact with the adherend, conditioned for 24 h in ambient and wet conditions and then peeled at a rate of 300 mm/min. Peel adhesion results for (B) steel and (C) HDPE adherends (Failure Modes: C–cohesive, A–adhesive, and AT–adhesive transfer). A vertical dashed line separates the results of the low (left) and high (right) M_w PSAs. Statistical analysis was performed using a one-way analysis of variance (ANOVA) and Tukey's multiple comparisons post-test to verify significant differences ($p<0.05$). Data are expressed as mean±standard deviation (N=5 independent test samples). A summary of statistical test results for the peel adhesion tests are presented in Supplementary Tables S5-S8.

Catechol-PSA adhesion was also evaluated using the 180°C peel adhesion test. This test measures the average force required to peel a PSA tape from a rigid test substrate (Fig. 4A). For the low molecular weight PSAs tested in dry conditions, PSA-L achieved a peel force

of 3.3±0.2 N/25 mm on steel whereas the peel force of PSA-5DMA-L increased to 19.7±0.3 N/25 mm (Fig. 4B); both samples failed cohesively. A similar trend in peel strength was observed on HDPE, although in this case the failure mode was adhesive rather than cohesive (Fig. 4C).

For the high molecular weight PSAs the dry peel behavior was more complex, with different trends observed for stainless steel and HDPE. For steel, the dry peel force increased from 14.47±1.3 N/25 mm for PSA-H to 70±4.3 N/25 mm for PSA-5DMA-H, which failed via adhesive transfer (AT) wherein the polymer detached from the PET backing material and remained adhered onto the stainless steel. This behavior can be attributed to the strong interactions of catechols toward metals. Further increasing the catechol content to 10 wt% reduced the dry peel adhesion to 41.6±20.4 N/25 mm. Dry peel adhesion of phenethyl-containing polymers on stainless steel increased as a function of PMA monomer concentration, peaking at 55.1±13.0 N/25 mm for PSA-10PMA-H.

The assay for wet peel strength was designed to be challenging and involved bringing the PSA and test substrate into contact under water and then further conditioning in water for 24 h before testing. For the PSAs investigated here, wet peel strength was almost always lower than dry peel strength. Notable exceptions were PSA-10PMA-H, which had similar values for dry and wet performance on both steel and HDPE, and PSA-10DMA-H, which had significantly higher wet vs dry peel strength. Wet peel strength on steel increased with catechol content, achieving the highest value of 46.6±3.4 N/25 mm for PSA-10DMA-H. An interesting finding is that PMA-polymers outperformed DMA-polymers on HDPE in both dry and wet peel conditions (Fig. 4C). Dry peel adhesion for both catechol PSAs decreased as compared to the control polymer PSA-H, although the failure mode changed from cohesive to adhesive failure, which is preferred in applications where no residue should be left on the substrate after the PSA has been peeled off. The stark difference in peel adhesion results of the catecholic PSAs on stainless steel as compared to HDPE emphasizes the importance of strong interactions of catechols toward polar and metallic surfaces as compared to low surface energy and nonpolar, organic adherends. This observation also agrees with the colloidal probe spectroscopy results discussed in the previous section.

Lastly, we also measured tack adhesion using the loop tack test (Fig. 5A), which assesses the ability of a PSA to quickly adhere onto surfaces with minimal applied force. High tack PSAs are generally soft and viscoelastic materials capable of rapid deformation and wetting of the surface. Tackifiers and/or plasticizers are often incorporated to lower the storage modulus of the polymer and optimize the tack of commercial PSA formulations.[1, 44, 56] As shown in Fig. 5B and Fig. 5C, it can be seen that every PSA exhibited lower tack adhesion on HDPE than on steel, illustrating the challenges associated with adhesion to polyolefins. A notable result is that catechol polymer PSA-5DMA-L showed the highest tack adhesion among all the aromatic PSAs, for both steel and HDPE.

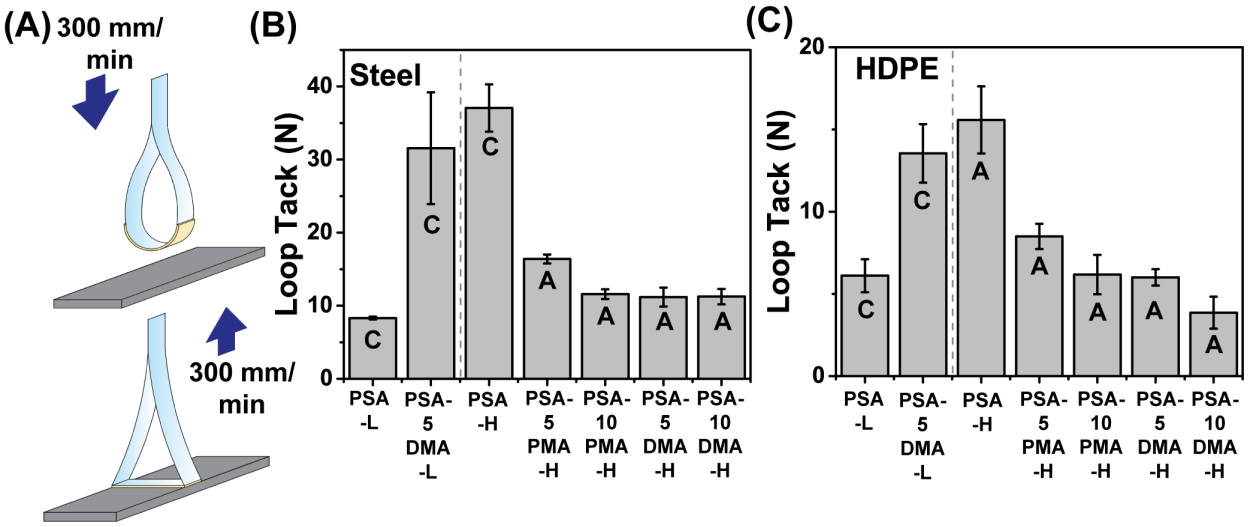

Figure 5.5: Loop tack test on PSA polymers. (A) Loop tack (quickstick) test with a pull rate of 300 mm/min, and a bonded surface area of 2.5 cm×3 cm. Tack adhesion test results for (B) steel and (C) HDPE (Failure Modes: C–cohesive and A–adhesive). A vertical dashed line separates the results of the low (left) and high (right) M_w PSAs. Statistical analysis was performed using a one-way analysis of variance (ANOVA) and Tukey's multiple comparisons post-test to verify significant differences ($p<0.05$). Data are expressed as mean±standard deviation (N=5 independent test samples). A summary of statistical test results for the loop tack tests are presented in Supplementary Tables S9-S10.

5.4 Conclusions

Taken together, the colloidal probe (Table 2), shear, peel adhesion and tack results identify certain circumstances under which PSA performance clearly benefits from the presence of catechols, and other situations where the benefit is less clear. Colloidal force spectroscopy revealed that the work required to detach polystyrene and silica colloidal probes from a catechol PSA was 2.5-6 times greater compared to a catechol-free PSA. The adhesion promoting ability of catechols was also evident in static shear and 180° peel measurements, where both the shear holding power and peel adhesion of catechol PSAs were dramatically higher than a conventional PSA in both dry and wet conditions. The DMA concentration, however, should not exceed 10 wt% in order to keep the T_g of the polymers low and maintain the ability of PSA's to wet out and adhere onto surfaces. In the case of nonpolar organic substrates, the potential benefit of catechol PSAs is less obvious as indicated by the good peel performance of PSAs containing non-phenolic aromatic groups on both steel and HDPE. This is suggestive of more general aromatic contributions to PSA performance, possibly arising from interfacial or bulk π-π stacking interactions, although further studies will be necessary to

confirm this. Finally, it is important to note that DOPA does not work in isolation in mussel adhesive proteins; rather, it functions in concert with many other amino acids.[57] Although catechols make sense as an initial focus of study, they should be considered a starting point only. Another unique feature of mussel adhesive proteins that may be worth mimicking in PSAs is the close proximity of catechols (DOPA) and amines (Lys, His and Arg).[57, 58] Recent model adhesion studies conducted by surface forces apparatus and single molecule force spectroscopy suggest an enhancement of catechol adhesion in partnership with nearby amino functional groups.[14, 40, 59–62] Accordingly, in the future it may be possible to further enhance catechol PSA performance through introduction of amine containing monomers into the polymer structure.[63] Moreover, structurally related derivatives of catechols may function as well or even better than catechols. For example, the trihydroxyphenyl (gallol) functional group offers additional possibilities for adhesive building blocks, as gallol containing biomolecules and synthetic polymers have been reported to be adhesive to surfaces.[22, 64]

5.5 Supplementary Figures

Fabrication of PSA tapes

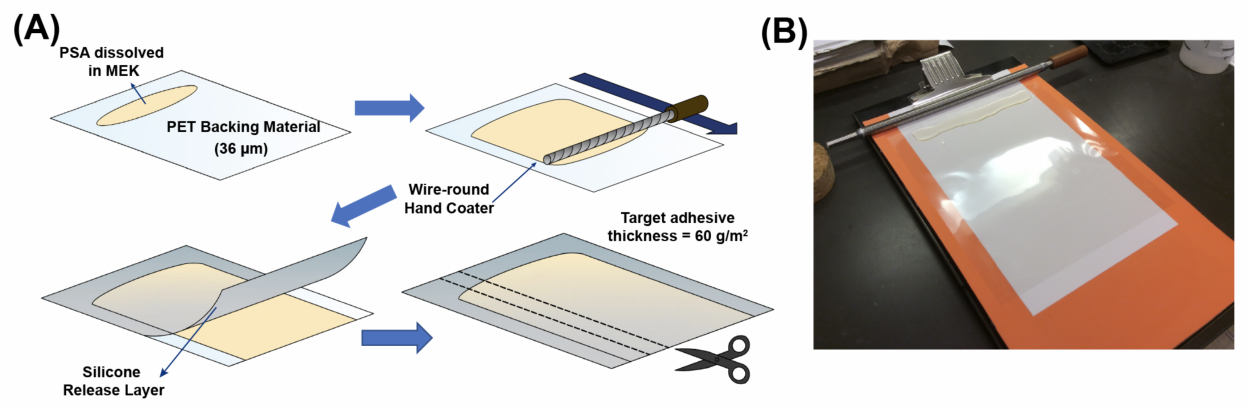

Figure S5.1: (A) Fabrication of the pressure sensitive adhesives tapes. (B) Draw-down coating with a target thickness of 60 gsm.

Colloidal Probe Spectroscopy Data

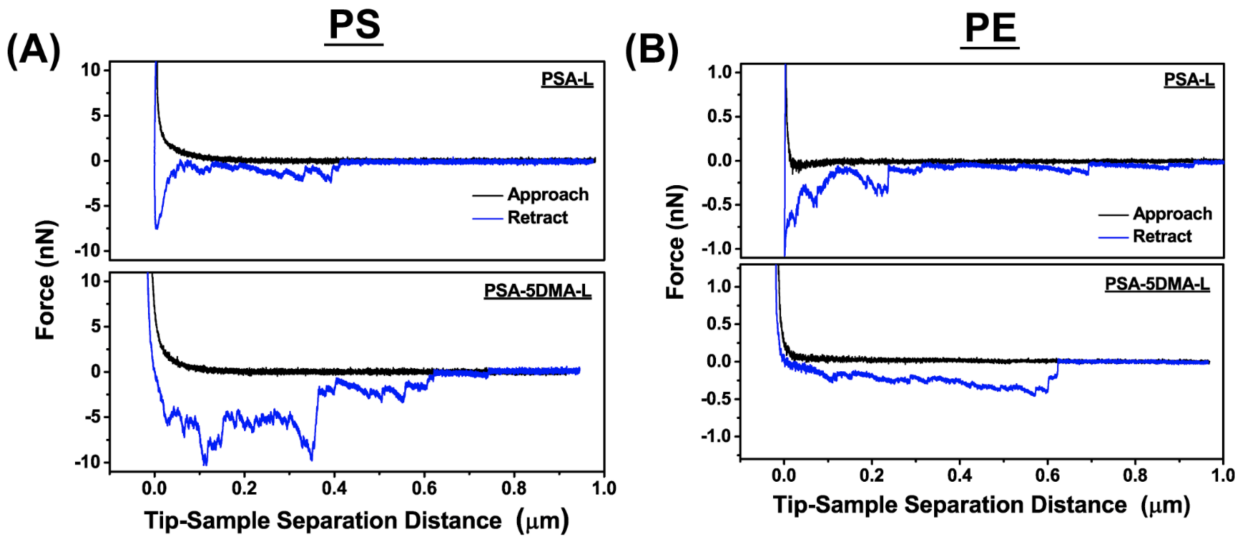

Figure S5.2: Representative colloidal probe spectroscopy F-D curves for PSA-L and PSA-5DMA-L collected using (A) PS (d=14.45 μm) and (B) PE probes (D=10 μm).

Summary of Statistical Differences Between Test Samples via One-Way ANOVA and Tukey Test ($p<0.05$)

Table S5.1: Summary of statistical analysis results for the shear test on stainless steel in dry conditions. 0, not significant; 1, significant with $p<0.05$.

Shear - Dry - Steel						
	PSA-L	PSA-5DMA-L	PSA-H	PSA-5PMA-H	PSA-10PMA-H	PSA-5DMA-H
PSA-5DMA-L	0					
PSA-H	0	0				
PSA-5PMA-H	1	0	0			
PSA-10PMA-H	1	1	1	1		
PSA-5DMA-H	1	1	1	1	1	
PSA-10DMA-H	1	1	1	1	1	1

Table S5.2: Summary of statistical analysis results for the shear test on HDPE in dry conditions. 0, not significant; 1, significant with $p<0.05$.

Shear - Dry - HDPE						
	PSA-L	PSA-5DMA-L	PSA-H	PSA-5PMA-H	PSA-10PMA-H	PSA-5DMA-H
PSA-5DMA-L	0					
PSA-H	0	0				
PSA-5PMA-H	1	1	1			
PSA-10PMA-H	1	1	1	1		
PSA-5DMA-H	1	1	1	1	1	
PSA-10DMA-H	1	1	1	1	1	1

Table S5.3: Summary of statistical analysis results for the shear test on stainless steel after underwater assembly of test samples and 10 min underwater conditioning. 0, not significant; 1, significant with $p<0.05$.

Shear - Wet - Steel						
	PSA-L	PSA-5DMA-L	PSA-H	PSA-5PMA-H	PSA-10PMA-H	PSA-5DMA-H
PSA-5DMA-L	0					
PSA-H	0	0				
PSA-5PMA-H	0	0	0			
PSA-10PMA-H	1	1	1	1		
PSA-5DMA-H	1	1	1	1	1	
PSA-10DMA-H	1	1	1	1	0	0

Table S5.4: Summary of statistical analysis results for the shear test on HDPE after underwater assembly of test samples and 10 min underwater conditioning. 0, not significant; 1, significant with $p<0.05$.

Shear - Wet - HDPE						
	PSA-L	PSA-5DMA-L	PSA-H	PSA-5PMA-H	PSA-10PMA-H	PSA-5DMA-H
PSA-5DMA-L	0					
PSA-H	0	0				
PSA-5PMA-H	0	0	0			
PSA-10PMA-H	1	1	0	0		
PSA-5DMA-H	1	1	1	1	1	
PSA-10DMA-H	1	1	1	1	0	1

Table S5.5: Summary of statistical analysis results for the 180° peel adhesion test on stainless steel after 24 hr storage in dry conditions. 0, not significant; 1, significant with $p<0.05$.

Peel - Dry - Steel						
	PSA-L	PSA-5DMA-L	PSA-H	PSA-5PMA-H	PSA-10PMA-H	PSA-5DMA-H
PSA-5DMA-L	0					
PSA-H	0	0				
PSA-5PMA-H	1	1	1			
PSA-10PMA-H	1	1	1	0		
PSA-5DMA-H	1	1	1	1	0	
PSA-10DMA-H	1	1	1	0	0	1

Table S5.6: Summary of statistical analysis results for the 180° peel adhesion test on HDPE after 24 hr storage in dry conditions. 0, not significant; 1, significant with $p<0.05$.

Peel - Dry - HDPE						
	PSA-L	PSA-5DMA-L	PSA-H	PSA-5PMA-H	PSA-10PMA-H	PSA-5DMA-H
PSA-5DMA-L	1					
PSA-H	1	1				
PSA-5PMA-H	1	1	1			
PSA-10PMA-H	1	1	0	1		
PSA-5DMA-H	0	1	1	1	1	
PSA-10DMA-H	1	1	1	1	1	0

Table S5.7: Summary of statistical analysis results for the 180° peel adhesion test on stainless steel after underwater assembly of test samples and 24 hr underwater conditioning. 0, not significant; 1, significant with $p<0.05$.

Peel - Wet - Steel						
	PSA-L	PSA-5DMA-L	PSA-H	PSA-5PMA-H	PSA-10PMA-H	PSA-5DMA-H
PSA-5DMA-L	1					
PSA-H	0	0				
PSA-5PMA-H	1	1	1			
PSA-10PMA-H	1	1	1	1		
PSA-5DMA-H	1	1	1	1	0	
PSA-10DMA-H	1	1	1	1	1	1

Table S5.8: Summary of statistical analysis results for the 180° peel adhesion test on HDPE after underwater assembly of test samples and 24 hr underwater conditioning. 0, not significant; 1, significant with $p<0.05$.

Peel - Wet - HDPE						
	PSA-L	PSA-5DMA-L	PSA-H	PSA-5PMA-H	PSA-10PMA-H	PSA-5DMA-H
PSA-5DMA-L	1					
PSA-H	1	0				
PSA-5PMA-H	1	1	1			
PSA-10PMA-H	1	1	1	1		
PSA-5DMA-H	0	1	0	1	1	
PSA-10DMA-H	0	0	0	1	1	0

Table S5.9: Summary of statistical analysis results for the loop tack test on stainless steel. 0, not significant; 1, significant with $p<0.05$.

Loop Tack - Dry - Steel						
	PSA-L	PSA-5DMA-L	PSA-H	PSA-5PMA-H	PSA-10PMA-H	PSA-5DMA-H
PSA-5DMA-L	1					
PSA-H	1	0				
PSA-5PMA-H	1	1	1			
PSA-10PMA-H	0	1	1	0		
PSA-5DMA-H	0	1	1	0	0	
PSA-10DMA-H	0	1	1	0	0	0

Table S5.10: Summary of statistical analysis results for the loop tack test on HDPE. 0, not significant; 1, significant with $p<0.05$.

Loop Tack - Dry - HDPE						
	PSA-L	PSA-5DMA-L	PSA-H	PSA-5PMA-H	PSA-10PMA-H	PSA-5DMA-H
PSA-5DMA-L	1					
PSA-H	1	0				
PSA-5PMA-H	0	1	1			
PSA-10PMA-H	0	1	1	0		
PSA-5DMA-H	0	1	1	0	0	
PSA-10DMA-H	0	1	1	1	0	0

Underwater Mussel-Inspired Sticky Notes

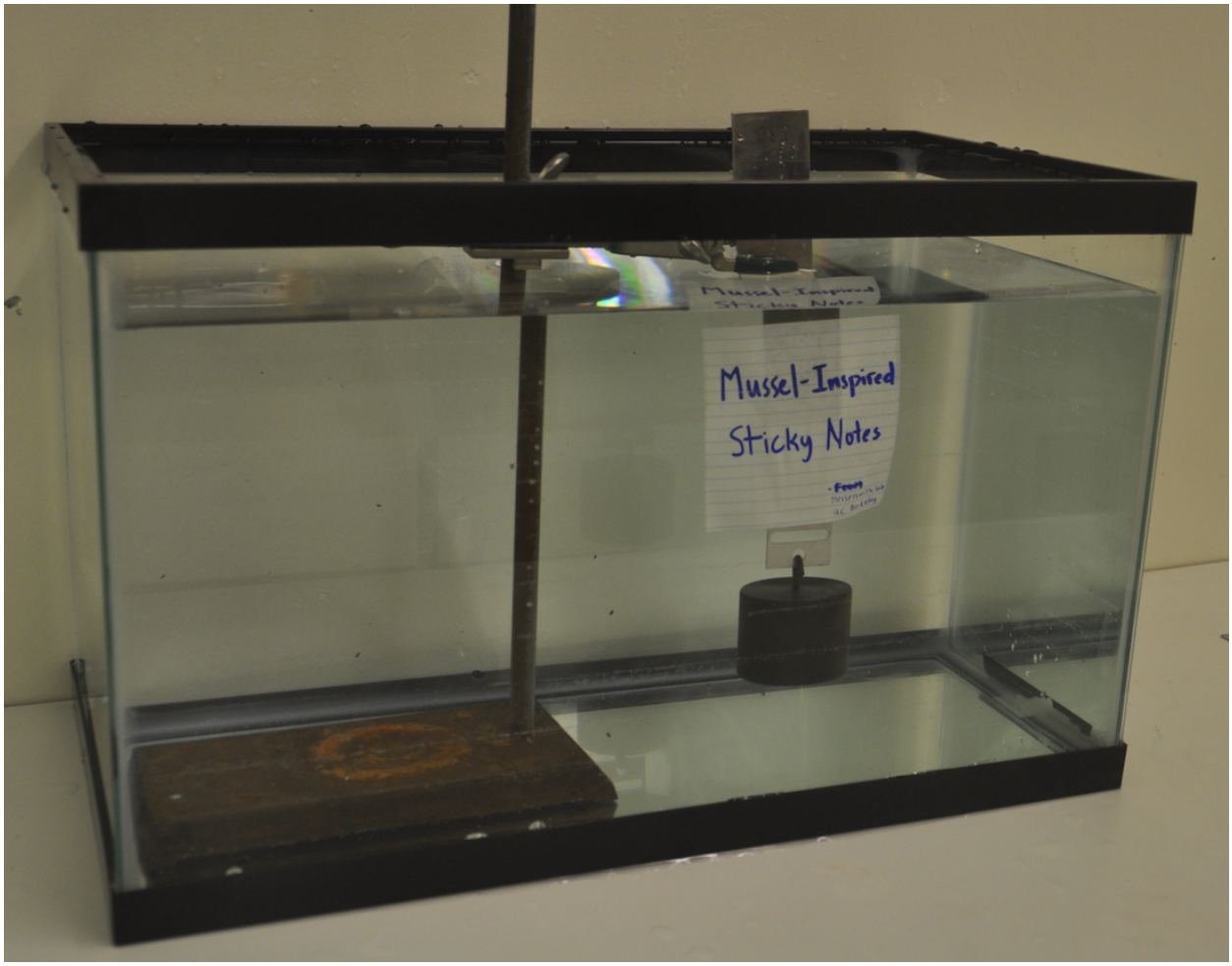

Figure S5.3: Digital image of a piece of water-resistant "Rite in the Rain" paper with one end coated with PSA-5DMA-H and attached directly to stainless steel under deionized water. The bottom end of the paper is attached to a piece of PET film also coated with PSA-5DMA-H and looped into the shear test clip, where the 1 kg weight is hooked into.

References

[1] Alphonsus V Pocius. *Adhesion and adhesives technology: an introduction*. Carl Hanser Verlag GmbH Co KG, 2012. ISBN: 3446431772 (cit. on pp. 108, 116, 120).

[2] Steven Abbott. *Adhesion science: principles and practice*. DEStech Publications, Inc, 2015 (cit. on p. 108).

[3] Wiebke Maassen, Michael A. R. Meier, and Norbert Willenbacher. "Unique adhesive properties of pressure sensitive adhesives from plant oils". In: *International Journal of Adhesion and Adhesives* 64 (2016), pp. 65–71 (cit. on p. 108).

[4] H. Schonhorn and R. H. Hansen. "Surface treatment of polymers for adhesive bonding". In: *Journal of Applied Polymer Science* 11.8 (1967), pp. 1461–1474 (cit. on p. 108).

[5] Amaia Agirre et al. "Improving adhesion of acrylic waterborne PSAs to low surface energy materials: Introduction of stearyl acrylate". In: *Journal of Polymer Science Part A: Polymer Chemistry* 48.22 (2010), pp. 5030–5039 (cit. on p. 108).

[6] Preetika Karnal et al. "Importance of Substrate Functionality on the Adhesion and Debonding of a Pressure-Sensitive Adhesive under Water". In: *ACS Applied Materials Interfaces* 9.48 (2017), pp. 42344–42353 (cit. on p. 108).

[7] "Post-it® Extreme Notes, 3 in. x 3 in., Green, Yellow, Orange, 3 Pads/Pack, 45 Sheets/Pad". In: $CORP_FUZEExp_US$ (). URL: https://www.post-it.com/3M/en_US/post-it/products/~/Post-it-Extreme-Notes-3-in-x-3-in-Green-Yellow-Orange-3-Pads-Pack-45-Sheets-Pad/?N=4327+3290627424+3294529207&rt=rud%20https://www.post-it.com/3M/en_US/post-it/products/~/Post-it-Extreme-Notes-3-in-x-3-in-Green-Yellow-Orange-3-Pads-Pack-45-Sheets-Pad/?N=4327+3290627424+3294529207&preselect=8750143+3293786499&rt=rud (cit. on p. 108).

[8] G. A. Young. "Response to, and selection between, firm substrata by Mytilus edulis". In: *Journal of the Marine Biological Association of the United Kingdom* 63.3 (1983), pp. 653–659 (cit. on p. 109).

[9] J. Herbert Waite. "Mussel adhesion – essential footwork". In: *Journal of Experimental Biology* 220.4 (2017), pp. 517–530 (cit. on p. 109).

[10] Bruce P. Lee et al. "Mussel-Inspired Adhesives and Coatings". In: *Annual Review of Materials Research* 41.1 (2011), pp. 99–132 (cit. on p. 109).

[11] Matthew J. Harrington, Franziska Jehle, and Tobias Priemel. "Mussel Byssus Structure-Function and Fabrication as Inspiration for Biotechnological Production of Advanced Materials". In: *Biotechnology Journal* 13.12 (2018), p. 1800133 (cit. on p. 109).

[12] Haeshin Lee, Norbert F. Scherer, and Phillip B. Messersmith. "Single-molecule mechanics of mussel adhesion". In: *Proceedings of the National Academy of Sciences of the United States of America* 103.35 (2006), pp. 12999–13003 (cit. on pp. 109, 115).

[13] Qi Lin et al. "Adhesion mechanisms of the mussel foot proteins mfp-1 and mfp-3". In: *Proceedings of the National Academy of Sciences* 104.10 (2007), pp. 3782–3786 (cit. on p. 109).

[14] Greg P. Maier et al. "Adaptive synergy between catechol and lysine promotes wet adhesion by surface salt displacement". In: *Science* 349.6248 (2015), pp. 628–632 (cit. on pp. 109, 122).

[15] Yiran Li et al. "Single Molecule Evidence for the Adaptive Binding of DOPA to Different Wet Surfaces". In: *Langmuir* 30.15 (2014), pp. 4358–4366 (cit. on p. 109).

[16] J. Saiz-Poseu et al. "The Chemistry behind Catechol-Based Adhesion". In: *Angewandte Chemie International Edition* 58.3 (2019), pp. 696–714 (cit. on pp. 109, 115).

[17] Pegah Kord Forooshani and Bruce P. Lee. "Recent approaches in designing bioadhesive materials inspired by mussel adhesive protein". In: *Journal of Polymer Science Part A: Polymer Chemistry* 55.1 (2017), pp. 9–33 (cit. on pp. 109, 115).

[18] Anton H. Hofman et al. "Bioinspired Underwater Adhesives by Using the Supramolecular Toolbox". In: *Advanced Materials* 30.19 (2018), p. 1704640 (cit. on p. 109).

[19] Michael North, Chelsey A. Del Grosso, and Jonathan James Wilker. "High Strength Underwater Bonding with Polymer Mimics of Mussel Adhesive Proteins". In: *ACS Applied Materials & Interfaces* (2017) (cit. on p. 109).

[20] Ying Xu et al. "Mussel-Inspired Polyesters with Aliphatic Pendant Groups Demonstrate the Importance of Hydrophobicity in Underwater Adhesion". In: *Advanced Materials Interfaces* 4.22 (2017), p. 1700506 (cit. on p. 109).

[21] Heather J. Meredith, Courtney L. Jenkins, and Jonathan J. Wilker. "Enhancing the Adhesion of a Biomimetic Polymer Yields Performance Rivaling Commercial Glues". In: *Advanced Functional Materials* 24.21 (2014), pp. 3259–3267 (cit. on p. 109).

[22] Kan Zhan et al. "Tunicate-Inspired Gallol Polymers for Underwater Adhesive: A Comparative Study of Catechol and Gallol". In: *Biomacromolecules* 18.9 (2017), pp. 2959–2966 (cit. on pp. 109, 122).

[23] Grozdana Bilic et al. "Injectable candidate sealants for fetal membrane repair: bonding and toxicity in vitro". In: *American Journal of Obstetrics and Gynecology* 202.1 (2010), 85.e1–85.e9 (cit. on p. 109).

[24] Hui Shao, Kent N. Bachus, and Russell J. Stewart. "A Water-Borne Adhesive Modeled after the Sandcastle Glue of P. californica". In: *Macromolecular Bioscience* 9.5 (2009), pp. 464–471 (cit. on p. 109).

[25] Bum Jin Kim et al. "Mussel-Mimetic Protein-Based Adhesive Hydrogel". In: *Biomacromolecules* 15.5 (2014), pp. 1579–1585 (cit. on p. 109).

[26] Sang-Bae Lee et al. "Catechol-Functionalized Synthetic Polymer as a Dental Adhesive to Contaminated Dentin Surface for a Composite Restoration". In: *Biomacromolecules* 16.8 (2015), pp. 2265–2275 (cit. on p. 109).

[27] Chaehoon Kim, Hirotaka Ejima, and Naoko Yoshie. "Non-swellable self-healing polymer with long-term stability under seawater". In: *RSC Advances* 7.31 (2017), pp. 19288–19295 (cit. on p. 109).

[28] Jincai Li, Hirotaka Ejima, and Naoko Yoshie. "Seawater-Assisted Self-Healing of Catechol Polymers via Hydrogen Bonding and Coordination Interactions". In: *ACS Applied Materials & Interfaces* 8.29 (2016), pp. 19047–19053 (cit. on p. 109).

[29] Yun-Hui Yan et al. "Mussel-Inspired Hydrogel Composite with Multi-Stimuli Responsive Behavior". In: *Macromolecular Materials and Engineering* 304.7 (2019), p. 1800720 (cit. on p. 109).

[30] Qiang Zhang et al. "Synthesis of well-defined catechol polymers for surface functionalization of magnetic nanoparticles". In: *Polymer Chemistry* 7.45 (2016), pp. 7002–7010 (cit. on p. 109).

[31] Emilie Faure et al. "Functional Nanogels as Platforms for Imparting Antibacterial, Antibiofilm, and Antiadhesion Activities to Stainless Steel". In: *Advanced Functional Materials* 22.24 (2012), pp. 5271–5282 (cit. on p. 109).

[32] Emilie Faure et al. "Clay and DOPA Containing Polyelectrolyte Multilayer Film for Imparting Anticorrosion Properties to Galvanized Steel". In: *Langmuir* 28.5 (2012), pp. 2971–2978 (cit. on p. 109).

[33] Haosheng Wu et al. "Transfer Printing of Metallic Microstructures on Adhesion-Promoting Hydrogel Substrates". In: *Advanced Materials* 27.22 (2015), pp. 3398–3404 (cit. on p. 109).

[34] Debabrata Payra et al. "Rational design of a biomimetic glue with tunable strength and ductility". In: (2017) (cit. on p. 109).

[35] Juan Yang et al. "The effect of molecular composition and crosslinking on adhesion of a bio-inspired adhesive". In: 6.16 (2015), pp. 3121–3130 (cit. on pp. 109, 112).

[36] Paul Glass et al. "Enhanced Reversible Adhesion of Dopamine Methacrylamide-Coated Elastomer Microfibrillar Structures under Wet Conditions". In: *Langmuir* 25.12 (2009), pp. 6607–6612 (cit. on p. 109).

[37] Bruce P. Lee et al. "Synthesis of 3,4-dihydroxyphenylalanine (DOPA) containing monomers and their co-polymerization with PEG-diacrylate to form hydrogels". In: *Journal of Biomaterials Science, Polymer Edition* 15.4 (2004), pp. 449–464 (cit. on p. 109).

[38] Haeshin Lee, Bruce P. Lee, and Phillip B. Messersmith. "A reversible wet/dry adhesive inspired by mussels and geckos". In: *Nature* 448.7151 (2007), pp. 338–341 (cit. on p. 109).

[39] Glenn Westwood, Trinity N. Horton, and Jonathan J. Wilker. "Simplified Polymer Mimics of Cross-Linking Adhesive Proteins". In: *Macromolecules* 40.11 (2007), pp. 3960–3964 (cit. on p. 109).

[40] Sean K. Clancy et al. "Marine Bioinspired Underwater Contact Adhesion". In: *Biomacromolecules* 17.5 (2016), pp. 1869–1874 (cit. on pp. 109, 122).

[41] Jannis Lübbe et al. "Determining cantilever stiffness from thermal noise". In: *Beilstein Journal of Nanotechnology* 4.1 (2013), pp. 227–233 (cit. on p. 110).

[42] Patent. 1961/02/28 1961. URL: `https://patents.google.com/patent/US2973286A/en` (cit. on p. 112).

[43] Istvan Benedek and Mikhail M. Feldstein. *Technology of Pressure-Sensitive Adhesives and Products*. CRC Press, 2008, p. 570. ISBN: 978-1-4200-5941-0 (cit. on p. 112).

[44] Donatas Satas. *Handbook of pressure sensitive adhesive technology*. Vol. 1. Van Nostrand Reinhold New York, 1989 (cit. on pp. 112, 120).

[45] Hans-Jürgen Butt, Brunero Cappella, and Michael Kappl. "Force measurements with the atomic force microscope: Technique, interpretation and applications". In: *Surface Science Reports* 59.1 (2005), pp. 1–152 (cit. on p. 114).

[46] Johann Erath, Stephan Schmidt, and Andreas Fery. "Characterization of adhesion phenomena and contact of surfaces by soft colloidal probe AFM". In: *Soft Matter* 6.7 (2010), pp. 1432–1437 (cit. on p. 114).

[47] A. Zosel. "Adhesion and tack of polymers: Influence of mechanical properties and surface tensions". In: *Colloid and Polymer Science* 263.7 (1985), pp. 541–553 (cit. on p. 114).

[48] Adriana Paiva et al. "Study of the Surface Adhesion of Pressure-Sensitive Adhesives by Atomic Force Microscopy and Spherical Indenter Tests". In: *Macromolecules* 33.5 (2000), pp. 1878–1881 (cit. on p. 114).

[49] Michael Kappl and Hans-Jürgen Butt. "The Colloidal Probe Technique and its Application to Adhesion Force Measurements". In: *Particle and Particle Systems Characterization* 19.3 (2002), pp. 129–143 (cit. on p. 114).

[50] Robert W. Carpick, D. Frank Ogletree, and Miquel Salmeron. "A General Equation for Fitting Contact Area and Friction vs Load Measurements". In: *Journal of Colloid and Interface Science* 211.2 (1999), pp. 395–400 (cit. on p. 114).

[51] Kim Hyonchol et al. "Quantification of fibronectin and cell surface interactions by AFM". In: *Colloids and Surfaces B: Biointerfaces* 25.1 (2002), pp. 33–43 (cit. on p. 114).

[52] Bettye L. Smith et al. "Molecular mechanistic origin of the toughness of natural adhesives, fibres and composites". In: *Nature* 399.6738 (1999), pp. 761–763 (cit. on p. 114).

[53] Eugene Kim et al. "Microbially Synthesized Repeats of Mussel Foot Protein Display Enhanced Underwater Adhesion". In: *ACS Applied Materials Interfaces* 10.49 (2018), pp. 43003–43012 (cit. on p. 114).

[54] Chuan Leng et al. "Interfacial Structure of a DOPA-Inspired Adhesive Polymer Studied by Sum Frequency Generation Vibrational Spectroscopy". In: *Langmuir* 29.22 (2013), pp. 6659–6664 (cit. on p. 115).

[55] Emiliano M. Ciannamea and Roxana A. Ruseckaite. "Pressure Sensitive Adhesives Based on Epoxidized Soybean Oil: Correlation Between Curing Conditions and Rheological Properties". In: *Journal of the American Oil Chemists' Society* 95.4 (2018), pp. 525–532 (cit. on p. 116).

[56] James J. Gallagher, Marc A. Hillmyer, and Theresa M. Reineke. "Acrylic Triblock Copolymers Incorporating Isosorbide for Pressure Sensitive Adhesives". In: *ACS Sustainable Chemistry Engineering* 4.6 (2016), pp. 3379–3387 (cit. on p. 120).

[57] J. Herbert Waite and Xiaoxia Qin. "Polyphosphoprotein from the Adhesive Pads of Mytilus edulis". In: *Biochemistry* 40.9 (2001), pp. 2887–2893 (cit. on p. 122).

[58] J. Herbert Waiter. "Reverse Engineering of Bioadhesion in Marine Mussels". In: *Annals of the New York Academy of Sciences* 875.1 (1999), pp. 301–309 (cit. on p. 122).

[59] Michael V. Rapp et al. "Defining the Catechol–Cation Synergy for Enhanced Wet Adhesion to Mineral Surfaces". In: *Journal of the American Chemical Society* 138.29 (2016), pp. 9013–9016 (cit. on p. 122).

[60] Matthew A. Gebbie et al. "Tuning underwater adhesion with cation– interactions". In: *Nature Chemistry* advance online publication (2017) (cit. on p. 122).

[61] Yiran Li et al. "Single-molecule study of the synergistic effects of positive charges and Dopa for wet adhesion". In: *Journal of Materials Chemistry B* (2017) (cit. on p. 122).

[62] Ying Li et al. "Hidden complexity of synergistic roles of Dopa and lysine for strong wet adhesion". In: *Materials Chemistry Frontiers* 1.12 (2017), pp. 2664–2668 (cit. on p. 122).

[63] James D. White and Jonathan J. Wilker. "Underwater Bonding with Charged Polymer Mimics of Marine Mussel Adhesive Proteins". In: *Macromolecules* 44.13 (2011), pp. 5085–5088 (cit. on p. 122).

[64] Tadas S. Sileika et al. "Colorless Multifunctional Coatings Inspired by Polyphenols Found in Tea, Chocolate, and Wine". In: *Angewandte Chemie International Edition* 52.41 (2013), pp. 10766–10770 (cit. on p. 122).

Chapter 6

High Performance Adhesives via Cooperativity of Catechols and Amines

* This chapter is adapted based on the research originally appeared as a peer-reviewed article co-first-authored by me published in Angewandte Chemie.
B. D. B. Tiu[†], P. Delparastan[†], M. R. Ney, M. Gerst, and P. B. Messersmith, Cooperativity of Catechols and Amines in High Performance Dry/Wet Adhesives. Angew. Chem. Int. Ed. 2020, 59, 16616

Abstract

The outstanding adhesive performance of mussel byssal threads has been a beacon of inspiration for materials scientists over the past few decades. Historically, presence of a significant amount of the unique catecholic amino acid dihydroxyphenylalanine (Dopa) has been considered to play a key role in strong dry and wet adhesive properties of the byssal interfacial proteins. In recent years, molecular and microscopic level studies using short peptides or small molecule analogs have investigated the roles of other amino acids in mussel adhesion. In particular, these studies have highlighted the cohesive role of cation-π interactions as well as the adhesive synergy between Dopa and flanking lysine residues. Inspired to design advanced synthetic adhesives that exploit amino-catechol synergy, we synthesized polymeric pressure sensitive adhesives (PSAs) by copolymerizing traditional PSA monomers, butyl acrylate and acrylic acid, with mussel-inspired lysine- and aromatic-rich monomers. Of particular interest was to compare the consequences of decoupling amino and catechol moieties from each other (i.e. incorporated as separate monomers) versus a monomer architecture in which the catechol and amine were coupled together in a fixed orientation in the monomer side chain. Comprehensive multi-scale adhesion assays were used to probe performance at

the molecular, microscopic and macroscopic levels through a combination of AFM-assisted force spectroscopy, peel and static shear adhesion. We showed that coupling of catechols and amines together within the same monomer side chain produced optimal cooperative effects in improving macroscopic adhesion performance. The findings in this study improve our understanding of underlying principles of mussel adhesion and provide a solid framework for rational design of high-performance bioinspired adhesives.

6.1 Introduction

The remarkable wet adhesion of marine mussel byssus has been a major source of bioinspiration for materials scientists during the recent decades.[1–4] These sessile organisms are able to tenaciously attach to various surfaces in turbulent, wet, and saline habitats using their byssal threads.[1, 5] Since many man-made adhesives fail in the presence of moisture, surface contaminants or salts, incorporation of concepts from mussel adhesives into synthetic materials has been a long-standing pursuit for researchers.[6, 7] To achieve this goal, many fundamental studies have been conducted in order to understand the underlying principles of mussel adhesion. Early investigations attributed the unique adhesive properties of mussel plaques to the presence of unusually high contents (20-30 mol%) of the post-transitionally modified 3,4-dihydroxyphenylalanine (Dopa) residues in the mussel foot proteins (Mfps-3,5) at the protein-substrate interface.[1, 8, 9] Fundamental studies later confirmed the critical role of catechol moiety in adhesive and cohesive properties of these interfacial proteins using surface forces apparatus (SFA) and single molecule force spectroscopy (SMFS).[10–12] These initial observations sparked an era of substantial scientific interest in designing catechol-containing synthetic peptides and polymers to mimic the mussel plaque adhesion.[13–15] Although incorporating catechols alone shows great promise in improving adhesive performance,[15–17] such simplified approaches are unable to capture the complex interplay between different amino acids in Mfps.

Recently, a few seminal studies have suggested the critical role of other amino acids beside Dopa on the strong adhesion of Mfps. For instance, a possible synergy between Dopa and positively charged amino acids such as lysine (Lys) and arginine (Arg) has been proposed.[18–20] These amino acids are frequently positioned adjacent to Dopa residues in Mfps.[1] Although still a subject of active investigation, presence of these cationic residues and their close proximity to Dopa are thought to improve the interfacial adhesion by providing additional surface binding opportunities as well as repelling the hydration layer and thus preparing a pristine surface for effective catechol interaction.[18–22] In addition to acting as surface primer, amine groups are also believed to amplify the cation-π interactions and enhance cohesive properties.[23, 24] Cation-π interactions are among the most important non-covalent interactions employed in nature to stabilize and tune the structure and function of many biological molecules.[25, 26] In particular, interactions between hydrophobic aromatic amino acids such as phenylalanine and tyrosine with cationic residues has been shown to play an essential role in self-assembly, molecular cohesion and adhesion, as well

as formation of secondary structures in proteins and peptides.[27–29] Interestingly, a few recent investigations have suggested that the aromatic-rich nature of Mfps provide a clue as to the important function of cation-π interactions in tuning the underwater adhesion of mussel plaques.[23, 28–31]

Although these recent findings have improved our understanding of the underlying mechanisms for the remarkable adhesion of Mfps, many important questions still remain unanswered. For instance, it is not clear whether the synergistic effects between catechols and amines are limited to only enhancing the interfacial adhesion or if cohesive properties are also affected. More importantly, a controversy still exists on whether the adjacency of the catecholic and cationic moieties is crucial in establishing the cooperative effects. In addition, it remains unclear whether catechol groups are inherently essential to observe strong synergy with amines or if similar properties can be achieved by employing phenyl instead of catechol in the bioinspired molecular designs. Finally, most of the previous investigations have focused on studying the adhesion of nanometer thin films of small molecules or short peptides using SFA measurements. Although these experiments provide invaluable molecular mechanistic insights, validity of translating these results across many length scales to design polymer adhesives for practical applications remains an open question. Here, we examined the cooperative effects of amine and aromatic groups incorporated into a common pressure sensitive adhesive polymer based on acrylic acid (AA) and butyl acrylate (BA). The polymers were subjected to a variety of multi-scale adhesion measurements including AFM-based force spectroscopy at molecular and microscopic levels as well as macroscopic peel and static shear adhesion, providing fundamental insights into the mechanism and strength of the interfacial interactions between the polymers and the surface. The rational approach to polymer design combined with comprehensive multi-scale adhesion characterizations allowed us to decouple the interfacial adhesive and intermolecular cohesive contributions of each functional motif on the overall performance and provided new insights into mussel adhesion principles.

6.2 Materials and Methods

Methods

Polymer Synthesis & Characterization: A detailed description of materials used and steps undertaken to synthesize and characterize monomers and polymers is provided in the published article in Angewandte Chemie journal.

Differential scanning calorimetry (DSC): was conducted using the Mettler Toledo DSC1 STARe system under nitrogen to determine the glass transition temperature (T_g) of the polymers. The T_g was measured during the second heating cycle at a heating rate of 10°C/min was recorded.

Fabrication of pressure-sensitive adhesive (PSA) tape samples: The synthesized

PSAs were dissolved in methyl ethyl ketone (MEK) in a 1:1 (w/v) ratio and coated onto Hostaphan RN36 poly(ethylene terephthalate) films (thickness=36 μm) with a wet coating thickness of 120 μm using a wire-round K-bar hand coater (Testing Machines, Inc., New Castle, DE) to target a final coating thickness of 60 gsm (g/m^2) (Supplementary Fig. S1). The PET films coated with PSAs were heated at 100°C for 5 min to remove the solvent and stored in ambient conditions for 24 h prior to use. To temporarily protect the adhesive layer, the PSA-coated PET films were adhered onto silicone release layers. Then, 1 in.-wide strips of PSA-coated films were cut for PSA evaluation tests (static shear and 180° peel).

Preparation of test panels: Performance of PSA tapes was tested against stainless steel test plates. 4 cm×20 cm test panels for 180° peel were generously provided by BASF SE (Ludwigshafen, Germany) while 5 cm×7.5 cm test panels for static shear tests were purchased from ChemInstruments (Fairfield, OH). Based on the FINAT Technical Handbook, the substrates were cleaned prior to testing by dispensing ethyl acetate onto the surface and wiping it dry with Kimwipes. The process was repeated at least three times. Acetone was used in the last rinse. The cleaned substrates were placed in a vacuum desiccator for at least an hour before testing.

Static shear test: The shear holding power of the PSA tapes was measured using a Room Temperature 10 Bank shear tester (ChemInstruments, Fairfield, OH) according to FINAT Test Method no. 8. The silicone release layer was removed from the prepared 1 in.-wide strip, which was then adhered on a clean test plate in such a way that a 25 mm×25 mm area of the PSA-coated PET film was attached onto the substrate. Initially, contact was made using light finger pressure. To standardize the applied pressure, the standard 2 kg hand roller was rolled twice in each direction at approximately 10 mm/s. The other end of the tape was looped through a shear test clip (part STC-100, ChemInstruments) and carefully attached back on itself. The test sample (test plate with attached PSA strip and shear test clip) was mounted onto the substrate holder of the shear tester. Then, a 500 g weight was carefully inserted into the shear test clip. The static shear test was performed in both dry and wet conditions, which means that the contact between the PSA and the test panel and the 'roll-down' methodology to standardize the applied pressure were done either in a dry/ambient condition or while submerged under water. For the wet condition, the PSA attached to the test panel was patted dry with a sheet of Kimwipes and was placed in a shear tester. Shear test results of five samples per condition were averaged and reported.

180° Peel Adhesion: The peeling resistance of the PSA samples was measured by the conventional 180° peel adhesion test as defined by FINAT Test Method no. 1. The PSA tape was cut into 25 mm×175 mm strips and, after removing the release layer, was adhered onto the test substrates using light finger pressure. To achieve similar contact between the adhesive layer and the substrate, a standard FINAT 2 kg hand roller was rolled twice in each direction at approximately 10 mm/s. The test samples were stored in ambient conditions for 24 h before testing. The end of the tape was pulled back at 180°, mounted in an Instron 3345

single column universal testing system, and pulled at 300 mm/min. Peel tests were repeated five times, and the results averaged. In addition to the dry 180° peel test, the peel adhesion after immersion in deionized water for 24 h was also measured. The setup for the "wet" 180° peel test is similar to the dry test except that the test samples were assembled and stored under water for 24 h before measuring the peel adhesion. First, the test substrate was submerged in water. The silicone release layer of the pressure-sensitive tape was removed, and the PSA was adhered onto the test substrate while still submerged under water. Contact between the adhesive and the substrate was standardized by rolling the FINAT hand roller twice in each direction at 10 mm/s. The test samples were then incubated in water for 24 h, dried with a lint-free wipe, and then mounted in the Instron tensile testing system for the peel adhesion test.

Colloidal Probe and Single Molecule Force Spectroscopy: Colloidal probe and single molecule force spectroscopy experiments were performed using a JPK ForceRobot 300 Atomic Force Microscope (JPK Instruments AG, Berlin, Germany). For CPS experiments, AFM probes with colloidal SiO_2 particles of 3.5 μm in diameter and nominal spring constant of $\sim$0.2 N/m were obtained from sQube (Bickenbach, Germany). For SMFS experiments, soft silicon nitride cantilevers (MLCT from Bruker Nano Inc., USA) of typical spring constant of 50-60 pN/nm were used. The experiments were performed after allowing the cantilever to equilibrate in solution and calibrating the sensitivity and spring constant of all the cantilevers using the equipartition theorem.[32] Samples were prepared by drop casting a solution of polymers in ethanol at a concentration of 1 wt% on mica substrates (Ted Pella, Inc, Redding, CA) that were previously mechanically cleaved in order to provide with a clean and pristine surface. After evaporation of solvent, the polymer-coated mica substrates were rinsed with ethanol and placed in AFM sample holder. Since the AFM-assisted force spectroscopy experiments require a good-solvent condition to enable stretching of single polymer chains, the sample chamber was filled with 95% ethanol:5% H_2O (v/v). In this solvent mixture ethanol satisfies the good-solvent requirement while addition of 5% water ensures hydration of the substrate surface. In a typical measurement, the cantilever was approached to the surface with a piezo velocity of 1000 nm/s and a dwelling time (contact time between probe and surface) of 1s over a z-piezo range of 1 μm. For either of CPS or SMFS experiments more than thousands of F-D curves were collected on multiple samples (n=3-5) to achieve statistically representative datasets. For the analysis of data obtained in CPS experiments, the area under the retraction trace in F-D curves were calculated using the JPK data processing software and histograms of the values were plotted using the Origin Pro software. Data obtained in the SMFS experiments were analyzed using the JPK data processing software and a home-written procedure in IgorPro (Wavemetrics) for fitting the spikes in the F-D curves with the Worm-like Chain (WLC) model to measure the corresponding rupture force. Histograms of the rupture forces were plotted using the OriginPro software.

6.3 Results & Discussion

Pressure-sensitive adhesives (PSAs) have become an integral component in many consumer products with widespread applications including adhesive tapes, labels, protective coatings, and medical bandages.[33–36] Among different classes of PSAs, linear or slightly cross-linked acrylic based polymers with a high content of BA or other monomers with low glass transition temperature (T_g) are extensively used in these contexts.[35, 37] Although the conventional PSA formulations show satisfactory performance for non-demanding applications there are a few challenges associated these compositions.[34, 36] For instance, the adhesive properties of PSAs in wet conditions are generally significantly inferior to their performance in ambient.[36] In a previous effort to improve their wet adhesion, we applied the mussel inspiration principles to the base PSA polymers and showed that catechol PSAs outperformed conventional benchmarks in different industry standard tests even at a low ∼3mol% catechol content.[14] In addition to the inferior under water performance, another major shortcoming of conventional PSAs is their poor cohesive strength and low toughness. PSAs commonly take the form of viscoelastic polymers with a sufficiently low modulus to allow for good contact with the substrate upon application of light pressure.[37, 38] However, the low modulus can lead to poor cohesive strength which can substantially limit the use of PSAs to low stress applications.[35, 38] Although a few strategies have been previously proposed to improve the cohesive strength of PSAs, optimizing the adhesive and cohesive properties of PSAs has proven to be a challenging task, as improving one property often comes at the expense of another.[14, 36, 38]

The promising results of our earlier study motivated us to take a step further and apply the recently highlighted mussel adhesion propositions to our PSA design in order to tackle the above challenges. To examine the synergy between catechols and cationic amine groups in PSAs, we designed and synthesized several mussel-inspired Lys- and aromatic-rich monomers (Fig. 1). The monomer designs were inspired by the high Dopa and Lys content and common appearance of adjacent Lys-Dopa pairs in Mfps, as well as recent findings regarding the potential of cation-π interactions between cationic and aromatic residues in tuning the adhesive performance.[18, 20, 23] Acrylic-based PSAs can be considered an ideal platform for studying the effects of mussel-inspired monomers in improving the adhesive performance owing to their widespread practical use and their synthetic modularity in monomer composition. Thus, we proceeded to polymerize our mussel-inspired monomers with AA and BA co-monomers using conventional free-radical polymerization to yield high molecular weight PSAs (Fig. 1). Full synthetic schemes and experimental details for monomer and polymer preparation are provided in the published article. The library of the synthesized polymers along with the selective deprotection of the amine and catechol moieties (Supplementary Scheme S1) allowed us to effectively decouple the adhesive and cohesive contributions of each functional group on the overall adhesive performance and investigate possible cooperative effects.

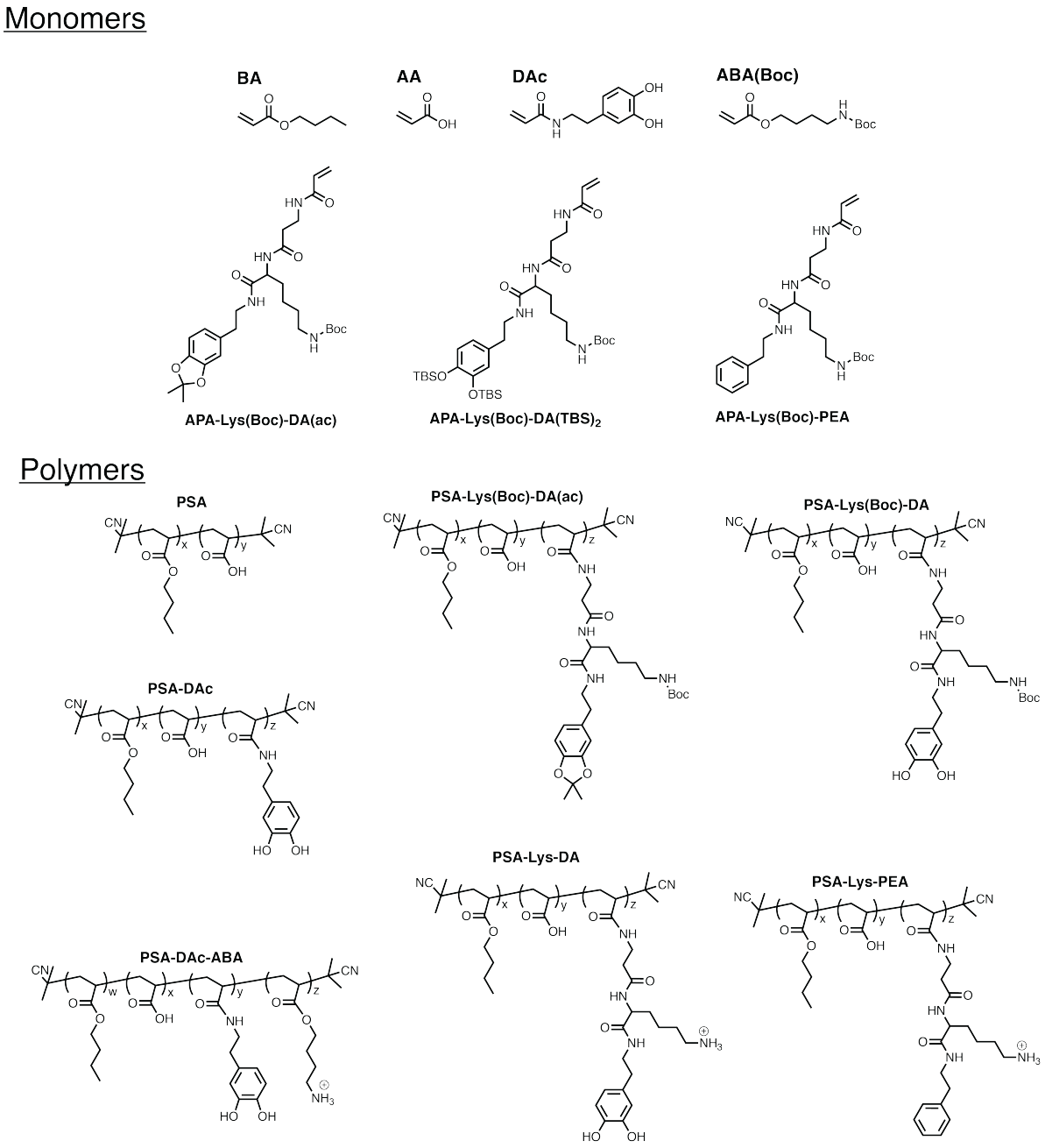

Figure 6.1: Structure of PSA monomers and polymers. Structure of conventional and various mussel-inspired monomers used to synthesize a library of PSAs via free-radical polymerization.

In order to isolate the effect of composition on adhesion, we chose to keep the functional monomer feed ratio fixed at 2.85 mol% (Table 1), as this concentration of catechol

Table 6.1: Monomer feed composition (mol%), molecular weight values, dispersity index, and T_g of synthesized PSAs.

Polymer	Feed Composition (mol%)					M_n	M_w	D	T_g
	BA	AA	Dipeptide Monomer	DAc	ABA	(kDa)	(kDa)		(°C)
PSA	91.40	8.60	-	-	-	116	346	3.0	-41
PSA-DAc	88.40	8.74	-	2.85	-	280	599	2.14	-32
PSA-Lys(Boc)-DA(ac)	88.40	8.74	2.85	-	-	157	377	2.4	-30
PSA-Lys(Boc)-DA	88.40	8.74	2.85	-	-	204	413	2.03	-32
PSA-Lys-DA	88.40	8.74	2.85	-	-	233	827	3.54	-28
PSA-Lys-PEA	88.40	8.74	2.85	-	-	153	352	2.3	-30
PSA-DAc-ABA	85.60	8.74	-	2.85	2.85	193	544	2.82	-23

was demonstrated to be sufficient for boosting the adhesive performance of acrylic PSAs.[14] Molecular weight and T_g values of polymers were measured using gel permeation chromatography (GPC) and differential scanning calorimetry (DSC) and are listed in Table 1 (also Supplementary Table S1). Compared to the control PSA polymer (BA91.4%:AA8.6%), the functional polymers had higher M_w which can be attributed to the enhanced non-covalent and covalent interactions between the polymer chains owing to the presence of catechol groups, as described previously in more detail.[14] The small variations observed between the molecular weight and T_g of the functional polymers can further underline that physical properties of PSAs are not expected to be a major contributor to the differences noticed in their adhesive performance.[39]

After a thorough physical and chemical characterization of PSAs, we proceeded to evaluate their interfacial adhesion using an Atomic Force Microscope (AFM). Owing to its high force resolution and displacement sensitivity, AFM-assisted force spectroscopy has been recognized as a versatile technique in studying physical behavior and mechanical properties of polymeric films.[40–44] Depending on the cantilever probe used in the measurements, a range of molecular or micro-scale interfacial phenomena can be investigated using this technique. For example, colloidal probe spectroscopy (CPS) is a widely employed method to measure adhesive forces acting between a colloidal particle (i.e., micrometer-sized spherical particle) attached to a cantilever beam and a planar substrate.[45–48] Single molecule force spectroscopy (SMFS) is another powerful AFM-based characterization method which is well suited to investigate and quantitively measure the strength of chemical bonds as well as adhesive interactions acting between molecules and surfaces.[49, 50] This technique has been widely used in the past for studying the adhesion of mussel-inspired peptides and polymers and advances have been summarized in a recent review by Li et al.[10] SMFS measurements are complementary to the CPS experiments and when combined together can provide a more comprehensive picture of the molecular basis underlying adhesive and cohesive properties of materials. In the present work, we utilized both SMFS and CPS techniques to study adhesive performance of PSA polymers in order to decouple cohesive contributions from interfacial adhesive interactions acting between polymer chains and the surface.

SMFS experiments were performed initially to gain a fundamental insight into the molecular phenomena underlying the interfacial adhesive properties of PSAs. In our experiments a sharp AFM cantilever (tip radius ∼10-20 nm) was brought into contact with PSA films on mica substrate and retracted at a specified speed while the force of interaction between the probe and the polymer film was measured. A schematic of the experimental setup as well as a representative F-D curve for PSA-Lys-DA is shown in Fig. 2a. The sequential rupture of polymer-surface interactions during retraction of the cantilever lead to the appearance of sawtooth-like peaks in the F-D curves (Fig. 2a), reminiscent of what is observed during unfolding of globular polyproteins during stretching.[43, 51] These rupture events can then be fitted using polymer elasticity models to confirm single molecule behavior and extract the strength of polymer-surface interactions. Histograms and average values of rupture force for PSAs are presented in Fig. 2 and Table 2, respectively (also Supplementary Table S2 and Supplementary Fig. S3). We first tested the control PSA polymer where an average rupture force of 118 pN was measured (Fig. 2b). This value is in the range of weak non-covalent interactions such as hydrogen bonding and charge-charge interactions and can be attributed to the presence of AA in the polymer which can accommodate these interactions with the substrate.[52] Results of measurements on PSA-DAc indicated that incorporation of catechol groups into the polymer can lead to a notable increase in the average rupture force to ∼236 pN, possibly owing to the myriad of interfacial interactions that catechol can form with the mica surface including strong hydrogen bonding and bidentate complexation.

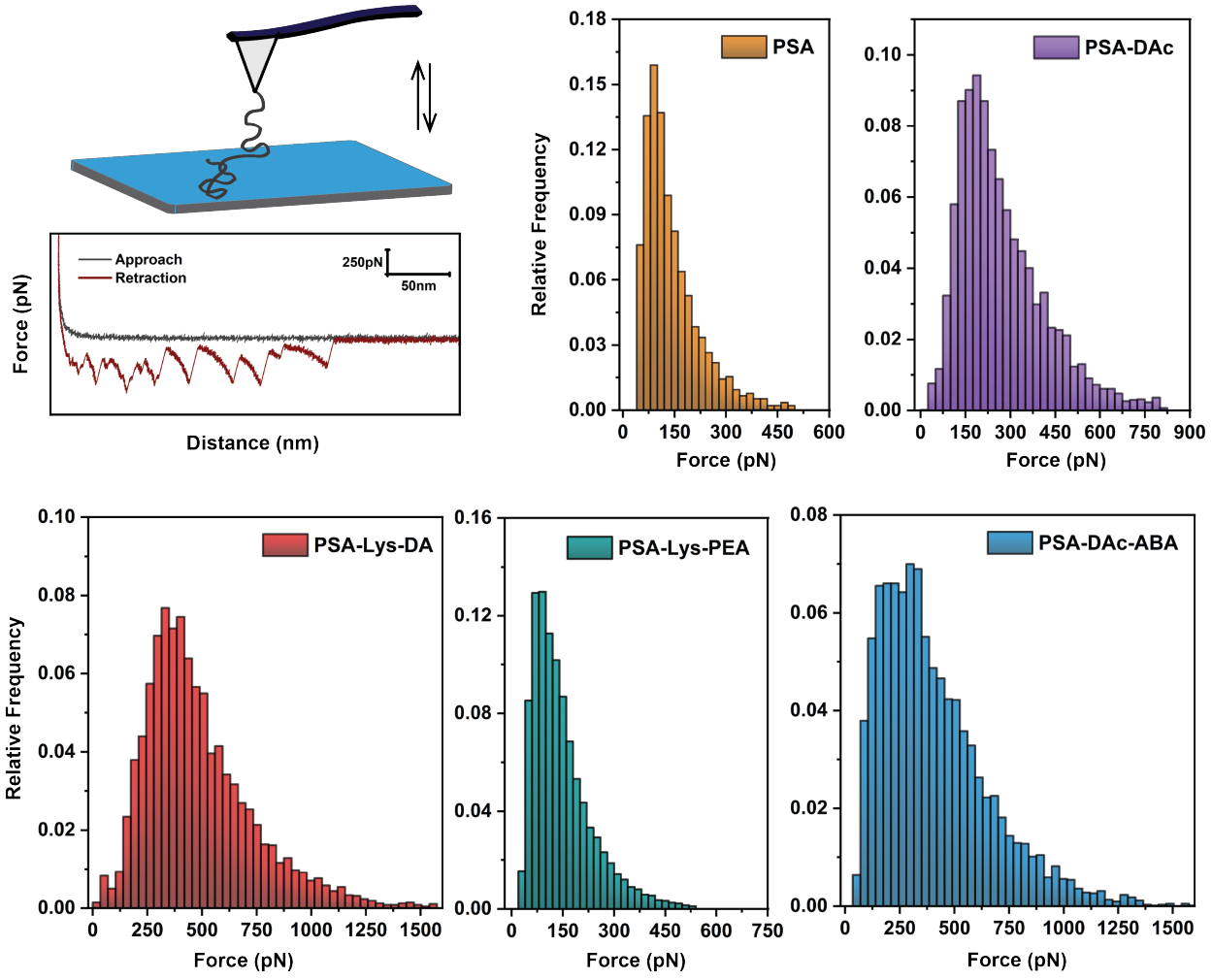

Figure 6.2: SMFS characterization of PSA polymers. (a) experimental schematic and a representative F-D curve for PSA-Lys-DA are shown. Histograms of the rupture forces are shown in (b) PSA, (c) PSA-DAc, (d) PSA-Lys-DA, (e) PSA-Lys-PEA, (f) PSA-DAc-ABA.

We observed a stark increase in the average rupture force for PSA-Lys-DA compared to PSA and PSA-DAc polymers, confirming the cooperative effects between catechols and positively charged amines at the single molecule level. The elevated rupture forces for PSA-Lys-DA can be attributed to the potential role of positive charges of Lys in removal of solvation layer from the surface for a more effective catechol interaction as well as possible cooperative surface binding leading to an increased interaction strength and lifetime as suggested previously by Cao and colleagues.[18–20] Next, we proceeded to study the interfacial adhesion of PSA-Lys-PEA to evaluate the effects of cation-π interactions in improving the

polymer-surface interactions. Interestingly, we observed an average rupture force of 125 pN for PSA-Lys-PEA. The sharp contrast in the rupture forces detected for PSA-Lys-DA and PSA-Lys-PEA clearly highlights the advantages of catechols over unsubstituted phenyl rings for improving interfacial interactions with substrates.

After observing the performance of PSA-Lys-DA we were intrigued to study the effects of the molecular architecture and adjacency of amine and catechol groups on the interfacial adhesion. Since Lys and Dopa residues are most commonly positioned adjacent to each other along the backbone in Mfp-3 and 5, it was initially hypothesized that the close proximity of the cationic Lys residues and catecholic motifs are necessary to establish the synergistic effects.[18, 20] However, recently it has been suggested that the adjacency of the two functional motifs might not be required for the synergistic effects and only co-presence of cationic and catecholic groups might lead to major improvements in adhesive performance.[21] To further test this notion we studied interfacial adhesion of PSA-DAc-ABA. The average rupture force for PSA-DAc-ABA was ∼351 pN, much higher than that of the of amine-free PSA-DAc and only modestly less than the values observed for PSA-Lys-DA. Compared to PSA-Lys-DA, in PSA-DAc-ABA catechol- and amine-containing monomers are located randomly along the backbone, resulting in a stochastic distribution of spacing between DAc and ABA groups in the polymer chains. The SMFS results indicate that even when randomly distributed, the amine groups can possibly be partially effective in desolvating the surface and facilitating the interaction of catechols with the substrate. More importantly, in SMFS measurements the polymer chains can be picked up at any random point along their contour length. Owing to this random attachment to the probe as well as flexibility of the backbone and the presence of a large number of amine and catechol groups in polymer molecules, the synergistic effect due to the simultaneous rupture of catechol- and amine-surface interactions might still be observed, leading to elevated rupture forces as compared to PSA-DAc.

Next, we proceeded to perform CPS experiments on PSAs in order to complement the SMFS studies and to gain a microscopic view of adhesion performance.[47, 48] In our measurements an AFM cantilever with a colloidal probe of silica (SiO_2, diameter=3.5 μm) was used and brought into contact with a PSA film adsorbed on mica substrate. Schematic of the experimental setup as well as a representative F-D curve for PSA-Lys-DA are shown in Fig. 3a. A characteristic feature in most of the collected F-D curves was the appearance of multiple spikes in the retraction trace. The presence of these spikes can be attributed to detachment of multiple polymer chains from either the colloidal probe or the substrate upon retraction of the AFM cantilever, or alternatively to rupture of specific polymer-surface adhesive interactions between individual chains and the surface. As a result, extracting only the maximum detachment force from the F-D curves is not a proper measure of the overall adhesive interactions. More importantly, owing to the viscoelastic nature of the polymer as well as roughness and asperities on the colloidal particle, accurate determination of the contact geometry and radius can be challenging.[45–47, 53] Hence, the adhesion energy values calculated based on the contact mechanics models can be subject to large errors introduced from the estimated contact radius. An alternative approach to estimate the magnitude of the overall adhesive strength between the polymer film and the substrate in the contact area is to

integrate the area under the retraction trace in the F-D curves.[54] The calculated quantity has the units of energy and will be referred to as separation work (W) here.[14, 55–57] The separation work calculated here is related to the energy that is required to detach the probe from the substrate.[46]

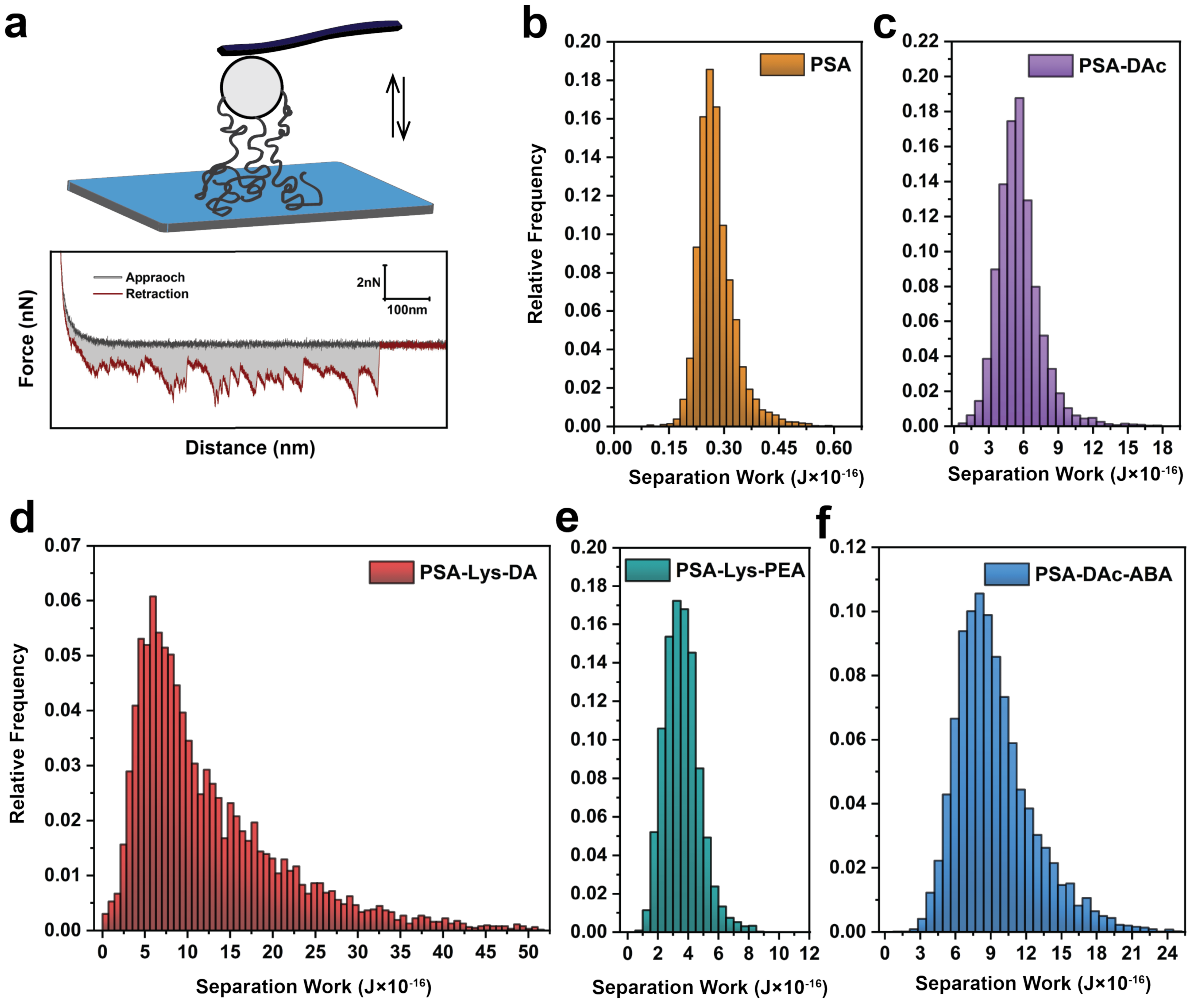

Figure 6.3: CPS characterization of PSA polymers. (a) experimental schematic and a representative F-D curve for PSA-Lys-DA are shown. Histograms of the separation work are shown in (b) PSA, (c) PSA-DAc, (d) PSA-Lys-DA, (e) PSA-Lys-PEA, (f) PSA-DAc-ABA.

Histograms and average values of W for the PSA polymers are presented in Fig. 3 and Table 2, respectively (also Supplementary Table S2 and Supplementary Fig. S3). CPS results show that incorporating catechol as DAc into the polymer backbone can lead to a 20-fold increase in the separation work. A similar trend was observed in our earlier study where incorporating 5 wt% dopamine methacrylamide into PSAs resulted in a significant

increase in the separation work for SiO_2 probes.[14] The large increase in adhesion to silica upon incorporation of DAc may be attributed to strong binding mechanisms such as hydrogen bonding and bidentate complexation as described in detail previously.[3, 11, 14] As expected, incorporating a protected form of the bifunctional monomer Lys-DA into the polymer backbone did not result in major changes in adhesion compared to the control PSA polymer (Supplementary Fig. S2). However, upon removal of the protecting groups the resulting PSA-Lys-DA outperformed all other polymers by showing a remarkable ∼36-fold increase in the separation work compared to the control PSA. This striking increase further highlights that co-presence of amine and catechol groups can lead to significant improvements in adhesive performance of PSA polymers. The cooperative effects between amines and catechols can be attributed to the role of positive charges of amines in removing solvation layer and providing an immaculate surface for catechol interaction or resulted from a better load distribution through synergistic surface binding of the two groups as suggested in previous molecular studies.[18–21]

To determine if similar adhesive performance can be achieved by substituting phenyl for catechol groups in the monomer design, we tested the adhesion of PSA-Lys-Phe. Although the results showed a notable ∼10x improvement in the separation work compared to the control PSA, PSA-Lys-Phe underperformed both PSA-Lys-DA and PSA-DAc. Considering the results obtained in CPS and SMFS experiments together, the findings indicate the potential benefits of cation-π interactions in improving the cohesive interactions between the macromolecules leading to an enhanced adhesion as measured here in the CPS experiments as well as in previous SFA studies.[23, 28, 29] Nevertheless, the SMFS results imply that Lys-PEA pairs have minimal effects in strengthening the interfacial adhesive interactions with surfaces. In other words, due to the nature of the CPS and SFA experiments where detachment of an ensemble of molecules is studied, cohesive interactions between the molecules can affect the measured values for separation work or work of adhesion. Thus, possible contributions of intermolecular cohesive and interfacial adhesive interactions on the improved performance cannot be equivocally deconvoluted solely based on the results these measurements.

To gauge the possible role of molecular architecture and proximity of catechol and amine groups on the adhesive performance of PSAs, we performed CPS experiments on PSA-DAc-ABA. Interestingly, the polymer displayed an average separation work close to that of PSA-Lys-DA polymer. The trend observed in CPS measurements is similar to what was noted earlier in SMFS experiments and can indicate that architecture of the polymer and the adjacency of catechol- and amine-containing groups might not be necessary in establishing the cooperative effects to improve the adhesion, at least when measured at the microscopic or molecular levels. Similar observations have been made recently by Degen et al.,[21] where results of SFA measurements implied that incorporating glycine residues as spacer between the cationic and catecholic groups did not lead to significant changes in the force required to separate peptide-coated mica surfaces.

Despite the wealth of mechanistic information that interfacial adhesion measurements on thin-films can provide, the bulk behavior still cannot be unambiguously predicted from CPS and SMFS experiments that probe the microscopic and molecular levels, respectively.

Thus, we proceeded to perform static shear and 180° peel measurements as industry-standard macroscale adhesion tests. Combined with the results obtained in the interfacial adhesion measurements, this holistic multi-scale approach could allow us to decouple the adhesive and cohesive contributions as well as effects of polymer composition and architecture on the PSA performance.

For the macroscopic adhesion measurements, the PET films were coated with PSAs, dried and then cut into 1 inch-wide strips to prepare test samples for the tests (Supplementary Fig. S1). The shear holding power of the adhesives was evaluated in both dry and wet conditions by adhering the PSA tapes onto a stainless steel test plate and measuring the time to rupture under the influence of a constant shear force (Supplementary Fig. S4). This test simulates a constant load creep condition and can be used for determining the shear failure time, a measure of the cohesive strength or shear holding power of the adhesive. Similar to the results obtained in our previous study, incorporation of catechol groups into the polymer backbone led to a substantial increase in the failure time for PSA-DAc as compared to the control PSA, from 14 and 8 to 123 and 77 minutes under dry and wet conditions, respectively (Fig. 4a). While the improved shear holding power of the PSA-DAc can be mostly attributed to the enhanced cohesive and intermolecular interactions due to the presence of catechol groups, we should note that in addition to the chemical composition, the shear failure times are also dependent on additional factors including M_w, T_g, and the degree of physical or chemical cross-linking of the polymer, all of which can be affected by incorporation of catechols into the polymer.

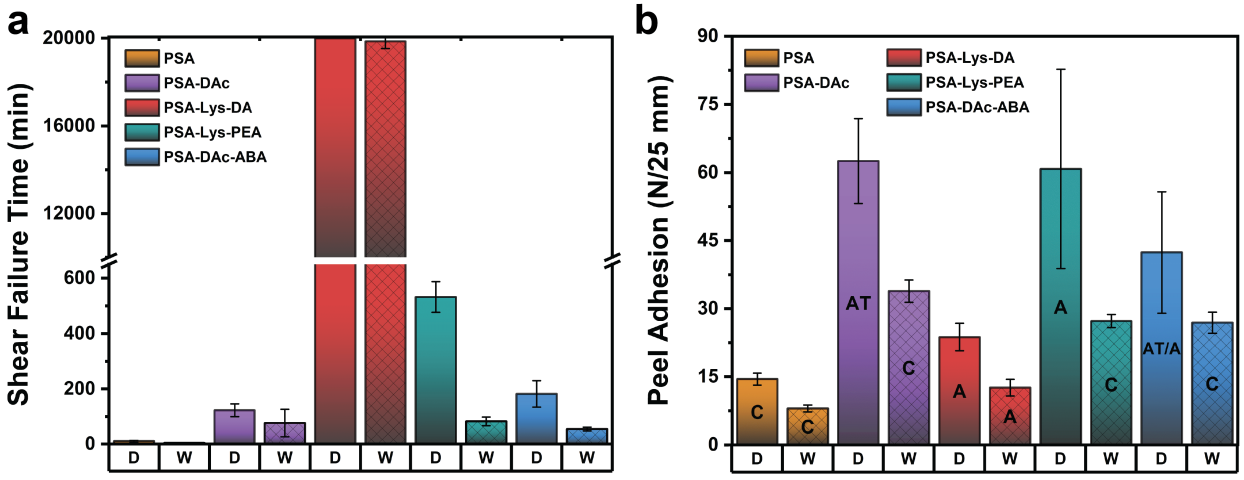

Figure 6.4: Macroscopic characterization of PSA tapes. (a) Shear failure time after 10 min conditioning in ambient (D) and wet (W) conditions. (b) 180° peel adhesion after 24 h conditioning in ambient (D) and wet (W) conditions. The failure modes are denoted as: C=cohesive, A=adhesive, and AT=adhesive transfer.

The most interesting finding was the remarkably large failure times observed for PSA-

Lys-DA, which was on the order of 20,000 minutes or more compared to ¡600 minutes for all other samples. This outstanding performance can indicate the significant enhancements in the intermolecular interactions in PSA-Lys-DA, possibly owing to the augmented covalent and non-covalent interactions such as additional hydrogen bonding due to the presence of amine groups as well as strong cation-π interactions between the charged amine and catechol motifs, in a similar manner to their recently highlighted role in improving cohesive strength of Mfps.[23, 58]

To understand the effects of the aromatic molecular structure on the strength of the cohesive cation-π interactions, we tested the shear holding power of PSA-Lys-PEA. Interestingly, the failure time in wet condition was not statistically different from that shown by PSA-DAc, although PSA-Lys-PEA outperformed other polymers except for PSA-Lys-DA when considering dry shear holding power. The results underline the key role of cation-π interactions in boosting the cohesive strength of the adhesive films. However, when compared against PSA-Lys-DA, the catechol-containing polymer displayed significantly larger failure times, both in ambient and wet conditions. Such a notable difference between failure times of PSA-Lys-DA and PSA-Lys-PEA polymers can possibly be attributed to the role of hydroxyl groups of the catechol in providing additional opportunities for intermolecular hydrogen bonding as well as acting as an anionic site for auxiliary charge interactions with cationic Lys groups.

To evaluate the possible impact of molecular design on cation-π interactions and cohesive strength of catechol-amine containing polymers, we studied shear holding power of PSA-DAc-ABA. Surprisingly, we did not observe a substantial increase in the dry and wet failure times as compared to PSA-DAc. Unlike the behavior noted at the molecular level in this study and recent SFA measurements by others,[21] the static shear test results indicate that close proximity of cation-aromatic binding pairs can significantly affect the macroscopic cohesive strength. The results might also explain why marine mussels have evolved to secrete adhesive proteins with Dopa and Lys pairs located mostly adjacent to each other rather than separated by spacer amino acids such as glycine. The findings here also motivates further studies to investigate the effects of proximity of catechol and cationic amine moieties in mussel inspired adhesives across many length scales.

In addition to shear, conventional 180° peel adhesion tests were performed both in dry conditions and after immersion in water for 24 hours prior to the measurement (Supplementary Fig. S5). The results of the peel adhesion for PSA-DAc show that both dry and wet adhesion increase ∼4-fold (Fig. 4b and Table 2). More importantly, the failure mode also changes from cohesive to adhesive transfer in ambient condition as compared to control PSA. This behavior can be attributed to the strong interactions of catechol with the metal substrate as compared to the PET backing material which leads to detachment of the polymer from the backing layer. In the case of PSA-Lys-DA polymer, although both dry and wet performance was improved compared to PSA, the increase in peel adhesion was not as significant as that observed for PSA-DAc. However, the most interesting observation was the change in the failure mode from cohesive to adhesive for both dry and wet measurements. This behavior can be ascribed to the magnified intermolecular and cohesive forces

Table 6.2: Summary of the adhesion characterization results of PSAs measured using SMFS, CPS, static shear test, and 180° peel adhesion experiments. The values in parenthesis for SMFS and CPS results correspond to the total number of events used to calculate the averages.

	Single Molecule Force Spectroscopy	**Colloidal Probe Spectroscopy (CPS)**	**Shear Failure Time (min)**		**Peel Adhesion (N/25mm)**	
Polymer	Median Rupture Force (pN)	Median Separation Work (Joules × 10^{-16})	Dry	Wet	Dry	Wet
PSA	118 (2862)	0.27 (10996)	10.5±3.3	3.9±1.3	14.5±1.3	8±0.7
PSA-DAc	235.8 (6088)	5.41 (8061)	122.9±23.5	76.7±50	62.5±9.3	33.9±2.4
PSA-Lys-DA	430 (4822)	9.72 (6292)	>20000	19858.6±327.4	23.7±3	12.6±1.8
PSA-Lys-PEA	125 (29728)	3.51 (8850)	531.6±55.6	82.9±15.4	60.8±22	27.3±1.5
PSA-DAc-ABA	350.7 (7568)	8.76 (8020)	182.1±47.8	55.2±7	42.4±13.4	26.9±2.3

between the polymer chains in PSA-Lys-DA owing to the presence of cation-π interactions. The adhesive and cohesive performance of PSA-Lys-DA, in terms of both force values and failure mode, may be attractive for many practical applications of PSAs.

Peel adhesion results of PSA-Lys-PEA showed significant improvements in comparison to the control PSA which can partly be attributed to the increase in the T_g and consequently changes in the mechanical properties at room temperature. In dry condition, adhesive failure was observed, which can further underline enhancements in the intermolecular interactions resulting from cation-aromatic pairs in the polymer backbone. The PSA-DAc-ABA polymer showed average peel adhesion values between those measured for PSA-DAc and PSA-Lys-DA. However, since the T_g of this polymer is somewhat different from those of the other two polymers, interpretation and direct comparison between the peel adhesion values should be done with caution.

Overall, the results of the static shear and peel adhesion measurements highlight the importance of balancing adhesive and cohesive properties to achieve optimal performance of mussel-inspired PSAs. In this sense, the performance shown by PSA-Lys-DA clearly stands out compared to all other polymers for its remarkable shear strength conferred by strong cohesive interactions between catechol and amine functional groups. In addition, PSA-Lys-DA also showed improvements in both dry and wet peel adhesion compared to the control PSA, and more importantly we observed a change in the failure mode from cohesive to adhesive which is preferred for many practical applications.

6.4 Conclusions

Altogether, in this work we applied the recently highlighted compositional and structural aspects of Mfps into our modular PSA designs and investigated the effects of molecular architecture and aromatic structure on the cooperative adhesive effects of catechols and amines. An important finding of this work is that comprehensive adhesion measurements

across different length scales are crucial in decoupling contributions from interfacial adhesive and intermolecular cohesive interactions on overall PSA performance, highlighting the benefits of a multi-scale approach. Our results from AFM-based molecular and microscopic force spectroscopy experiments showed significant improvements in interfacial adhesion of catechol-amine PSAs compared to the amine-free polymers, possibly owing to the synergistic effects between catechols and amines. Macroscopic adhesion results further indicated that coupling catechol and amine moieties in a hybrid monomer architecture can lead to optimization of overall performance of the catechol-amine adhesives and developing PSAs with remarkable resistance to flow under shear. Moreover, by substituting phenyl for catechol in the hybrid monomer structure we showed that incorporating phenyl-amine pairs into polymer backbone cannot provide a clear benefit in improving interfacial adhesion with surfaces. However, PSA with phenyl and amine groups coupled together demonstrated a satisfactory performance in macroscopic shear and peel adhesion tests, underlining the key role of cation-aromatic pairs as compelling molecular modules in enabling robust cohesion of mussel-inspired adhesives and hydrogels. Finally, since the precise positioning of catechol and amine motifs adjacent to each other in a fixed architecture is synthetically demanding, the intriguing possibility of achieving similar synergistic effects through a random distribution of these groups motivated us to study adhesive performance of PSA polymer with catechol and amine moieties incorporated as separate monomers. Interestingly, both SMFS and CPS results indicated that molecular architecture and adjacency of these groups is not necessary for establishing the synergistic effects. However, the cooperative effects between catechols and amines were not observed at macroscopic level in static shear or peel adhesion tests when amine and catechol groups were decoupled from each other in monomer architecture.

6.5 Supplementary Figures

Fabrication of the pressure-sensitive adhesive tapes

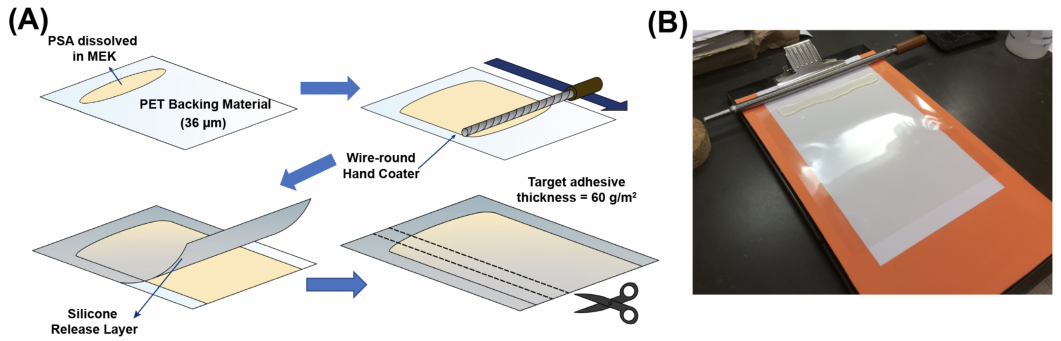

Figure S6.1: (A) Fabrication of the pressure-sensitive adhesive tapes. (B) Draw-down coating with a target thickness of 60 gsm.

Polymer Synthesis and Characterization

Synthesis of Polymers with Protecting Groups

Several PSA samples have been prepared based primarily on a butyl acrylate (95 wt% or 91 mol%)-acrylic acid (5 wt% or 8.6 mol%) copolymer. Catechol or catechol-lysine PSAs were synthesized by replacing a portion of the butyl acrylate monomer with either the protected catechol monomer DAc(ac) or the branched-type monomers with adjacent catechol and lysine motifs with varying protecting groups. The molar feed% of all catechol monomers was fixed to 2.85 mol%, which is the optimized composition from our previous study. For PSA-DAc(ac)-ABA(Boc), the molar% of the monofunctional lysine monomer ABA(Boc) was also set to 2.85% to be comparable with the 1:1 catechol-lysine ratio of the branched-type monomers.

Table S6.1: Monomer feed composition (mol%), molecular weight values, dispersity index, and T_g of synthesized PSAs.

Polymer	Feed Composition (mol%)					M_n (kDa)	M_w (kDa)	D	T_g (°C)
	BA	AA	Dipeptide Monomer	DAc	ABA				
PSA	91.40%	8.60%	-	-	-	116	346	3	-41
PSA-DAc(ac)	88.40%	8.74%	-	2.85%	-	102	348	3.42	-34
PSA-DAc	88.40%	8.74%	-	2.85%	-	280	599	2.14	-32
PSA-Lys(Boc)-DA(ac)	88.40%	8.74%	2.85%	-	-	157	377	2.4	-30
PSA-Lys(Boc)-DA	88.40%	8.74%	2.85%	-	-	204	413	2.03	-32
PSA-Lys(Boc)-DA$(TBS)_2$	88.40%	8.74%	2.85%	-	-	132	385	2.92	-31
PSA-Lys-DA	88.40%	8.74%	2.85%	-	-	233	827	3.54	-28
PSA-Lys(Boc)-PEA	88.40%	8.74%	2.85%	-	-	151	361	2.4	-31
PSA-Lys-PEA	88.40%	8.74%	2.85%	-	-	153	352	2.3	-30
PSA-DAc(ac)-ABA(Boc)	85.60%	8.74%	-	2.85%	2.85%	109	390	3.58	-29
PSA-DAc-ABA	85.60%	8.74%	-	2.85%	2.85%	193	544	2.82	-23

Acetonide and/or Boc-Deprotection of PSA-DAc(ac), PSA-DAc(ac)-ABA(Boc), PSA-Lys(Boc)-DA(ac), and PSA-Lys(Boc)-PEA

Acetonide and Boc protecting groups of PSA-DAc (ac), PSA-DAc(ac)-ABA(Boc), PSA-Lys(Boc)-DA(ac), and PSA-Lys(Boc)-PEA were cleaved using trifluoroacetic acid (TFA) and triisopropyl silane (TIPS) to produce PSA-DAc, PSA-DAc-ABA, PSA-Lys-DA, and PSA-Lys-PEA respectively (Scheme S6).

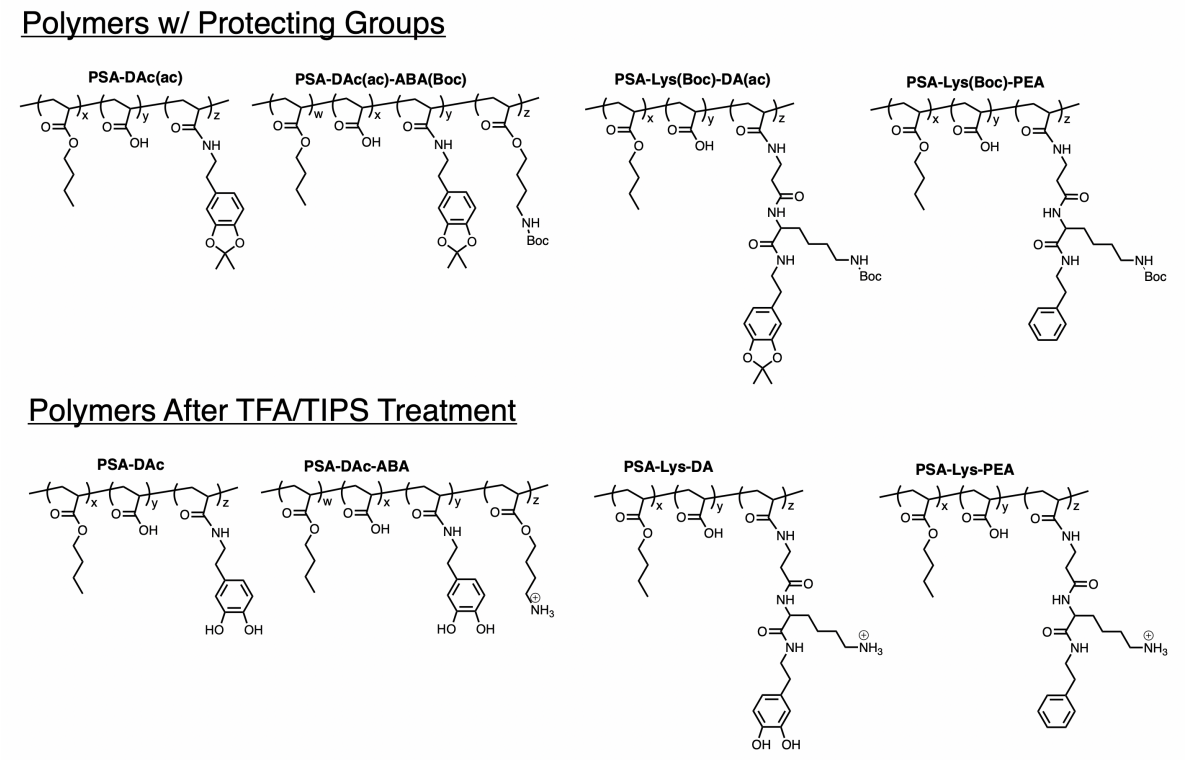

Scheme S6.1: Acetonide and/or Boc deprotection of PSA-DAc(ac), PSA-DAc(ac)-Lys(Boc), PSA-Lys(Boc)-DA(ac), and PSA-Lys(Boc)-PE via TFA/TIPS treatment.

Colloidal Probe Force Spectroscopy on Protected PSA-Lys(Boc)-DA(ac) and PSA-Lys(Boc)-DA

In order to investigate the contribution of each functional group in Lys-DA pairs on the overall adhesive performance, we analysed PSA-Lys(Boc)-DA(ac), PSA-Lys(Boc)-DA, and PSA-Lys-DA by CPS measurements. As expected, incorporating bifunctional monomer Lys-DA into the polymer backbone did not result in major changes in the adhesion compared to the control PSA polymer when both Lys and DA groups were still protected. Next, we removed the acetonide protecting group of DA while keeping the Boc protecting group of Lys intact. Interestingly, although the average value for separation work was almost doubled after deprotection of catechols, we did not observe a substantial increase similar to that of PSA-DAc in comparison to control PSA polymer. This might possibly attributed to the presence of the bulky, hydrophobic Boc protecting groups in close proximity to the catechols which might hinder the effective interaction of catechol with the surface and lead to attenuating its potential to improve adhesive performance. However, after removal of the protecting groups the resulting PSA-Lys-DA outperformed all other polymers by showing a remarkable ∼36-fold increase in the separation work compared to the control PSA. This meaningful increase further highlights that co-presence of amines and catechols can lead to major improvements in the interfacial adhesive performance possibly due to synergistic effects between the two groups.

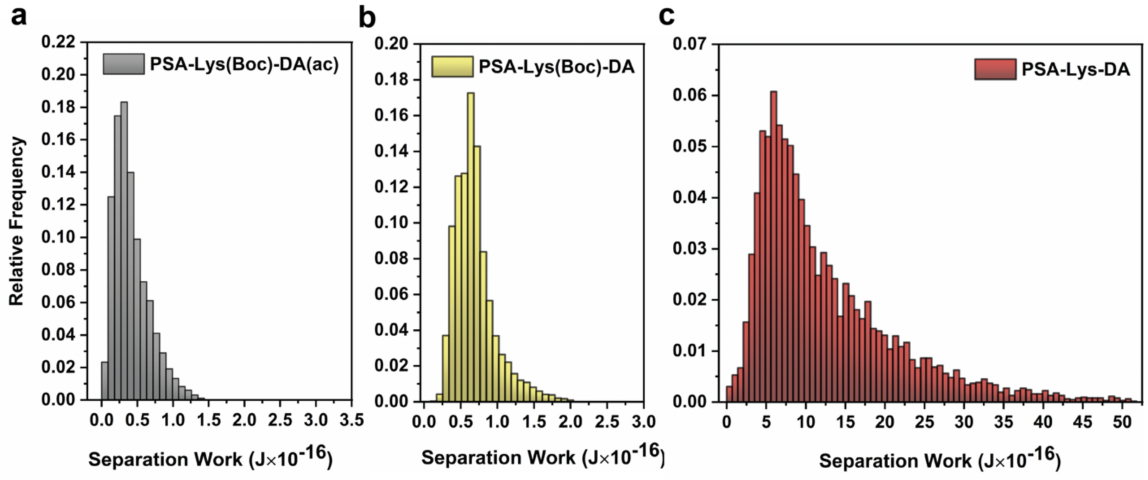

Figure S6.2: CPS measurements on Lys-DA incorporated polymers. Histograms of separation work are shown for (a) PSA-Lys(Boc)-DA(ac) (b) PSA-Lys(Boc)-DA (c) PSA-Lys-DA.

Summary and Statistical Analysis of AFM-based SMFS and CPS Interfacial Adhesion Results

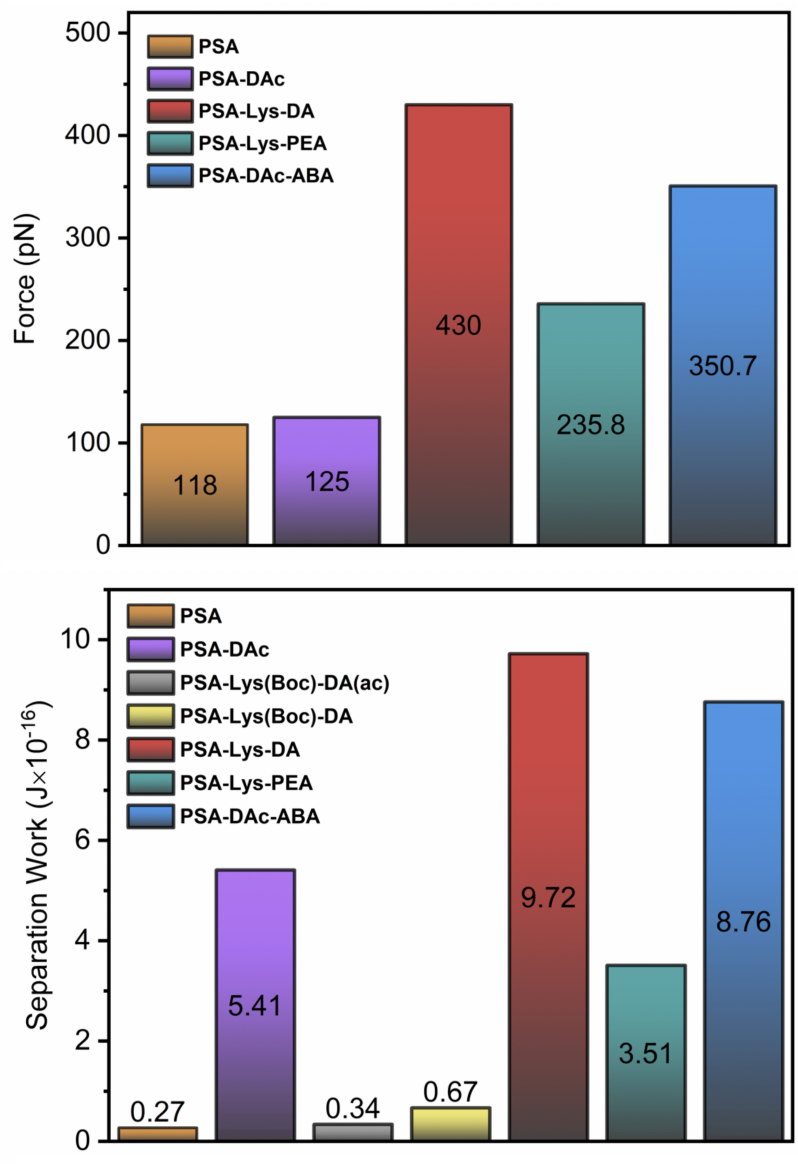

Figure S6.3: AFM-based SMFS and CPS Interfacial Adhesion Results. Median rupture force values from SMFS (top) and Median separation work values from CPS (bottom).

Static Shear Measurements on Protected PSA-Lys(Boc)-DA(ac) and PSA-Lys(Boc)-DA

Results of static shear measurements showed that incorporation of catechol groups into the polymer backbone in PSA-DAc can lead to a substantial increase in the failure time compared to the control PSA polymer. A similar trend was observed for the PSA-Lys(Boc)-DA(ac) and PSA-Lys(Boc)-DA polymers. While the improved shear holding power of the PSA-DAc can be mostly attributed to the enhanced cohesive and intermolecular interactions due to the presence of catechol groups, we should note that in addition to the chemical composition, the shear failure times are also dependent on additional factors including M_w, T_g, and the degree of physical or chemical cross-linking of the polymer, all of which can be affected by incorporation of catechols into the polymer. Thus, the increase in the shear holding power of the PSA-Lys(Boc)-DA(ac) and PSA-Lys(Boc)-DA compared to the PSA polymer can be attributed to the changes in the above characteristics, for instance an increase in the T_g from -40 to about -29°C.

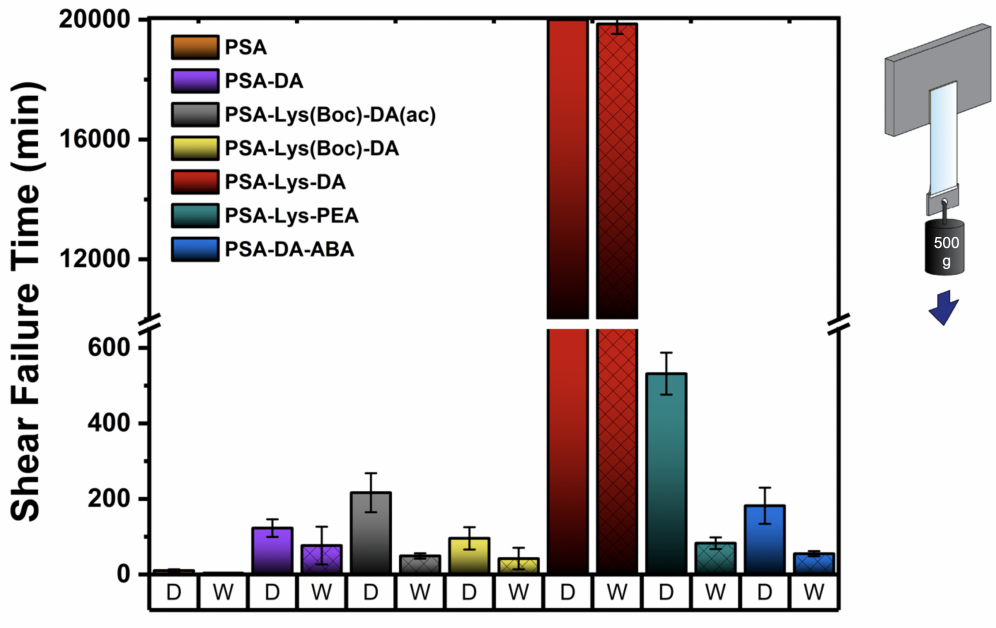

Figure S6.4: Static shear measurements on PSAs. Shear failure time after 10 min conditioning in ambient (D) and wet (W) conditions. Schematic of the experimental setup is shown on the right.

Failure Modes Observed in 180° Peel Measurements

Peel adhesion test measures the average force required to peel a PSA tape from a rigid substrate. It is worth mentioning that although the peel adhesion results can provide valuable insights into the adhesive properties of the material, a number of other material characteristics such as elastic modulus and toughness can have major influence on the measured forces. Therefore, in order to properly evaluate the adhesive performance, it is critical to note the failure modes when interpreting the peel adhesion results. Adhesive tapes typically leave residues behind as they are removed from a surface. This behavior is generally known as cohesive failure and can be easily identified in the peel adhesion measurements through detecting residual material left on both the substrate as well as the PET backing layer after peeling off the tape. Cohesive failure observed in the peel tests indicates that while the adhesive interactions with the substrate can endure under stress and remain intact, cohesive interactions in the material are not strong enough to withstand the applied stress, and as a result, the failure occurs in the bulk rather than in the interface with the substrate or the backing layer. Adhesive failure, on the other hand, relates to the condition in which cohesive intermolecular interactions between the polymer chains are strong enough to withstand the applied stress, however, the bonding between the surface and the polymer is relatively week and as a result failure occurs at the polymer-substrate interface. In adhesive transfer mode the adhesive interactions between the polymer and the substrate are substantially stronger than those between the polymer and the backing layer, thus, the polymer coating will be entirely removed from the backing layer and be transferred to the substrate.

180° Peel Measurements on Protected PSA-Lys(Boc)-DA(ac) and PSA-Lys(Boc)-DA

The results of the peel adhesion of PSA-DAc show with incorporating catechol into the backbone both dry and wet adhesion increase compared to PSA. The behavior observed for the PSA-Lys(Boc)-DA(ac) and PSA-Lys(Boc)-DA polymers was more complex and a different trend was observed after removal of acetonide protecting groups. Although the failure mode observed for PSA-Lys(Boc)-DA was adhesive in both ambient and wet conditions, the peel adhesion values dropped compared to PSA-Lys(Boc)-DA(ac). As described in the main text, bulk mechanical properties of polymers such as modulus can affect the force values measured in the peel adhesion test, and the trend observed for the protected polymers can be attributed to differences in these characteristics.

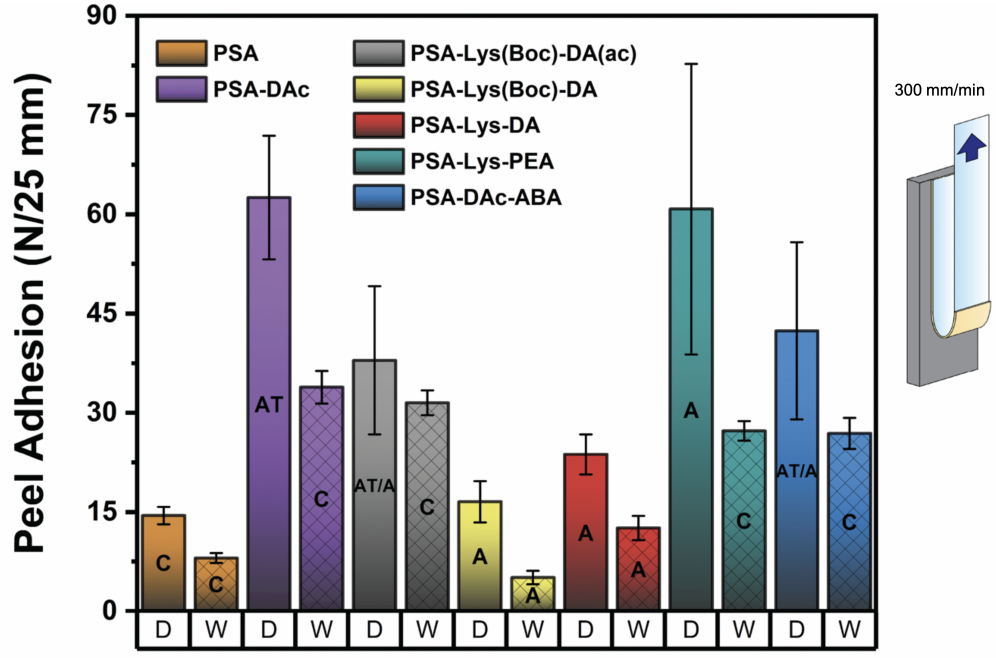

Figure S6.5: 180° peel adhesion measurements on PSAs after 24 h conditioning in ambient (D) and wet (W) conditions. The failure modes are denoted as: C=cohesive, A=adhesive, AT=adhesive transfer.

Overall Summary of the Adhesion Characterization Results of PSAs

Table S6.2: Summary of values obtained in SMFS, CPS, static shear test, and 180° peel adhesion experiments for all the PSAs (protected and deprotected) tested. The values in parenthesis for SMFS and CPS results correspond to the total number of events used to calculate the averages.

	Single Molecule Force Spectroscopy	**Colloidal Probe Spectroscopy (CPS)**	**Shear Failure Time (min)**		**Peel Adhesion (N/25mm)**	
Polymer	Median Rupture Force (pN)	Median Separation Work (Joules $\times 10^{-16}$)	Dry	Wet	Dry	Wet
PSA	118 (2862)	0.27 (10996)	10.5±3.3	3.9±1.3	14.5±1.3	8±0.7
PSA-DAc	235.8 (6088)	5.41 (8061)	122.9±23.5	76.7±50	62.5±9.3	33.9±2.4
PSA-Lys(Boc)-DA(ac)	N/A	0.34 (8602)	216.5±51.7	49.1±7.1	38±11.2	31.5±1.9
PSA-Lys(Boc)-DA	N/A	0.67 (6587)	95.9±29.5	42.3±28.6	16.6±3.1	5.1±1
PSA-Lys-DA	430 (4822)	9.72 (6292)	>20000	19858.6±327.4	23.7±3	12.6±1.8
PSA-Lys-PEA	125 (29728)	3.51 (8850)	531.6±55.6	82.9±15.4	60.8±22	27.3±1.5
PSA-DAc-ABA	350.7 (7568)	8.76 (8020)	182.1±47.8	55.2±7	42.4±13.4	26.9±2.3

Statistical Analysis of PSA Adhesion Test Results

Results obtained in the macroscopic adhesion experiments, static shear and 180° peel, on PSA tapes have been subjected to One-Way ANOVA analysis and mean values have been compared against each other using Tukey Test ($p<0.05$). Summary of the results for different experiments are provided below:

Table S6.3: Summary of statistical analysis results for the shear test in dry conditions. 0, not significant; 1, significant with $p<0.05$

Polymer	PSA	PSA-DAc	PSA-Lys(Boc)-DA(ac)	PSA-Lys(Boc)-DA	PSA-Lys-DA	PSA-Lys-PEA	PSA-DAc-ABA
PSA							
PSA-DAc	1						
PSA-Lys(Boc)-DA(ac)	1	1					
PSA-Lys(Boc)-DA	1	0	1				
PSA-Lys-DA	1	1	1	1			
PSA-Lys-PEA	1	1	1	1	1		
PSA-DAc-ABA	1	0	0	1	1	1	

Table S6.4: Summary of statistical analysis results for the shear test in wet conditions. 0, not significant; 1, significant with $p<0.05$

Polymer	PSA	PSA-DAc	PSA-Lys(Boc)-DA(ac)	PSA-Lys(Boc)-DA	PSA-Lys-DA	PSA-Lys-PEA	PSA-DAc-ABA
PSA							
PSA-DAc	1						
PSA-Lys(Boc)-DA(ac)	1	0					
PSA-Lys(Boc)-DA	1	0	0				
PSA-Lys-DA	1	1	1	1			
PSA-Lys-PEA	1	0	0	0	1		
PSA-DAc-ABA	1	0	0	0	1	0	

Table S6.5: Summary of statistical analysis results for the 180° peel test in dry conditions. 0, not significant; 1, significant with $p<0.05$

Polymer	PSA	PSA-DAc	PSA-Lys(Boc)-DA(ac)	PSA-Lys(Boc)-DA	PSA-Lys-DA	PSA-Lys-PEA	PSA-DAc-ABA
PSA							
PSA-DAc	1						
PSA-Lys(Boc)-DA(ac)	1	1					
PSA-Lys(Boc)-DA	0	1	0				
PSA-Lys-DA	0	1	0	0			
PSA-Lys-PEA	1	0	1	1	1		
PSA-DAc-ABA	1	0	0	1	0	0	

Table S6.6: Summary of statistical analysis results for the 180° peel test in wet conditions. 0, not significant; 1, significant with $p<0.05$

Polymer	PSA	PSA-DAc	PSA-Lys(Boc)-DA(ac)	PSA-Lys(Boc)-DA	PSA-Lys-DA	PSA-Lys-PEA	PSA-DAc-ABA
PSA							
PSA-DAc	1						
PSA-Lys(Boc)-DA(ac)	1	0					
PSA-Lys(Boc)-DA	0	1	1				
PSA-Lys-DA	1	1	1	1			
PSA-Lys-PEA	1	1	1	1	1		
PSA-DAc-ABA	1	1	1	1	1	0	

References

[1] B. P. Lee et al. "Mussel-Inspired Adhesives and Coatings". In: *Annual Review of Materials Research, Vol 41* 41 (2011), pp. 99–132 (cit. on p. 137).

[2] M. J. Harrington, F. Jehle, and T. Priemel. "Mussel Byssus Structure-Function and Fabrication as Inspiration for Biotechnological Production of Advanced Materials". In: *Biotechnology Journal* 13.12 (2018) (cit. on p. 137).

[3] Pegah Kord Forooshani and Bruce P. Lee. "Recent approaches in designing bioadhesive materials inspired by mussel adhesive protein". In: *Journal of Polymer Science Part A: Polymer Chemistry* 55.1 (2017), pp. 9–33 (cit. on pp. 137, 148).

[4] H. Lee et al. "Mussel-inspired surface chemistry for multifunctional coatings". In: *Science* 318.5849 (2007), pp. 426–430 (cit. on p. 137).

[5] J. H. Waite. "Mussel adhesion - essential footwork". In: *Journal of Experimental Biology* 220.4 (2017), pp. 517–530 (cit. on p. 137).

[6] D. W. R. Balkenende, S. M. Winkler, and P. B. Messersmith. "Marine-inspired polymers in medical adhesion". In: *European Polymer Journal* 116 (2019), pp. 134–143 (cit. on p. 137).

[7] A. H. Hofman et al. "Bioinspired Underwater Adhesives by Using the Supramolecular Toolbox". In: *Advanced Materials* 30.19 (2018) (cit. on p. 137).

[8] D. G. DeMartini et al. "A cohort of new adhesive proteins identified from transcriptomic analysis of mussel foot glands". In: *Journal of the Royal Society Interface* 14.131 (2017) (cit. on p. 137).

[9] J. H. Waite. "Natures Underwater Adhesive Specialist". In: *International Journal of Adhesion and Adhesives* 7.1 (1987), pp. 9–14 (cit. on p. 137).

[10] Y. R. Li and Y. Cao. "The molecular mechanisms underlying mussel adhesion". In: *Nanoscale Advances* 1.11 (2019), pp. 4246–4257 (cit. on pp. 137, 143).

[11] H. Lee, N. F. Scherer, and P. B. Messersmith. "Single-molecule mechanics of mussel adhesion". In: *Proceedings of the National Academy of Sciences of the United States of America* 103.35 (2006), pp. 12999–13003 (cit. on pp. 137, 148).

[12] Q. Lin et al. "Adhesion mechanisms of the mussel foot proteins mfp-1 and mfp-3". In: *Proc Natl Acad Sci U S A* 104.10 (2007), pp. 3782–6 (cit. on p. 137).

[13] B. K. Ahn et al. "High-performance mussel-inspired adhesives of reduced complexity". In: *Nature Communications* 6 (2015) (cit. on p. 137).

[14] B. D. B. Tiu et al. "Enhanced Adhesion and Cohesion of Bioinspired Dry/Wet Pressure-Sensitive Adhesives". In: *Acs Applied Materials Interfaces* 11.31 (2019), pp. 28296–28306 (cit. on pp. 137, 141, 143, 147, 148).

[15] B. K. Ahn. "Perspectives on Mussel-Inspired Wet Adhesion". In: *Journal of the American Chemical Society* 139.30 (2017), pp. 10166–10171 (cit. on p. 137).

[16] J. H. Waite. "Translational bioadhesion reserach: embracing biology without tokenism". In: *Philosophical Transactions of the Royal Society B-Biological Sciences* 374.1784 (2019) (cit. on p. 137).

[17] Y. Li et al. "Hidden complexity of synergistic roles of Dopa and lysine for strong wet adhesion". In: *Materials Chemistry Frontiers* 1.12 (2017), pp. 2664–2668 (cit. on p. 137).

[18] G. P. Maier et al. "Adaptive synergy between catechol and lysine promotes wet adhesion by surface salt displacement". In: *Science* 349.6248 (2015), pp. 628–632 (cit. on pp. 137, 141, 145, 146, 148).

[19] M. V. Rapp et al. "Defining the Catechol-Cation Synergy for Enhanced Wet Adhesion to Mineral Surfaces". In: *Journal of the American Chemical Society* 138.29 (2016), pp. 9013–9016 (cit. on pp. 137, 145, 148).

[20] Y. R. Li et al. "Single-molecule study of the synergistic effects of positive charges and Dopa for wet adhesion". In: *Journal of Materials Chemistry B* 5.23 (2017), pp. 4416–4420 (cit. on pp. 137, 141, 145, 146, 148).

[21] G. D. Degen et al. "Impact of Molecular Architecture and Adsorption Density on Adhesion of Mussel-Inspired Surface Primers with Catechol-Cation Synergy". In: *Journal of the American Chemical Society* 141.47 (2019), pp. 18673–18681 (cit. on pp. 137, 146, 148, 150).

[22] M. Shin et al. "The position of lysine controls the catechol-mediated surface adhesion and cohesion in underwater mussel adhesion". In: *Journal of Colloid and Interface Science* 563 (2020), pp. 168–176 (cit. on p. 137).

[23] M. A. Gebbie et al. "Tuning underwater adhesion with cation-pi interactions". In: *Nat Chem* 9.5 (2017), pp. 473–479 (cit. on pp. 137, 138, 141, 148, 150).

[24] Q. Y. Lu et al. "Nanomechanics of Cation Interactions in Aqueous Solution". In: *Angewandte Chemie-International Edition* 52.14 (2013), pp. 3944–3948 (cit. on p. 137).

[25] J. P. Gallivan and D. A. Dougherty. "Cation-pi interactions in structural biology". In: *Proceedings of the National Academy of Sciences of the United States of America* 96.17 (1999), pp. 9459–9464 (cit. on p. 137).

[26] A. S. Mahadevi and G. N. Sastry. "Cation-pi Interaction: Its Role and Relevance in Chemistry, Biology, and Material Science". In: *Chemical Reviews* 113.3 (2013), pp. 2100–2138 (cit. on p. 137).

[27] P. B. Crowley and A. Golovin. "Cation-pi interactions in protein-protein interfaces". In: *Proteins-Structure Function and Bioinformatics* 59.2 (2005), pp. 231–239 (cit. on p. 138).

[28] D. S. Hwang et al. "Adhesion mechanism in a DOPA-deficient foot protein from green mussels". In: *Soft Matter* 8.20 (2012), pp. 5640–5648 (cit. on pp. 138, 148).

[29] S. Kim et al. "Cation-pi interaction in DOPA-deficient mussel adhesive protein mfp-1". In: *Journal of Materials Chemistry B* 3.5 (2015), pp. 738–743 (cit. on pp. 138, 148).

[30] H. Birkedal. "Cation-pi Interactions Mimicking Mussel Mechanics". In: *Nature Chemistry* 9.5 (2017), pp. 408–409 (cit. on p. 138).

[31] H. L. Fan et al. "Adjacent cationic-aromatic sequences yield strong electrostatic adhesion of hydrogels in seawater". In: *Nature Communications* 10 (2019) (cit. on p. 138).

[32] N. F. Della Vecchia et al. "Building-Block Diversity in Polydopamine Underpins a Multifunctional Eumelanin-Type Platform Tunable Through a Quinone Control Point". In: *Advanced Functional Materials* 23.10 (2013), pp. 1331–1340 (cit. on p. 140).

[33] I. Webster. "Recent developments in pressure-sensitive adhesives for medical applications". In: *International Journal of Adhesion and Adhesives* 17.1 (1997), pp. 69–73 (cit. on p. 141).

[34] Istvan Benedek and Mikhail M. Feldstein. *Technology of pressure-sensitive adhesives and products*. a Handbook of pressure-sensitive adhesives and products. Boca Raton, FL: CRC Press, 2009 (cit. on p. 141).

[35] R. D. Adams. "Adhesive bonding: science, technology and applications". In: *Adhesive bonding: science, technology and applications*. Ed. by R. D. Adams. Woodhead Publishing, 2005 (cit. on p. 141).

[36] Alphonsus V. Pocius. "Adhesion and Adhesives Technology". In: *Adhesion and Adhesives Technology (Third Edition)*. Ed. by Alphonsus V. Pocius. Hanser, 2012, pp. I–XVI (cit. on p. 141).

[37] S. M. Sun, M. L. Li, and A. Liu. "A review on mechanical properties of pressure sensitive adhesives". In: *International Journal of Adhesion and Adhesives* 41 (2013), pp. 98–106 (cit. on p. 141).

[38] Adam L. Dobson, Nicholas J. Bongiardina, and Christopher N. Bowman. "Combined Dynamic Network and Filler Interface Approach for Improved Adhesion and Toughness in Pressure-Sensitive Adhesives". In: *ACS Applied Polymer Materials* 2.3 (2020) (cit. on p. 141).

[39] Y. J. Cui et al. "Decoupling the roles of the catechol content from those of glass transition temperature and dynamic mechanical modulus in determining self-healing and anti-corrosion of mussel-inspired polymers". In: *Polymer* 185 (2019) (cit. on p. 143).

[40] Hans-Jürgen Butt, Brunero Cappella, and Michael Kappl. "Force measurements with the atomic force microscope: Technique, interpretation and applications". In: *Surface Science Reports* 59.1 (2005), pp. 1–152 (cit. on p. 143).

[41] E. M. Puchner and H. E. Gaub. "Force and function: probing proteins with AFM-based force spectroscopy". In: *Current Opinion in Structural Biology* 19.5 (2009), pp. 605–614 (cit. on p. 143).

[42] X. Zhang, C. J. Liu, and Z. Q. Wang. "Force spectroscopy of polymers: Studying on intramolecular and intermolecular interactions in single molecular level". In: *Polymer* 49.16 (2008), pp. 3353–3361 (cit. on p. 143).

[43] A. Noy. "Force spectroscopy 101: how to design, perform, and analyze an AFM-based single molecule force spectroscopy experiment". In: *Current Opinion in Chemical Biology* 15.5 (2011), pp. 710–718 (cit. on pp. 143, 144).

[44] C. Friedsam, H. E. Gaub, and R. R. Netz. "Probing surfaces with single-polymer atomic force microscope experiments". In: *Biointerphases* 1.1 (2006), Mr1–Mr21 (cit. on p. 143).

[45] Johann Erath, Stephan Schmidt, and Andreas Fery. "Characterization of adhesion phenomena and contact of surfaces by soft colloidal probe AFM". In: *Soft Matter* 6.7 (2010), pp. 1432–1437 (cit. on pp. 143, 146).

[46] A. Zosel. "Adhesion and tack of polymers: Influence of mechanical properties and surface tensions". In: *Colloid and Polymer Science* 263.7 (1985), pp. 541–553 (cit. on pp. 143, 146, 147).

[47] Adriana Paiva et al. "Study of the Surface Adhesion of Pressure-Sensitive Adhesives by Atomic Force Microscopy and Spherical Indenter Tests". In: *Macromolecules* 33.5 (2000), pp. 1878–1881 (cit. on pp. 143, 146).

[48] M. Kappl and H. J. Butt. "The colloidal probe technique and its application to adhesion force measurements". In: *Particle Particle Systems Characterization* 19.3 (2002), pp. 129–143 (cit. on pp. 143, 146).

[49] V. T. Moy, E. L. Florin, and H. E. Gaub. "Intermolecular Forces and Energies between Ligands and Receptors". In: *Science* 266.5183 (1994), pp. 257–259 (cit. on p. 143).

[50] L. F. Milles et al. "Molecular mechanism of extreme mechanostability in a pathogen adhesin". In: *Science* 359.6383 (2018), pp. 1527–1532 (cit. on p. 143).

[51] Yi Cao and Hongbin Li. "Polyprotein of GB1 is an ideal artificial elastomeric protein". In: *Nat Mater* 6.2 (2007), pp. 109–114 (cit. on p. 144).

[52] J. S. Kim et al. "Mechanically Stretching Folded Nano-pi-stacks Reveals Pico-Newton Attractive Forces". In: *Advanced Materials* 21.7 (2009), pp. 786–789 (cit. on p. 144).

[53] R. W. Carpick, D. F. Ogletree, and M. Salmeron. "A general equation for fitting contact area and friction vs load measurements". In: *Journal of Colloid and Interface Science* 211.2 (1999), pp. 395–400 (cit. on p. 146).

[54] S. Okada et al. "Adhesion properties of polyacrylic block copolymer pressure-sensitive adhesives and analysis by pulse NMR and AFM force curve". In: *Journal of Applied Polymer Science* 136.29 (2019) (cit. on p. 147).

[55] Kim Hyonchol et al. "Quantification of fibronectin and cell surface interactions by AFM". In: *Colloids and Surfaces B: Biointerfaces* 25.1 (2002), pp. 33–43 (cit. on p. 147).

[56] Bettye L. Smith et al. "Molecular mechanistic origin of the toughness of natural adhesives, fibres and composites". In: *Nature* 399.6738 (1999), pp. 761–763 (cit. on p. 147).

[57] Eugene Kim et al. "Microbially Synthesized Repeats of Mussel Foot Protein Display Enhanced Underwater Adhesion". In: *ACS Applied Materials Interfaces* 10.49 (2018), pp. 43003–43012 (cit. on p. 147).

[58] Tobias Priemel et al. "Compartmentalized processing of catechols during mussel byssus fabrication determines the destiny of DOPA". In: *Proceedings of the National Academy of Sciences* 117.14 (2020), p. 7613 (cit. on p. 150).

Conclusions

The preceding chapters in this dissertation should provide a flavor of the mix of the achievements, expectations, and existing challenges regarding the creation of novel functional materials utilizing mussel-inspired catechol- and catecholamine-based molecules. The ubiquity of catecholic compounds in nature and their unique properties and versatile reaction chemistries have fueled their implementation in a wide range of functional materials. These catecholic motifs exhibit multiple intrinsic properties such as metal chelation, dynamic complexation with multitude of ligands, interfacial adhesion to a variety of substrates, redox potential and radical scavenging as well as broadband light absorbance, which can provide elegant solutions to many multifaceted problems encountered in materials development for a wide range of applications. However, despite the outstanding progress that has been accomplished in the design of catecholic functional materials, there are still numerous challenges that must be met before this research area can become a mature field for translation into technological platforms. For instance, structure elucidation of many hierarchical catechol-based assemblies such as pDA and eumelanin remains a subject of ongoing investigations. Unlike the vast majority of synthetic polymers, structure of pDA and eumelanin can only be portrayed in terms of a statistical description of a heterogeneous mixture of protomolecules and building blocks rather than a well-defined chemical structure. The notorious difficulties in the structural investigation of these functional assemblies, mainly due to the amorphous character and the marked insolubility in most common solvents have rendered a deeper understanding of their structure-property-processing relationship extremely challenging. Although pDA and melanin-mimetic materials satisfy many of the requisite physicochemical properties essential in design of novel engineering materials, the true potential of these bioinspired materials cannot be realized unless a unified perspective aiming at elucidating their structure is established. Particularly noteworthy is delineating the final steps of assembly in order to develop rational strategies to improve processability and tailor and fine-tune their properties for target applications.

Furthermore, despite their overall exemplary properties, relatively weak stability of the catechol-based molecules has been widely acknowledged as one of their major drawbacks. For instance, catechols are susceptible to spontaneous oxidation upon exposure to air, which makes the process of constructing the engineering materials from these catecholic molecules challenging. Moreover, due to the relatively weak intermolecular interactions present in their structures, most of the catechol-based assemblies in their current form do not ex-

hibit great resistance to delamination and wear, limiting their widespread adaptation into mechanically-demanding applications. Therefore, more efforts should be devoted to improving their mechanical performance without compromising the inherent chemical versatility of these molecules to support secondary reactions. It is thus critical to devise new experimental approaches to conquer these shortcomings in order to facilitate the widespread incorporation of these building blocks into design of emerging multi-component materials. Finally, I would like to conclude by acknowledging the ability of catechol-based molecules to form a myriad of strong reversible and irreversible interactions which has long inspired researchers for creation of unique and versatile platforms for developing complex materials with enhanced performance. However, it is essential to note that these catechol-based molecules in the natural systems do not perform in isolation; instead, they often function in parallel, serving multiple roles and collaborate closely with other available functionalities and structural motifs to yield unique properties. A better understanding of the fundamental principles and multifunctionality that these building blocks exhibit in nature will foster further progress in exploitation and harnessing their full potential as alternative solutions to many outstanding engineering challenges.